

A 3D MONOFILAMENT BIOSUTURE FOR MICROVASCULAR SURGERY APPLICATIONS

Kara Mia de la Harpe

A dissertation submitted to the Faculty of Health Sciences, University of the Witwatersrand,
in fulfilment of the requirements for the degree Master of Pharmacy.



Supervisor: Professor Yahya Essop Choonara, Department of Pharmacy and Pharmacology,
Faculty of Health Sciences, University of the Witwatersrand, South Africa.

Co-supervisor: Professor Pierre Pavan Demarco Kondiah, Department of Pharmacy and
Pharmacology, Faculty of Health Sciences, University of the Witwatersrand, South Africa.

Co-supervisor: Professor Thashree Marimuthu, Department of Pharmacy and
Pharmacology, Faculty of Health Sciences, University of the Witwatersrand, South Africa.

January 2022, Johannesburg, South Africa

DECLARATION

I, Kara de la Harpe, declare that this dissertation is my own, unaided work. It is being submitted for the Degree Master of Pharmacy at the University of the Witwatersrand, Johannesburg. It has not been submitted before for any degree or examination at any other University.

(Signature of candidate)

26th day of January 2022 in Johannesburg, Gauteng, South Africa.

DEDICATION

I dedicate this work firstly to my Heavenly Father, Jesus Christ, without whom I am nothing, and secondly to my earthly father, Prof. Stephen de la Harpe, without whom I would not be who I am today.

PUBLICATIONS

Review articles

1. de la Harpe, K.M., Kondiah, P.P., Choonara, Y.E., Marimuthu, T., du Toit, L.C. and Pillay, V., 2019. The hemocompatibility of nanoparticles: a review of cell–nanoparticle interactions and hemostasis. *Cells*, 8(10), p.1209. **Impact factor: 4.33. Citations: 70.** (Appendix A 1).
2. de la Harpe, K.M., Kondiah, P.P., Marimuthu, T. and Choonara, Y.E., 2021. Advances in carbohydrate-based polymers for the design of suture materials: A review. *Carbohydrate Polymers*, p.117860. **Impact factor: 9.381. Citations: 1.** (Appendix A 2).

Research articles

1. de la Harpe, K.M., Kondiah, P.P., Marimuthu, T., Du Toit, L.C., Kumar, P., Choonara, Y.E. and Pillay, V., 2020. An advanced 3D monofilament biosuture. *South African Pharmaceutical Journal*, 87(1), pp.45-48. **Impact factor: 1.325. Citations: 1.** (Appendix A 3).
2. de la Harpe, K.M., Kondiah, P.P., Marimuthu, T., P. Kumar, Ubanako, P. and Choonara, Y.E. Synthesis of a novel monofilament bioabsorbable suture for biomedical applications. Submitted to the *Journal of Biomedical Materials Research: Part B*. **Impact factor: 3.368.** (Appendix A 4).

RESEARCH OUTPUTS

Podium presentations

1. de la Harpe, K.M., Kondiah, P.P., Choonara, Y.E., Marimuthu, T., du Toit, L.C. and Pillay, V., September 2019. An advanced 3D monofilament biosuture. 10th Wits Cross-faculty Postgraduate Symposium, University of the Witwatersrand, Johannesburg, South Africa (Appendix B 1).
2. de la Harpe, K.M., Kondiah, P.P., Choonara, Y.E., Marimuthu, T., du Toit, L.C. and Pillay, V., October 2019. An advanced 3D monofilament biosuture. Academy of Pharmaceutical Sciences, 2019 Conference and Young Scientist Competition, Pretoria, South Africa. (Appendix B 2).
3. de la Harpe, K.M., Kondiah, P.P., Marimuthu, T., Du Toit, L.C., Kumar, P. and Choonara, Y.E., October 2020. Evolution of the suture – where to in the future? Faculty of Health Sciences, 2020 Biannual Research Day, University of the Witwatersrand, Johannesburg, South Africa. (Appendix B 3).
4. de la Harpe, K.M., Kondiah, P.P., Marimuthu, T., Kumar, P., Ubanako, P. and Choonara, Y.E., November 2021. Synthesis of a novel monofilament bioabsorbable suture for biomedical applications. International BRICS Symposium, Wits Advanced Drug Delivery Platform (WADDP), University of the Witwatersrand, Johannesburg, South Africa.

Poster presentations

1. de la Harpe, K.M., Kondiah, P.P., Marimuthu, T., Du Toit, L.C., Kumar, P. and Choonara, Y.E., September 2021. A novel monofilament, absorbable, drug-eluting biopolymeric suture. Faculty of Health Sciences, 2021 Biannual Research Day, University of the Witwatersrand, Johannesburg, South Africa. (Appendix B 4).

Accolades

1. Master's Scholarship: National Research Foundation (NRF) Freestanding bursary, 2019 – 2021.
2. Postgraduate Merit Award, University of the Witwatersrand, 2019 – 2020. (Appendix C 1).
3. Winner of the Academy of Pharmaceutical Sciences' Young Scientist Award at the 2019 Conference and Young Scientist Competition, Pretoria, South Africa. "An advanced 3D monofilament biosuture". (Appendix C 2).
4. Winner of the best student poster presentation at the Faculty of Health Sciences, 2021 Biannual Research Day, University of the Witwatersrand, Johannesburg, South Africa. "A novel monofilament, absorbable, drug-eluting biopolymeric suture". (Appendix C 3).

ABSTRACT

With a huge global market of over \$ 3.7 billion annually and employment in more than 12 million procedures per year, sutures are one of the most widely used medical devices of the day. Yet, the ideal suture material does not exist, and surgeons battle on a daily basis with the various complications caused by these key medical devices. The ideal suture should create an environment that not only supports, but also encourages wound healing by delicately approximating the wound edges without contributing to the damage and inflammatory activity of the wound. Regrettably, most suture materials have no inherent therapeutic activity and contrarily cause damage to the tissue through effects such as 'sawing' and 'cheese-wiring', that can delay the wound healing process. Hence, there is an urgent need for a more advanced suture material that is, not only biocompatible and safe, but also inherently bioactive and able to either prevent complications or contribute to the wound healing process.

The aim of this study is to design, fabricate and evaluate a novel absorbable, monofilament biosuture material, that consist only of natural biopolymers with established biocompatibility and biodegradability. The biosuture will be transformed into a drug delivery device, that can provide localized, sustained drug release to help address complications such as ischemic reperfusion injury and the dreaded 'no-reflow' phenomenon during microvascular surgery. Various biopolymers, such as alginate, pectin, nanocellulose and gelatin, were investigated during the preliminary design phase, to obtain an optimized biosuture formulation that could meet the United States Pharmacopoeia's requirements for suture tensile strength. The optimized formulation consisted of alginate (6% w/v), pectin (0.1% w/v), gelatin (3% w/v) and glycerol (4% v/v). Different methods of drug loading were also investigated and the optimal method, namely a lipid-drug coating, selected for further characterization. The biosutures displayed excellent mechanical properties with a maximum load failure of 4.14 N in the straight configuration. SEM images revealed a smooth surface morphology and even coating of the biosuture with the lipid-drug layer. The lipid-drug coating displayed a suitable loading capacity (53 – 101 ug/cm) and provided controlled drug release over a period of seven days. The biosutures degraded by means of surface erosion and were fully eroded after 5 weeks of incubation. The physicochemical and thermal properties of the biosutures were investigated by means of FTIR, XRD, TGA and DSC) and showed favourable results. The biosutures also displayed excellent biocompatibility and improved cell viability over a period of 48 hours. The biosutures displayed good hemocompatibility with no haemolytic or platelet activating abilities. The results are very encouraging warrant further *in vivo* investigation of the newly developed biosuture material.

AKNOWLEDGEMENTS

This degree has been quite challenging from the start and when it all felt like an unsurmountable task, the following quote, cited to me by my father, helped me to get started:

“Begin at the beginning and end at the end” – Alice in Wonderland.

My dad, Prof. Stephen de la Harpe, passed away on 18 February 2021, and wasn't there to give me a similar quote when the degree drew to an end. Ironically, this same quote gave me just as much solace and encouragement when I faced the final hurdles of the degree, as it did in the beginning – if not more. *Dankie pappa, vir die sterk akademiese fondasie wat pappa in my lewe gelê het. Hierdie graad en my akademiese lewenspad het heel waarskynlik begin by my Graad 1 verjaarsdag geskenk ('n boek van my keuse) wat baie vining 'n jaarlikse tradisie geword het. Dankie dat pappa my gewys het hoe om objektief te dink, hard te werk, mense en situasies te waardeer vir wat dit is en om bowenal die lewe te geniet. Ek is baie lief vir pappa.*

I would like to express my gratitude to Prof. Yahya E. Choonara, Prof. Thashree Marimuthu and Prof. Pierre P.D. Kondiah for their guidance, encouragement, and useful critique to this research work. Thank you also to Prof. Pradeep Kumar and Prof. Lisa C. du Toit, for their continued support. I would also like to acknowledge the technical support staff at WAPPD – Hillary, Tshidi, Bafana, KB (Kleinboo) and Mr. Sello Ramarumo for their help with acquiring chemicals and just about anything else I needed to complete the project. WADDP provided me with amazing opportunities, pushed me further than I thought I could go, and taught me life lessons beyond what I expected. This journey would not have been the same without my colleagues and friends, Eemaan, Abu, Taskeen, Henna, Divesha, Shazia, Courtney, Kate, Leschika, Kruti, Ayesha, Thope, Alex, and Cuthbert. Thank you for all the stories, jokes, Paul's ice cream, cry sessions, long invigilations and pep talks – I will always treasure the times we weathered the postgraduate storms together.

I would also like to thank my friends outside of WADDP, Carli, Yollie, Ilze, Anri, Driekie, Margo, Petroné, Heinrich, Chanté, Mariska, Charolize, Mareli and the many others who helped break the academic pressure when needed. Additionally, I would like to express my gratitude towards my aunts, uncles and cousins, my dear extended Stellenbosch family and my Every Nation church family for their support, love, continued interest, and innumerable prayers. Lastly, a very special thank you to my close family – my mother, Dr. Hanri Elisabeth de la Harpe and sisters, Shani, Lana, and Janke. You mean more to me than words can say, and I love you with my whole heart.

TABLE OF CONTENTS

DECLARATION	ii
DEDICATION.....	iii
PUBLICATIONS.....	iv
Review articles	iv
Research articles.....	iv
RESEARCH OUTPUTS	v
Podium presentations.....	v
Poster presentations.....	v
Accolades.....	v
ABSTRACT.....	vi
ACKNOWLEDGEMENTS.....	vii
TABLE OF CONTENTS	viii
LIST OF TABLES.....	xi
LIST OF FIGURES	xii
LIST OF EQUATIONS	xvi
CHAPTER 1: INTRODUCTION AND OVERVIEW OF THE STUDY	1
1.1 Introduction.....	1
1.2 Rational and motivation	4
1.3 Novelty of the study	7
1.4 Aims and objectives.....	7
1.5 Overview of the dissertation.....	8
CHAPTER 2: ADVANCES IN CARBOHYDRATE-BASED POLYMERS FOR THE DESIGN OF SUTURE MATERIALS – A REVIEW	10
2.1 Introduction.....	10
2.2 Cellulose and its derivatives	12
2.2.1 The use of oxidized cellulose in the development of novel suture materials	12
2.2.2 The use of plant derived nanocellulose in the development of suture materials. .	14
2.2.3 The use of bacterial derived nanocellulose for novel suture material development	16
2.3 Chitin and its derivatives.....	17
2.3.1 Chitin as a potential biomaterial for surgical suture material applications	18
2.3.2 Chitosan from chitin as a potential biomaterial for surgical suture applications....	23
2.4 Alginate and its derivatives	28
2.4.1 Advancements in the use of alginate to develop novel suture materials	29
2.5 Potential impact and future prospects.....	32
2.6 Conclusion.....	36
CHAPTER 3: PRELIMINARY BIOSUTURE DESIGN AND STUDY OF THE INFLUENCE OF FORMULATION PARAMETERS ON THE MECHANICAL PROPERTIES OF THE BIOSUTURE	40
3.1 Introduction.....	40
3.2 Theoretical basis for the selection of key materials.....	41
3.2.1 Polymer base: Sodium alginate.....	41
3.2.2 Crosslinking agents: Barium chloride and epichlorohydrin.....	43
3.2.3 Reinforcing agents: Pectin, nanocellulose and gelatin.....	44
3.2.4 Plasticizers: Polypropylene glycol, triethyl citrate and glycerol.....	48
3.3 Materials.....	49
3.4 Methods	49

3.4.1 Polymer characterization by Fourier Transform Infrared Spectroscopy (FTIR)	49
3.4.2 Determination of the fibre forming ability of sodium alginate.....	52
3.4.3 Methods of biosuture fabrication	52
3.4.4 Tensile testing procedure	53
3.4.5 Influence of formulation components and processing conditions on the mechanical properties of the biosuture.	54
3.5 Results and discussion	57
3.5.1 Polymer characterization by Fourier Transform Infrared Spectroscopy (FTIR)	57
3.5.2 Determination of the fibre forming ability of sodium alginate.....	62
3.5.3 Methods of biosuture fabrication	63
3.5.4 Influence of formulation components and processing conditions on the mechanical properties of the biosuture.	65
3.6 Conclusion.....	87
CHAPTER 4: APPROACHES TO THE CONFIGURATION OF A DRUG-ELUTING BIOSUTURE WITH OPTIMAL METHOD SELECTION.	88
4.1 Introduction.....	88
4.2 Materials and methods	90
4.2.1 Materials	90
4.2.2 Methods of drug loading.....	90
4.2.3 Evaluation of the drug loading capacity of the different drug-loaded biosutures ..	92
4.2.4 Evaluation of the drug release behaviour of the different drug-loaded biosutures	93
4.2.5 Determination of the degradation profiles of the different drug-loaded biosutures	94
4.2.6 Evaluation of the mechanical properties of each drug loaded biosuture	94
4.2.7 Selection of the optimal drug loading method for the specific study.....	95
4.3 Results and discussion	95
4.3.1 Drug loading capacity of the different drug-loaded biosutures	95
4.3.2 Drug release behaviour of biosutures prepared with drug loading methods A – D.	97
4.3.3 Degradation profile of the different drug-loaded biosutures	102
4.3.4 Mechanical properties of the different drug-loaded biosutures.....	104
4.3.5 Selection of the optimal drug loading method for the specific study.....	106
4.3.6 Conclusion.....	109
CHAPTER 5: PHYSIOCHEMICAL AND PHYSICOMECHANICAL CHARACTERIZATION OF THE OPTIMIZED MONOFILAMENT, ABSORBABLE, DRUG-ELUTING BIOSUTURE.....	110
5.1 Introduction.....	110
5.2 Materials and methods	110
5.2.1 Materials	110
5.2.2 Preparation of the optimized biosutures	110
5.2.3 Evaluation of vibrational transitions within the biosuture by means of Fourier Transform Infrared Spectroscopy (FTIR).....	111
5.2.4 Evaluation of the relative crystallinity of materials by means of Powder X-ray Diffraction (XRD).....	112
5.2.5 Thermal evaluation of the biosutures by means of Thermogravimetric analysis (TGA) and Differential Scanning Calorimetry (DSC).....	112
5.2.6 Evaluation of the surface morphology of biosutures by means of light microscopy and Scanning Electron Microscope (SEM) imaging.....	113
5.2.7 Evaluation of the mechanical properties of the biosutures.....	113
5.2.8 Evaluation of the <i>in vitro</i> drug loading and release behaviour of the biosutures.	114
5.2.9 Evaluation of the <i>in vitro</i> swelling and degradation behaviour of the biosutures	114

5.3 Results and discussion	115
5.3.1 Preparation of the optimized biosutures	115
5.3.2 Evaluation of vibrational transitions within the biosuture by means of Fourier Transform Infrared Spectroscopy (FTIR).....	116
5.3.3 Evaluation of the relative crystallinity of materials by means of Powder X-ray Diffraction (XRD).....	121
5.3.4 Thermal evaluation of the biosutures by means of Thermogravimetric analysis (TGA) and Differential Scanning Calorimetry (DSC).....	123
5.3.7 Evaluation of the mechanical properties of the biosutures.....	131
5.2.8 Evaluation of the <i>in vitro</i> drug loading and release behaviour of the biosutures.	133
5.2.9 Evaluation of the <i>in vitro</i> swelling and degradation behaviour of the biosutures	134
5.4 Conclusion.....	137
 CHAPTER 6: ANALYSIS OF THE <i>IN VITRO</i> BIOCOMPATIBILITY OF THE NEWLY DEVELOPED BIOSUTURES	 138
6.1 Introduction.....	138
6.2 Materials and methods	139
6.2.2 Materials	139
6.2.2 Evaluation of the <i>in vitro</i> cytotoxicity of the biosutures.....	139
6.2.3 Evaluation of cellular attachment to the biosutures.....	140
6.2.4 Evaluation of the haemolytic activity of the biosutures.....	140
6.2.5 Evaluation of the platelet activation ability of the biosutures	141
Statistical analysis.....	141
6.3 Results and discussion	142
6.3.1 Evaluation of the <i>in vitro</i> cytotoxicity of the biosutures.....	142
6.3.2 Evaluation of cellular attachment to the biosutures.....	144
6.3.3 Evaluation of the haemolytic activity of the biosutures.....	146
6.3.4 Evaluation of the platelet activation ability of the biosutures	149
6.4 Conclusion.....	153
 CHAPTER 7: CONCLUSIONS, RECOMMENDATIONS, AND FUTURE PROSPECTS	 155
7.1 Conclusions.....	155
7.2 Recommendations and future prospects.....	156
 REFERENCES	 158
APPENDICES.....	185
Appendix A: Publications	185
Appendix B: Research outputs (oral and poster presentations)	190
Appendix C: Accolades	196
Appendix D: Ethical clearance	199

LIST OF TABLES

Table 2.1 Advantages and disadvantages of synthetic- and natural polymer sutures.....	11
Table 2.2 Mechanical properties of the BC-loaded yarns indicating the ultimate stress and ultimate strain of fibres with different diameters and BC concentrations.....	17
Table 2.3 Mechanical properties of the chitosan and the chitosan-N-acetyl-D-Glucosamine (GlcNAc) sutures – non-knotted and knotted – tested in dry and wet conditions..	24
Table 3.1: Basic requirements of a safe and effective drug-loaded suture material.....	40
Table 3.2: Band assignments for the determination of protein secondary structures.....	51
Table 3.3: Proportions of solutions required to measure the isoelectric point of gelatin.....	51
Table 3.4: Different concentrations of BaCl ₂ and ECH used to crosslink the polymer blend and produce biosutures.....	56
Table 3.5: Calculation of the M/G ratio of sodium alginate.....	58
Table 3.6: Observations made for fibres of varying sodium alginate concentrations while in the crosslinker solution and after being air dried.....	62
Table 3.7: Mechanical properties of biosutures produced with different fabrication methods in the straight and knotted configuration.....	64
Table 3.8: USP limits on average diameter and knot pull tensile strength of respective suture gauge numbers.....	66
Table 3.9: Mechanical properties of biosutures produced from only sodium alginate.....	68
Table 3.10: Mechanical properties of biosutures containing different concentrations of glycerol, in the straight and knot configuration.....	70
Table 3.11: The load failure, tensile strength, and elongation at break of biosutures containing different concentrations of CNF, in the straight and knot configuration.....	77
Table 3.13: Mechanical properties of biosutures containing different concentrations of gelatin.....	79
Table 3.13: Mechanical properties of biosutures crosslinked with different BaCl ₂ concentrations.....	81
Table 3.14: Mechanical properties of biosutures crosslinked with varying concentrations of ECH, in the straight and knotted configuration.....	83
Table 3.15: Diameter and mechanical properties of biosutures dried under different drying conditions, in the straight and knotted configuration.....	85
Table 4.1 Composition of lipid-drug solutions used for coating the biosuture material.....	92
Table 4.2 The drug loading capacity of biosutures prepared using methods A – D.....	96
Table 4.3 The average values of key parameters used to study the mechanical properties of the original and drug loaded biosutures.....	104
Table 4.4 Summary of the methods that performed best in each of the investigated categories.....	109
Table 5.1 Composition of the optimised biosuture formulation.....	111
Table 5.2 Mechanical properties of the uncoated and coated biosutures.....	132

LIST OF FIGURES

Figure 1.1: A) End-to-end anastomosis using the popular triangulation technique and B) end-to-side anastomosis using interrupted sutures. Adapted with permission from A) (Wain, <i>et al.</i> , 2016) and B) (MacDonald, 2005).	3
Figure 1.2: Schematic representation of the tissue damaging inflammatory response of ischemic reperfusion injury. Reused with permission from (Sánchez-Hernández <i>et al.</i> , 2020).	6
Figure 1.3: Schematic representation of the outline of the dissertation.....	9
Figure 2.1: A) The in vitro degradation of tempo-mediated oxidized regenerated cellulose (TORC) sutures at different oxidation times (15, 30, 45, 60, and 90 minutes after PBS impregnation) mean \pm S.D., n = 10. B) Carboxyl content of ORC sutures at the same different oxidation times. Adapted with permission from (Li <i>et al.</i> , 2019).	14
Figure 2.2: Immunocytochemistry shows the attachment of the cells of the suture surface. The human adipose mesenchymal stem cells (hASC) exhibited elongated cytoplasmic intermediate filaments (stained red with phalloidin), especially on the crosslinked suture fibres. Nuclei were counterstained in blue with DAPI. Scale bars 50 μ m. Used with permission from (Mertaniemi <i>et al.</i> , 2016).	15
Figure 2.3: Fabrication process of chitin-graphene oxide sutures. (A) Chitin gel spun into a coagulation bath; (B) suture solidification stretching and moulding; (C, D) stretched chitin and chitin-graphene oxide sutures in an elution bath, respectively; (E) chitin suture; (F) chitin-graphene oxide suture. Reused with permission from (Zhang <i>et al.</i> , 2019).	20
Figure 2.4: Representative images of the wound healing process after treatment with DAC suture (A) and the control Vicryl® Plus suture (B) during a 3-week observation period. Bars represent 5 mm. Reprinted with permission from (Shao <i>et al.</i> , 2016).	23
Figure 2.5: Optical microscopy images of a) monofilament and b) multifilament chitosan fibres. Adapted with permission from (Costa Da Silva <i>et al.</i> , 2020).	27
Figure 2.6: A) Photo of the alginate/BSA composite fibres. Scale bar: 3 cm. B) Stress-strain curves of alginate/BSA composite fibres. The curves with different colours represent three parallel tensile tests. C) Confocal microscopy image of the alginate/BSA composite fibres co-cultured with adeno-carcinomic human alveolar basal epithelial cells (A549). Scale bar: 20 μ m. A549 cells are stained with calcein-AM (green)/PI (red) in phosphate buffered saline solution. Adapted with permission from (Zhang, Sun, <i>et al.</i> , 2020).	30
Figure 2.7: The different areas of suture performance that can be impacted by the development of novel sutures made from natural carbohydrate polymers.	32
Figure 3.1: Chemical structure of sodium alginate showing the α -D-guluronic (G), acid β -D-mannuronic acid (M) and heterogeneous MG blocks. Adapted with permission from (Daemi & Barikani, 2012).	42
Figure 3.2: Eggbox model of ionic crosslinking between a divalent cation and sodium alginate. Adapted with permission from (Paul & Sharma, 2015).	42
Figure 3.3: Suggested method of crosslinking between alginate and epichlorohydrin. Adapted with permission from (Pawar & Edgar, 2012).	44
Figure 3.4: (A) Co-linear model for the organization of pectin in smooth and hairy regions. (B) The chemical structure of the smooth region – homogalacturonan. Used with permission from (Liu <i>et al.</i> , 2007).	45

Figure 3.5: Structural representation of how ionic interaction and hydrogen bonding can take place between sodium alginate and gelatin. Adapted with permission from (Samp, 2017). .	48
Figure 3.6: A) Graphical representation of suture fabrication via hand. B) 3D spiral design used to extrude the polymer solution via the 3D Bioplotter. C) Texture Analyser setup during suture fabrication and polymer extrusion using the universal syringe rig.	53
Figure 3.7: FTIR spectra of sodium alginate, pectin and nanocellulose fibrils.	57
Figure 3.8: FTIR spectrum of pectin showing the peaks used to determine the degree of esterification of the polymer.	58
Figure 3.9: FTIR spectrum of gelatin, showing all major amide regions.	59
Figure 3.10: Gaussian deconvolution of the FTIR spectra of amide I and amide III of gelatin, as obtained by means of the second derivative method. The sum of the fitted curves is shown as a red line, closely overlapping the experimental data trace, which is shown as a full black line. The secondary structure, as derived from Table 3.2, is indicated above each peak.	60
Figure 3.11: The pH of solutions before and after the addition of gelatin; the corresponding zeta-potential and the PI of gelatin with a graphical representation of its determination.	61
Figure 3.12: A) Test tube 1 – 6 presenting as clear solutions before the addition of methanol. B) Test tubes 1 – 6 with different degrees of flocculation after the addition of methanol. Arrow indicates maximum flocculation in test tube 2 (pH 5.25).	61
Figure 3.13: Crosslinked fibres made with varying concentrations of sodium alginate (A) 1%, B) 2%, C) 4%, D) 6%, E) 8%, F) 10%), showing the range between 4 – 8% as most appropriate for biosuture fabrications.	63
Figure 3.14: Schematic representation of a typical stress-strain curve. Adapted with permission from (Cooke, F.W., Lemons, J.E. and Ratner, 1996).	67
Figure 3.15: A) Representative load vs displacement curve of pure sodium alginate biosutures. B) Representative stress vs strain curve of pure sodium alginate biosutures.	68
Figure 3.16: Stress-strain curves of biosutures containing 4% v/v glycerol in the straight (A) and knotted (B) configuration.	71
Figure 3.17: Morphology of biosutures consisting of alginate alone (1. A) and alginate plus pectin (1. A) and the corresponding diameter of each biosuture fibre – alginate alone (2. A) and alginate plus pectin (2. B).	73
Figure 3.17: The force required to extrude the alginate (blue) and alginate – pectin (red) solutions through a 23G needle into a crosslinker solution as measured with the Texture Analyser (T.A.X.T Plus).	74
Figure 3.18: Load failure (N) and tensile strength (N/mm ²) of biosuture samples containing different concentrations of pectin in the straight (A & C) and knot (B & D) configuration.	75
Figure 3.19: Elongation at break (%) of biosuture samples containing different concentrations of pectin in the straight (A) and knotted (B) configuration.	76
Figure 3.20: A) Microscopic image of the cellulose nanofibrils (CNF), illustrating their tendency to entangle and agglomerate. B) Microscopic image of biosutures consisting of alginate and CNF (top) and alginate alone (bottom). Arrows indicate CNF agglomerates. Note that fibres are in the wet, swollen state and diameters do not correlate with the final dry biosuture fibre diameter.	78
Figure 3.21: Representative stress-strain graphs (straight configuration) of biosutures containing different concentrations of gelatin.	81
Figure 3.22: A) Tensile strength and B) Elongation at break of biosutures crosslinked with different concentrations of the crosslinkers, Barium chloride (BaCl ₂) and Epichlorohydrin (ECH), in the straight and knotted configuration.	84
Figure 3.23: Stress-strain curves of biosutures dried under different drying conditions, as evaluated in the straight configuration.	85

Figure 4.1: Calibration curve of (A) dexamethasone 21-phosphate disodium salt and (B) dexamethasone, indicating the linear regression equation and R ² values, as well as the confidence and prediction intervals for each curve.	93
Figure 4.2: Chemical structures of the drug and lipids used in the study and possible interactions and attractive/repulsive forces that may occur.	97
Figure 4.3: Cumulative drug release over 7 days in A) amount (ug/mL) and B) percentage (%) from biosutures prepared with method A – D.	98
Figure 4.4: Cumulative drug release over 7 days in A) amount (ug/mL) and B) percentage (%) for biosutures prepared with method A. C) Graphical representation of the proposed drug release mechanism and D) the degradation profile of biosutures prepared with method A..	99
Figure 4.5: Cumulative drug release over 7 days in A) amount (ug/mL) and B) percentage (%) for biosutures prepared with method B. C) Graphical representation of drug migration to the surface of the biosuture during drying and subsequent burst release from the surface.	100
Figure 4.6: Cumulative drug release over 7 days in A) amount (ug/mL) and B) percentage (%) for biosutures prepared with method C and C) Graphical representation of the proposed drug release mechanism from biosutures prepared with method C.	101
Figure 4.7: Cumulative drug release over 7 days in A) amount (ug/mL) and B) percentage (%) for biosutures prepared with method D.....	102
Figure 4.8: <i>In vitro</i> degradation profile of the original biosuture and of biosutures prepared with different methods (A – D) of drug loading.....	103
Figure 4.9: Representative stress – strain curves of the original and drug loaded biosutures in the (A) straight configuration and (B) knotted configuration.....	105
Figure 5.1: Images taken during the biosuture fabrication process; A) biopolymer solution, B) extrusion into the crosslinker, C) drying in a fume hood, D) coating with lipid-drug layer, E) drying of the coated biosutures F) final coated biosutures.....	115
Figure 5.2: FTIR spectra of the biosuture formulation components in their pristine form, top to bottom: alginate, pectin, gelatin and glycerol.....	116
Figure 5.3: FTIR spectra of the biosuture before (black) and after crosslinking (red) with BaCl ₂	119
Figure 5.4: FTIR spectra of the lipid-drug coating that consists of soy phosphatidyl choline and dexamethasone.	120
Figure 5.5: FTIR spectra of the lipid-drug coated biosuture.....	121
Figure 5.6: XRD spectra of the pristine biopolymers; top to bottom: alginate, pectin and gelatin.	122
Figure 5.7: XRD spectra of the uncoated (top) and coated (bottom) biosutures, showing additional sharp peaks in the coated biosuture spectrum that are indicative of dexamethasone.	122
Figure 5.8: A) TGA and B) DTG curves of pristine sodium alginate.....	123
Figure 5.9: A) DSC curve of the pristine polymers and the uncoated and coated biosuture. B) Enlarged DSC curve of pectin, showing its glass transition (T _g) temperature.....	124
Figure 5.10: A) TGA and B) DTG curves of pristine pectin.	125
Figure 5.11: A) TGA and B) DTG curves of pristine gelatin	126
Figure 5.12: A) TGA and B) DTG curves of the uncoated biosuture and C) TGA and D) DTG curves of the coated biosuture.	128
Figure 5.13: Macroscopic appearance of the biosuture at different temperature points (x3 magnification).....	129
Figure 5.14: SEM images of the uncoated biosuture (A) and coated biosuture (B). Image (C) provides an enlarged (1.05K magnification) image of the coated biosuture without damage by the electron beam. Image (D) and (E) show in lens SEM images of the biosuture in the straight and knotted configuration, respectively. Light microscope images (F) and (G) show the	

morphology of tightened knots made with biosutures and (H) the diameter (103.02 μm) of a coated biosuture.	131
Figure 5.15: Stress – strain curves of the uncoated and coated biosutures in the (A) straight configuration and (B) knotted configuration.	133
Figure 5.16: Cumulative drug release from coated biosutures expressed as (A) amount ($\mu\text{g}/\text{cm}$) and B) percentage (%) of drug released over a period of 12 days.	134
Figure 5.17: Swelling ratio (A) and degradation expressed as percentage weight loss (B) of the uncoated (black) and coated (blue) biosutures as a function of time immersed in phosphate buffered saline (pH = 7.4) at 37°C. C) SEM images of biosuture samples after 7 (i), 14 (ii) and 28 (iii) days of degradation.	135
Figure 6.1: Percentage cell viability of HEK 293 cells after A) 24 hours and B) 48 hours, with $p < 0.05$ indicated as (*) and $p < 0.01$ as (**).	142
Figure 6.2: Percentage cell viability of NIH-3T3 cells after A) 24 hours and B) 48 hours, with $p < 0.05$ indicated as (*) and $p < 0.01$ as (**).	143
Figure 6.3: Light microscope images (60x magnification) of the biosutures, showing cell attachment after i) 1 hour, ii) 24 hours and iii) 48 hours of incubation; iv) synthetic polypropylene suture (Prolene®) after incubation with cells for 48 hours.	145
Figure 6.4: A) Percentage haemolysis of sheep blood and images indicating the respective supernatants of the erythrocyte suspensions after centrifugation, as treated with B) the positive and negative control, C) the uncoated biosuture (indirect and direct method) and D) the coated biosuture (indirect and direct method).	147
Figure 6.5: A) Percentage haemolysis of human blood and images indicating the respective supernatants of the erythrocyte suspensions after centrifugation, as treated with B) the positive and negative control, C) the uncoated biosuture (indirect and direct method) and D) the coated biosuture (indirect and direct method).	148
Figure 6.6: Platelet morphology according to increasing degrees of activation, (R) round, (D) dendritic, (SD) spread dendritic, (S) spread and (FS) fully spread.	149
Figure 6.7: Sheep platelet morphology after incubation with A) the positive control, B) the negative control, C) uncoated biosutures (indirect method), D) uncoated biosutures (direct method), E) coated biosutures (indirect method) and F) coated biosutures (direct method).	150
Figure 6.8: Human platelet morphology after incubation with A) the positive control, B) the negative control, C) uncoated biosutures (indirect method), D) uncoated biosutures (direct method), E) coated biosutures (indirect method) and F) coated biosutures (direct method).	151
Figure 6.9: Adhesion of human platelets to the biosuture surface.	152

LIST OF EQUATIONS

Equation 3. 1.....	50
Equation 3. 2.....	50
Equation 3. 3.....	50
Equation 4. 1.....	94
Equation 4. 2.....	94
Equation 4. 3.....	95
Equation 4. 4.....	95
Equation 5. 1.....	114
Equation 5. 2.....	114
Equation 6. 1.....	140
Equation 6. 2.....	141

CHAPTER 1: INTRODUCTION AND OVERVIEW OF THE STUDY

1.1 Introduction

Sutures are one of the most widely used, yet ill performing medical devices on the market (Ajmeri & Ajmeri, 2006; Byrne & Aly, 2019). The number of available surgical sutures is approaching 300 different types, which signifies, on the one hand, the extensive need for an assortment of suture materials, but on the other hand, signifies the dissatisfaction with the quality of available sutures (Baybekov *et al.*, 2018). There are over 10 well-known suture related complications, ranging from wound dehiscence and infection to osteolysis and severe granulomatous reactions, that occur at alarming rates and carry devastating consequences for patients worldwide (Abhari *et al.*, 2017; Devick, 2021). These complications can largely be ascribed to the poor performance and inappropriate characteristics of suture materials, which continue to flame the search for more advanced surgical sutures. The ideal suture must meet several criteria, foremost of which are adequate tensile strength, good handling properties and excellent knot security (Karaman *et al.*, 2017). Other important characteristics include low tissue reactivity, minimal tissue trauma, no capillary action, sterility, cost efficiency and a reliable, timely degradation profile, without the release of damaging degradation products (Açan & Hapa, 2018). All encompassing, a suture material should create an environment that supports, and even encourages, wound healing by delicately approximating the wound edges without contributing to the damage and inflammatory activity of the wound (Burkhardt & Lang, in press). Regrettably, none of the sutures that are currently on the market, comply with all these requirements and the need for a new suture material with improved safety and efficacy is pertinent (Domnick, 2014).

Sutures are classified based on structure (monofilament or multifilament), lifespan (permanent or absorbable) and origin (natural or synthetic) (Chu, 2018). Monofilament sutures are generally preferred due to the high friction coefficient of braided/multifilament sutures, which causes unnecessary trauma as the suture saws through the tissue. Additionally, multifilament sutures increase the risk of infection by providing multiple niduses for bacteria to adhere and accumulate (Domnick, 2014). Yet, several common suture materials, including silk and polyglactin 910 (Vicryl®), must be braided in order to achieve satisfactory mechanical strength and handling abilities, which necessitates a compromise between preferred characteristics and renders these sutures less than optimal (Bloom & Goldberg, 2007).

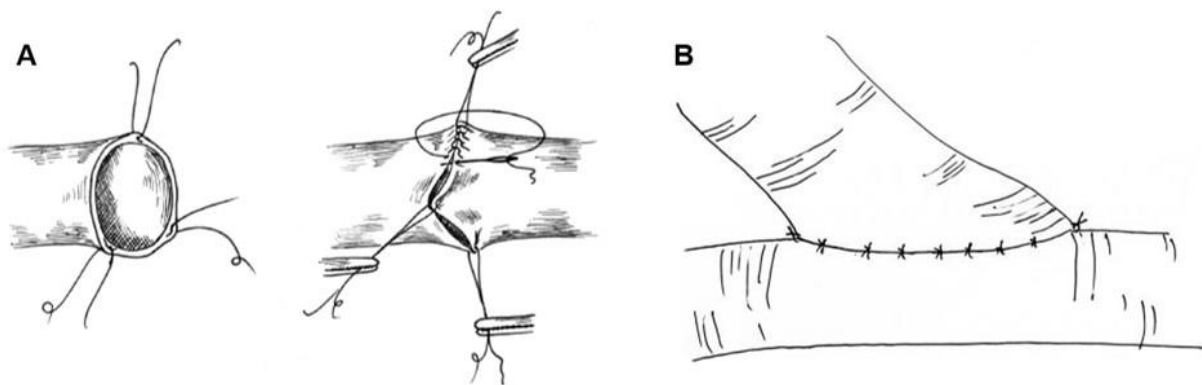
In terms of lifespan, absorbable sutures are the preferred option, in most surgical procedures, as it eliminates the need for a second removal procedure, which not only saves time but also decreases patient anxiety and pain (Greenberg & Clark, 2009). Additionally, non-absorbable

1 or permanent suture, such as polyester (Fibrewire[®] and Ethibond[®]), are known for their rigidity
2 and tendency to cut into tissues, a complication referred to as 'cheese wiring' (Akgun *et al.*,
3 2018). The ideal absorbable suture should only remain in the body until the wound has
4 regained sufficient strength to support itself and the edges no longer require artificial
5 approximation (Gazivoda *et al.*, 2015). If the suture remains in the body longer than necessary,
6 its continued presence can result in persisting cellular reactions and chronic inflammatory
7 responses that has been shown to interfere with the normal wound healing process
8 (Greenberg & Clark, 2009). Yet, the absorbable sutures that are currently available, e.g.,
9 polyglycolic acid (Daxon[®]) and polyglyconate (Maxon[®]), have unnecessarily long absorption
10 times of between 60 and 150 days, which is far longer than is required by most surgical
11 procedures (Bloom & Goldberg, 2007).

12 The origin of a suture material, is also of critical importance as the degree of tissue reaction
13 largely depends on the chemical properties of the starting materials (Salthouse, 1980). Natural
14 sutures, i.e., silk and catgut, are notorious for inciting severe inflammatory responses *in vivo*,
15 as a result of their proteolytic degradation products (Rose, 2019). Synthetic polymer sutures,
16 degrade by means of hydrolysis which releases less immunogenic degradation products and
17 makes synthetic sutures the option of choice for most surgeons (Barrows, 2017). Yet, synthetic
18 sutures remain inherently foreign to the body and still incite notable inflammatory responses
19 that have been reported to cause extreme granulomatous reactions, interfere with the
20 proliferative phase of wound healing and result in necrotic exudative wound tissue (Conn *et al.*,
21 1974; Greenberg & Clark, 2009; Ollivere *et al.*, 2014). In light of the great advances in
22 natural polymer material sciences and the pronounced biocompatibility and biodegradability
23 of natural polymers, it is shocking that silk and catgut – two of the oldest suture materials
24 known to man – remain the only natural polymer sutures on the market (Ajmeri & Ajmeri,
25 2006). There is a clear void in terms of natural polymer-based suture material development
26 that can be ascribed to the limited tensile strength of natural polymers, and the lack of effective
27 and well-defined suture fabrication methods that employ natural polymers (de la Harpe *et al.*,
28 2021).

29 The need for more advanced and better performing suture materials is more pressing than
30 what is generally assumed. It is estimated that globally over 3 million individual sutures are
31 implanted every single day (Gazivoda *et al.*, 2015). This gives sutures unprecedented power
32 to influence the health of unnumerable patients worldwide, but also places a heavy
33 responsibility on these materials to perform optimally and not deter the success of the
34 procedures they are used in (Kukreja *et al.*, 2018). Microvascular surgery (MVS), is one of the
35 many procedures that are directly reliant on the performance of suture materials for a
36 successful outcome (Rickard & Hudson, 2014). Despite the development of new anastomotic

1 devices, interrupted or continuous sutures (Figure 1.1), remain the gold standard and preferred
2 method for achieving microvascular anastomosis (Wain *et al.*, 2016). Hence, if the suture
3 material does not perform optimally, but for example breaks unexpectedly or significantly
4 damages the vessel wall, as was described by Polykandriotis *et al.*, surgical failure will ensue
5 with detrimental consequences for the patient (Polykandriotis *et al.*, 2019). However, MVS is
6 also complicated by other factors such as thrombosis, stenosis, ischemic reperfusion injury
7 (IRI) and the dreaded no-reflow phenomenon. These events further threaten the success of
8 MVS and require additional measures, over and above the improvement of the suture material
9 used, to ensure complete patency in every case of microvascular anastomosis (Carroll &
10 Esclamado, 2000).



11
12 **Figure 1.1:** A) End-to-end anastomosis using the popular triangulation technique and B) end-
13 to-side anastomosis using interrupted sutures. Adapted with permission from A) (Wain, R.A.J.,
14 Hammond, D., McPhillips, M., Whitty, J.P.M. and Ahmed, 2016) and B) (MacDonald, 2005).

15 Suture materials, if developed correctly, can open up an interesting avenue for addressing
16 unavoidable surgical complications, such as IRI and no-reflow in MVS (Dennis *et al.*, 2016).
17 Drug-eluting sutures have received significant attention in recent years due to their ability to
18 deliver a drug directly to the site of injury in a slow, controlled manner (Arora *et al.*, 2019).
19 Sutures, as drug delivery devices, pose several alluring benefits, that include localized drug
20 delivery which avoids the risk of systemic side effects, lowers the amount of drug needed, and
21 decreases the overall cost of treatment (Tummalapalli *et al.*, 2016a). Additionally, since
22 sutures are already used in most medical procedures, there is no need to introduce a second
23 foreign object to the surgical field, thereby lowering the chances of infection, while saving the
24 surgeon valuable time (Deng *et al.*, 2021). Moreover, continued hospitalization is not
25 necessary to achieve sustained drug administration and if the suture material is absorbable,
26 a second procedure to remove the drug delivery device is not necessary, which again saves
27 time and money, but also spares the patient unnecessary pain and discomfort (Dennis *et al.*,
28 2016; Leaper *et al.*, 2017; Weldon *et al.*, 2012).

1 In the present project, we set out to address the need for a superior suture material by
2 developing and advanced 3D monofilament biosuture that consists of natural polymers and is
3 capable of localized, sustained drug delivery. Only natural polymers, with established
4 biocompatibility and biodegradability, was considered for inclusion in the biosuture
5 formulation, to ensure optimal safety and *in vivo* degradation. A new method of suture material
6 fabrication, that is appropriate for natural polymer-based formulations and does not rely on
7 harsh organic chemicals, was developed. Different methods of drug loading were explored in
8 order to find a method that did not interfere with the mechanical performance of the biosuture
9 material and provided a desirable drug release profile. Through the development of this novel
10 biosuture material we aimed to provide a device that can improve the patency rates of MVS
11 procedures and pave the way for future natural polymer-based suture materials.

12 **1.2 Rational and motivation**

13 Biosutures, here defined as any suture materials that consist of natural biopolymers (i.e.,
14 polymers derived from plant or animal materials that are abundantly found in nature), have the
15 potential to transform the surgical field as we know it (Hassan *et al.*, 2019). Natural polymers
16 have a unique trump card over synthetic polymers in the form of their biological properties and
17 close similarity to the native extracellular matrix (ECM) (Nam & Park, 2018). The ECM, which
18 primarily consists of proteins and carbohydrates, plays a critical role in tissue regeneration by
19 providing structural support to cells, maintaining homeostasis, and facilitating key cellular
20 functions such as adhesion, signalling, differentiation, and proliferation (Altomare *et al.*, 2018).
21 There is an interesting correlation between the basic functions of the ECM, and that of a suture
22 material, which include providing mechanical support, achieving haemostasis, and facilitating
23 effective wound healing (Tan *et al.*, 2003). Yet, synthetic polymer sutures do not actively
24 contribute to the wound healing process as they lack the necessary bioactive moieties that
25 would allow for cellular interactions (Chandra *et al.*, 2020). Natural protein polymers such as
26 gelatin, on the other hand, contain the same RDG (arginine-glycine-aspartic) amino acid
27 sequence found in the native ECM, which allows them to facilitate and encourage cellular
28 adhesion, proliferation, differentiation and ultimately, tissue regeneration (Koshy *et al.*, 2016).
29 Hence, by developing novel biosutures with bioactive moieties, that are inherently part of their
30 structure, the therapeutic value of suture materials can instantly be elevated to a new level
31 where they actively support and facilitate the wound healing process (Joseph *et al.*, 2017).

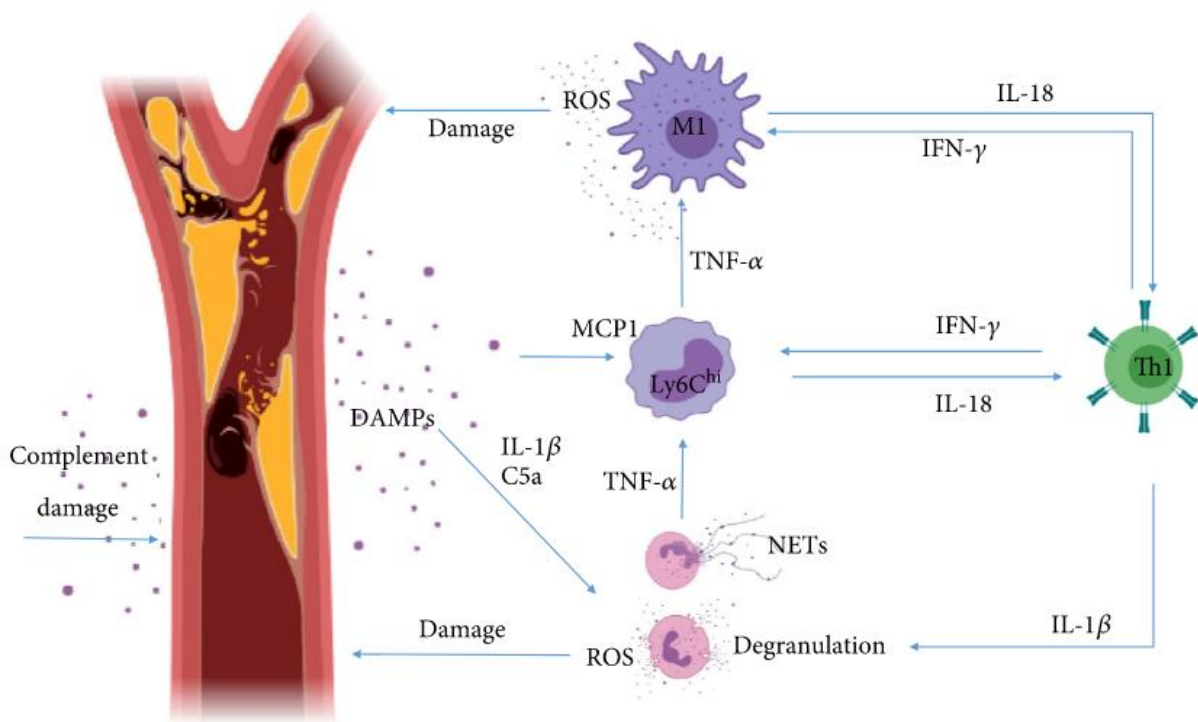
32 In addition to improving the therapeutic efficacy of suture materials, natural polymers possess
33 several other benefits that also advocate for their use in suture material development. These
34 include their sustainable and environmentally friendly nature, low cost, and wide availability
35 (Kurakula *et al.*, 2020). Natural polymers are also highly adaptable and can easily be
36 manipulated to obtain specific properties, such as more rapid degradation or greater tensile

1 strength, to meet the specific requirements of the biomaterial that is being developed
2 (Doppalapudi *et al.*, 2015). Moreover, there are several promising natural polymers available
3 that undergo hydrolytic degradation *in vivo* to release safe, nonimmunogenic and nonantigenic
4 degradation products that are easily metabolised and excreted from the body (Rajeswari,
5 2017). In fact, all the natural polymers employed in this study, are approved by the FDA as
6 'generally regarded as safe' (GRAS), meaning they have been bestowed the highest level of
7 safety and can freely be included in the human diet (Qin *et al.*, 2018).

8 Undoubtedly, natural polymers have improved the outcome of various medical procedures
9 through the development of more advanced medical devices such as absorbable stents, novel
10 wound dressings and several tubular prosthesis (Petersen & Gatenholm, 2011). Microvascular
11 surgery, which has greatly expanded in recent years to include plastic and reconstructive
12 surgery, free tissue transfers and organ transplants, is one of the fields that have yet to benefit
13 from a natural polymer counterpart, to the extensively used synthetic suture (Brown *et al.*,
14 2020). The urgent need for a more effective biosuture counterpart is highlighted by the various
15 complications (e.g., hyperproliferation and stenosis, thrombosis, necrosis, and chronic
16 inflammation) that find their origin in the synthetic nature of currently employed suture
17 materials (de la Harpe *et al.*, 2021). These synthetic sutures have been shown to place
18 unnecessary strain on the vessel wall, cause significant endothelial damage and release
19 harmful degradation products that cause local pH-shifts and are onerous to remove from the
20 body (Benlier *et al.*, 2007; Hadlock & Varvares, 2002; Metz *et al.*, 1989; Seitz *et al.*, 2015; Wu
21 *et al.*, 2021). Hence, MVS can clearly benefit from the development of a novel biosuture with
22 appropriate tensile strength, excellent biocompatibility, a timely degradation profile and safe
23 degradation products, as we will endeavour to achieve in this project.

24 Ischemic reperfusion injury (IRI) and the widely encountered no-reflow phenomenon, is
25 currently one of the greatest threats to the success of microvascular and vascular procedures
26 (Seyid *et al.*, 2021). Reperfusion injury has been described to hold several significant
27 consequences, including vast oedema and stenosis, but the most common is indisputably the
28 no-reflow phenomenon, which has been recorded to occur in 60% of percutaneous coronary
29 interventions, 58% of failed digital replantation surgeries and a staggering 82% of free flap
30 transfers (Bouleti *et al.*, 2015; Wang, 2009; Wang *et al.*, 2011). IRI and the no-reflow
31 phenomenon are complicated events, and the reader is referred to an in-dept review published
32 by Carroll *et al.*, on IRI within the framework of MVS (Carroll & Esclamado, 2000). Briefly, MVS
33 necessitates a transient period of ischemia during which toxic metabolites and pro-
34 inflammatory mediators accumulate. Once the vessel clamps are removed and blood flow is
35 restored, an influx of activated neutrophils, oxygen free radicals and proteolytic enzymes
36 causes irreversible damage to the vessel wall (Figure 1.2) (Sánchez-Hernández *et al.*, 2020).

1 No-reflow, in turn, is a continuous event that worsens over time and is thought to be the result
 2 of interstitial oedema and endothelial swelling, loss of adrenergic control of vascular tone and
 3 plugging of the vessel lumen with leucocytes (Rezkalla, 2002a). No-reflow is a dangerous and
 4 lethal process as it cuts off all nutrients to distal tissues, at which point it is extremely difficult
 5 to stop or reverse (Carroll & Esclamado, 2000). Additionally, the risk of fatal secondary events,
 6 such as ischemic stroke, myocardial infarctions and organ failure, increases exponentially.
 7 Prevention of IRI and no-reflow is therefore of utmost importance during MVS, yet an effective
 8 protocol to achieve such prevention does not exist (Niccoli *et al.*, 2010).



9
 10 **Figure 1.2:** Schematic representation of the tissue damaging inflammatory response of
 11 ischemic reperfusion injury. Reused with permission from (Sánchez-Hernández *et al.*, 2020).

12 Dexamethasone (DEX) has been shown to be beneficial in the prevention of IRI during MVS,
 13 most likely due to its anti-inflammatory activity, even though several authors maintain that the
 14 exact mechanism is not known (Lu & Chiang, 2008; Sánchez-Hernández *et al.*, 2020; Tu *et*
 15 *al.*, 2020). Dolan *et al.*, showed that DEX significantly improves ischemic flap survival using a
 16 rat model, while other authors have reported reduced macromolecular clearance during
 17 reperfusion, improved reflow and greater flap viability with the use of DEX during MVS
 18 (Breitbart *et al.*, 1989; Chen *et al.*, 1996; Dolan *et al.*, 1995a). Yet, there are several challenges
 19 with the use of DEX for the prevention of IRI and no-reflow, which has hindered its routine use
 20 in MVS (Askar & Bozkurt, 2002). One of the biggest challenges is the high risk of detrimental
 21 systemic side effects, such as suppressed immunity, at the high doses of DEX that are
 22 necessary to achieve successful prevention of reperfusion injury (Tritto *et al.*, 2013).

1 Additionally, no-reflow has been found to occur up to seven days after reperfusion and thus
2 requires continued DEX administration to be circumvented, which is impractical and costly in
3 the surgical and hospital setting (Giammalva *et al.*, 2017). There is clearly a dire need for a
4 new drug delivery device, such as the drug-eluting biosuture proposed by this study, that can
5 provide local, sustained release of DEX, without the risk of systemic side effects or
6 unnecessary high cost and time expenditures, to help prevent IRI and the no-reflow
7 phenomenon in MVS.

8 **1.3 Novelty of the study**

9 It is of critical importance that the therapeutical efficacy of suture materials be improved. Even
10 though an impressive number of sutures have been developed, the current study is novel in
11 the fact that:

- 12 • The new biosuture material was developed from natural biopolymers that have not
13 previously been used as raw materials for suture fabrication.
- 14 • An innovative method of biosuture fabrication, that does not involve the use of harsh
15 organic solvents like most suture production methods, was employed.
- 16 • The biosuture had an additional feature, i.e., localized drug delivery and could provide
17 sustained release of dexamethasone to help prevent ischemic reperfusion injury and no-
18 reflow during microvascular surgery.

19 **1.4 Aims and objectives**

20 The aim of this study was to design, formulate and evaluate a novel 3D monofilament
21 biosuture that can provide sustained, localized drug release for microvascular surgery (MVS)
22 applications. We proposed to use natural biopolymers with established biocompatibility and
23 similarity to the native ECM components, to ensure that the biosuture has optimal
24 biocompatibility and provides an environment supportive of wound healing. To achieve this
25 aim, the following objectives were set:

- 26 1. To develop a biosuture formulation that consist of natural biopolymers, in the correct
27 concentrations and molar ratios, to yield a material that has satisfactory mechanical
28 performance and handling properties.
- 29 2. To develop a reliable, environmentally friendly method of biosuture fabrication that can
30 produce biosutures with consistent diameter, morphology, and strength.
- 31 3. To transform the newly created biosuture material into a drug delivery device with an
32 acceptable sustained drug release profile.
- 33 4. To evaluate the physiochemical, mechanical, thermal, and morphological properties of the
34 optimized biosuture material by studying the infrared spectrum, x-ray diffraction spectrum,
35 thermograms, tensile strength and surface properties of the biosuture.

- 1 5. To evaluate the *in vitro* swelling, degradation, and drug release behaviour of the optimized
2 biosuture material for the development of the drug delivery device.
- 3 6. To evaluate the *in vitro* biocompatibility of the optimized biosuture material by means of a
4 cytotoxicity assay and cellular attachment study, according to ISO 10993-5 standards.
- 5 7. To evaluate the *in vitro* hemocompatibility of the optimized biosuture material according to
6 ISO 10993-4 and ASTM F756 guidelines to account for blood-biosuture interactions.

7 **1.5 Overview of the dissertation**

8 The content of each chapter in this dissertation is based on the aforementioned aim and the
9 outlined objectives. Figure 1.3 provides a schematic representation of the overview of the
10 dissertation.

11 **Chapter 1** introduces the subject at hand and specifies the rationale and motivation behind the
12 study. The novelty of the study is also highlighted while the specific aim and objectives that
13 were undertaken are described.

14 **Chapter 2** is a literature review that exposes the latest and most important advancements in
15 suture material development while digging deep into how natural, carbohydrate polymers can
16 serve to advance this field.

17 **Chapter 3** is focussed on the development of the novel biosuture formulation and investigates
18 the effect of different formulation components, such as biopolymers, plasticizers and
19 crosslinkers, on the mechanical properties of the biosuture material. The ideal biosuture
20 fabrication method was identified in this chapter and the influence of different fabrication
21 factors, such as crosslinking time and drying method, on the mechanical properties of the
22 biosuture, investigated. Finally, an optimized biosuture formulation, that yields a biosuture with
23 satisfactory mechanical properties, was identified.

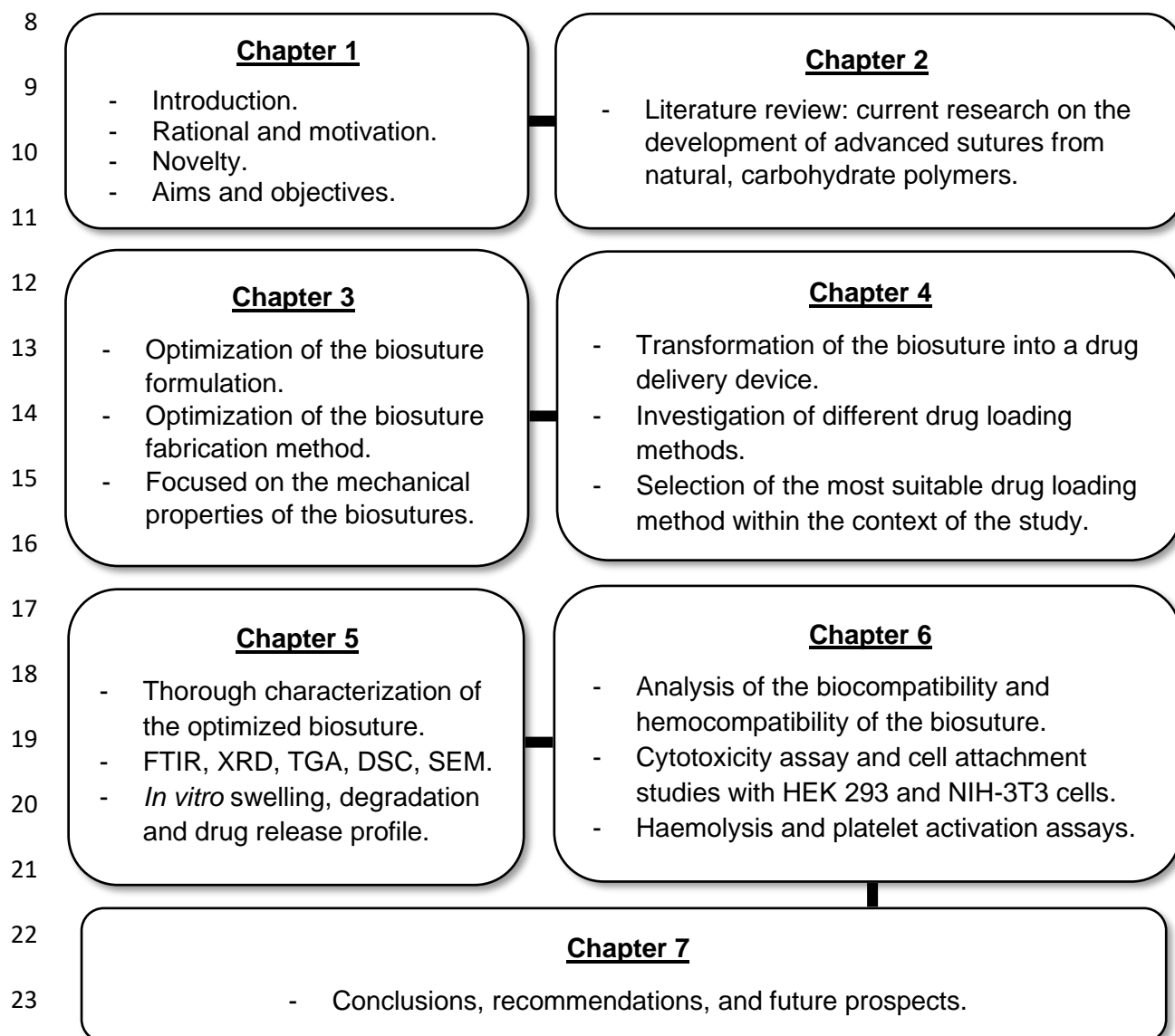
24 **Chapter 4** is concerned with the transformation of the newly developed biosuture material into
25 a drug delivery device. Different methods of drug loading, that include immersion, drop coating
26 and direct incorporation into the polymer matrix, were explored in order to find a method that
27 did not compromise the mechanical properties of the biosuture and provided the desired drug
28 release profile.

29 **Chapter 5** finds its focal point in the characterization of the optimized biosuture material,
30 before and after drug loading. The infrared and powder x-ray diffraction spectra of the
31 biosutures were contrasted with that of the pristine polymers to expose any chemical
32 transitions and changes in crystallinity. The thermal properties of the biosutures were also
33 investigated by means of thermogravimetric analysis and differential scanning calorimetry,
34 while the surface morphology of the biosutures is discussed based on scanning electron

1 images. The *in vitro* swelling, degradation, and drug release behaviour of the optimized
2 biosutures are also analysed and elaborated on in this chapter.

3 **Chapter 6** is an in-depth report of the biocompatibility and hemocompatibility of the biosutures
4 and describes the results of a cytotoxicity assay and cell attachment study that was performed
5 on HEK 293 and NIH-3T3 cells, in addition to a haemolysis and platelet activation assay.

6 **Chapter 7** is the closing chapter and provides a conclusion to and summary of the work that
7 was done, as well as future recommendations for how this study can be further enhanced.



24 **Figure 1.3:** Schematic representation of the outline of the dissertation.

CHAPTER 2: ADVANCES IN CARBOHYDRATE-BASED POLYMERS FOR THE DESIGN OF SUTURE MATERIALS – A REVIEW

2.1 Introduction

A suture is any string of material, either natural or synthetic, that is used to ligate blood vessels or approximate tissues, in order to achieve proper wound healing (Azhahia *et al.*, 2008). Sutures were first introduced by the forefathers of medicine, nearly 4000 years ago, when they used strips of linen, tendons and even horsetail hair to close common wounds (Sahoo *et al.*, 2017). Today, surgical sutures are primarily made of synthetic polymers and used to treat a more diverse scope of wounds ranging from surgical incisions and severed vessels, to any form of traumatized tissue such as tendons, nerves and muscles (Ajmeri & Ajmeri, 2006). The successful outcome of these procedures rely heavily on the behaviour of the suture material within the biological milieu, which in turn depends on the intrinsic properties of the starting material and its proper formulation into a suitable suture material (Tummalapalli *et al.*, 2016b). In light of the primary role of sutures in achieving a successful surgical outcome, one would expect these materials to have been refined and perfected over the many years that they have been in use. Yet, the ideal suture material remains a much sought-after target and future dream of scientists and surgeons alike (Rengasamy & Ghosh, 2010).

In recent years, several authors have suggested that the demands of modern surgery, drastically exceed the abilities of available synthetic polymer sutures (Pillai & Sharma, 2010; Tanasă & Zănoagă, 2011; Zhukovskii, 2008). Hence, a new trend has emerged where scientists are looking towards natural polymers, which hold several promising properties, such as supreme biocompatibility and high tensile strength with a balanced measure of elasticity, to develop novel suture materials with improved safety and efficacy (Cruz *et al.*, 2016). The potential of natural polymers to produce first-rate suture materials, was first alluded to by Zhukovskii, who stated that the only way to advance the field of surgical sutures, is to develop new strong and elastic fibres made of biocompatible, absorbable natural polymers, such as the polyoxyalkanoates, collagen, chitin and alginate (Zhukovskii, 2008). Yet, the greatest argument in favour of employing natural polymers in suture material development, can perhaps be found in a simple comparison of the advantages and disadvantages of synthetic- and natural polymer sutures, as provided in Table 2.1

1 **Table 2.1:** Advantages and disadvantages of synthetic- and natural polymer sutures.

Advantages	Disadvantages
<i>Synthetic polymer sutures</i>	
1. Good mechanical strength (Szycher, 2017)	1. Poor biocompatibility and causes severe inflammatory reactions (Yunus, <i>et al.</i> , 2019).
2. Familiar to most surgeons (Halepas <i>et al.</i> , 2020)	2. Release harmful degradation products (Islam <i>et al.</i> , 2017).
3. High reproducibility (Hosseini, <i>et al.</i> , 2020)	3. Longer recovery times (Shao <i>et al.</i> , 2016).
4. Wide variety available (Matsuzaki <i>et al.</i> , 2019)	4. Does not support cellular interactions (Cassimjee <i>et al.</i> , 2020).
5. Can be coated to improve handling properties (Byrne & Aly, 2019)	5. Low pliability and poor handling properties (Trentadue <i>et al.</i> , 2021).
6. Absorbable and non-absorbable variants (Sheik-Ali & Guets, 2018)	6. Irregular degradation and sudden loss of tensile strength (Alsarhan <i>et al.</i> , 2018).
	7. High risk of bacterial adherence and infection (Mahesh <i>et al.</i> , 2019).
<i>Natural polymer sutures</i>	
1. Excellent biocompatibility (Centeno-Cerdas <i>et al.</i> , 2018).	1. Variation depending on source of polymer (Guambo <i>et al.</i> , 2020).
2. Environmentally friendly / Green (Islam <i>et al.</i> , 2017).	2. Ethical considerations (Phelan & Council, 2019).
3. Inexpensive (Kaczmarek <i>et al.</i> , 2019).	3. Unfamiliar to surgeons (Fan <i>et al.</i> , 2020).
4. Improved wound healing (Shao <i>et al.</i> , 2016).	
5. Supports cell proliferation (Peng <i>et al.</i> , 2020).	
6. Inherent antimicrobial activity (da Silva <i>et al.</i> , 2019).	
7. Mimics the extra cellular matrix (Li <i>et al.</i> , 2017).	
8. Safe degradation products (Kim <i>et al.</i> , 2015).	
9. Sustained drug release (Padmakumar <i>et al.</i> , 2016).	

2

1 In this chapter, we review the latest advancements in the field of suture materials by taking a
2 closer look at three profound natural carbohydrate polymers, namely cellulose, chitin and
3 alginate and how they have been employed to create novel, advanced suture materials. The
4 specific properties and unique attributes of these three natural polymers, which make them
5 especially suitable for suture material applications, are discussed. Furthermore, significant
6 breakthroughs that have been made in recent years, through the use of these polymers in
7 suture development, are studied in detail. The potential impact and future prospects of these
8 developments are also highlighted. Through this review, we hope to gain new insight into the
9 potential of natural polymers as advanced suture materials and the novel, interesting methods
10 that can be employed to manufacture natural polymer-based sutures.

11 **2.2 Cellulose and its derivatives**

12 Cellulose is the most abundant polymer of natural origin and has enjoyed much attention in
13 the field of biomedical research (Mohite & Patil, 2014). As a biomaterial, cellulose offers
14 numerous advantages such as nontoxicity, high availability, renewability, low cost,
15 biodegradability and other quintessential physical and chemical properties (Liu *et al.*, 2015).
16 These properties have led to its widespread use as a biomaterial with applications such as
17 wound dressings, dialysis membranes, controlled drug delivery systems and tissue
18 engineering scaffolds (Flynn *et al.*, 2013; Hakkarainen *et al.*, 2016; Mansoor *et al.*, 2019;
19 Sindhu *et al.*, 2014; Ullah *et al.*, 2016). However, the poor solubility of cellulose in water and
20 other common solvents, has prevented its full utilization in the biomedical and related fields
21 (Petersen & Gatenholm, 2011). Hence, different derivatives of this promising natural polymer,
22 such as oxidized regenerated cellulose, hydroxyethyl cellulose and cellulose nanofibrils, have
23 been developed (Roy *et al.*, 2009). These derivatives exhibit improved solubility, as well as
24 other desirable chemical properties, including the presence of several functional groups that
25 can be readily activated (Hou *et al.*, 2009). As a result of its key structural role in plant cell
26 walls, cellulose and its derivatives also demonstrate notable mechanical strength, making
27 them ideal candidates for new, innovative suture materials (Halib *et al.*, 2017).

28 **2.2.1 The use of oxidized cellulose in the development of novel suture materials**

29 Traditionally, cellulose cannot be degraded in the human body due to the absence of cellulase,
30 the enzyme responsible for cellulose degradation (Cassimjee *et al.*, 2020; Yadav *et al.*, 2019).
31 In this regard, oxidized cellulose, which is both biocompatible and biodegradable, is a valuable
32 option for the fabrication of highly sought after, absorbable suture materials (Harris *et al.*,
33 2010). Additionally, oxidized cellulose has bactericidal properties, against some of the most
34 prominent infectious organisms, and has been found to facilitate wound healing through the
35 suppression of matrix metalloproteinases (MMP) activity, which results in reduced
36 inflammatory responses (Alfieri *et al.*, 2011; Liu *et al.*, 2012). Despite these advantageous

1 properties and the demonstrated benefit of using oxidized cellulose in wound healing, there is
2 currently no oxidized cellulose suture product on the market (Zhang *et al.*, 2020).

3 A study done by Li *et al.*, in 2019, however, suggests that this could change in the near future.
4 The authors managed to successfully produce absorbable surgical sutures from oxidized
5 regenerated cellulose (ORC), with favourable biodegradability and ideal mechanical
6 properties. Their work signified a breakthrough in both the field of suture manufacturing and
7 that of cellulose processing (Li *et al.*, 2019). In contrast to previously employed non-selective
8 oxidation methods, that were difficult to execute and required both high temperature (343 K)
9 and high pressure (70 atm), the authors employed a selective 2,2,6,6 – tetramethylpiperidine-
10 1-oxyl (TEMPO)-mediated oxidation method (Coseri *et al.*, 2013). This method allows for
11 expert control over the extend of oxidation and enabled the authors to obtain the ideal carboxyl
12 content, that ensured both biodegradability and sufficient mechanical strength in the novel
13 suture formulation (Li *et al.*, 2019). In fact, the knot-pull tensile strength of the ORC sutures,
14 demonstrated values exceeding 10.0 N, which is more that the required strength specified by
15 the United States Pharmacopeia (USP) (Rockville (MD): United States Pharmacopeial
16 Convention, 1976). These values are especially significant, as knot-pull tensile strength is the
17 main determining factor of the success and applicability of suture materials (Kim *et al.*, 2007).
18 The fabricated ORC sutures also demonstrated good knot security and satisfactory handling
19 properties, pointing to the feasibility of using cellulose based sutures in the clinical setting (Li
20 *et al.*, 2019).

21 Additionally, the ORC sutures displayed a model degradation profile that could easily be
22 adapted (illustrated in Figure 2.1 A). As can be seen in Figure 2.1 B, TEMPO-mediated
23 oxidation significantly increased the carboxyl content of the material which also increased the
24 spacing between the molecular chains and subsequently decreased the inter anatomic forces
25 between the cellulose molecules. Water could, therefore, easily penetrate the suture fibre,
26 allowing it to slightly swell and eventually degrade. This method of suture fabrication provides
27 an added benefit of controlled degradation that can easily be adapted by varying the extend
28 of oxidation. Alternatively, it provides a valuable opportunity for controlled, localized drug
29 delivery through the functionalization of active pharmaceutical ingredients onto the suture
30 surface, that can ultimately expand the versatility of novel cellulose-based suture materials
31 (Dennis *et al.*, 2016).

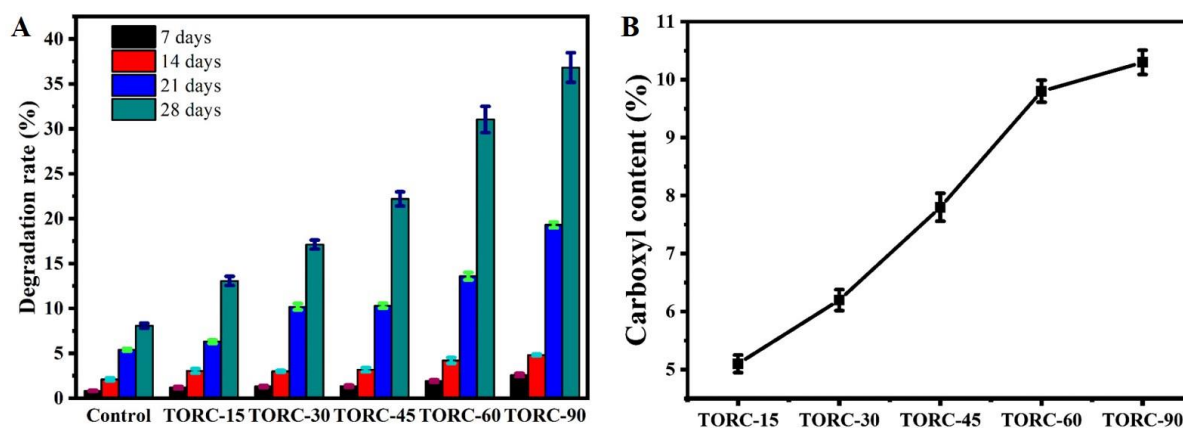


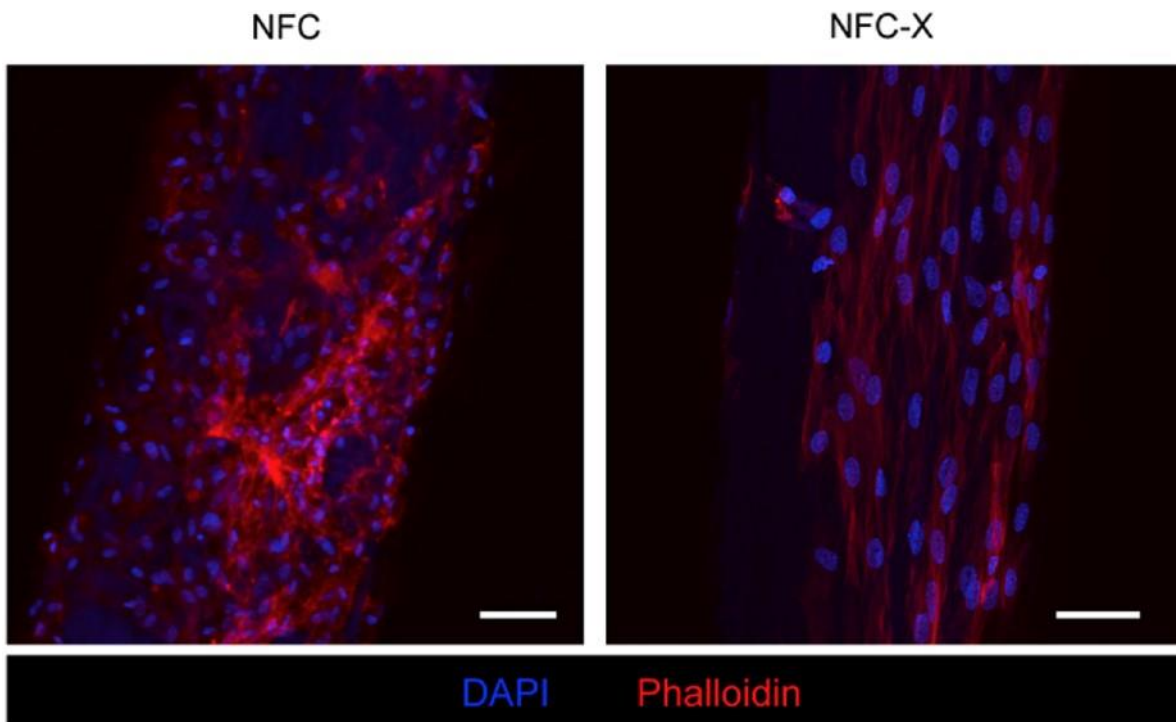
Figure 2.1: A) The in vitro degradation of tempo-mediated oxidized regenerated cellulose (TORC) sutures at different oxidation times (15, 30, 45, 60, and 90 minutes after PBS impregnation) mean \pm S.D., n = 10. B) Carboxyl content of ORC sutures at the same different oxidation times. Adapted with permission from (Li *et al.*, 2019).

2.2.2 The use of plant derived nanocellulose in the development of suture materials.

Nanocellulose (NC) is another form of cellulose that provides an exciting combination of the structural elements of pristine cellulose, with the unique features of nanoscale materials (Gatenholm & Klemm, 2010). NC can be derived from either plant materials, that undergo extensive chemical and mechanical treatment, or from bacteria (e.g. *Gluconacetobacter xylinus*) that produce NC as an exopolysaccharide (Klemm *et al.*, 2006). The unique scale and structure of NC gives it certain desirable qualities, such as a large specific surface area, tailorable morphology and stability over a wide range of temperatures and pH levels, amongst others (Bacakova *et al.*, 2019). However, it is the characteristically high Young's modulus, which is in the range of 100 – 200 GPa and comparable to the strength of steel, that makes NC a useful polymer in terms of suture fabrication (Yadav *et al.*, 2019).

In a promising study, Mertaniemi *et al.*, produced NC sutures capable of harbouring and delivering stem cells directly to an injured area (Mertaniemi *et al.*, 2016). They demonstrated that native cellulose nanofibers could be prepared into cross-linked suture threads with high mechanical strength, even under wet cell culture or surgery conditions, which has been a challenge with other cellulosic materials (Yadav *et al.*, 2019). Even after being soaked in water for one week, the cross-linked NC sutures maintained 40% of their dry tensile strength, resulting in a wet tensile strength within the range of the strongest tendons in the human body (Mathew *et al.*, 2012, 2013). Additionally, these suture fibres created an optimal environment for human adipose mesenchymal stem cells (hASC) to adhere, migrate and proliferate, even without added surface modifiers (Figure 2.2). An *ex vivo* experiment on pig skin revealed that the cells remain on the suture material after intradermal suturing, without displaying any

1 morphological changes or reduction in metabolic activity (Mertaniemi *et al.*, 2016). This state-
2 of-the-art research opened up a new avenue for stem cell therapy, where surgical sutures can
3 be used to directly deliver and retain cells at the target site, thereby improving the efficacy of
4 the treatment and preventing unnecessary spread and deposition of cells in other organs
5 (Dennis *et al.*, 2016). Moreover, these innovative NC sutures, can allow for facile surface
6 modification to allow for the addition of different molecules or adhesion of various cell types,
7 thereby creating a generic platform for surgical cell delivery via sutures, that can help fight
8 post-operative inflammation, chronic stubborn wounds and several other difficult to treat
9 conditions (Mertaniemi *et al.*, 2016).



10
11 **Figure 2.2:** Immunocytochemistry shows the attachment of the cells of the suture surface.
12 The human adipose mesenchymal stem cells (hASC) exhibited elongated cytoplasmic
13 intermediate filaments (stained red with phalloidin), especially on the crosslinked suture fibres.
14 Nuclei were counterstained in blue with DAPI. Scale bars 50 μ m. Used with permission from
15 (Mertaniemi *et al.*, 2016).

16 Another study on NC based sutures was completed in 2019 by Yunus *et al.*, who evaluated
17 the utilization of NC from oil palm empty-fruit-bunches for the manufacturing of surgical
18 sutures. During an *in vivo* trial using male Wistar rats, they found that the NC surgical threads
19 caused less inflammation than the control groups (silk and polyvinyl alcohol sutures) and had
20 a favourable influence on the wound healing process (Yunus *et al.*, 2019). This is in line with
21 other studies done on NC wound dressings that have been found to promote healing and
22 reduce pain (Czaja *et al.*, 2006). A major benefit noted in this study, and other investigations

1 of NC fabrication from oil palm empty-fruit-bunches, is that the transformation of this abundant
2 biomaterial into NC, could help address the large amount of unutilized biomaterial waste (\pm
3 17.37 million tons per year) by creating value added products that can help ease the growing
4 burden on the environment (Dungani *et al.*, 2018; Fahma *et al.*, 2010; Hastuti *et al.*, 2018).

5 **2.2.3 The use of bacterial derived nanocellulose for novel suture material development**

6 Bacterial nanocellulose (BC), which is produced by several strains of bacteria, is an especially
7 distinguished polymer that has certain advantages above plant-based NC that can lead to its
8 inclusion in suture materials (Shah *et al.*, 2013). When NC is removed from plants, the raw
9 material usually contains several impurities in the form of ash or hemicellulose that must be
10 removed before use. Bacterial cellulose (BC) on the other hand is a very pure material that
11 can be used without further processing (Iguchi; *et al.*, 2000). Another limiting factor of plant-
12 based NC is the inability to change the size and shape of the nanofibers, while BC
13 demonstrates great moldability during cultivation, allowing for the desired size and shape to
14 be obtained (Shoseyov *et al.*, 2019). Another interesting property of BC, is its striking similarity
15 to collagen, a protein found in the native extracellular matrix (ECM), which could explain the
16 impressive biocompatibility and lack of inflammation witnessed with implanted BC (He *et al.*,
17 2005; Li *et al.*, 2017). However, some of the noble properties of BC, such as a high degree of
18 polymerization and crystallinity, can cause suture materials to lose their elasticity and become
19 brittle, if this distinguished polymer is not employed correctly (Klemm *et al.*, 2006).

20 Yet, in 2018, Wu *et al.*, managed to develop regenerated chitin fibres that could meet the
21 requirements of surgical sutures, precisely through the incorporation of BC into the formulation
22 (Wu *et al.*, 2018a). They used BC to improve the mechanical strength of chitin fibres, which
23 were previously too weak to be used as functional suture materials (Maslova *et al.*, 2016; Viju
24 & Thilagavathi, 2013). As the amount of BC was increased in the formulation, the ultimate
25 stress increased while the strain slightly decreased, the effect of which can be seen in Table
26 1 (Wu *et al.*, 2018a). This is in line with other studies which found that the addition of BC can
27 increase the strength of a matrix but will simultaneously decrease the extensibility (Lee *et al.*,
28 2016; Saralegi *et al.*, 2013; Wang *et al.*, 2015). The authors, however, managed to find a
29 sweet spot at 10 mL of 5% (w/v) BC, where the main aim of improved mechanical strength
30 was achieved, while maintaining sufficient extensibility for the fibres to function as surgical
31 sutures. At this concentration, the BC-loaded fibres achieved a knot-pull tensile strength of 9.8
32 ± 0.6 N, which meets the strength requirements mandated by the USP (Chen *et al.*, 2015). An
33 enzymatic degradation study revealed an added benefit of tuneable degradation that could be
34 achieved by varying the concentration of BC in the fibres. Lastly, good biocompatibility and
35 ease of use was noted during an *in vivo* animal trial and the authors concluded that the BC-

1 loaded fibres might be considered as good candidates for surgical suture applications (Wu *et*
2 *al.*, 2018a).

3 **Table 2.2:** Mechanical properties of the BC-loaded yarns indicating the ultimate stress and
4 ultimate strain of fibres with different diameters and BC concentrations (mean \pm S.D., n = 20).
5 Reused with permission from (Wu *et al.*, 2018b).

Volume of BC added (mL)	Yarn diameter (μ m)	Ultimate stress (MPa)	Ultimate strain (%)
0	20.5 \pm 1.7	126.5 \pm 11.4	9.7 \pm 1.1
5	21.2 \pm 1.5	157.6 \pm 11.8	8.8 \pm 1.0
10	22.4 \pm 1.6	186.2 \pm 12.4	8.3 \pm 0.7
15	23.5 \pm 1.8	153.3 \pm 13.5	7.8 \pm 0.7

6
7 Recently, a patent (US 2013/0309295 A1) entitled, 'Biosynthetic functional cellulose (BC)
8 fibres as surgical sutures and reinforcement of implants and growing tissue' was filed by Paul
9 Gatenholm, Riner, VA (US). The principal embodiment of this invention is strong and stiff, yet
10 flexible fibres, consisting of BC, that can be used as surgical sutures. The patent discloses a
11 novel method of growing BC inside permeable tubes, whereby a compact gel in the form of
12 cylindrical fibres can be produced and then dehydrated to obtain unique suture-like fibres.
13 According to the inventor, the surface of the fibre consists of nano-structured cellulose which
14 promotes cell migration, tissue integration and wound healing. The published patent
15 application also provides a method of loading the fibres with growth factors, drugs and other
16 antimicrobial agents that can aid the wound healing process (United States patent no.
17 13/983,709, 2013). This patent as well as the other studies discussed above, highlight the
18 fascinating and almost inexhaustible methods that can be employed to utilize cellulose, as
19 well as its significant potential as a suture biomaterial.

20 **2.3 Chitin and its derivatives**

21 Chitin is another ubiquitous and useful natural polymer, found in the exoskeleton of arthropods
22 such as crabs and shrimps, or in cell walls of fungi and yeast (Cheba, 2011). Besides
23 conceivable properties such as biocompatibility, biodegradability and non-toxicity, which
24 stems from its natural origin, chitin also holds several other useful properties (Öktem, 2003).
25 These include a basic nature, which stands in stark contrast to the acidic or neutral nature of
26 most natural polymers, as well as a high charge density with the ability to chelate metal ions,
27 high surface area, exceptional porosity and other optical structural characteristics, that has
28 ensured its use in a myriad of biomedical applications and makes it a promising futuristic
29 suture material (Badwan *et al.*, 2015; Benesch & Tengvall, 2002; Gupta & Ravi Kumar, 2000;
30 Obulapuram *et al.*, 2020; Shelma *et al.*, 2008).

1 Chitin is chiefly found in two forms namely, pristine chitin as extracted from crustacean shells,
2 and its deacetylated form, chitosan, which has an acetylation degree below 50% and higher
3 solubility than chitin (Shen *et al.*, 2015). These polymers are naturally broken down in the
4 human body by native enzymes (e.g. lysozyme) into relatively pure oligosaccharide and
5 glycosaminoglycan moieties (Niekraszewicz & Niekraszewicz, 2009). Some of these moieties,
6 such as N-acetyl glucosamine (NAGA), which is the most pertinent component of chitin, is
7 also present in essential human glycoproteins that make up connective tissues like hyaluronic
8 acid and keratin sulphate. This glucosamine is widely used in tissue engineering and wound
9 healing applications for its esteemed ability to regenerate cartilage tissue and facilitate the
10 ordered deposition of collagen (Mndlovu *et al.*, 2019a; Pillai & Sharma, 2010). Other moieties,
11 such as N-acetyl-D-glucosamine (GlcNAc), which is released upon depolymerization of
12 chitosan, can initiate fibroblast proliferation and stimulate hyaluronic acid synthesis, that will
13 ultimately lead to faster wound healing and less scar formation (Shelma *et al.*, 2008).
14 Numerous reports have indicated that both chitin and chitosan have accelerating effects on
15 wound healing, making them distinguished materials for wound dressings and suture
16 formulations (Badwan *et al.*, 2015; Brigham, 2017; Sashiwa & Aiba, 2004; Singh & Ray, 2000).

17 Accelerated wound healing is, however, only the start of the beneficial properties displayed by
18 chitin and its derivatives (Khor, 2014). These polymers exhibit a variety of biological functions
19 such as haemostatic, anti-tumour, anti-inflammatory, anti-scarring, anti-bacterial, anti-viral and
20 anti-fungal activities, that can all be used to obtain the ideal suture material (Kucharska *et al.*,
21 2019). The exact mechanism of action behind the inherent bioactivity of chitin, is not yet fully
22 understood but progress is being made at a staggering rate to better understand this
23 impressive polymer (Kong *et al.*, 2010; Riaz *et al.*, 2020). Despite our limited knowledge on
24 how this polymer functions *in vivo*, chitin has already moved to the forefront of suture material
25 development, primarily due to present research studies and development efforts focussing on
26 the development of absorbable suture materials with multiple functionalities, including the
27 antibacterial and haemostatic activities seen with chitin (Chu, 2013; Padmakumar *et al.*, 2016).
28 A wide chasm remains in terms of chitin-based fibre formulations with applicable suture
29 properties and functional methods for the production of chitin-based sutures. Yet, the immense
30 potential and importance of chitin as an absorbable suture material is evident and can be
31 witnessed in the great number of relevant research papers, recently published on the subject
32 (Singh *et al.*, 2017).

33 **2.3.1 Chitin as a potential biomaterial for surgical suture material applications**

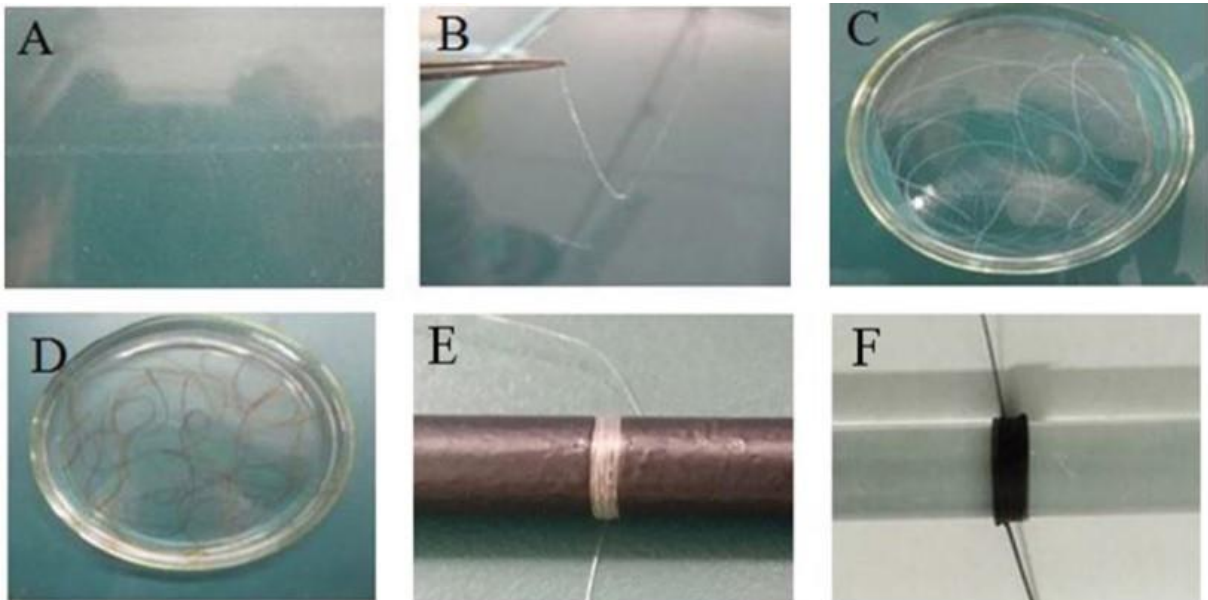
34 In mid-2019, Zhang *et al.*, published a research paper wherein they propose chitin as an ideal,
35 degradable surgical suture material (Zhang *et al.*, 2019). The authors suggest that chitin-
36 based suture materials can help overcome some of the disadvantages and limitations of

1 current synthetic absorbable suture materials, such as the inevitable inflammatory responses
2 and tissue reactions that are normally witnessed (Yaltirik *et al.*, 2003). In a previous
3 unpublished work, the authors proved the applicability of pure chitin sutures but identified the
4 need to further improve their mechanical strength in order to enable suturing of areas that bear
5 high loads and require significant tensile strength. As was seen in Section 2.2 on cellulose,
6 there are two basic, yet effective, methods to improve the mechanical strength of biopolymers,
7 namely crosslinking and the addition of nanofillers (Garavand *et al.*, 2017; Jamróz *et al.*, 2019).
8 In the present study, Zhang *et al.*, employed graphene oxide (GO) as nanofiller and
9 epichlorohydrin as crosslinker, to obtain a novel, monofilament chitin surgical suture with
10 admirable mechanical strength (Zhang *et al.*, 2019).

11 In the development of novel natural polymer-based suture materials, the selected crosslinker
12 plays a pivotal role in not only the mechanical, but also the biological properties of the final
13 suture product. Crosslinking is the process whereby different molecular chains of a polymer
14 are joined through the formation of chemical bond, that can range from ionic interaction to
15 hydrogen bonding, to form a stronger, more rigid three-dimensional polymer network
16 (Garavand *et al.*, 2017). In the case of suture fabrication, crosslinking allows the researcher
17 to produce a thin, insoluble suture-like thread with substantial tensile strength, from a simple
18 polymer solution. The type of crosslinker that can be used, depends of the functional groups
19 present on the polymer itself, the desired mechanical properties, as well as biocompatibility,
20 since many of the most effective crosslinkers are also cytotoxic (Chen *et al.*, 2019).

21 In the case of chitin, glutaraldehyde is one of the most well studied and widely used
22 crosslinkers, due to its excellent ability to covalently crosslink chitosan and dramatically
23 increase the tensile strength of the polymer network. Yet, strong covalent bonds may also lead
24 to more brittle fibres that cannot tie effective knots, and is not necessarily the best option
25 during suture fabrication (Beppu *et al.*, 2007). Additionally, glutaraldehyde is highly toxic and
26 will diminish the biocompatibility of the natural polymer-based suture. There are, however,
27 several safer crosslinkers available, including genipin, ECH and heparin, that have received
28 increasing attention in recent years due to their much greater biocompatibility than
29 glutaraldehyde (Kildeeva *et al.*, 2020; Liu *et al.*, 2019). In the study presented here, sutures
30 crosslinked with ECH, displayed good cell viability with values above 90%, indicating than
31 ECH did not significantly affect the biocompatibility of the chitin sutures (Yu *et al.*, 2021).
32 Furthermore, ECH, in contrast with glutaraldehyde, has been shown to only react with the
33 hydroxy groups of chitins, while preserving the cationic amine function. Consequently, not all
34 of the available functional groups will be crosslinked by ECH, which could lead to better
35 mechanical properties without excessive brittleness as was shown by Zhang *et al.*, (Zhang *et al.*,
36 2019).

1 With the impact of the manufacturing process on the tensile strength of suture materials in
2 mind, the authors developed an innovative method of stretching the suture fibres (Figure 2.3),
3 that allowed for better alignment of the chitin building blocks along the suture axis, and
4 significantly improved its tensile strength (Wang *et al.*, 2011; Zhang *et al.*, 2019). This
5 stretching method also resulted in a smoother suture surface with a smaller friction coefficient,
6 that will allow the novel chitin sutures to easily penetrate tissues and drastically reduce the
7 damage caused by insertion of the suture material (Viju & Thilagavathi, 2013). Moreover, this
8 monofilament fabrication process, which is not often seen in polymeric sutures with a high
9 tensile strength, decreases the risk of infection as the contact area between the suture and
10 tissue fluid is limited (Geiger *et al.*, 2005). The potential of the novel chitin-GO suture for clinical
11 application was confirmed by *in vivo* and histological studies that revealed good
12 biocompatibility, a lack of serious inflammatory responses and an improved wound healing
13 effect (Zhang *et al.*, 2019).



14
15 **Figure 2.3:** Fabrication process of chitin-graphene oxide sutures. (A) Chitin gel spun into a
16 coagulation bath; (B) suture solidification stretching and moulding; (C, D) stretched chitin and
17 chitin-graphene oxide sutures in an elution bath, respectively; (E) chitin suture; (F) chitin-
18 graphene oxide suture. Reused with permission from (Zhang *et al.*, 2019).

19 In another recent study, Wu *et al.*, reinforced regenerated chitin, named as such because of
20 the dissolution and re-precipitation process it underwent, with nanocellulose (NC) to obtain a
21 novel surgical suture material with good biocompatibility and mechanical performance (Wu *et al.*
22 *et al.*, 2018). Instead of the standard crosslinking method, the authors set out to develop and
23 optimize a wet spinning process, with well-defined parameters, that can offer an alternative
24 route to producing chitin fibres that are able to meet the demands of suture materials. They

1 employed a custom-made apparatus, designed in their laboratory, to extrude a 5% (w/w) chitin
2 solution through a commercial spinneret plate into a coagulation bath of 10% (v/v) aqueous
3 sulfuric acid solution (Wu *et al.*, 2016). The wet-spun fibres were then twisted together and
4 coated with another chitin layer to further improve their mechanical performance and handling
5 properties (Wu *et al.*, 2018a).

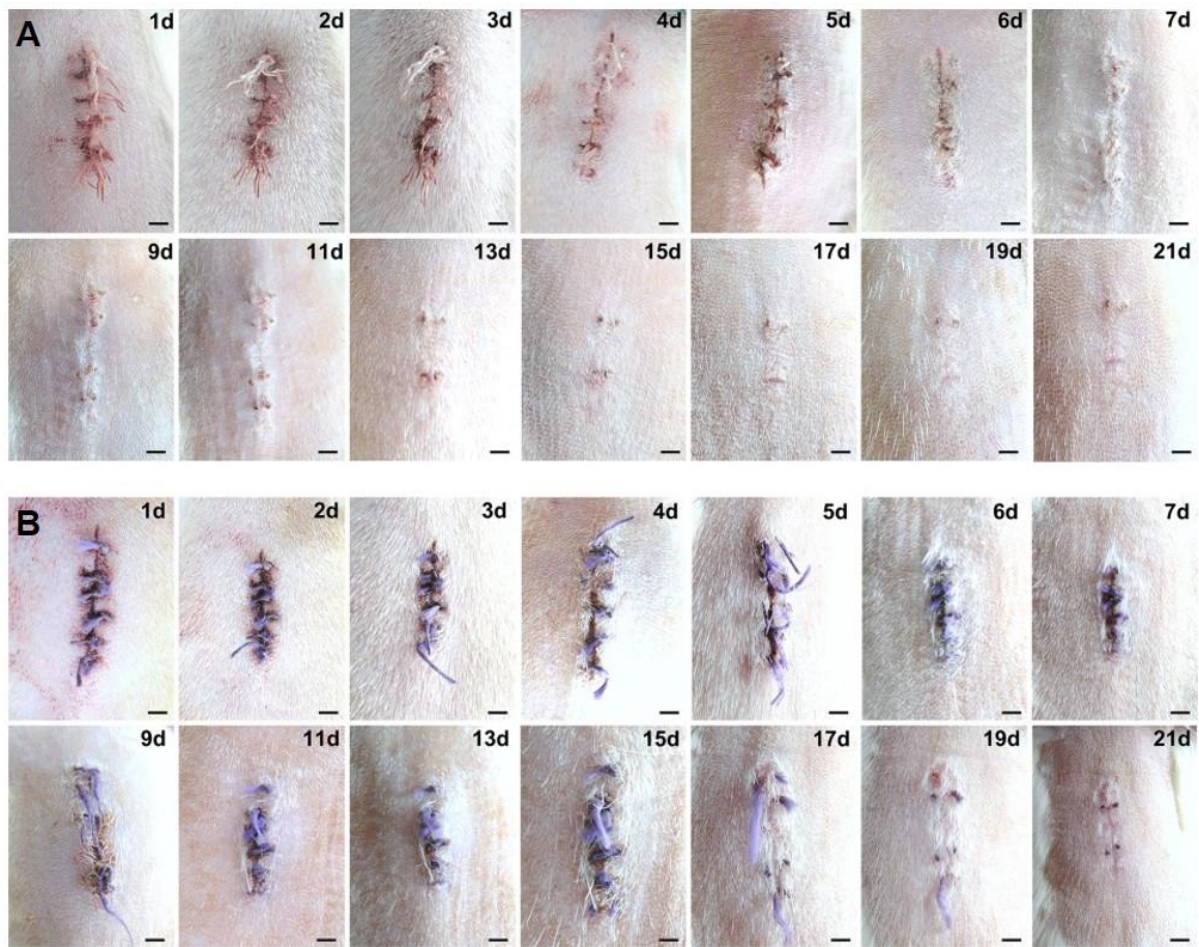
6 In an *in vivo* trial, based on a trusted BALB/c mouse model, the produced chitin-NC sutures,
7 displayed good biocompatibility and a clear ability to improve wound healing. These properties
8 were ascribed to the natural origin of the polymers and the bioactive properties of chitin,
9 respectively. Additionally, an *in vitro* cytocompatibility essay revealed a higher cell density on
10 the chitin-NC fibres compared to the control, while the cell morphologies remained the same
11 for all conditions. The clear enhanced adhesion and proliferation of cells on the chitin-NC fibre,
12 suggests that, as suture material, it will create an ideal environment for cell proliferation and
13 play a role in the promotion of effective wound healing, as was confirmed by the *in vivo* animal
14 trial. In terms of handling properties, the chitin-NC fibres showed a good balance between
15 elasticity and tensile strength, making them fully appropriate for application as suture materials
16 (Wu *et al.*, 2018a). Nevertheless, certain factors need to be reviewed before a stage of clinical
17 application is reached. Particular attention should be paid to the degradation profile and the
18 reliability thereof, since consistent and controllable biodegradation of acylated chitin
19 formulations can be troublesome (Kurita *et al.*, 2000).

20 On the other hand, there is currently a patent available that specifically provides a method of
21 obtaining a chitin-based suture material with unparalleled and highly controlled degradability.
22 The invention describes a suture that is fabricated from chitin, or a derivative thereof, and has
23 a chitin degrading enzyme, such as chitinase derived from *Pyrococcus furiosus*, incorporated
24 into the suture material (United States patent no. 13/442,002., 2012). The rate of
25 biodegradation can then be precisely controlled by varying the enzyme type, quantity,
26 concentration, activity, and the like, which allows for easier and more accurate control over
27 the degradation profile than with conventional methods (Yang *et al.*, 2007). According to the
28 inventors, a suture can be obtained, that firstly maintains its tensile strength for the duration
29 of the surgery and then undergoes gradual degradation that can be fashioned to suit any
30 particular application (United States patent no. 13/442,002., 2012). An added benefit is that
31 the suggested enzymes are highly heat-resistant and remain stable for long periods, even at
32 extreme temperatures (70 – 100 °C). This not only allows for high-temperature treatment
33 during the suture manufacturing process, but also results in sutures with excellent long-term
34 storage stability (Toharisman *et al.*, 2005). Moreover, due to the chitin constituents of the
35 suture material, the inventors suggest that properties such as an enhanced wound healing

1 and haemostatic effect, can be expected in addition to excellent biocompatibility in the newly
2 invented chitin suture material (United States patent no.13/442,002., 2012).

3 Yet, the study that most expertly portrays the benefits of employing chitin as a suture material,
4 was undoubtedly published by Shao *et al.*, who developed a novel mono-component,
5 multifilament diacetyl chitin (DAC) suture, for the treatment of superficial skin wounds (Shao
6 *et al.*, 2016). To assess the feasibility of the produced DAC sutures, an extensive *in vivo* trial
7 was conducted by employing a full thickness wound model with the popular and widely used
8 Vicryl® Plus sutures as control. The DAC sutures had comparable mechanical properties to
9 that of the synthetic suture, which meets the standard suture strength requirements, and
10 managed to maintain a staggering 63% of its original strength at 14 days post-implantation
11 (Gartti-Jardim *et al.*, 2013). Particularly good handling properties, with ease of knot-tying, was
12 noted for the DAC sutures and ascribed to the excellent pliability and modest swelling property
13 of the DAC material. The histological evaluation revealed the expected pronounced
14 inflammatory reaction towards Vicryl® Plus sutures, which again highlights the urgent need for
15 absorbable sutures with improved biocompatibility, while the DAC suture elicited no
16 remarkable tissue response (Shao *et al.*, 2016).

17 The most impressive results of the study, however, were seen during the analysis of the wound
18 healing process. After only six days postoperatively, the linear wounds treated with DAC
19 sutures had regained sufficient tensile strength to maintain their own shape and by day 13 the
20 wound healing process was fully completed, compared to 20 days in the control (Figure 2.4).
21 Additionally, the wound breaking strength of the DAC suture group, was significantly higher
22 ($p < 0.05$) than both the untreated group and the control group. Moreover, at two weeks the
23 linear wound in the DAC suture group, was completely re-epithelized with epidermal cells fully
24 differentiated, basal cells closely arranged and a small amount of sebaceous gland cells and
25 hair follicle cells visible. The control group, also at two weeks, only displayed inflammatory
26 cells with little evidence of wound healing. Still the authors delved deeper in an effort to
27 understand the enhanced wound healing witnessed in the DAC suture group. They discovered
28 a more orderly arrangement of collagen fibres which ran parallel to the epidermal layer of
29 normal skin in the DAC suture group, while the collagen fibres of the control group ran
30 perpendicular to the normal epidermal layer. This explains both the higher wound breaking
31 strength and smoother appearance of the wounds treated with DAC sutures and was ascribed
32 to the N-acetyl glucosamine (NAGA) content of the chitin sutures, and its ability to facilitate
33 the orderly deposition of collagen. With right, the authors of this auspicious study concluded
34 that the produced DAC suture has the potential to break the monopoly of synthetic polymer
35 sutures in the wound closure market (Shao *et al.*, 2016).



1
2 **Figure 2.4:** Representative images of the wound healing process after treatment with DAC
3 suture (A) and the control Vicryl® Plus suture (B) during a 3-week observation period. Bars
4 represent 5 mm. Reprinted with permission from (Shao *et al.*, 2016).

5 **2.3.2 Chitosan from chitin as a potential biomaterial for surgical suture applications**

6 Previously, chitosan was mostly employed as a suture coating material and managed to
7 improve various suture characteristics such as biocompatibility, capillarity, immunogenicity
8 and handling properties, with great success (Viju & Thilagavathi, 2013). More recently,
9 chitosan coatings were employed to convey biological activity, such as antibacterial and
10 haemostatic properties, to already established surgical sutures (Debbabi *et al.*, 2017; Saxena
11 *et al.*, 2011; Zhang *et al.*, 2020). Through these studies, the vast potential of chitosan as a
12 possible raw material for suture fabrication, became evident and in the last few years, research
13 on this subject has been on the increase (Mohammadi *et al.*, 2020).

14 In 2019, da Silva *et al.*, developed an absorbable chitosan suture, enriched with N-acetyl-D-
15 Glucosamine (GlcNAc), a component of its own biodegradation (da Silva *et al.*, 2019). GlcNAc
16 is an essential component of the epithelium and has been found to stimulate fibroblast
17 proliferation, collagen synthesis and hyaluronic acid production in wounds, promoting quick
18 repair and preventing complications related to the process of tissue restoration (Bissett, 2006;

1 Ueno, 2001). This ability of GlcNAc to improve the wound healing process, as well as its
 2 similarity to chitosan which will ensure its proper incorporation into the suture formulation, was
 3 the basis for its selection as an added bioactive molecule (da Silva *et al.*, 2019).

4 The novel chitosan-GlcNAc fibres showed promising results in terms of mechanical
 5 performance, handling properties and drug release, signifying that the produced fibres could
 6 function as surgical sutures with combined mechanical and therapeutic activity. The authors
 7 did a thorough analysis of the mechanical performance of the developed chitosan sutures and
 8 studied both the straight and knotted tensile strength under dry and wet conditions, as can be
 9 seen in Table 2. The addition of GlcNAc to the chitosan formulation, decreased its tensile
 10 strength, which still remained high and exceeded the mean values indicated in the USP, under
 11 both wet and dry conditions. The elasticity and percentage elongation at break (also shown in
 12 Table 2) of the chitosan-GlcNAc sutures were near ideal. The values indicated high pliability
 13 of the suture material and suggested that under wet *in vivo* conditions the material will be able
 14 to stretch as the wound swells and then regain its original shape and length as the wound
 15 retracts when the swelling subsides. This high pliability also conveyed good handling
 16 characteristics and knot security to the chitosan-GlcNAc sutures (da Silva *et al.*, 2019).

17 **Table 2.3:** Mechanical properties of the chitosan (CS) and the chitosan-N-acetyl-D-
 18 Glucosamine (GlcNAc) sutures – non-knotted and knotted – tested in dry and wet conditions.
 19 Reused with permission from (da Silva *et al.*, 2019).

Filament type	Sample	Breaking strength (N)	Elongation at break (%)	Young Modulus (MPa)	Stress at Break (MPa)
Non-knotted	CS Dry	4.3 ± 0.5	8.9 ± 1.1	25.2 ± 0.1	261.0 ± 25.1
	CS Wet	2.9 ± 0.5	15.9 ± 5.3	6.2 ± 0.3	170.9 ± 29.8
	CS/GlcNAc Dry	3.4 ± 0.7	8.6 ± 1.0	21.7 ± 2.0	181.9 ± 71.5
	CS/GlcNAc Wet	2.8 ± 0.8	17.2 ± 3.9	7.2 ± 0.2	159.4 ± 39.0
Knotted	CS Dry	2.4 ± 0.5	10.5 ± 4.3	17.8 ± 0.2	127.1 ± 32.8
	CS Wet	2.7 ± 0.7	11.4 ± 2.8	1.2 ± 0.3	104.4 ± 22.3
	CS/GlcNAc Dry	1.9 ± 0.2	9.2 ± 2.6	9.1 ± 0.2	95.4 ± 26.1
	CS/GlcNAc Wet	1.8 ± 0.7	16.6 ± 5.4	4.8 ± 1.4	88.3 ± 51.1

20 In addition to these favourable mechanical properties and handling characteristics, the suture
 21 fibres also displayed commendable topographical surface properties. Scanning electron
 22 microscopy (SEM) images of the chitosan-GlcNAc sutures revealed a remarkably smooth,
 23 compact, and homogenous morphology that can be ascribed to the expert incorporation of

1 GlcNAc into the chitosan solution. It was believed that GlcNAc was immobilized by a
2 combination of covalent, ionic and hydrogen bondages within the suture formulation which
3 was corroborated by X-ray diffraction (XRD) results. This expansive combination of bonding
4 interactions was speculated to, not only contribute to the appreciable mechanical properties
5 of the suture material, but also to the valuable drug release profile thereof (da Silva *et al.*,
6 2019).

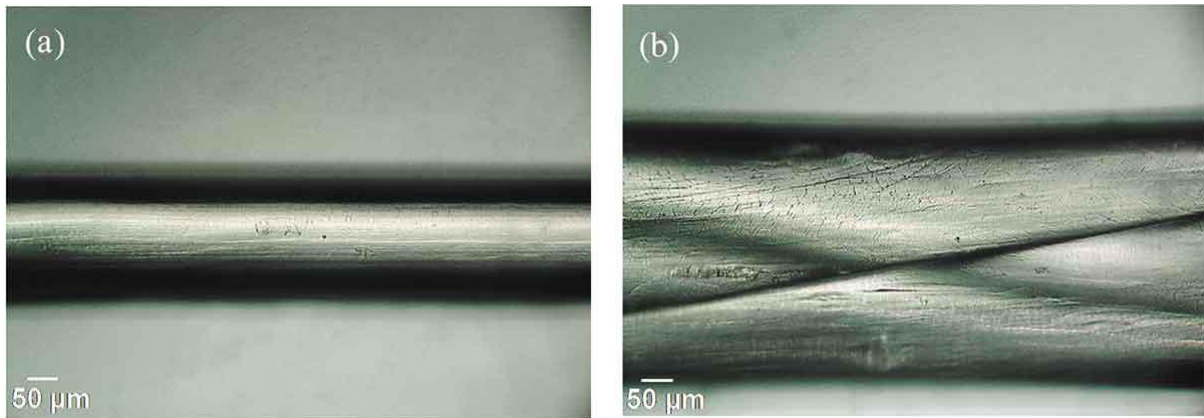
7 Analysis of the drug release kinetics revealed a linear relationship that is dosage independent
8 and highly desirable in any sustained release formulation, as it will prevent oscillating drug
9 concentrations (Dash *et al.*, 2010). In combination with the biodegradation study, it was
10 concluded that drug release was controlled, simply through the diffusion and surface erosion
11 that transpired in the novel chitosan-GlcNAc suture material. Hence, the distinctive
12 degradation profile of this characteristically dense suture material, ensured that it can function
13 as a sustainable drug delivery platform whereby constant drug levels, within the desired
14 therapeutic range, can be maintained for an extended period of time (da Silva *et al.*, 2019).
15 The novel chitosan-GlcNAc suture, therefore, signifies a momentous breakthrough, not only
16 in terms of new suture materials based on natural polymers, but also as a potential localized
17 drug delivery platform that can possibly enhance the wound healing process.

18 The true worth of the study discussed above can be seen by comparing the results with those
19 of another study where Cruz *et al.*, set out to develop a novel chitosan suture material, that
20 would hopefully further the approximation of an ideal suture (Cruz *et al.*, 2016). They
21 investigated two variables, namely polymer concentration and solvent type, in a hope to find
22 suitable parameters for the production of chitosan sutures. Even though they could clearly
23 identify the influence of different solvents and polymer concentrations on the final suture
24 properties, none of the parameters yielded a suture formulation with sufficient tensile strength
25 to meet the minimum requirements specified in the USP (Geiger *et al.*, 2005). The produced
26 fibres varied significantly in terms of fibre dimension, density, and tendency to swell, which
27 was ascribed to the different steric effects of the various acidic solvents that were employed.
28 It was found that denser fibres tend to have higher mechanical properties and lesser tendency
29 to swell, which correlates with the above study where the characteristically dense suture that
30 was produced, displayed admirable mechanical strength that exceeded the USP requirements
31 (da Silva *et al.*, 2019). Nonetheless, Cruz *et al.*, concluded that the fibres produced in their
32 study showed good potential for application as suture materials (Cruz *et al.*, 2016).

33 It is worth noting that at the end of 2017 a patent, titled 'Chitosan fibre', was published wherein
34 the preferred application of the fibre is as a surgical suture. The invention addresses the issue
35 of high swelling ratios in chitosan fibres by providing a new method of manufacturing chitosan

1 fibres with 'n maximum swelling ratio of 100%, deeming them useful as suture materials
2 (United States patent no. 9,771,668, 2017). This corresponds with the previous study where
3 the high swelling tendencies of chitosan fibres resulted in low densities and poor mechanical
4 properties, which impeded their performance as new suture materials (Cruz *et al.*, 2016). The
5 patent application specified several advantages of the moderate swelling properties of the
6 invented chitosan fibres. This included the ability to support suture channels and close them
7 to prevent bleeding in certain applications (e.g., vascular anastomosis), maintenance of
8 sufficient mechanical strength even when swollen, and the prevention of unwanted tissue
9 compression that can be caused by excessive fibre swelling. Additionally, the inventors
10 provide an interesting method of removing the chitosan fibres from the body, namely through
11 the partial dissolution of the fibre with a solvent applied from outside the body (*ex vivo*). The
12 different exemplary embodiments of the invention displayed good mechanical properties in
13 the range of 7.0 – 16.9 N which meets the USP requirement for suture tensile strength (United
14 States patent no. 9,771,668, 2017).

15 Recently, da Silva *et al.*, published yet another research paper on the development of
16 monofilament and multifilament chitosan fibres through a wet spinning process, for potential
17 application as suture materials (Costa Da Silva *et al.*, 2020). The chitosan fibres were
18 exclusively evaluated for their morphology and breaking strength to determine if the fibres
19 comply with USP standards and have potential for use as surgical sutures. Optical microscopy
20 (OM) images showed that the monofilament chitosan fibres were smooth, compact, and
21 cylindrical with no surface porosity, while the multifilament fibres were not as smooth and
22 showed clear undulations and grooves, probably due to the braiding and twisting process. Yet,
23 the OM images revealed that both the mono- and multifilament fibres have a relatively smooth
24 and dense area and that the two monofilaments that make up the multifilament fibre,
25 maintained their original morphological characteristics, as shown in Figure 2.5. The smooth
26 morphology of the fibres suggest that they will carry a low infection risk, cause minimal tissue
27 damage and display uniform distribution of force along the fibre, which will all be beneficial to
28 their application as a suture material (Im *et al.*, 2007; Lapointe *et al.*, 2015).



1
2 **Figure 2.5:** Optical microscopy images of a) monofilament and b) multifilament chitosan fibres.
3 Adapted with permission from (Costa Da Silva *et al.*, 2020).

4 The mechanical properties of the chitosan fibres were evaluated in terms of breaking strength,
5 in the straight and knotted configuration, and were dramatically different for the mono- and
6 multifilament fibres. The monofilament chitosan fibres had an average diameter of 0.137 mm,
7 which corresponds with a 6-0 suture size, and requires a minimum breaking strength of 1.77N
8 according to the USP (*Tensile Strength. United States Pharmacopeia and National Formulary*
9 (*USP 29-NF 24*)). The multifilament chitosan fibres, were nearly double that size (0.239 mm),
10 which was expected since the multifilament fibres consisted of two monofilament fibres that
11 are braided together, and corresponded with a 4-0 suture size with a minimum breaking
12 strength of 7.5 N. Surprisingly, the monofilament chitosan fibres far exceeded the standard
13 breaking strength in the straight configuration and showed an average of 3.0 ± 0.2 N, while
14 the multifilament fibres, which were expected to be dramatically stronger, only exceeded the
15 standard value by 0.4 N with an average breaking strength of 7.9 ± 0.1 N. In the knotted
16 configuration, the monofilament chitosan fibres still adhered to the Pharmacopoeia
17 specifications with an average breaking strength of 2 ± 0.8 N, while the multifilament fibres fell
18 short, with an average of only 4.3 ± 0.8 N compared to the required 7.5 N. According to the
19 authors, the knot made the multifilament fibres brittle to breakage which is not ideal for surgical
20 sutures (Costa Da Silva *et al.*, 2020). This displays a valuable truth namely, that multifilament
21 fibres may appear stronger upon initial inspection but may not necessarily perform best under
22 surgical conditions. The authors concluded that the newly developed monofilament chitosan
23 sutures, displayed great potential for application as surgical suture materials.

24 It is safe to say that chitin and chitosan have already extended the frontiers of surgical sutures
25 by providing viable options for localized drug delivery while simultaneously offering inherent
26 bioactivity. These natural polymers have the exact properties needed to formulate advanced
27 suture materials that can address the current issues of acute and chronic inflammatory
28 responses, poor wound healing strength, scar formation, wound dehiscence etc. that are

1 experienced with the synthetic sutures on the market today. There are, however, certain
2 downfalls such as harsh acidic dissolution conditions and high fibre swelling properties that
3 require a substantial amount of attention. Yet, the studies discussed here give a clear
4 indication that these hurdles can be overcome and potentially open up a way to the ideal
5 suture material.

6 **2.4 Alginate and its derivatives**

7 The third natural polymer, that stands out as a viable option for the fabrication of novel suture
8 materials, with expert biocompatibility and potential bioactivity, is alginate (Brinsko, 2010).
9 Marine brown algae are the main source of alginate, which is a linear polysaccharide
10 consisting of two different monomeric units namely β -D-mannuronic acid (M blocks) and α -L-
11 guluronic acid (G blocks). The composition and sequence of M and G blocks in alginate,
12 depend on the growth conditions and type of seaweed that the polymer was derived from
13 (Radhakrishnan, 2014). This M/G ratio has a profound influence on the chemical and physical
14 behaviour of alginate and creates a unique avenue for manipulating certain properties such
15 as the stiffness and swelling capacity (Rinaudo, 2006). To date, alginate has been investigated
16 for various pharmaceutical applications, including controlled drug delivery, tissue engineering
17 and wound management (Sun & Tan, 2013; Tamayol *et al.*, 2015; Wanawananon *et al.*, 2016).
18 Yet, as a result of the valuable inherent biocompatibility, biodegradability, non-toxicity and
19 related properties of alginate, researchers are still searching for new ways to extend its field
20 of application (Niekraszewicz & Niekraszewicz, 2009).

21 As with cellulose and chitin, alginate can be found in various forms. During the extraction
22 process, alginate is primarily obtained in the form of alginic acid which can be converted to
23 various salt forms such as calcium, magnesium and sodium alginate derivatives (Paul &
24 Sharma, 2015). Amongst these, sodium alginate is the only form that is soluble in water,
25 making it, not only the most established derivative, but also the one with the greatest clinical
26 relevance (Wang *et al.*, 2010). Alginate is characteristically described by properties such as
27 hydrophilicity, ease of gelation, high swelling, and water absorption capacity, as well as ion
28 exchanging abilities that donates reversible solubility to the polymer. These properties that
29 have made alginate one of the most important materials in wound management and an
30 indispensable component of modern wound dressings (Varaprasad *et al.*, 2020).

31 Clinical studies have found that alginate wound dressings can promote wound healing and
32 wound closure to ensue smaller fibrotic lesions with better aesthetic appearances than
33 traditional materials (e.g. cotton and viscose fibres) (Alamgir, 2017; Kazi & Yamamoto, 2019;
34 Zhou *et al.*, 2018). This significant ability of alginate can also be of great value in surgical
35 suture applications where rapid wound closure, with proper wound healing and little scar

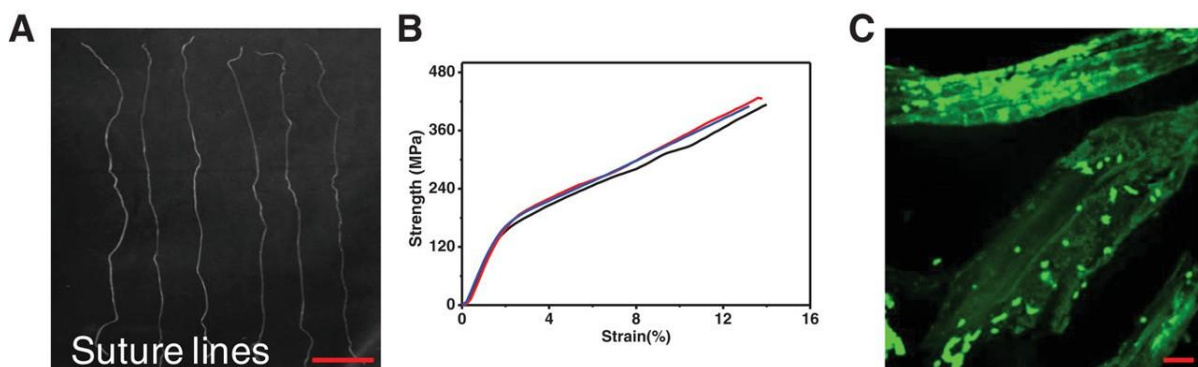
1 formation is viewed as the ideal treatment outcome (Al-Mubarak & Al-Haddab, 2013). It is
2 believed that alginate promotes wound healing by stimulating macrophage and other
3 proinflammatory mediators to initiate the wound healing process. Therefore, when applied to
4 chronic wounds, alginate immediately sets the wound healing process into motion and
5 improves the treatment of difficult-to-heal wounds such as pressure sores and leg ulcers
6 (Chang *et al.*, 2012). Additionally, *in vitro* studies and wound scratch assays revealed that
7 alginates can facilitate cell movement and create the ideal microenvironment for cell
8 proliferation that will further aid the wound healing process (Costa-Almeida *et al.*, 2018; Kazi
9 & Yamamoto, 2019).

10 Moreover, the adhesive nature of alginate fibres plays a significant role in closing the wound
11 and sealing it off to prevent the invasion of unwanted foreign bodies, which can have a
12 favourable effect on the final outcome of wound healing (Hong *et al.*, 2018). These exceptional
13 abilities of alginate, together with its remarkable biosorption that is a result of its hydrophilic
14 and porous nature, make this unmatched natural polymer an interesting option for the
15 development of advanced absorbable suture materials with inherent bioactivity
16 (Niekraszewicz & Niekraszewicz, 2009). Yet, very few researchers have investigated the
17 potential of alginate as a suture material. This could be because of the relatively low
18 mechanical strength of alginate fibres and other formulation factors that make the production
19 of alginate-based suture materials a challenging endeavour (He *et al.*, 2012; Lee *et al.*, 2009).
20 Nonetheless, several intriguing studies with unique approaches to suture development
21 through the use of alginate, have recently made it to the forefront of material sciences.

22 **2.4.1 Advancements in the use of alginate to develop novel suture materials**

23 To find inspiration for the production of strong, biocompatible fibres that can be used as suture
24 materials, Zhang *et al.*, looked to some of the high-performance biomaterials, such as spider
25 and silkworm fibres, found in nature (Zhang *et al.*, 2020). They ascribed the exceptional
26 mechanical properties and sophisticated functionalities of these fibres, to the structural
27 proteins with characteristic hierarchical structures such as α -helix or β -sheets, within the fibres
28 (Chen *et al.*, 2019). Based on these observations, Zhang *et al.*, developed a series of protein
29 reinforced fibres and tested the most promising material, which consisted of alginate and
30 bovine serum albumin (BSA) in a 9:1 ratio, for its potential application as a suture material.
31 They engineered a facile microfluidic strategy that allows for easy, scalable construction of
32 biological fibres whilst preserving the hierarchical structure of the proteins (Zhang *et al.*, 2020).
33 This new method produced fibres with surprisingly high mechanical strength that outperformed
34 many of the existing artificial protein fibres, including those made from recombinant spider or
35 silkworm silks (Li *et al.*, 2020; Zhang, *et al.*, 2020).

1 By employing alginate as a base polymer and reinforcing it with BSA, which demonstrated
2 astonishing breaking strength and toughness, the authors successfully produced fibres that
3 could be used for surgical suture applications (Figure 2.6 A). The alginate/BSA composite fibre
4 displayed outstanding mechanical properties with a high breaking strength of ≈ 420 MPa and
5 a Young's modulus of ≈ 10 GPa, which exceeds that of human recombinant collagen fibres
6 (Figure 2.6 B). The authors investigated the cytocompatibility of the novel fibres and found
7 that adeno-carcinomic human alveolar basal epithelial cells (A549) anchor and spread over
8 the smooth alginate/BSA composite fibres (Figure 2.6 C), which points to good and acceptable
9 cytocompatibility. Additionally, the produced alginate/BSA composite fibres were used in
10 various wound closure experiments that included rat, minipig and porcine skin, liver, and
11 stomach models, to illustrate their applicability as suture materials. The alginate/BSA
12 composite fibres were able to close all the wound incisions without breakage and displayed
13 admirable mechanical strength and flexibility. Overall, the results indicated that the novel
14 alginate/BSA composite fibres can be considered as good candidates for new absorbable
15 suture materials due to their robust mechanical performance and good biocompatibility (Zhang
16 *et al.*, 2020).



17 **Figure 2.6:** A) Photo of the alginate/BSA composite fibres. Scale bar: 3 cm. B) Stress-strain
18 curves of alginate/BSA composite fibres. The curves with different colours represent three
19 parallel tensile tests. C) Confocal microscopy image of the alginate/BSA composite fibres co-
20 cultured with adeno-carcinomic human alveolar basal epithelial cells (A549). Scale bar: 20
21 μm . A549 cells are stained with calcein-AM (green)/PI (red) in phosphate buffered saline
22 solution. Adapted with permission from (Zhang *et al.*, 2020).
23

24 This expert research article, published early 2020, demonstrates that with innovative thinking
25 and advanced manufacturing strategies, it is possible to create new alginate-based fibres that
26 are capable of suturing and closing wounds. Another interesting approach is given by a very
27 recent patent that describes a unique method of producing multifilament sutures, with
28 enhanced braid strength, through click chemistry (United States patent no. 10,196,762 5,
29 2019). The disclosed suture fibres consist of at least two distinct filaments, each with a polymer

1 core and a reactive group, known to have click reactivity, on its surface. The two reactive
2 groups are complementary such that they react to covalently bond the two filaments together.
3 Alginate is one of the suitable natural, biodegradable polymers that can be pre-
4 functionalized and used to prepare the polymer core of the disclosed fibres. Click chemistry
5 reactions include Huisgen cycloaddition, Diels-Alder, thiol-alkene and maleimide-thiol
6 reactions, some of which take place in aqueous environments, such as physiological fluids,
7 that can lead to *in situ* strengthening of sutures as the braided filaments are covalently bonded
8 upon implantation (Escorihuela *et al.*, 2015). Alginate gels, consisting of sodium and calcium
9 alginate, can also be used to coat the disclosed suture fibres through one of several known
10 methods such as dipping, spraying, and full immersion, to enhance the surface properties of
11 the suture material. This patent reveals one of the many undiscovered methods that can be
12 used to employ alginate as a suture material and thereby obtain novel suture fibres with
13 enhanced mechanical properties (United States patent no. 10,196,762 5, 2019).

14 Khan *et al.*, studied yet another technique of surface modification that can lead to improved
15 mechanical strength in alginate fibres and render them suitable for suture applications (Md.
16 Khan *et al.*, 2013). As opposed to the plasma treatment suggested in the patent discussed
17 above, Khan *et al.*, employed a γ -irradiation technique, which is both environmentally friendly
18 and economically viable, to graft polyethylene glycol (PEG) onto the surface of calcium
19 alginate fibres, to improve the physio-mechanical properties thereof (Khan *et al.*, 2013). The
20 process of γ -irradiation holds several unique advantages, such as the ability to enhance the
21 antimicrobial activity of calcium alginate, that make it highly suitable for this application (Kume
22 *et al.*, 2002). PEG, on the other hand, also has a range of benefits including, promoting the
23 proliferation of cells, enhancing the elasticity of a system and increasing the stability thereof,
24 that can prove valuable for alginate-based suture formulations (D'souza & Shegokar, 2016).

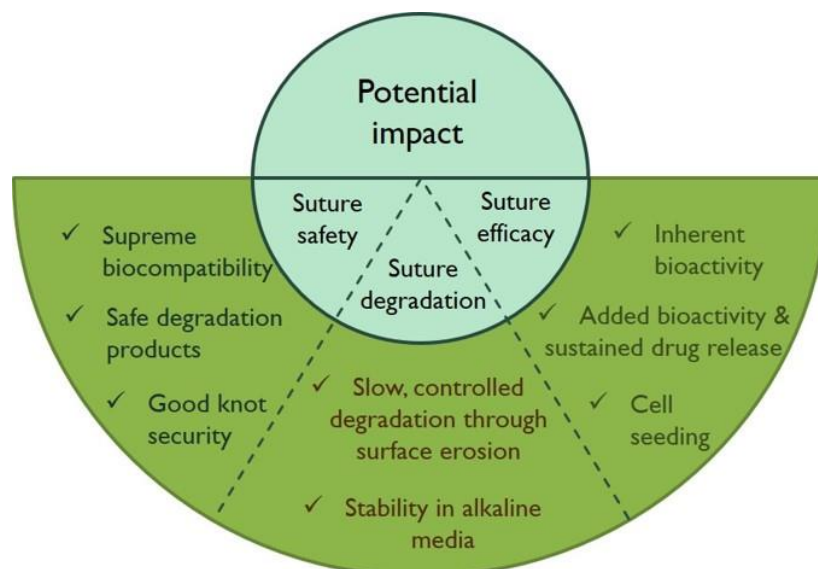
25 Through a detailed optimization process, the authors found that grafting conditions of 2.5 kGy
26 irradiation with 50% PEG, yielded fibres with the highest tensile strength, which was three
27 times that of pristine calcium alginate fibres. The addition of PEG significantly improved the
28 elasticity and percentage elongation at break of the fibres which increases their potential for
29 application as a novel suture material. Importantly, the γ -irradiation process decreased the
30 water absorption ability of the calcium alginate fibres, which is normally too high for suture
31 applications. This resulted in better interaction of the fibres with simulated body fluids and
32 confirms their potential for biomedical applications such as surgical sutures (Khan *et al.*, 2013).

33 It should be noted that in all the discussed studies, the interchangeability of alginate which
34 allows it to be easily converted from either alginic acid or sodium alginate to insoluble calcium
35 alginate, was employed (Fu *et al.*, 2011). This process of crosslinking allows for immediate

1 fibre formation and adjustable mechanical strength in the produced fibre (Chen *et al.*, 2001).
2 The convenient interchangeability of alginate was, therefore, embraced and then combined
3 with different approaches to enhance the mechanical strength thereof, and ultimately obtain a
4 fibre with suitable characteristics for use as a suture material. The recent nature of these
5 publications suggest that we have only scratched the surface of alginate's potential as a novel
6 suture material and that more work is needed to fully uncover the possibilities and
7 breakthroughs that this valuable natural polymer can offer (Khan *et al.*, 2013; Thomas, 2019;
8 Zhang *et al.*, 2020). On this account, the current research project is focussed on finding a new
9 way to fully utilize alginate as an absorbable, monofilament suture material with added
10 bioactivity and enhanced biocompatibility that will serve to extend the frontiers of suture
11 material sciences (de la Harpe *et al.*, in press).

12 **2.5 Potential impact and future prospects**

13 Sutures made from natural polymers, can help to overcome some of the most crippling
14 complications and troubling problems experienced with the synthetic sutures that are currently
15 available (Kulkarni *et al.*, 2012). The three areas of suture performance, that can be profoundly
16 impacted by the development of novel, high quality natural polymer sutures, are suture safety,
17 suture degradation and suture efficacy (Figure 2.7). Improvement of these three areas will
18 serve to firstly, change the general performance of suture materials available on the market
19 today, while secondly, decreasing the rate of suture related complications and lastly,
20 potentially close the gap to the ideal suture material (Chen *et al.*, 2017; Dennis *et al.*, 2016;
21 Seitz *et al.*, 2015).



22

23 **Figure 2.7:** The different areas of suture performance that can be impacted by the
24 development of novel sutures made from natural carbohydrate polymers.

1 The ability of natural polymer sutures to improve suture safety, lies in their characteristically
2 high biocompatibility and harmless degradation products. In fact, the primary reason why
3 natural polymers have attracted such a great amount of attention, particularly in the fields of
4 wound healing and drug delivery, is their high level of safety and excellent biocompatibility
5 (Malafaya *et al.*, 2007; Shi *et al.*, 2016). The monomeric subunits of natural polymers closely
6 resemble macromolecules that are normally recognized by, and found in the human body
7 (Mogoşanu & Grumezescu, 2014). Because of this similarity, sutures made of natural
8 polymers, do not elicit the same degree of inflammatory and immunological reactions as
9 synthetic sutures, which are undeniably foreign to the body (Mohammadi *et al.*, 2020).
10 Additionally, the degradation products of synthetic sutures can be harmful, as they often cause
11 local pH shifts and enlarged inflammatory responses, which have been found to prolong and
12 even prevent wound healing (Washington *et al.*, 2018). The degradation products of natural
13 polymers on the other hand, are harmless to the extent that they can be further used by the
14 body for the production of other macromolecules, or effortlessly eliminated through renal
15 clearance (Asghari *et al.*, 2017).

16 Natural polymer sutures, can also help to improve the safety of suture materials by overcoming
17 common suture problems like knot slippage, suture breakage and excessive wound tension.
18 Various synthetic suture materials are notorious for their poor handling properties, which
19 makes it difficult for the surgeon to tie a proper knot at the appropriate tension, without the
20 suture breaking or the knot slipping (Avoine *et al.*, 2016). Some of these synthetic suture
21 materials, for example Ethibond polyester sutures, despite having a multifilament nature that
22 is supposed to ensue good knot security, are highly prone to knot slippage. This often leads
23 to the spontaneous unravelling of knots and increases the risk of complications like infection
24 and wound dehiscence (Smith *et al.*, 2013). Other synthetic sutures, especially nonabsorbable
25 sutures and those made of metallic alloys, are extremely rigid and even though they possess
26 favourable and excellent mechanical strength, can cause unwanted high levels of intrinsic
27 tension in the wound which often leads to ischemic necrosis (Duarah *et al.*, 2018; Lendlein &
28 Langer, 2002).

29 On the other hand, suture fibres made of natural polymers display an impressive balance
30 between tensile strength and elasticity which allows them to expand and contract as the wound
31 swells and recoils. This adaptability also prevents unnecessary tension at the wound site and
32 creates an environment suitable for wound healing (Song *et al.*, 2018). The characteristically
33 porous nature of natural polymer sutures and their high pliability also conveys good knot
34 security to these materials which will ensure that the wound stays closed, and infection risks
35 low (Mogoşanu & Grumezescu, 2014). Thus, the excellent properties and unique abilities of

1 sutures consisting of natural polymers like cellulose, chitin and alginate, convey first-rate safety
2 profiles to these materials which far transcends that of current commercial suture materials.

3 The degradation profile of synthetic suture materials, which is vastly unsatisfactory in the
4 majority of cases, can also readily be improved on through the development of suture
5 materials from natural polymers (Abhari *et al.*, 2017). One of the key characteristics of the
6 ideal suture material, is that it should degrade in a predictable manner and preferably lose its
7 tensile strength at the same rate that the tissue regains strength (Samadian *et al.*, 2020). Yet,
8 synthetic suture materials degrade by means of swelling and bulk erosion which leads to a
9 rapid loss of tensile strength and irregular, unpredictable degradation rates (Seitz *et al.*, 2015).
10 The early and unexpected loss of tensile strength of degradable synthetic sutures, is a major
11 concern of many surgeons who have witnessed first-hand the detrimental effects of such
12 undesirable suture behaviour (Campbell *et al.*, 2014). Sutures made of natural polymers,
13 however, have been found to degrade through surface erosion, which leads to a gradual loss
14 in tensile strength and more predictable degradation profiles (Pitt & Schindler, 2019).
15 Additionally, the degradation rate of natural polymer sutures, can easily be controlled through
16 the variation of simple factors such as the degree of crosslinking and polymer composition
17 (Wu *et al.*, 2018a). Through the use of natural polymers, scientist can, therefore, develop
18 suture materials that degrade at the same rate as which the wound heals, to ensure that
19 adequate mechanical support is provided for the duration of the wound healing process
20 (Chiaoprakobkij *et al.*, 2019).

21 Another problem, often encountered with synthetic suture materials, is that they swiftly
22 degrade in the harsh basic conditions of the infected urinary track, bile conducts or pancreatic
23 juice released in the duodenum (Tomihata *et al.*, 2001). This is especially problematic in the
24 case of urinary surgery where permanent sutures cannot be used as their presence induces
25 the formation of urinary calculi (Wang *et al.*, 2019). Sutures, made of natural polymers like
26 chitin for example, which has an inherently basic nature and is therefore stable in conditions
27 with high pH levels, can help address this problem by providing surgeons with durable suture
28 materials that will slowly degrade, even under challenging basic conditions (Shahidi &
29 Abuzaytoun, 2005). Natural polymers can therefore provide surgeons with valuable, reliable
30 suture materials that undergo predictable degradation irrespective of the physiological
31 conditions in which they are used (Mohammadi *et al.*, 2020).

32 When it comes to the efficacy of suture materials, various factors including the ability of the
33 material to close the wound and to create an environment suitable for wound healing, play a
34 role (Selvi *et al.*, in press). The first factor, depends largely on the tensile properties of the
35 polymer used, while the latter can be achieved through the incorporation of appropriate APIs

1 into the suture formulation or, in the case of natural polymers, through the utilization of their
2 inherent wound healing properties (Lee *et al.*, 2017). Since all suture materials inevitably
3 cause some form of damage upon insertion, induce a measure of inflammation and hold a risk
4 of infection, albeit at different degrees, the only way to overcome these complications is
5 through bioactivity (Somasekharan *et al.*, 2020; Tajirian & Goldberg, 2010). Natural polymers
6 have an advantage in this area, as they already have inherent bioactive properties such as
7 antimicrobial and accelerated wound healing effects (Torres-Giner & Pérez-Masiá, 2016).
8 Natural polymers, with their reliable degradation profiles and low temperature preparation
9 methods, also allow for the effective incorporation and sustained delivery of various APIs, such
10 as anaesthetics that can help reduce the pain experienced by patients, or antineoplastic
11 agents that can help improve the aesthetic appearance of the recovered wound, which is of
12 particular interest in cosmetic surgery (Guambo *et al.*, 2020; Lee *et al.*, 2017).

13 Additionally, the structural properties of natural polymers closely resemble the native
14 extracellular matrix (ECM) and can create the ideal environment for wound healing by allowing
15 the diffusion of nutrients, metabolites and growth factors, while providing the optimal
16 microenvironment for cell proliferation, migration and differentiation (Ghorbani *et al.*, 2020).
17 Hence, natural polymers play a major role in the field of tissue regeneration and can potentially
18 be used to transform suture materials into tissue engineering platforms (Guyette *et al.*, 2013).
19 The cellulose based sutures produced by Mertaniemi *et al.*, for example, effectively supported
20 the adherence, migration and proliferation of human adipose mesenchymal stem cells, and
21 could successfully deliver these stem cells to an injured area of the body, thereby creating a
22 new, exciting avenue for tissue regeneration. Cell seeding has the potential to significantly
23 improve suture efficiency, especially in cases such as Achilles tendon ruptures, where blood
24 perfusion is low, and the body is unable to repair the wound without external support (Yao *et al.*,
25 2008). Ultimately, the efficiency of a suture material, is measured by the success of the
26 surgical procedure for which it was employed. The inherent bioactivity of natural polymer
27 sutures and the addition of APIs, growth factors, cells and the like, to natural polymer sutures,
28 can potentially lead to a 100% success rate of the procedures they were used in, thereby also
29 conveying full efficacy to the suture materials (Gierek *et al.*, 2018). However, this will require
30 great specificity in terms of the particular application of each developed suture material. In
31 fact, in terms of the future prospects of suture materials, we suspect that an ideal suture
32 material, for every unique application, is on the horizon.

33 Given the wide range of applications for which suture materials are indicated, from basic skin
34 lacerations to intricate microvascular anastomosis, it is highly unlikely that one suture material
35 can be ideal for all suture requiring operations (Tanasă & Zănoagă, 2011; Teo *et al.*, 2021).
36 We, therefore, envisage that researchers and material scientist will soon start to develop

1 suture materials with singular applications, beginning with procedures that are troubled by
2 high rates of complications. For example, sutures indicated for microvascular surgery (MVS)
3 applications can be loaded with anti-inflammatory agents to help lower the incidence of
4 detrimental ischemic reperfusion injury, during MVS (Askari *et al.*, 2006; Caiazzo *et al.*, 2020).
5 Additionally, such sutures might be developed to have mechanical properties similar to that of
6 the micro-vessels, which might be lower than the tensile strength mandated by the USP but
7 more suitable for this particular application (Klemm *et al.*, 2001; Özkan & Özgentaş, 2005). In
8 this way, natural polymers might not lead to a single ideal suture material but pave the way to
9 a variety of suture materials that are ideal for their particular application.

10 **2.6 Conclusion**

11 Undeniably, the field of suture material sciences is moving in the direction of employing
12 natural, and often carbohydrate-based, polymers to develop innovative suture materials with
13 improved biocompatibility and efficacy (Deng & Qasim, 2021). This comes after thousands of
14 years of customary suture usage and experimentation with a myriad of materials that have all
15 failed to fulfil the high demands of an ideal suture material (Rengasamy & Ghosh, 2010). We
16 are now at a stage where the downfalls and shortcomings of current, synthetic degradable
17 sutures, such as localized pH shifts, high levels of inflammation and debilitating cellular
18 necrosis, can no longer be ignored but warrant urgent attention (Gabrielli *et al.*, 2001; Teo *et al.*,
19 2021). Additionally, biomedical sciences and surgical procedures have advanced to such
20 a level that there is no longer room for suture materials with the singular function of tissue
21 approximation. Rather there is an imperative need for a dynamic approach where suture
22 materials can actively participate in the wound healing process and increase the chances of a
23 successful surgical outcome (Alshomer *et al.*, 2017). Hence, researchers are now looking
24 towards natural polymers with suitable properties such as good biocompatibility, high
25 mechanical strength, safe degradation products and inherent bioactivity to develop novel
26 suture materials (Islam *et al.*, 2017). Despite the favourable properties of natural polymers,
27 innovative techniques and manufacturing processes are necessary to obtain fibres that are
28 suitable for suture material applications. In recent years, several researchers have made
29 profound breakthroughs in terms of suture material development through the use of natural
30 polymers such as cellulose, chitin and alginate, the most successful of which is shown in Table
31 2.4 (Halib *et al.*, 2017; Zhang *et al.*, 2020).

32 The novel natural polymer-based suture materials, shown in Table 2.4, have the potential to
33 change, not only the outcome of the numerous procedures in which sutures are employed,
34 but also the general approach to the treatment of difficult conditions such as chronic, non-
35 healing wounds (Mertaniemi *et al.*, 2016). There are three areas of suture performance that
36 can be dramatically impacted by the development of innovative natural polymer-based sutures

1 namely, suture safety, suture degradation and suture efficacy. The characteristically high
2 biocompatibility and harmless degradation products of natural polymers elicit a notably lower
3 inflammatory response in the body than synthetic polymers, which results in an unquestionably
4 superior safety profile for natural polymer-based sutures (Pillai & Sharma, 2010; Seitz *et al.*,
5 2015). As was seen throughout this review, natural polymers allow for tuneable degradation
6 that can readily be adapted to synchronize with the rate of wound healing to ensure that
7 adequate mechanical support is provided for the duration of the wound healing process (Pitt
8 & Schindler, 2019). In this manner, sutures made of natural polymers can improve on the
9 degradation profile of synthetic sutures which are prone to rapid and unpredictable
10 degradation *in vivo* (Campbell *et al.*, 2014). Yet, the greatest benefit of natural polymer sutures
11 can arguably be their ability to improve suture efficacy through their inherent bioactivity or their
12 capacity for sustained, local drug delivery (Lee *et al.*, 2017). The efficacy of suture materials
13 is ultimately measured by the success of the surgical procedures in which they are used. The
14 outcome of several procedures, including those riddled with complications such as infection
15 and chronic inflammation, can be dramatically improved through the localized delivery of APIs
16 via suture materials or by exploiting the inherent bioactive properties (e.g. antimicrobial, anti-
17 inflammatory and accelerated wound healing effects) of natural carbohydrate polymers,
18 thereby also improving the efficacy of the suture material itself (Arora *et al.*, 2019; Lee *et al.*,
19 2017).

20 In terms of future prospects, we propose that instead of finding one ideal suture material that
21 that fits all occasions, natural polymers will pave the way towards a more diverse range of
22 suture materials, each with a singular or more focused field of application. In this manner,
23 suture materials can be designed to meet the highly specialized requirements of modern
24 surgical procedures, while simultaneously meeting the basic requirements of any absorbable
25 suture material, i.e., sufficient mechanical strength, reliable biodegradation, and biosafety.

26 (De la Harpe, K.M., Kondiah, P.P., Marimuthu, T. and Choonara, Y.E., 2021. Advances in
27 carbohydrate-based polymers for the design of suture materials: A review. *Carbohydrate*
28 *Polymers*, p.117860.)

Table 2.4: The processing methods and physiochemical properties of the most successful carbohydrate-based suture materials, discussed in this article.

Suture material	Processing methods	Reinforcing agent	Crosslinker	Filament	USP size	Tensile strength (MPa)	Biocompatibility	Reference
Cellulose fibres from sisal plant	Standard chemical extraction and lyophilization	None	None	Monofilament	3-0	138.84	Good <i>in vivo</i> biocompatibility in a rat model with no signs of inflammation.	(Guambo <i>et al.</i> , 2020)
Oxidized regenerated cellulose (ORC)	Braiding with one core strand and eight shell strands	None	None	Multifilament	2-0	116.91	Not evaluated	(Li <i>et al.</i> , 2019)
Nano-cellulose fibres (NCF)	Crosslinking post extrusion with a Fab@Home experimental 3D printer	None	Glutaraldehyde	Monofilament	6-0	227	No <i>in vitro</i> cytotoxicity towards human adipose stem cells (hASC)	(Mertaniemi <i>et al.</i> , 2016)
Regenerated chitin	Wet spinning, weaving (30 strands) and coating	Bacterial nanocellulose crystals	Sulfuric acid	Multifilament	3-0	168.2	No cytotoxicity, promoted cell proliferation and wound healing	(Wu <i>et al.</i> , 2018a)
Chitin	Extrusion into an ethanol coagulation bath followed by vertical stretching	Graphene oxide	Epichlorohydrin	Monofilament	2-0	124.66	Good biocompatibility with L929 cells, cell viability above 90%	(Zhang <i>et al.</i> , 2019)

Diacetyl chitin	Wet spinning and weaving	None	None	Multifilament	2-0	144.37	No <i>in vivo</i> tissue reaction in a rat model	(Shao <i>et al.</i> , 2016)
Chitosan	Wet spinning	None	None	Monofilament	6-0	95.4	No cytotoxicity towards L929 cells	(da Silva <i>et al.</i> , 2019)
Chitosan	Wet spinning	None	None	Monofilament	6-0	72.2	Not evaluated	(Cruz <i>et al.</i> , 2016)
2-hydroxy-trimethyl ammonium chloride chitosan (HACC)	Coaxial electrospinning	None	Regenerated silk fibroin (RSF)	Monofilament	_	41.1	No cytotoxicity to Schwann cells	(Fan <i>et al.</i> , 2020)
Chitosan	Wet spinning	None	None	Monofilament	6-0	131.79	Not evaluated	(Costa Da Silva <i>et al.</i> , 2020)
Sodium alginate	Crosslinking with a microfluidic technique	Bovine serum albumin (BSA)	Glutaraldehyde	Monofilament	2-0	270 MPa	Good biocompatibility with A549 cells	(Zhang <i>et al.</i> , 2020)

CHAPTER 3: PRELIMINARY BIOSUTURE DESIGN AND STUDY OF THE INFLUENCE OF FORMULATION PARAMETERS ON THE MECHANICAL PROPERTIES OF THE BIOSUTURE.

3.1 Introduction

Suture materials have to meet a very unique set of requirements (outlined in Table 3.1) for the material to be considered both safe and effective. Many of these requirements are not only difficult to achieve in themselves, but also play up against each other, making the development of a novel suture material a particularly challenging task (Seitz *et al.*, 2010). For example, the ideal material should be strong and provide maximum tensile strength, but it should also be elastic and easily manipulated. This necessitates a somewhat flexible polymer network which will inevitably be softer and weaker than a more rigid, compact polymer network (Kim *et al.*, 2007). The suture material should also be as thin and smooth as possible to minimize damage to the tissue while suturing. Yet, a decrease in diameter and surface friction can lead to poor handling properties and knot slippage (Silver *et al.*, 2016). Therefore, in the development of a new suture material, a delicate balance must be achieved between the different inter-related properties. One way to obtain such a delicate balance, is by combining the right, carefully selected raw materials in optimal ratios, under well controlled processing conditions, while using the most effective available methods to yield a strong, flexible suture (Sánchez-Valdes *et al.*, 2013). Hence, this chapter explores various formulation parameters, including the addition of reinforcing polymers, the use of different plasticizers, different crosslinker concentrations, as well as different drying methods, to find a suitable formulation and methodology that will yield a strong, yet flexible biosuture.

Table 3.1: Basic requirements of a safe and effective drug-loaded suture material.

	Requirement	Reference
1.	Good stability both <i>in vivo</i> and <i>ex vivo</i> .	(Hermes, 1991; Seitz <i>et al.</i> , 2015)
2.	Optimal mechanical properties with maximum tensile strength (specified in the USP).	(Bloom & Goldberg, 2007; Costa Da Silva <i>et al.</i> , 2020)
3.	Minimum swelling and loss of tensile strength <i>in vivo</i> .	(Peng <i>et al.</i> , 2020; Shao <i>et al.</i> , 2016)
4.	Sufficient elasticity and flexibility (ease of knot tying).	(Marturello <i>et al.</i> , 2014)
5.	Appropriate diameter (specified in the USP).	(Guo <i>et al.</i> , 2019; Silver <i>et al.</i> , 2016)
6.	Excellent safety and biocompatibility.	(Maslova <i>et al.</i> , 2016)
7.	Slow, sustained drug release.	(Arora <i>et al.</i> , 2019)

From the different suture requirements mentioned in Table 3.1, the mechanical properties are of primary importance, since a weak suture material will not be able to perform the basic function of tissue approximation and the mechanical properties of the biosutures are, therefore, the focus of this preliminary design chapter. First, a sound theoretical basis will be drawn for the selection of key materials (i.e., polymers, crosslinkers and plasticizers). The influence of these materials, as well as other factors such as fabrication and drying methods, on the mechanical properties and foundational quality of the biosuture, will then be experimentally determined. Based on these results, a final fabrication method and biosuture formulation will be selected.

3.2 Theoretical basis for the selection of key materials

3.2.1 Polymer base: Sodium alginate

The merits of employing sodium alginate in suture material development has already been elucidated in Chapter 2. Briefly, sodium alginate, a linear polysaccharide that consists of alternating β -D-mannuronic acid (M) and α -D-guluronic acid (G) residues (Figure 3.1) has many valuable attributes such as biocompatibility, biodegradability, and water solubility. The following properties, however, have caused Sachan *et al.*, (Sachan *et al.*, 2009) to classify sodium alginate as a wonder polymer for controlled drug delivery, and further justify its use in the current study:

- It is readily available and relatively inexpensive.
- It has good blood compatibility and does not accumulate in any organ of the human body.
- It is water soluble which eliminates the use of noxious solvents and hence stability, toxicological and environmental problems associated with solvents can be minimized.
- It forms a gel under mild conditions, such as room temperature, and hence reduces the chance of destroying the activity of sensitive drugs under harsh processing conditions.
- It can be crosslinked with a variety of crosslinking agents, to form an insoluble gel, which can be used to delay the release of various drugs, including large proteins and peptides.
- It has been adopted by the European Pharmacopoeia (EP).
- It has been granted the 'generally recognized as safe' (GRAS) status by the Food and Drug Administration (FDA). The acceptable daily intake (ADI) for alginates is not specified which is the highest possible classification for food additives as both the FDA and World Health Organization (WHO) places no limitation on the daily consumption of alginates by man.

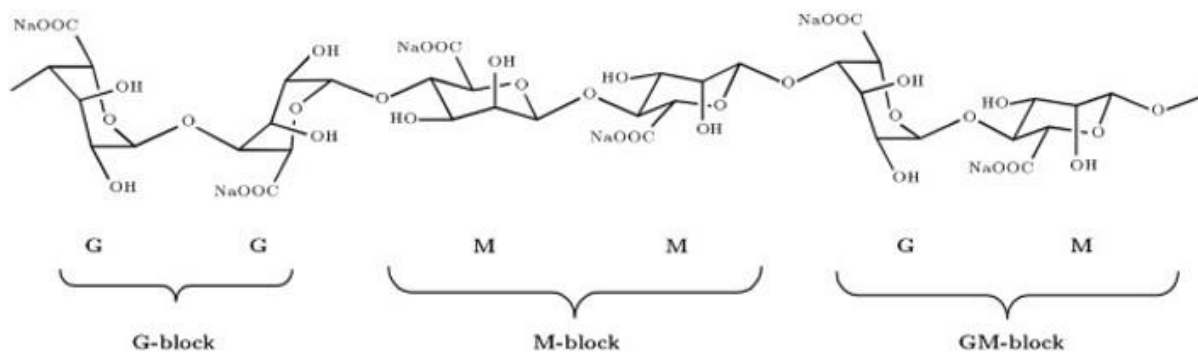


Figure 3.1: Chemical structure of sodium alginate showing the α-D-guluronic (G), acid β-D-mannuronic acid (M) and heterogeneous MG blocks. Adapted with permission from (Daemi & Barikani, 2012).

Amongst these favourable qualities, the most attractive attribute of alginate within the context of suture development, is arguably its ability to form an insoluble, rigid three-dimensional network upon exposure to appropriate crosslinkers. Crosslinkers are usually divided into three main types namely, physical, chemical or enzymatical crosslinkers that give rise to different bonds such as covalent, ionic or hydrogen bonds (Garavand *et al.*, 2017). Alginate is most commonly crosslinked by means of physical crosslinkers, such as divalent cations, where crosslinking is achieved through ionic interaction between the multivalent cation and the carboxylate acid groups of the galacturonate blocks on the alginate chain (Azeredo & Waldron, 2016). This interaction is best defined by the “eggbox model”, first described by Grant *et al.*, (Grant, *et al.*, 1973). According to this model, the cation fits into the electronegative cavity formed by alginate chains, like an egg in an eggbox as shown in Figure 3.2.

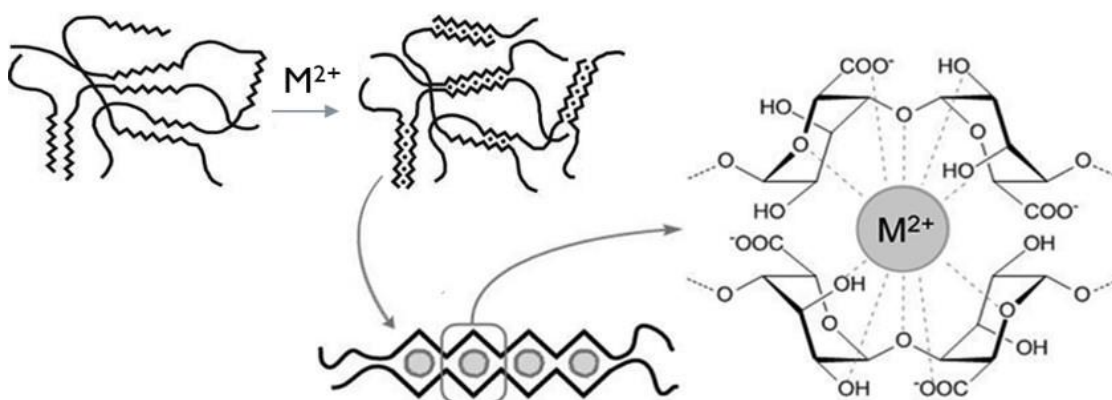


Figure 3.2: Eggbox model of ionic crosslinking between a divalent cation and sodium alginate. Adapted with permission from (Paul & Sharma, 2015).

In this study, a dual crosslinking approach that involves physical crosslinking of alginate with barium chloride (BaCl₂), as well as chemical crosslinking with epichlorohydrin (ECH), was investigated as a potential method of producing strong, yet flexible fibres that can successfully act as suture materials.

3.2.2 Crosslinking agents: Barium chloride and epichlorohydrin

It has long since been established that the crosslinking ion has a profound impact on various properties of the resulting crosslinked network, including the tensile strength, elasticity, swelling and drug release properties (Bajpai & Sharma, 2004). In 1965, Haug and Smidrøds, experimentally determined that the concentration of multivalent cations needed to induce gelation and precipitation of sodium alginate were, in increasing order (Haug, 1965):

Ba < Pb < Cu < Sr < Cd < Ca < Zn < Ni < Co < Mg

This order closely resembles the affinity of alginate for alkaline earth metals and suggests that barium chloride can lead to the formation of stable alginate gels at lower concentrations than the widely used calcium chloride (Siew *et al.*, 2005). This is desirable in the case of suture material development, as a high salt concentration will result in a more brittle fibre (Sriamornsak, 2007). Additionally, several authors have found that Ba²⁺ crosslinked alginate gels are more stable and have a higher crosslinking density and Young's modulus than Ca²⁺ crosslinked gels (Alizadeh Sardroud *et al.*, 2017; Jejurikar *et al.*, 2011; Kaygusuz *et al.*, 2016). Das and Senapati, who studied alginate microspheres made with different crosslinking agents (Ca²⁺, Ba²⁺ and Al³⁺), found that those formed with Ba²⁺ were stronger, displayed smaller voids and lower water uptake. This was ascribed to the large radius of barium (1.74 Å compared to 1.17 Å for calcium and 0.68 Å for aluminium), that can be expected to fill a large space between the alginate molecules, thus producing a tight arrangement with smaller voids (Das, 2008). The selection of BaCl₂ as physical crosslinking agent, can thus be justified on the basis that it will produce a stronger, more stable biosuture that is less prone to swelling, compared to the other available cations. Additionally, Bajpai and Sharma have shown that the small amount of barium released from crosslinked alginate is non-toxic and can easily be eliminated from the body along with other waste materials (Bajpai & Sharma, 2004).

However, physically crosslinked alginate networks, are held together by relatively weak bonds and can still swell inappropriately in body fluids that contain varying ratios of interchangeable ions (Merakchi *et al.*, 2019). This can be overcome by further crosslinking the network with a chemical crosslinker, such as epichlorohydrin (ECH), that will result in covalent bonds and successfully retain the structural integrity of the crosslinked network, even in aqueous media with a wide range of ionic strengths (Maitra & Shukla, 2014). ECH acts as a crosslinker by reacting with the hydroxyl groups on the alginate chain, through nucleophilic attack of the alcoholate anion, while a new epoxide is formed by chloride displacement, as shown in Figure 3.3 (Pawar & Edgar, 2012). Fundueanu *et al.*, found that the chemical structure of alginate microparticles, produced with ECH, were highly elastic and displayed reversible swelling, i.e., after a process of drying and reswelling the structure of the microparticles remained

unchanged (Fundueanu *et al.*, 1999). This suggests that crosslinking with ECH can convey a degree of elasticity to the biosutures and ensure, not only a lower degree of swelling, but also a reversible swelling behaviour. Asnani and Kokare showed that dual crosslinking with ECH can be used to obtain excellent sustained drug release from alginate microparticles, which further justifies its use in this study (Asnani & Kokare, 2018). Importantly, Zhao *et al.*, showed that films crosslinked with epichlorohydrin are fully biocompatible and demonstrate both good cytocompatibility and hemocompatibility (Zhao *et al.*, 2015).

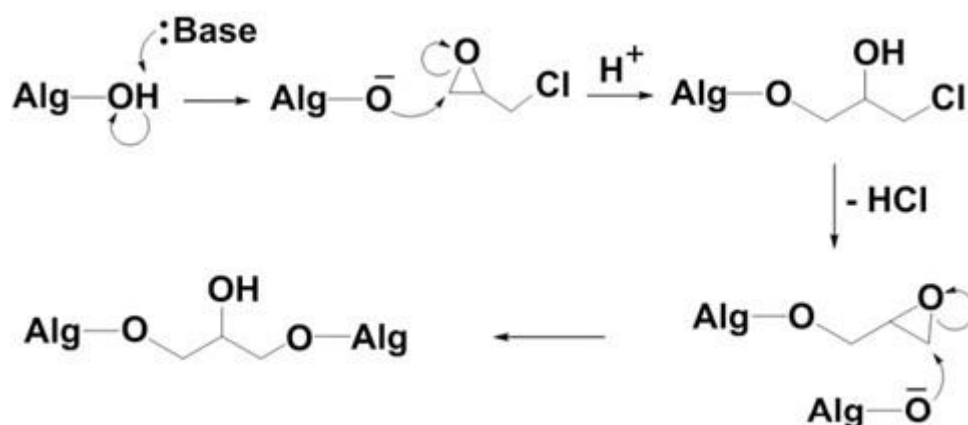


Figure 3.3: Suggested method of crosslinking between alginate and epichlorohydrin. Adapted with permission from (Pawar & Edgar, 2012).

The combination of ECH with a divalent cation like BaCl_2 is, however, crucial for biosuture fabrication. The reaction between BaCl_2 and alginate is rapid and allows for immediate solidification while the reaction between ECH and alginate is a slow and time-consuming process that does not allow any control over the morphology of the crosslinked network (Mammarella & Rubiolo, 2003). Hence, one-step, dual crosslinking process, where both crosslinkers are added to the same solution and allowed to simultaneously crosslink the polymer network, is explored in this study.

3.2.3 Reinforcing agents: Pectin, nanocellulose and gelatin

In addition to crosslinking, the alginate polymer network can easily be reinforced through the addition of more crystalline polymers such as pectin or nanocellulose, or through combination with proteins such as gelatin. Each of these polymers has a unique set of properties, that can be used to develop a novel polymer blend with selectively enhanced properties, that are not only superior to that of the individual components, but also highly suitable for biosuture material applications (Vroman & Tighzert, 2009).

Pectin is an extremely complex polysaccharide with great structural diversity but also astonishing similarity, compatibility, and synergy with alginate. Essentially, pectin consists of α -1,4-linked partially methyl-esterified α -D-galacturonic acids (Naqash *et al.*, 2017). However,

the structure of pectin also hinges on alternating ‘smooth’ and ‘hairy’ regions, where the substituted rhamnogalacturonans (RG-I and RG-II) constitute the ‘hairy’ regions, and the linear backbone of homogalacturonans (HG’s) form the ‘smooth’ regions as depicted in Figure 3.4 (Liu *et al.*, 2007). Similar to alginate, pectin can also be crosslinked by divalent cations that interact with the polygalacturonate chains of the polymer, at so-called junction zones, and can accurately be described by the same eggbox model used to define the ionic crosslinking of alginate (Kumar *et al.*, 2010). Pectin is also on equal footing with alginate in terms of its abundance in nature, biocompatibility, water-solubility and biodegradability, which make pectin a particularly suitable polymer for inclusion in this study (Bierhalz *et al.*, 2012).

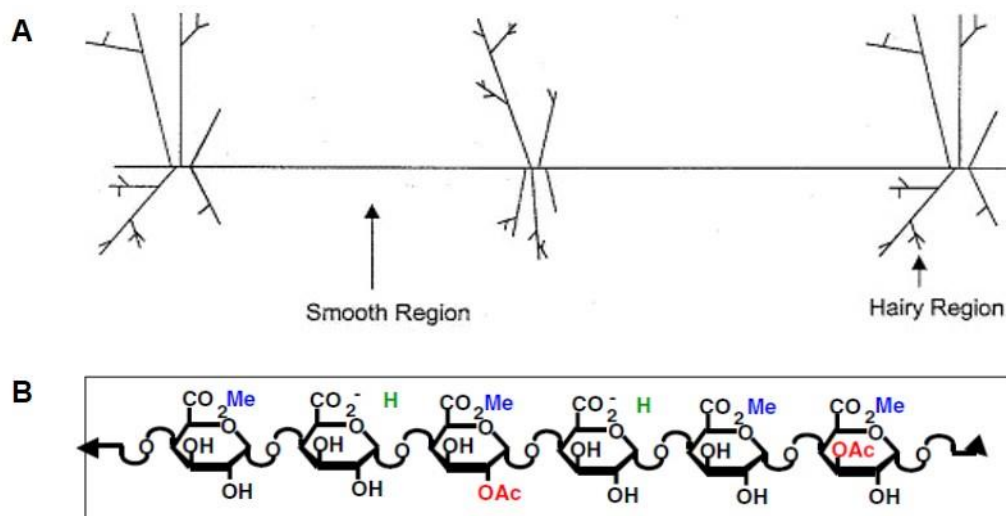


Figure 3.4: (A) Co-linear model for the organization of pectin in smooth and hairy regions. (B) The chemical structure of the smooth region – homogalacturonan. Used with permission from (Liu *et al.*, 2007).

Yet, the most important benefit of pectin is that it has the potential to improve the mechanical properties of an alginate network, if it is used in the correct concentration and ratio (Gohil, 2011). Pectin is crystalline in nature, which is evident from distinctly crystalline sharp peaks witnessed on the X-ray diffractogram of this polymer and can, therefore, be used to increase the overall crystallinity of the polymer network (Mishra *et al.*, 2008). An increased degree of crystallinity will result in a more closely packed internal structure and higher tensile strength, but also carries the risk of increased brittleness (Balani *et al.*, 2015). Excessive brittleness, however, can be circumvented by keeping the concentration of pectin aptly low and through the addition of suitable plasticizers such as glycerol.

Moreover, pectin can improve the tensile strength of the network by acting synergistically with alginate during crosslinking with divalent cations. This synergism is speculated to stem from a heterogeneous association of the poly-G blocks of alginate and the methyl ester regions of

pectin, which results in rigid ribbons (Bekhit *et al.*, 2016; Silva *et al.*, 2009; Walkenström *et al.*, 2003). Thom *et al.*, who conducted an in-depth study of the interaction between alginate and pectin, showed with the help of molecular modelling, that the poly-G and methyl ester regions, not only form rigid ribbons, but they also pack together in parallel twofold crystalline arrays (Thom *et al.*, 1982). This suggests that, if pectin and alginate are used in combination, stronger fibres with greater tensile strength can be obtained, than when the polymers are used on their own. Moreover, pectin has the same fast crosslinking potential as alginate and a greater affinity for Ba²⁺, compared to other divalent cations, just like alginate (Cernencu *et al.*, 2019). In the past, pectin has not been used for the exclusive purpose of enhancing the mechanical properties of an alginate matrix and the influence in terms of elasticity, brittleness and tensile strength remains to be seen. Indeed, at the time of this writing, there are no reports on the characterization of alginate-pectin fibres and the current study will, therefore, for the first time elucidate the characteristics of alginate-pectin fibres using different blend ratios.

Another avenue of enhancing the tensile strength of the biosuture, that will be explored in this study, is the use of a nanofiller namely, cellulose nanofibrils (CNF). Among the nanofillers available, nanocellulose has received considerable attention in the biomedical and pharmaceutical field due to its renewable nature, abundance, high elongation moduli and tensile strengths, biodegradability and excellent compatibility with other biopolymers (Chaichi *et al.*, 2017). According to Eichhorn *et al.*, CNF has been reported as one of the best biopolymer reinforcement materials due to its specific stiffness, ability to effectively reduce the interstitial spaces in the polymer network and form strong polymer-filler interactions, which significantly enhances the mechanical properties of the material (Eichhorn *et al.*, 2010). Several authors have found that the addition of CNF to films made of natural polymers, such as alginate and chitin improved, not only the tensile strength, but also the flexibility and elongation at break of the film (Chaichi *et al.*, 2017; Kanagaraj *et al.*, 2007; Li *et al.*, 2020; Meneguín *et al.*, 2017). This was ascribed to the concurrent structured and unstructured regions of nanocellulose that relate to both crystalline and amorphous phases where the first phase conveys rigidity and the other flexibility to the polymer network (Meneguín *et al.*, 2017). The addition of CNF to the biosutures might, therefore, have a favourable influence on the mechanical properties of the fibre in terms of both tensile strength and elongation at break.

Gelatin, an abundant natural protein derived from denatured collagen, is the most prominent protein of the extracellular matrix and can be employed to improve, not only the mechanical properties of the fibre, but also the *in vivo* interaction of the fibre with cells (Li *et al.*, 2008). Gelatin has a three-chain helical structure with positive, negative, and hydrophobic domains which gives it a characteristic amphoteric nature (Sakai *et al.*, 2018). As in the case of most natural polymers, gelatin displays excellent biocompatibility, ease of biodegradation and

general non-toxicity. Gelatin also has other valuable merits, such as its inexpensive nature, water solubility, good fibre forming ability and lack of antigenicity, which is often experienced with collagen (Rosellini *et al.*, 2009).

In recent years, alginate-gelatin combinations received considerable attention due to the complementary relationship between the two polymers, where the one is able to cancel out the limitations of the other and vice versa (Sarika *et al.*, 2016). A major limitation of alginate, in terms of wound healing and tissue regeneration, is that it does not actively promote cell interactions and displays a low cell adhesion rate (Wu *et al.*, 2020). This can be circumvented by the addition of gelatin, which is known to promote cellular adhesion, proliferation and differentiation, through cellular information signals, such as the Arginine-Glycine-Aspartate (RGD) sequence, present in its structure (Liao *et al.*, 2009). Alginate also displays relatively slow degradation *in vivo*, due to the lack of degrading enzymes in the human body, which can be sped up by gelatin which swells and degrades at a more rapid rate (Sarker *et al.*, 2014). Gelatin, on the other hand, has poor thermal stability and low network rigidity which significantly limits its applicability and can be improved through combination with other polymers such as alginate (Xiao *et al.*, 2001a). This strategy, where proteins are combined with polysaccharides to produce proteo-saccharides, is now considered as one of the foremost methods of improving cellular regeneration due to the high biocompatibility and close similarity of the materials to the native ECM, which primarily consists of proteoglycans (long chain polysaccharides and proteins) (Cassimjee *et al.*, 2020).

Another incentive for the combination of gelatin with alginate in this study, is its amphoteric nature which can lead to ionic interaction with anionic polysaccharides, such as alginate and pectin, under the right conditions. Xiao *et al.*, found that blends of alginate and gelatin, had improved thermal stability and mechanical properties (i.e., tensile strength and elongation at break) compared to the individual polymers. Additionally, Maud *et al.*, found that at the right concentrations and polymer ratios, alginate-gelatin blends display excellent miscibility, which is often a challenge with protein-polysaccharide combinations. In both cases, the favourable observations were ascribed to the strong interaction between alginate and gelatin that resulted from intermolecular hydrogen bonds and ionic interaction, as illustrated in Figure 3.5. This suggests that in combining alginate, and potentially pectin, with gelatin, a stronger and more thermally stable biosuture can be obtained. Yet, the degree of interaction will have to be monitored to ensure that excessive gelation does not occur prior to crosslinking of the biosuture.

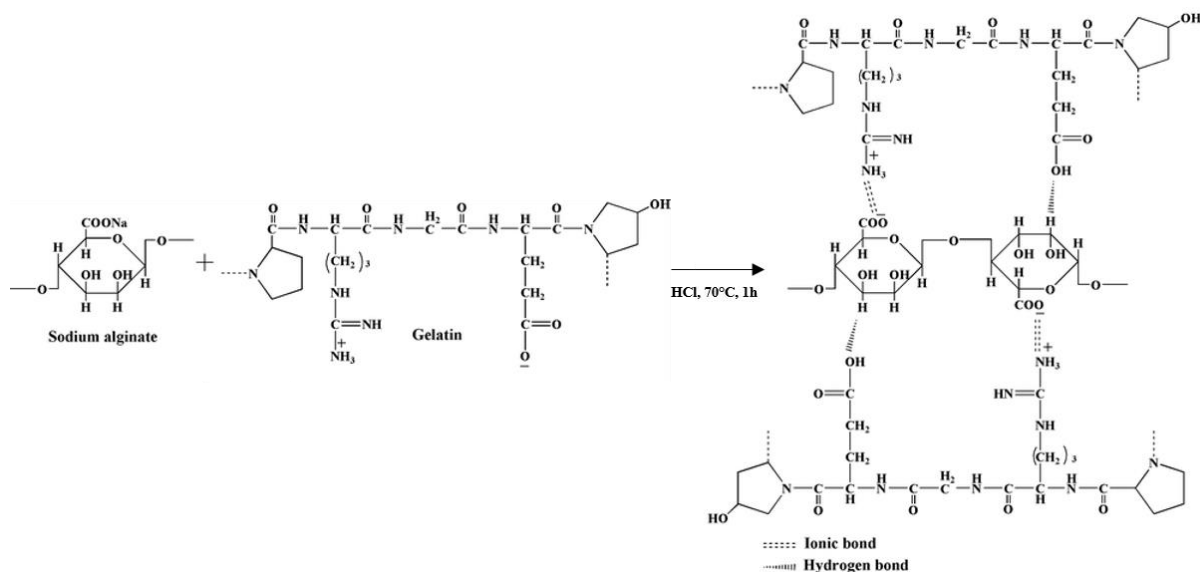


Figure 3.5: Structural representation of how ionic interaction and hydrogen bonding can take place between sodium alginate and gelatin. Adapted with permission from (Samp, 2017).

3.2.4 Plasticizers: Polypropylene glycol, triethyl citrate and glycerol

Natural polymer networks, especially those consisting of carbohydrates like sodium alginate, where the network is tightly held together by an abundance of hydrogen bonds, are rigid and brittle in nature. Consequently, these networks require the addition of a suitable plasticizer to improve their overall mechanical performance (Thakhiew *et al.*, 2010). Plasticizers are small molecules of substantially low volatility that, when added to a polymeric material, changes certain physical and chemical properties of that material (Sanyang *et al.*, 2015). Several theories have been proposed to explain the mechanism of plasticizer action (e.g. the 'lubricating theory', 'gel theory' and 'free volume theory') but the general consent is that these small molecules disrupt the original hydrogen bonds, or other forces holding the polymer chain together, to increase the mobility of the polymer chain (Ullah & Wu, 2013). The addition of plasticizers, therefore, decreases the tensile strength and young's modulus of the material while increasing the percentage elongation at break. In effect, the plasticizer makes the material weaker but easier to deform and bend, thereby adding to the toughness of the material. Hence, the optimum plasticizer content is a compromise between acceptable material strength and adequate material flexibility (Kunanopparat *et al.*, 2008).

The type of plasticizer selected, as well as its concentration, will affect the mechanical properties of the final material (Sanyang *et al.*, 2015). Polyols, particularly glycerol and sorbitol, are the most widely studied and commonly used plasticizers. They are especially favoured because of their non-volatile nature, hydrophilicity, non-toxicity and low cost (Silva *et al.*, 2009). In this study, we will investigate several plasticizers, including polypropylene glycol, triethyl citrate and glycerol, for their plasticizing effect on the biosutures. Yet, according to

Thakhiew *et al.*, plasticizer concentration is the most important parameter for the plasticizing effects of a polymer network (Thakhiew *et al.*, 2010). This was confirmed by Da Silva *et al.*, who showed that a very narrow range of plasticizer concentration (4-10%) will yield alginate films with acceptable mechanical properties. Films with plasticizer concentrations lower than 3% were brittle, while concentrations over 12% led to phase separation of the alginate films (Silva *et al.*, 2009). Therefore, care will be taken in this study to find the optimal plasticizer concentration that will result in biosutures with both adequate tensile strength and flexibility.

3.3 Materials

Sodium alginate, pectin from citrus peel, gelatin, and epichlorohydrin was purchased from Sigma-Aldrich (St. Louis, MO, USA). Barium chloride 2-hydrate and glycerol (Mw=92.1g/mol) was purchased from LabChem (Founders hill, Johannesburg, SA), and nanocellulose from DLD Scientific (Durban North, SA).

3.4 Methods

3.4.1 Polymer characterization by Fourier Transform Infrared Spectroscopy (FTIR)

Before initiating the design and fabrication of a novel suture material or drug delivery device, it is appropriate to first do a basic characterization of the polymers that will be used. Fourier Transform Infrared Spectroscopy (FTIR) is a non-destructive, rapid and easily employed technique to obtain valuable information about the chemical structure of polymers (Fan M, Dai D, 2012). For each of the four polymers investigated (i.e. sodium alginate, pectin, nanocellulose and gelatin), there is a specific property that will have a profound influence on its behaviour in the biosuture (Kulkarni *et al.*, 2012). These are the M/G ratio of alginate, the degree of esterification (DE) of pectin, the crystallinity index (CI) of nanocellulose, and the secondary structure of gelatin. Each of these properties were investigated using FTIR while the isoelectric point (PI) of gelatin was also determined through measurement of the protein's zeta-potential.

FTIR spectra of the pristine polymers were obtained using a PerkinElmer Spectrum 2000 ATR-FTIR (Waltham, MA, USA) fitted with a single-reflection diamond MIRTGS detector, with 64 scans taken at a wavenumber range of 4000 – 650 cm^{-1} . A simplified method, described by Sakugawa *et al.* and reported elsewhere (Mndlovu *et al.*, 2019a; Sakugawa *et al.*, 2004), was used to calculate the mannuronic acid and guluronic acid ratio (M/G) of sodium alginate from its FTIR spectra. Briefly, 600 mg of sodium alginate was dissolved in deionized water to obtain a 3% (w/v) aqueous solution of the sample. The solution was ejected through a syringe into a BaCl_2 (2% w/v) solution and left to crosslink for 1 hour, after which the precipitated alginate salt was collected and lyophilized. The FTIR spectra of three samples were recorded in absorbance with measurements repeated in triplicate. The mean value of absorbance strength

at the appropriate bands (A_{1023}/A_{1080}) was used to calculate the M/G ratio of each of the three alginate samples using Equation 3.1. The average M/G ratio of the three samples was taken as the final M/G ratio of the alginate sample.

$$\text{Alginate M/G ratio} = A_{1023}/A_{1080} \quad \text{Equation 3. 1}$$

The degree of esterification of pectin was determined according to a method described by Gnanasambandam and Proctor (Gnanasambandam, R., Proctor, 2000) and validated by Monsoor *et al.*, as well as Kohn *et al.*, who confirmed that the degree of esterification of pectin can be determined with an absolute error $\pm 1.3\%$ using FTIR (Filippov *et al.*, 1978; Monsoor *et al.*, 2001). Briefly, the FTIR spectra of a sample of unprocessed pectin powder was obtained in triplicate using the same parameters described above. The peak positions, peak height and peak areas representing the esterified and non-esterified carboxyl groups of pectin (at 1747 cm^{-1} and 1639 cm^{-1} respectively) were accurately determined using Spectrum™ 10 STD software. The degree of esterification (DE) was calculated using Equation 3.2.

$$\text{DE (\%)} = [A_{1747} / (A_{1747} + A_{1639})] \times 100 \quad \text{Equation 3. 2}$$

According to Ioelovich, M., IR-spectroscopy can be used to evaluate the crystallinity of nanocellulose samples by measuring the relative height of peaks (Ioelovich, 2017). A method proposed by Nelson and O'Connor, where the infrared ratio of peak heights at 1420 cm^{-1} and 2900 cm^{-1} is used to estimate the CI of nanocellulose, was employed (Nelson & O'Connor, 1964). Accordingly, the FTIR spectra of pristine nanocellulose was obtained using the same parameters described earlier and the CI determined according to Equation 3.3.

$$\text{CI} = \alpha_{1372 \text{ cm}^{-1}} / \alpha_{2900 \text{ cm}^{-1}} \quad \text{Equation 3. 3}$$

FTIR is also an established technique for characterizing protein structure, and especially for determining the secondary structure of proteins like gelatin (Yu, 2006). Table 3.2 provides typical band assignments for protein secondary structures and will be used to derive the secondary structure of the gelatin, used in this study. The amide I region is most commonly used for secondary structure determination, as the peak is typically the strongest absorbing peak of proteins. However, this strong peak, in the $1600 - 1700 \text{ cm}^{-1}$, region, also overlaps with an absorbance band of water which can make accurate analysis difficult (Bier *et al.*, 2013). The amide III region ($1200 - 1350 \text{ cm}^{-1}$), which is weaker than the amide I region, but equally sensitive to structural changes and not subject to interference, was therefore used to verify the secondary structure (Cai & Singh, 1999). Peaks of amide I and III were deconvoluted using the software Origin Pro 8.5 and the second derivative method, to reveal individual peaks in the relevant IR regions.

Table 3.2: Band assignments for the determination of protein secondary structures.

Region	Secondary structure	Band assignment (cm ⁻¹)
Amide I	Antiparallel β -sheet/ aggregated strands	1675–1695
	α – Helix	1648–1660
	Unordered	1640–1648
	β - Sheet	1625–1640
	Aggregated strands	1610–1628
Amide III	α – Helix	1295–1330
	β - Turns	1270–1295
	Random coils	1250–1270
	β - Sheet	1220–1250

Additionally, the isoelectric point (PI) of gelatin, which may be defined as the pH value at which the global charge of the molecule is null, was also determined (Macovescu *et al.*, 2018). PI is one of the most important parameters to reflect the molecular structure of amphoteric substances and can also be used to deduct the type (A or B) of gelatin (Zhang *et al.*, 2018). Gelatin that is obtained through an acid pre-treatment (gelatin type A) has a PI of 7 – 9 while gelatin prepared using a base (gelatin type B) has a PI of 4.7 – 5.4 (Siburian *et al.*, 2020). We determined the PI of gelatin used in this study according to a validated method that was developed by Macovescu *et al.*, and shown to have an accuracy of 99.8121% (Macovescu *et al.*, 2018). Briefly, solutions of 0.1 M sodium acetate, 0.1 M acetic acid and gelatin were added to six test tubes, according to proportions given in Table 3.3.

Table 3.3: Proportions of solutions required to measure the isoelectric point of gelatin.

Added reagents (mL)	Test tube number					
	1	2	3	4	5	6
0.1 M Sodium acetate	2	2	2	2	2	1.2
0.1 M Acetic acid	0.25	0.5	1	2	4	4.8
Distilled water	3.75	3.5	3	2	-	-
0.1% Gelatin solution	2	2	2	2	2	2

The pH of solutions was measured using a pH-meter (Mettler-Toledo, Greisensee, Switzerland) before and after the addition of 1% gelatin solutions in order to see the variation it causes. The zeta-potential of each test tube was measured using the ZetaSizer NanoZS (Malvern Instruments Ltd., Worcestershire, UK) with a 40 V field applied over a 10 mm electrode spacing at 25°C. The zeta-potential was plotted against pH variation and the data

extrapolated to obtain the isoelectric point at a potential of 0 mV. Three repeated measurements were performed on each sample and the average calculated. Additionally, methyl alcohol (10 mL) was added to each test tube to highlight the isoelectric point by means of turbidity.

3.4.2 Determination of the fibre forming ability of sodium alginate

The ability of sodium alginate to form suitable biosutures in the presence of the selected crosslinkers, namely BaCl₂ and ECH, was evaluated. Fibres of varying alginate concentrations (1%, 2%, 4%, 6%, 8% and 10% w/v, respectively) were prepared by dissolving the appropriate amount of sodium alginate in deionized water. The solutions were extruded into a crosslinker solution of BaCl₂ (1% w/v) and ECH (1% v/v) using a 10 mL syringe fitted with a 23 G needle and left to cure for 30 minutes. The resultant fibres were washed repeatedly, using baths of deionized water, and left to air dry in ambient conditions (25°C; 50% relative humidity). The fabricated fibres were observed and factors such as extrudability of the solution and morphology of the fibres, noted.

3.4.3 Methods of biosuture fabrication

Three different methods of suture fabrication were investigated, yet the chemistry and basic principles behind the fabrication process remained the same. Fibres were formed by extruding an alginate-based polymer solution, through a syringe and needle, into a crosslinker bath. As soon as the polymer solution came into contact with the crosslinker solution, the cations in the latter formed bonds between the polymer chains, which resulted in a more rigid, insoluble polymer matrix. The suture-like fibre morphology was the result of the combination of constant pressure applied to the plunger and spiral-shaped movement of either the crosslinker bath or the syringe. The three methods of extrusion that were investigated are:

- i. Extrusion via hand.
- ii. Extrusion via the 3D Bioplotter® (EnvisionTec, GmBH, Germany).
- iii. Extrusion via the Texture Analyser (TA.XTplus, StableMicroSystems, England).

For extrusion via hand, the polymer solution was loaded into a 5 mL luer-lock syringe, fitted with a 23 G needle, and manually extruded into a beaker with the crosslinker solution as shown in Figure 3.6. While pressure was being applied to the plunger, the syringe was simultaneously moved in a circular motion to allow for effective fibre formation.

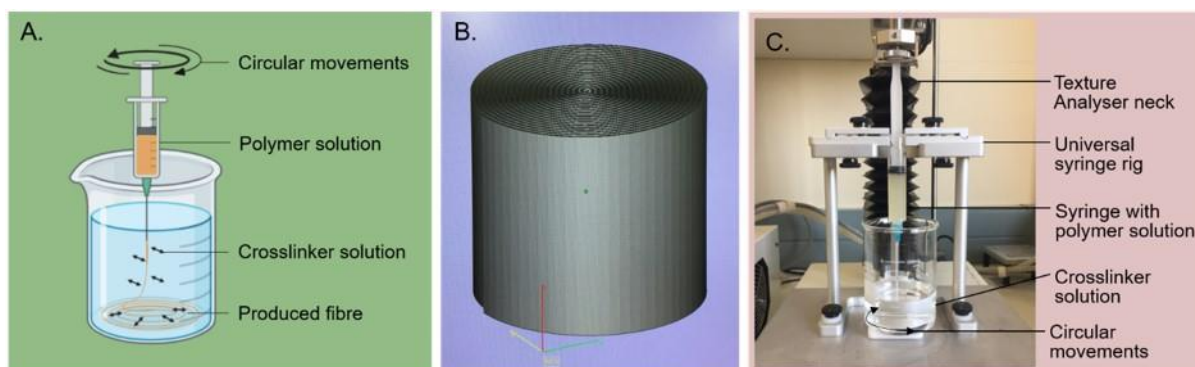


Figure 3.6: A) Graphical representation of suture fabrication via hand. B) 3D spiral design used to extrude the polymer solution via the 3D Bioplotter. C) Texture Analyser setup during suture fabrication and polymer extrusion using the universal syringe rig.

Prior to extrusion with the 3D Bioplotter, a unique spiral design was created using AutoCAD® (Autodesk) design software, which was then resized and sliced using Magics® V18 design software equipped with EnvisionTec® printing protocols (Figure 3.6 B). The polymer solution was loaded into a 3D Bioplotter syringe, fitted with a 23G needle tip, and inserted into the low temperature printing head of the 3D Bioplotter® (EnvisionTec, GmbH, Germany). Printing was executed directly into a petri dish, filled with the crosslinker solution, at a constant pressure of 0.7 bar and a speed of 70 mm/sec and a pre-flow and post-flow timing of 0 sec.

A special syringe rig (Universal Syringe Rig, A/USR, Stable Micro Systems, England) was used for extrusion via the Texture Analyser. The Texture Analyser setup is shown in Figure 3.6 C. The polymer solution was loaded into a 3 mL luer-lock syringe, fitted with a 23 G needle and the syringe secured onto the rig, using the provided clips. The Texture Analyser was set in the compression mode using the standard return to start T.A. sequence, with button mode as the trigger type and a distance of 30 mm as the target mode. An initial high-speed setting was used (2 mm/sec) to push the polymer solution through the needle and help unclog the tip. Once a proper flow was established, a lower speed of 0.6 mm/sec was used and the beaker, containing the crosslinker solution, moved in a circular direction.

After extrusion, all fibres were left to cure in the crosslinker solution for approximately 30 minutes after which they were washed repeatedly using five clean deionized water baths to remove any residual crosslinker from the fibres. The fibres were then placed on large ointment tiles and left to dry in ambient conditions ($25 \pm 2^\circ\text{C}$ and 50% relative humidity), until they reached a constant diameter (± 40 minutes).

3.4.4 Tensile testing procedure

Before tensile testing was initialized, the diameter of each biosuture formulation was measured using digital vernier callipers. The diameter was measured three times (N=3) along the active

length, at points corresponding to one-fourth, one-half and three-fourths of the fibre length, as described by the USP suture diameter standard (*Sutures—Diameter. United States Pharmacopeia and National Formulary (USP 29-NF 24)*). Tensile testing was performed with the Texture Analyser (TA.XTplus, Stable Micro Systems, England) in the tension mode and equipped with miniature tensile grips (A/MTG, Stable Micro Systems, England). The 5 kg load cell was calibrated prior to all tests. Biosutures were secured in the middle of the grips with a standard suture gauge length of 4 cm. All tests were performed under displacement control at a crosshead speed of two times the active gauge length (80 mm per minute) as specified by the USP standards for tensile testing (*Tensile Strength. United States Pharmacopeia and National Formulary (USP 29-NF 24)*).

For each biosuture formulation, a total of twenty biosutures (N=20) were tested using two configurations: straight-pull test (N=10) and knot-pull test (N=10), where a single overhand throw knot was placed in the centre of the biosuture. In all cases, failure occurred at the centre of the active length, indicating that the gripping points did not affect the results. Load (N) and elongation (mm) were collected throughout testing until failure and the average calculated for each formulation. The results were initially presented and analysed as load vs. displacement, as this is the most common method of presenting mechanical property data of suture materials (Naleway *et al.*, 2015). Additionally, the load data was converted to engineering stress by dividing the applied load (P), by the initial cross-sectional area (A). The displacement data was converted to engineering strain by dividing the change in active length (Δl) by the original active length (l_0). In certain cases, the young's modulus and toughness of the fibres were also calculated as the initial slope of the stress vs. strain curve and the area under the curve (AUC) of the stress vs. strain curve, respectively.

3.4.5 Influence of formulation components and processing conditions on the mechanical properties of the biosuture.

3.4.5.1 Pure sodium alginate biosuture

Biosutures consisting of sodium alginate, 6% w/v, alone were prepared according to the Texture Analyser method described in Section 3.4.3. The mechanical properties were evaluated as described in Section 3.4.4 and used as a baseline to compare all other biosuture formulations with.

3.4.5.2 Addition of a suitable plasticizer

Three different plasticizers namely, glycerol, polypropylene glycol and triethyl citrate were investigated for potential inclusion in the biosuture formulation, but only glycerol was found to be a viable option. Polypropylene glycol and triethyl citrate failed to plasticize the biosutures and hence, only glycerol was further investigated at different concentrations (2, 4, 6, 8 and 10%) to find a suitable concentration that will yield flexible, yet strong biosutures. Five polymer

solutions were prepared to have a final alginate concentration of 6% w/v and glycerol added to each solution according to the concentrations stated above. The polymer solutions were mechanically stirred for approximately 15 minutes until a homogenous mixture was obtained. Biosutures were then prepared from the polymer solutions according to the Texture Analyser method described in Section 3.4.3 and the mechanical properties evaluated as described in Section 3.4.4.

3.4.5.3 Addition of pectin as reinforcing agent

The same basic procedure used previously, was followed to fabricate the pectin reinforced biosutures but with different concentrations of pectin (2, 1, 0.5, 0.4, 0.3, 0.2 and 0.1% w/v respectively), first dissolved in deionized water through high-speed mechanical stirring and slight heating (30°C) on a hotplate magnetic stirrer (United Scientific, Goodwood, South Africa). Once cooled down, the pectin solutions were added to pre-dissolved sodium alginate solutions to yield a final alginate concentration of 6% w/v. Solutions were again mechanically stirred to obtain a homogenous mixture and the biosutures prepared according to the Texture Analyser method described in Section 3.4.3. The texture analyser continually records the force required to extrude the loaded hydrogel into the crosslinker and this data was analysed to compare the extrudability of the alginate solution, with and without the addition of pectin. The mechanical properties of the pectin reinforced biosutures were evaluated as described in Section 3.4.4.

3.4.5.4 Addition of nanocellulose as reinforcing agent

Biosutures were reinforced with 1, 0.5 and 0.25% w/v nanocellulose, respectively and the influence on the mechanical properties of the biosutures investigated. Prior to fabrication of the nanocellulose reinforced fibres, the nanoparticles were dispersed in deionized water and ultrasonicated (Ultrasonic Cleaner, SE-366, Scientech, India) for 30 minutes to ensure proper distribution of the nanofibers. The nanocellulose was then added to alginate solutions which was first mechanically stirred and then ultrasonicated for an additional 15 minutes to obtain a homogeneous polymer blend of 6% w/v alginate and the respective concentrations of nanocellulose. Biosutures were again prepared according to the Texture Analyser method described in Section 3.4.3 and the mechanical properties evaluated as described in Section 3.4.4. Images were taken of the hydrated cellulose fibrils using a Confocal Laser Scanning Microscope (CLSM, Leica Microsystems, Wetzlar, Germany) and the surface morphology of the nanocellulose reinforced fibres studied with a stereomicroscope (Olympus SZX – ILLD2-200, Olympus Corporation, Tokyo, Japan).

3.4.5.5 Addition of gelatin as reinforcing agent

Four concentrations of gelatin (i.e., 4, 3, 1.5 and 0.75% w/v) were investigated for their ability to improve the mechanical properties of the biosutures. Similar to pectin, the gelatin solutions were separately prepared through mechanical stirring and heating (30°C). The gelatin solutions were immediately added to pre-dissolved alginate (final concentration of 6% w/v) without prior cooling to prevent early setting of gelatin. The alginate-gelatin mixtures were mechanically stirred for 15 minutes to obtain a homogenous blend and biosutures prepared according to the Texture Analyser method described in Section 3.4.3. The mechanical properties were evaluated as described in Section 3.4.4.

3.4.5.6 Selection of the appropriate crosslinker concentration.

Biosutures were fabricated according to the Texture Analyser method described in Section 3.4.3, using a 6% sodium alginate solution reinforced with 0.1% pectin and 3% gelatin and plasticized with 4% glycerol. The effect of different crosslinker types and concentrations were evaluated against the latest biosuture formulation and not alginate alone in order to find the best crosslinker concentration for the final polymer blend. For the crosslinker solution, different concentrations of BaCl₂ and ECH were evaluated, as shown in Table 3.4. The mechanical properties were evaluated as described in Section 3.4.4.

Table 3.4: Different concentrations of BaCl₂ and ECH used to crosslink the polymer blend and produce biosutures.

Formulation	BaCl ₂ (% w/v)	ECH (% _{v/v})
A	1	0.5
B	2	0.5
C	4	0.5
D	2	-
E	2	0.25
F	2	0.5
G	2	1

3.4.5.7 Selection of the optimal drying method

Biosutures were fabricated according to the Texture Analyser method described in Section 3.4.3, using a 6% sodium alginate solution reinforced with 0.1% pectin and 3% gelatin and plasticized with 4% glycerol. Three different drying methods were investigated namely, normal air drying at room temperature (25 ± 2°C and 50% relative humidity), under lamellar flow in a fume hood, and at 35°C in a universal oven (Memmert, GmbH, Schwabach). Biosutures were dried until a constant diameter was achieved and kept in a desiccator until mechanical testing, which was performed as described in Section 3.4.4.

3.5 Results and discussion

3.5.1 Polymer characterization by Fourier Transform Infrared Spectroscopy (FTIR)

The FTIR spectra of sodium alginate, pectin and nanocellulose, with the most significant absorption bands visible, is provided in Figure 3.7. All three spectra show a broad, intense absorption band between 3600 and 3000 cm^{-1} , that can be related to -OH stretching vibrational modes present in all three carbohydrate polymers. For alginate, two characteristic bands were observed at 1594 and 1405 cm^{-1} , which can be ascribed to the asymmetric and symmetric stretching vibrations of the carboxylate salt ion ($-\text{COO}^-$), respectively. The later bands are highly significant and often used in the characterization of alginate and its derivatives. The bands observed at 1107 and 935 cm^{-1} were attributed to the C-O stretching vibration of the pyranosyl ring with contributions from C-C-H and C-O-H deformations. Peaks observed at 1080 and 1023 cm^{-1} respectively, represent the mannuronic and guluronic units of sodium alginate and the absorbance at these wavenumbers was used to calculate the M/G ratio of Ba^{2+} crosslinked sodium alginate as described in literature (Sakugawa *et al.*, 2004).

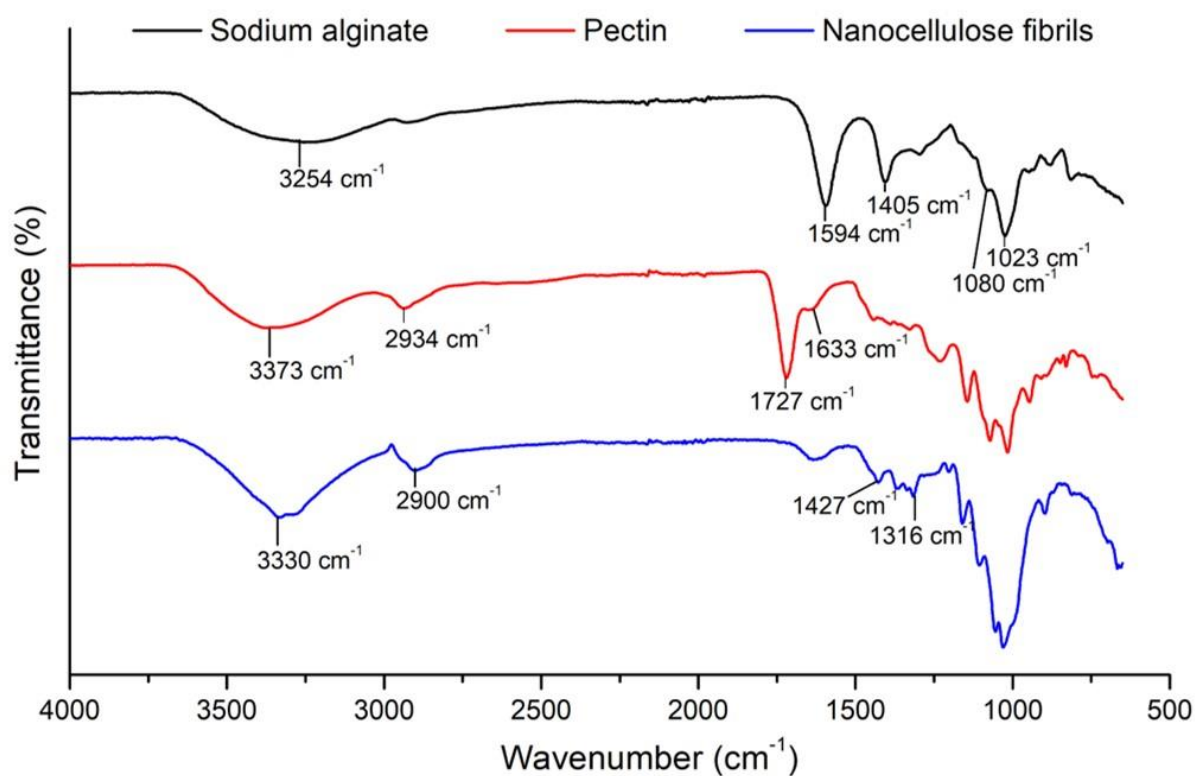


Figure 3.7: FTIR spectra of sodium alginate, pectin and nanocellulose fibrils.

The M/G ratio of sodium alginate was calculated as 1.45 (Table 3.5), which shows that this specific alginate sample has a higher mannuronic than guluronic acid content and will form more elastic fibres after crosslinking, due to the structural conformation of the M-block regions. As shown in Figure 3.1, the G-blocks have considerable steric hinderance around the carboxyl groups that leads to a rigid, folded structural conformation, while the linear M-block linages

result in a more flexible, ribbon-like chains (Yang *et al.*, 2011). This reaffirms that substantial steps need to be taken to improve the rigidity and tensile strength of the alginate sample. Table 3.5 shows the absorbance of three sodium alginate samples, the respective M/G ratios and the average M/G ratio of the sodium alginate used in this study.

Table 3.5: Calculation of the M/G ratio of sodium alginate.

Sample	Wavenumber (cm ⁻¹)	Absorbance	Wavenumber (cm ⁻¹)	Absorbance	M/G ratio
1.	1080	0.20	1023	0.29	1.45
2.	1080	0.26	1023	0.38	1.4615
3.	1080	0.16	1023	0.23	1.4375
Average					1.4496

In addition to the broad absorption band at ~3400 cm⁻¹, the FTIR spectrum of pectin displayed a band of moderate intensity at 2934 cm⁻¹ that was ascribed to CH, CH₂ and CH₃ stretching and bending vibrations. The strong absorption band observed at 1727 cm⁻¹ can be ascribed to the ester carbonyl (-COCH₃) groups, while the two moderate peaks at 1633 and 1400 cm⁻¹ represent the asymmetric and symmetric stretching of the carboxylate ion (-COO⁻). Kohn *et al.*, showed that, in the absorbance setting, the area under the latter peaks can be used to determine the degree of esterification of pectin with absolute error ± 1.3%. The DE of pectin was calculated as 86.44% and Figure 3.8 shows the spectrogram of pectin with the applicable wavelengths and areas. The sample can, therefore, be classified as a high methoxyl pectin (HMP) with more than 50% of the carboxyl groups being methyl esterified (Jindal *et al.*, 2013). This suggests that gelation of the polymer will be rapid and mostly based on hydrogen bonds and hydrophobic interactions at the methyl ester groups (Sharma *et al.*, 2006).

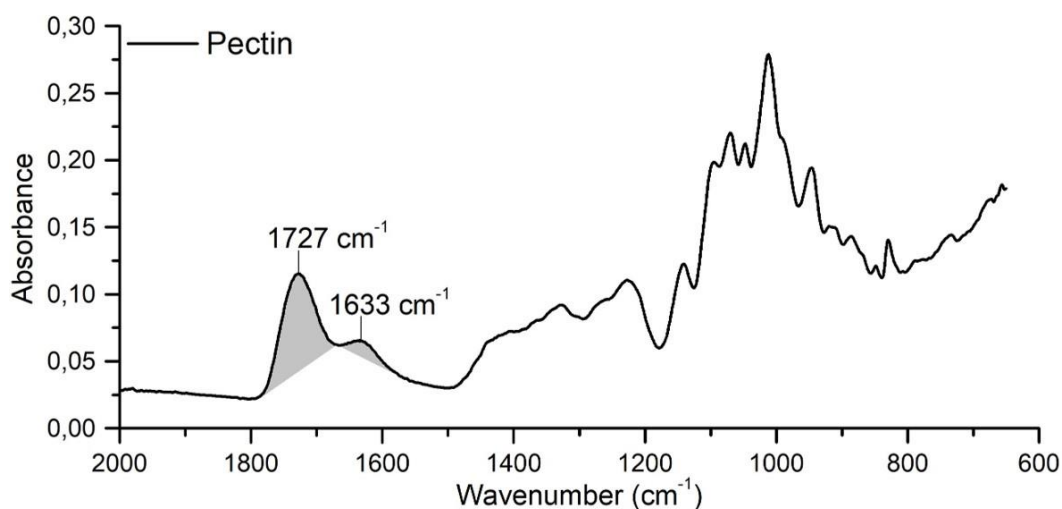


Figure 3.8: FTIR spectrum of pectin showing the peaks used to determine the degree of esterification of the polymer.

In the FTIR spectra of nanocellulose, the broad absorption band in the region of 3330 cm^{-1} which represents the -OH stretching vibrations, overlaps with the band at 3319 cm^{-1} , which can be ascribed to the stretching frequency of the -COO group. The band observed at 2900 cm^{-1} can be attributed to the stretching of the -CH of the saturated aliphatic structure of cellulose. The bands around 1427 and 1316 cm^{-1} can be assigned to -CH₂ scissoring and -OH bending vibrations, respectively while the broad band at 1030 cm^{-1} is representative of the CH-O-CH₂ stretching. The crystallinity index of the nanocellulose fibrils was found to be 0.52, which is in line with values reported in literature and predictably lower than that of nanocellulose crystals (Nelson & O'Connor, 1964; Sacui *et al.*, 2014).

As shown in Figure 3.9, the IR spectrum of gelatin displayed major peaks in all the expected amide regions: 3284 cm^{-1} (amide A), 2940 cm^{-1} (amide B), 1633 cm^{-1} (amide I), 1523 cm^{-1} (amide II) and 1234 cm^{-1} (amide III). Similar spectral bands were observed by Cebi *et al.*, and Almeida *et al.*, (Almeida *et al.*, 2012; Cebi *et al.*, 2016). The broad absorption peak at 3284 cm^{-1} , can be attributed to the stretching vibration of O-H bound to N-H groups in the amide A region. The amide B peak suggests the interaction of -NH₃ groups between peptide chains. Among the amide I, amide II and amide III absorption bands, the amide I vibration is primarily due to a C=O stretching vibration coupled to contributions from the C-N stretch, with C-C-N deformation and in-plane N-H bending modes. The amide II vibration modes can be ascribed to an out-of-phase combination of C-N stretching and in-plane N-H deformation modes of the peptide group (glycine backbone and proline sidechains). The amide III band, on the other hand, represents the combination of peaks from C-N stretching vibrations and N-H deformation from the amide linkages, as well as absorption bands arising from the wagging vibrations of C-H₂ groups in the glycine backbone and proline sidechains.

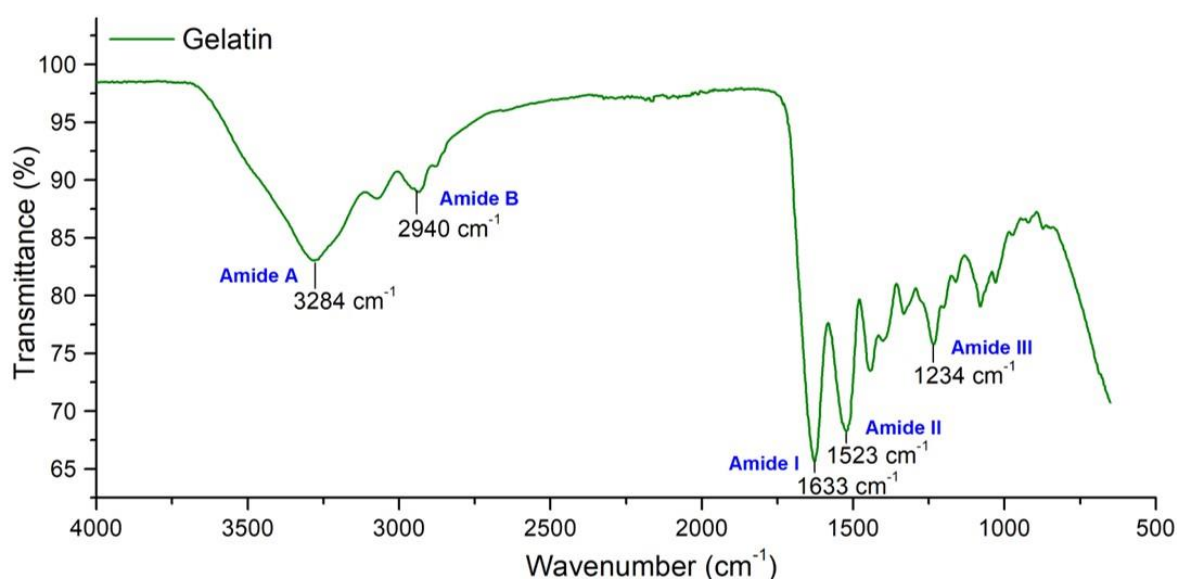


Figure 3.9: FTIR spectrum of gelatin, showing all major amide regions.

The secondary structure of a protein, plays an important structural or architectural role in the protein and has a direct impact of the mechanical properties thereof (Takano *et al.*, 2016). The three most common secondary structures are the α -helix, β -sheet, and random coil. These secondary structures, which normally vary throughout the polypeptide chain, arise from molecular interactions, in particular hydrogen bonds, between adjacent amino acids (Yang *et al.*, 2015). In comparison with the other secondary structures, β -sheets have a higher number of hydrogen bonds, due to full utilization of the hydrogen bonding capacity of the polypeptide backbone and can lead to stronger interchain interactions and hence stronger materials. Spider silk, for example, as well as other strong natural fibrous proteins, are known to have a higher β -sheet content than α -helices which is said to improve the mechanical properties of the material (Bortolini *et al.*, 2015). The deconvoluted peaks of the FTIR spectrum of amide I and amide III, shown in Figure 3.10, revealed a high β -sheet content combined with lower quantity of α -helices. This may be due to thermoplastic processing, which is known to increase the β -sheet content of polymers at the expense of α -helices. The β -sheet content of the gelatin, procured in this study, indicates that the polymer will have noteworthy mechanical strength that can potentially serve to improve the mechanical properties of the alginate biosutures.

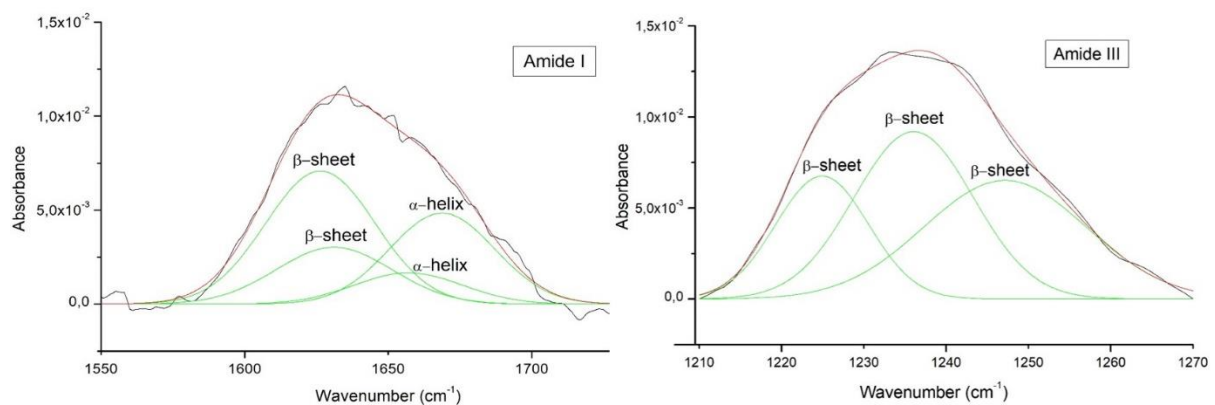


Figure 3.10: Gaussian deconvolution of the FTIR spectra of amide I and amide III of gelatin, as obtained by means of the second derivative method. The sum of the fitted curves is shown as a red line, closely overlapping the experimental data trace, which is shown as a full black line. The secondary structure, as derived from Table 3.2, is indicated above each peak.

The isoelectric point (PI) of gelatin was determined as 5.198, which indicates that the gelatin sample, used in the study, is a type B gelatin, obtained through treatment with a base. This would imply that the asparagine and glutamine amino acids of gelatin are almost completely converted to aspartic and glutamic acids respectively, and therefore, differ from the amino acid composition of original collagen (Liu *et al.*, 2020). This slight deviation in structure from native collagen, adds to the nonimmunogenicity and lack of antigenicity of the polymer and affirms the safety of its use in the study (Aramwit *et al.*, 2015). Figure 3.11 shows the pH of each test

tube before and after addition of gelatin (pH_0 and pH_1), the zeta-potential results, PI point as well as a graphical representation of the PI point determination of gelatin. A variation in pH in the range of 0.03 to 0.04 pH units, before and after the addition of pectin as was seen in this study, demonstrates stability of gelatin in the buffer solutions used.

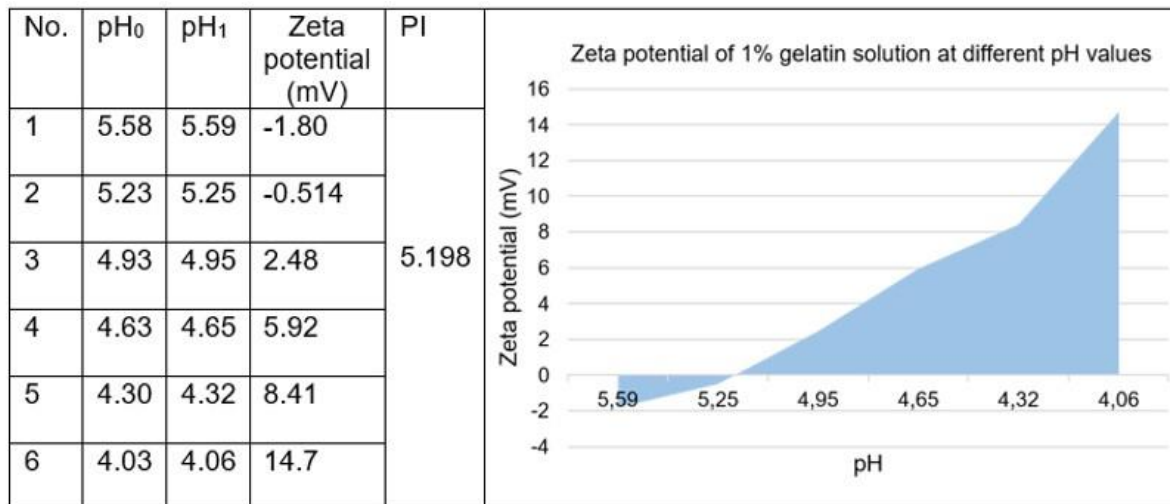


Figure 3.11: The pH of solutions before and after the addition of gelatin; the corresponding zeta-potential and the PI of gelatin with a graphical representation of its determination.

The isoelectric point can also be highlighted through the addition of methanol and consequent changes turbidity of the solutions, with maximum coagulation occurring at the pH nearest to the isoelectric point. Alcohol binds and extracts the water that normally hydrates protein molecules, leading to water-free micelles that flocculate. As shown in Figure 3.12, the highest degree of flocculation was seen in test tube 2 with pH 5.25, which is the measured pH closest to the calculated isoelectric point of gelatin and confirms the extrapolated data.

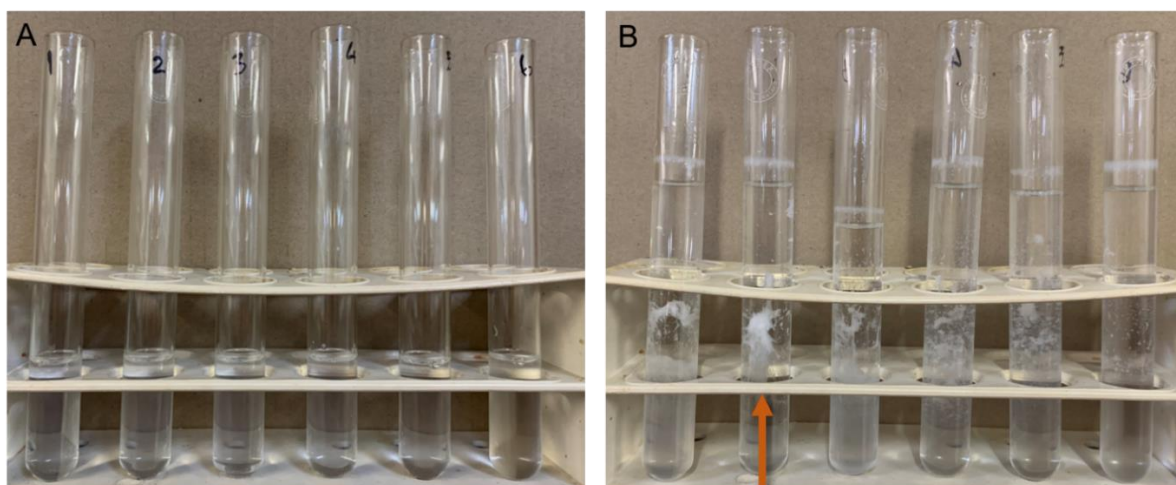


Figure 3.12: A) Test tube 1 – 6 presenting as clear solutions before the addition of methanol. B) Test tubes 1 – 6 with different degrees of flocculation after the addition of methanol. Arrow indicates maximum flocculation in test tube 2 (pH 5.25).

3.5.2 Determination of the fibre forming ability of sodium alginate

Solutions of different alginate concentrations were prepared and crosslinked to identify a concentration range that will yield adequate biosutures. Once sodium alginate came into contact with the cations in the crosslinker solution, it immediately solidified and formed fibres, due to the synergistic movement of the syringe and pressure on the plunger. Table 3.6 provides information on the characteristics of the fibres that were produced with different alginate concentrations. At concentrations below 4% w/v, fibres were crinkled and non-uniform, while concentrations above 8% w/v were difficult to extrude and resulted in clumped, short fibres (Figure 3.13). A concentration range of 4 – 8% w/v was determined as suitable for biosuture fabrication and a concentration of 6% w/v sodium alginate was used for further preliminary studies in this chapter.

Table 3.6: Observations made for fibres of varying sodium alginate concentrations while in the crosslinker solution and after being air dried.

Alginate (% w/v)	Observation	
	Extruded into crosslinker	Air dried
1	Fibres were crinkled and formed a web like mesh.	No adequate fibres were formed.
2	Fibres were thick, crinkled, and non-uniform.	Fibres were weak and broke instantly when handled.
4	Fibres were adequate but slightly crinkled and non-uniform.	Fibres maintained their structure when handled.
6	Adequate, straight, and uniform fibres.	Fibres were relatively strong and flexible but broke when strongly pulled.
8	Fibres were adequate but clumped slightly.	Fibres were robust and strong.
10	Fibres were short, clumped, and difficult to extrude due to the high viscosity of the solution.	No adequate fibres were formed.

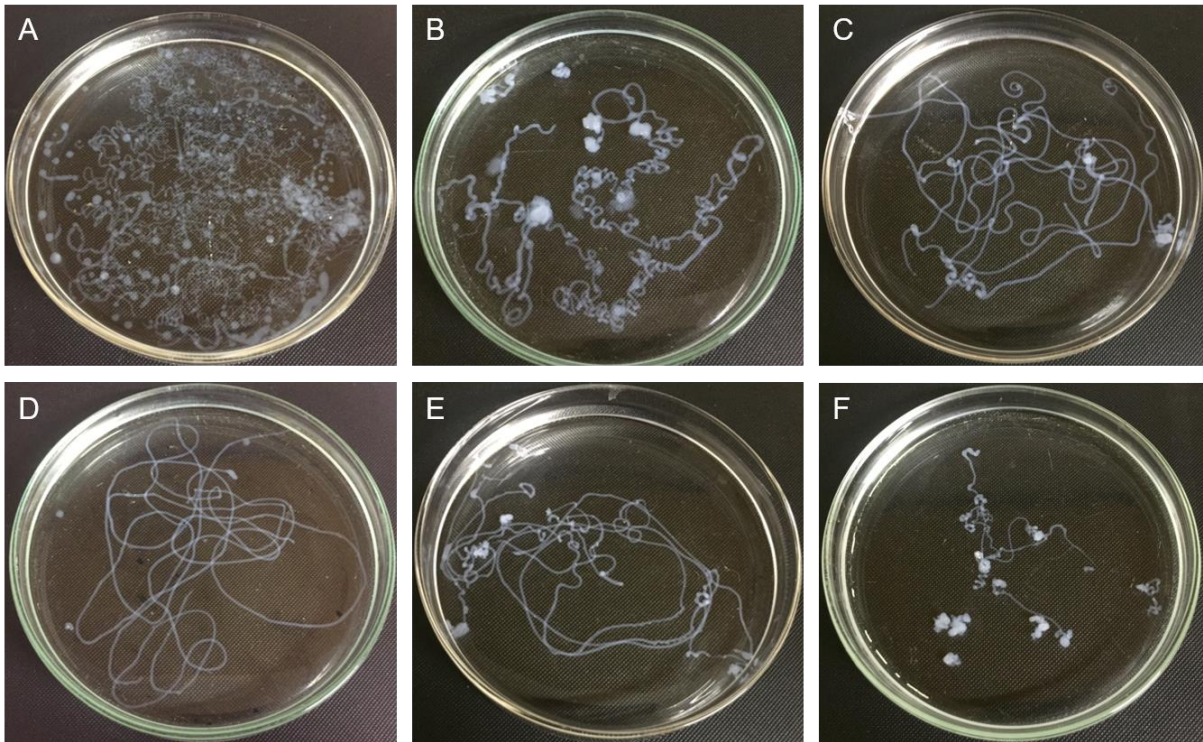


Figure 3.13: Crosslinked fibres made with varying concentrations of sodium alginate (A) 1%, B) 2%, C) 4%, D) 6%, E) 8%, F) 10%), showing the range between 4 – 8% as most appropriate for biosuture fabrications.

3.5.3 Methods of biosuture fabrication

3.5.3.1 Extrusion via hand

Extrusion of the polymer solution via hand produced fibres with varying diameters and an irregular morphology. This could be ascribed to the lack of constant, regulated pressure and human error. Extrusion via hand was physically challenging, especially for formulations with a high viscosity, and extremely time consuming. Yet, the produced fibres showed great similarity to commercial sutures in terms of appearance and handling properties but displayed great inter-fibre variation, not only in diameter but also in load failure and tensile strength (Table 3.7). Because of the irregularities found in manually produced biosutures, we decided to rather use an automated process, where parameters such as pressure and speed can be definitely controlled, for the biosuture fabrication method.

Table 3.7: Mechanical properties of biosutures produced with different fabrication methods in the straight and knotted configuration.

Fabrication method	Straight configuration		
	Load failure (N)	Tensile strength (N.mm ²)	Elongation at break (%)
Manual/hand	1.89 ± 5.2	167.11 ± 5.2	14.2 ± 6.3
3D Bioplotter	2.04 ± 0.64	180.38 ± 0.64	13.87 ± 0.41
Texture Analyser	2.07 ± 0.63	183.02 ± 0.63	13.77 ± 0.33
Knot configuration			
Manual/hand	1.25 ± 4.6	110.52 ± 4.6	4.31 ± 7.1
3D Bioplotter	1.31 ± 0.33	115.83 ± 0.33	4.39 ± 0.51
Texture Analyser	1.30 ± 0.37	114.91 ± 0.37	4.47 ± 0.43

3.5.3.2 Extrusion via the 3D Bioplotter® (EnvisionTec, GmbH, Germany)

A video of the 3D printing process can be viewed at <https://kapwi.ng/c/P9STLAXdMH> and pictures of the biosutures directly after crosslinking, found at <https://kapwi.ng/c/8pE0yW3AHD>.

There are several advantages to using the 3D Bioplotter for biosuture fabrication, such as tight control over both the pressure applied to the syringe plunger and the speed and pattern in which the syringe moves. There are, however, also many challenges in using the 3D Bioplotter, such as potential clogging of the needle tip. One of the well-known challenges of 3D bioprinting is to obtain a 3D printable bioink that has the correct texture and viscosity to allow for successful printing. Bioinks should preferably display thixotropic flow, be viscous enough to prevent leakage from the syringe prior to pressure being applied and solidify in a feasible manner (Gopinathan & Noh, 2018). Some of the formulations experimented with in the study did not conform to these requirements, but a solution of 6% sodium alginate, could successfully be printed into the predesigned pattern without leakage from the syringe and was readily solidified by a 1% BaCl₂ crosslinker solution. However, higher crosslinker concentrations lead to more rapid crosslinking that tended to clog the needle tip and prevent constant extrusion of the polymer solution. The concentration of the crosslinker solution has a direct impact on the mechanical properties of the biosuture and a lack of freedom to change this concentration is not desirable (Naghieh *et al.*, 2018).

The pressure used during 3D printing is a critical parameter as it influences the morphology and diameter of the final biosuture. When a too high pressure was used, the needle again clogged up rapidly while a too low pressure led to interrupted and irregular flow of the polymer solution. An ideal printing pressure for a 6% sodium alginate solution was found at 0.7 bar. The printing speed also affects the diameter of the fibre produced with a lower speed

producing thicker fibres. An optimal fibre diameter could be achieved with a printing speed of 70mm/sec. The biosutures produced with the 3D Bioplotter were uniform with very little inter-fibre variation in terms of diameter, load failure and tensile strength as shown in Table 3.7.

3.5.3.3 Extrusion via the Texture Analyser (TA.XTplus, StableMicroSystems, England)

Similar to the 3D Bioplotter, the Texture Analyser has several benefits, such as control over the compression speed, as well as certain challenges. The first challenge experience with the Texture Analyser was again clogging of the needle tip. This problem could, however, easily be overcome by using a higher compression speed and manually unclogging the needle tip with a spatula, which was not possible with the 3D Bioplotter as the head was constantly moving. The primary disadvantage of the Texture Analyser, is that the syringe cannot be moved, as in the case of extrusion via hand or with the 3D Bioplotter, which makes it difficult to obtain a long, continuous strand. However, this problem was circumvented by moving or stirring the crosslinker bath instead of the syringe, which also allowed for long, continuous fibre formation. The fibres produced with the Texture Analyser were uniform, linear, and closely resembled those produced with the 3D Bioplotter. The mechanical properties of the biosuture fibres prepared with the 3D Bioplotter and the Texture Analyser were also very similar, as shown in Table 3.7.

We selected the Texture Analyser as the optimal method of polymer extrusion and biosuture fabrication for several reasons. Firstly, various concentrations of both polymers and crosslinkers could successfully be utilized without excessive leakage or clogging of the needle tips as was seen with the 3D Bioplotter. This can be ascribed to the static nature of the syringe and needle which allows for the use of a needle lid and manual unclogging of the tip. Secondly, the Texture Analyser is more time efficient, user-friendly, and affordable than the 3D Bioplotter. There is no need for special 3D printer syringes or needle tips and different formulations can easily be extruded in sequence. Furthermore, the instrumental setup achieved with the Texture Analyser and universal syringe rig can easily be mimicked by other laboratories who have access to a general syringe pump. This method is also much more feasible in terms of large-scale production and keeps the production cost of the biosutures to a minimum.

3.5.4 Influence of formulation components and processing conditions on the mechanical properties of the biosuture.

A simple tensile test, as outlined in the United States Pharmacopoeia (USP), provides valuable information regarding the mechanical properties of suture materials, which are primarily described by the load failure (N), tensile strength (N/mm²) and elongation at break (%) of the suture material. Load failure refers to the maximum load (or force) that a single suture fibre can withstand before rupturing. The USP provides minimum values for the load failure of each

suture gauge as can be seen in Table 3.8 (*Tensile Strength. United States Pharmacopeia and National Formulary (USP 29-NF 24)*). Elongation at break gives an indication of the flexibility or ductility of the material, which can be defined as the degree to which the material can be stretched (and undergo plastic deformation) before failure. A certain degree of ductility is necessary for the suture to be able to elongate with wound oedema, but excessive ductility can easily lead to wound dehiscence, infection, and other debilitating complications (Chiaoprakobkij *et al.*, 2019). A higher elongation at break is also associated with better handling properties, knot-tying ability and knot pull tensile strength. Tensile strength, in turn, provides more information on the suture material's strength in relation to its size and is defined as the maximum strength in the stress-strain curve of the material. The tensile strength of the suture material must be high enough to ensure that failure will not occur during surgery and should be similar to the strength of the biological tissue it is used for (Akgun *et al.*, 2018).

Table 3.8: USP limits on average diameter and knot pull tensile strength of respective suture gauge numbers. Used with permission from (*Tensile Strength. United States Pharmacopeia and National Formulary (USP 29-NF 24)*).

USP Size	Metric Size (Gauge No.)	Limits on Average Diameter (mm)		Knot-Pull Tensile Strength (in N)	
		Min.	Max.	Limit on Average Min.	Limit on Individual Strand Min.
9-0	0.4	0.040	0.049	—	—
8-0	0.5	0.050	0.069	0.44	0.24
7-0	0.7	0.070	0.099	0.69	0.54
6-0	1	0.10	0.149	1.76	0.98
5-0	1.5	0.15	0.199	3.73	1.96
4-0	2	0.20	0.249	7.55	3.92
3-0	3	0.30	0.339	12.2	6.67
2-0	3.5	0.35	0.399	19.6	10.2
0	4	0.40	0.499	27.2	14.2
1	5	0.50	0.599	37.3	19.1
2	6	0.60	0.699	44.2	25.5
3	7	0.70	0.799	57.8	29.3
4	8	0.80	0.899	68.6	34.2

A more comprehensive picture of the mechanical properties of a suture material can be achieved by studying the engineering stress-strain curve of the material. This curve can be obtained by converting load-displacement data to engineering stress and engineering strain. As shown in Figure 3.14, other important parameters such as the young's modulus, yield stress and toughness of the material can be calculated from this curve. Young's modulus (MPa) is defined as the slope of the stress-strain curve in the linear (elastic) region and relates to the stiffness of the material and its ability to resist plastic deformation. A high young's modulus usually correlates with a high tensile strength and low elongation at break. The yield stress (N/mm²) represents the value beyond which the material undergoes plastic deformation where any deformation that takes place will be permanent and irreversible. Toughness (J.mm⁻³) refers to

the ability of the suture to absorb energy and deform before breaking. It is a very useful parameter to evaluate the mechanical properties of suture materials, as it provides an idea of the balance that is struck between strength and ductility.

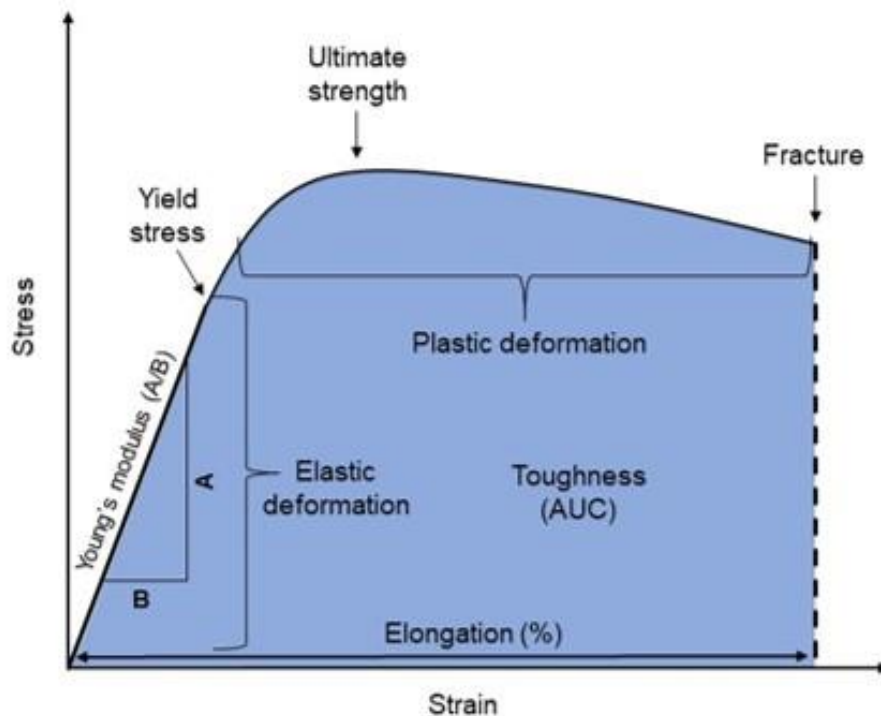


Figure 3.14: Schematic representation of a typical stress-strain curve. Adapted with permission from (Cooke *et al.*, 1996).

The load-displacement and stress-strain curves of each suture formulation was, therefore, carefully studied and each of the above-mentioned values calculated. This not only provided insight as to the influence of the different variables on the mechanical properties of the biosuture, but also allowed for the selection of appropriate formulation components.

3.5.4.1 Pure sodium alginate biosutures

A basic alginate biosuture, consisting of 6% sodium alginate only, and prepared according to the Texture Analyser method described in Section 3.4.3, was first evaluated, and used as a baseline to compare subsequent formulations with. The average diameter of the biosutures, after extrusion through a 23 G needle, was 0.10 mm and corresponds with a 6-0 suture size. Table 3.9 provides the average load at failure, tensile strength, young's modulus, elongation at break and toughness of the biosutures, while Figure 3.15 shows representative load-displacement and stress-strain graphs of the neat sodium alginate biosutures. From this figure, it is clear to see that the two graphs follow the exact same pattern and has the same shape but is expressed in different units. The knotted curve does not display the expected bimodal shape, as seen later in the study, presumably because the fibres ruptured before the knot was tightened, which signifies low elasticity and poor knot security.

Table 3.9: Mechanical properties of biosutures produced from only sodium alginate.

Pull configuration	Load failure (N)	Tensile strength (N/mm ²)	Young's modulus (MPa)	Elongation at break (%)	Toughness (J.mm ⁻³)
Straight	2.07 ± 0.9	183.12 ± 0.9	0.85 ± 0.3	13.77 ± 0.4	6.17 ± 0.7
Knotted	1.3 ± 0.6	116.18 ± 0.6	1.31 ± 0.7	4.47 ± 0.5	0.91 ± 0.6

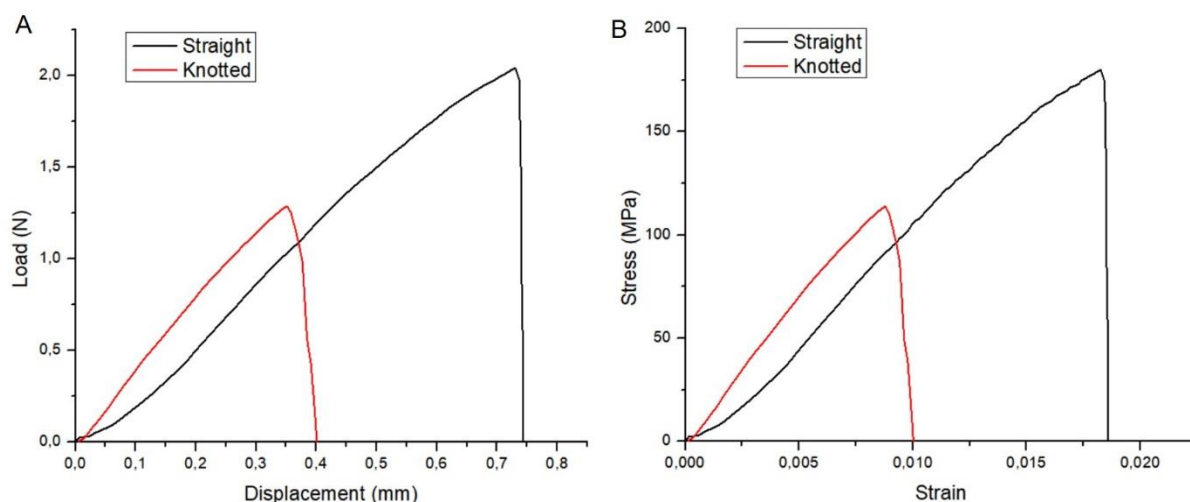


Figure 3.15: A) Representative load vs displacement curve of pure sodium alginate biosutures. B) Representative stress vs strain curve of pure sodium alginate biosutures.

The basic sodium alginate biosuture showed immense promise for application as a suture material with good handling properties and an acceptable diameter. However, the tensile strength, in both the straight and knotted configuration, was substandard and needed to be increased to ensure effective application as a suture material, as well as compliance with the USP requirements. The ductility of the pure alginate biosutures were not as high as expected, considering the high M/G ratio of the alginate used, and further work is needed to increase the ductility and improve the handling properties and knot tying ability of the biosutures.

3.5.4.2 Addition of a suitable plasticizer

Plasticizers are a critical part of most natural polymer-based formulations as they dramatically improve the flexibility and elasticity of the systems. Plasticizers are known to decrease the straight tensile strength of suture materials, while increasing their elongation at break (Sirviö *et al.*, 2018). A higher elongation at break usually improves the handling properties, knot-tying abilities, and knot tensile strength of suture materials, and could therefore, improve the performance of the alginate based biosutures. It is crucial to find the correct plasticizer concentration that will not dramatically decrease the tensile strength of the biosuture, but still improve the elasticity adequately (Naleway *et al.*, 2015). We investigated three different plasticizers namely, propylene glycol, glycerol and triethyl citrate.

Triethyl citrate could not be effectively incorporated into the polymer network and eventually lead to phase separation of the system. Propylene glycol, on the other hand, was easily incorporated into the system but could be observed diffusing out of the system, during crosslinking, and thereafter had a negligible effect on the mechanical properties of the biosutures. Glycerol, conversely, displayed strong plasticizing effects, good compatibility with the polymer network and effectively increased the percentage elongation of the biosutures. This is in accordance with the work of several other researchers who also reported that glycerol had the greatest effect on the mechanical properties of polysaccharides, compared to other plasticizers (Jantrawut *et al.*, 2017; Muscat *et al.*, 2012; Razavi *et al.*, 2015).

There could be several reasons for the poor plasticizing effect of propylene glycol, one being its low molecular weight (76.09 g/mol) compared to that of glycerol (92.06 g/mol). According to Mangavel *et al.*, plasticizer efficacy is dependent on plasticizer molecular weight, with higher molecular weight plasticizers displaying greater efficacy (Mangavel *et al.*, 2003). The large size of triethyl citrate (276,283 g/mol), however, could have prevented the molecule from being fully incorporated into the system, thereby limiting its plasticizing effect (Orliac *et al.*, 2003). Alternatively, the lack of interaction between propylene glycol and alginate, could be due to the relatively low polarity of propylene glycol, which has a dielectric constant of only 32.0 compared to 42.5 of glycerol. This suggests that propylene glycol may not have enough dipole strength to disrupt the intermolecular bonds between the alginate molecules and can, therefore, not position itself effectively between the polymer chains (Drive, 1993). Propylene glycol is also known to evaporate and migrate out of polymer networks, due to its relatively high volatility compared to that of other plasticizers, which would have resulted in the network reverting to its original stiffness (Suyatma *et al.*, 2005). Glycerol, on the other hand, is well known for its ability to remain entrapped within a polymer matrix as shown by Orliac *et al.*, who found no marked loss of glycerol from crosslinked films over a 3-month period (Orliac *et al.*, 2003). The strong plasticizing effect of glycerol, can also be ascribed to its asymmetric structure and three hydroxyl groups, which can form complex interactions with the polypeptide chain and affect the mechanical properties of the polymer network to a greater extent (Ullah & Wu, 2013).

Consequently, we selected glycerol as the most effective plasticizer for the biosutures and studied the influence of different concentrations (2, 4, 6, 8, and 10%) on the mechanical properties of the fibres in order to find the optimal concentration. Table 3.10 provides the mechanical properties of the different formulations in both the straight and knot pull configuration. Contrary to what was expected, the addition of glycerol at concentrations 2 – 4 % did not cause a decrease in strength, but resulted in an overall increase in load failure, tensile strength and elongation at break. This surprising increase in tensile strength can be

ascribed to the anti-plasticizing effect that is often observed when low concentrations of plasticizer are added to a polymeric system. The exact mechanism is not fully understood but according to Lourdin *et al.*, the small amount of plasticizer might act as a type of crosslinker by forming strong interactions with the polymer, that will decrease the free volume and mobility of the polymer chain. Additionally, a small amount of plasticizer could improve the reorganization of the polymer chains and encourage its arrangement in a crystal lattice, thereby increasing the strength of the material (Lourdin *et al.*, 1996).

Table 3.10: Mechanical properties of biosutures containing different concentrations of glycerol, in the straight and knot configuration.

Plasticizer	Straight configuration			
	Load failure (N)	Tensile strength (N/mm ²)	Elongation at break (%)	Toughness (J.mm ⁻³)
1. Glycerol (0%)	2.071 ± 0.91	183.116 ± 0.91	13.770 ± 0.43	6.168 ± 0.72
2. Glycerol (2%)	3,027 ± 0.62	267.645 ± 0.62	16.110 ± 0.38	15.128 ± 0.65
3. Glycerol (4%)	3.239 ± 0.79	286.390 ± 0.79	19.645 ± 0.61	18.524 ± 0.73
4. Glycerol (6%)	2.826 ± 0.59	249.873 ± 0.59	20.523 ± 0.74	16.199 ± 0.85
5. Glycerol (8%)	2.406 ± 0.82	212.737 ± 0.82	16.658 ± 0.68	10.521 ± 0.94
6. Glycerol (10%)	2.698 ± 0.93	238.555 ± 0.93	9.588 ± 0.79	8.331 ± 0.92
7. Glycerol (12%)	1.493 ± 0.57	132.010 ± 0.57	4.605 ± 0.46	1.223 ± 0.55

Plasticizer	Knot configuration			
	Load at failure (N)	Tensile strength (N/mm ²)	Elongation at break (%)	Toughness (J.mm ⁻³)
1. Glycerol (0%)	1.314 ± 0.62	116.183 ± 0.62	4.470 ± 0.51	0.913 ± 0.63
2. Glycerol (2%)	1.427 ± 0.56	126.174 ± 0.56	6.865 ± 0.72	1.373 ± 0.77
3. Glycerol (4%)	2.130 ± 0.75	188.333 ± 0.75	9.005 ± 0.87	2.558 ± 0.91
4. Glycerol (6%)	1.757 ± 0.83	155.352 ± 0.83	6.765 ± 0.70	1.611 ± 0.89
5. Glycerol (8%)	1.778 ± 0.32	157.209 ± 0.32	5.680 ± 0.63	1.725 ± 0.82
6. Glycerol (10%)	1.437 ± 0.60	127.058 ± 0.60	4.290 ± 0.75	1.113 ± 0.73
7. Glycerol (12%)	0.786 ± 0.72	69.497 ± 0.72	9.277 ± 0.98	0.390 ± 0.57

Yet, the percentage elongation at break was also notably increased with the addition of glycerol at low concentrations, which indicates that this phenomenon cannot be fully explained by the anti-plasticization effect. Similar effects was, however, seen by Gao *et al.*, who proved through X-ray diffraction analyses, that glycerol increases the mobility of alginate chains while also promoting the crystallization of the alginate with structural reorganization (Gao *et al.*, 2017). On the other hand, several other authors have suggested that the plasticizing effect of low concentrations of glycerol can be ascribed to the increase in water content of the polymer

system after incorporation of glycerol (Schmid, 2013; Talja *et al.*, 2007). Olivas and Barbosa-Cánovas found a significant increase in the moisture content of glycerol-plasticized alginate compared to alginate on its own and ascribed this to the increasing amount of hydroxyl groups brought by glycerol which binds water molecules through hydrogen bonding (Olivas & Barbosa-Cánovas, 2008). This suggests that, with the addition of glycerol at low concentrations, water acts as a plasticizer to increase the elongation at break while glycerol improves the structural organization of the alginate chains and thereby increases the tensile strength of the material.

The highest load failure values were found with the addition of 4% v/v glycerol, in both the straight and knot configuration (i.e., 3.2 and 2.1 N, respectively). At this glycerol concentration, the elongation at break was also substantially improved which suggests that it could potentially be the optimal concentration for inclusion in the biosuture formulation. As can be seen in Figure 3.16, the stress-strain curves of the biosutures that contain 4% v/v glycerol have vastly improved and show a bimodal structure in the knotted configuration, which confirms the improved elasticity and ability of the biosuture to tie and secure a knot before rupturing. Higher glycerol concentrations, however, lead to variable results where the tensile strength would decrease with increase in elasticity, (e.g., 6 and 8% v/v glycerol), or where the tensile strength would increase but the elasticity decrease (e.g., 10% v/v glycerol), or as in the case of 12% v/v glycerol, where both the tensile strength and elasticity decreased. The low elongation at break values seen with higher plasticizer concentrations, is not necessarily a reflection of poor elasticity but rather a detrimental decrease in tensile strength that causes the biosutures to break before maximum elongation is achieved. Gao *et al.*, also observed lower elongation at break values with the addition of higher amounts of glycerol to alginate films and ascribed this to a segregation/ exudation phenomena where the intermolecular and intramolecular bonding in the alginate network significantly decreases (Gao *et al.*, 2017).

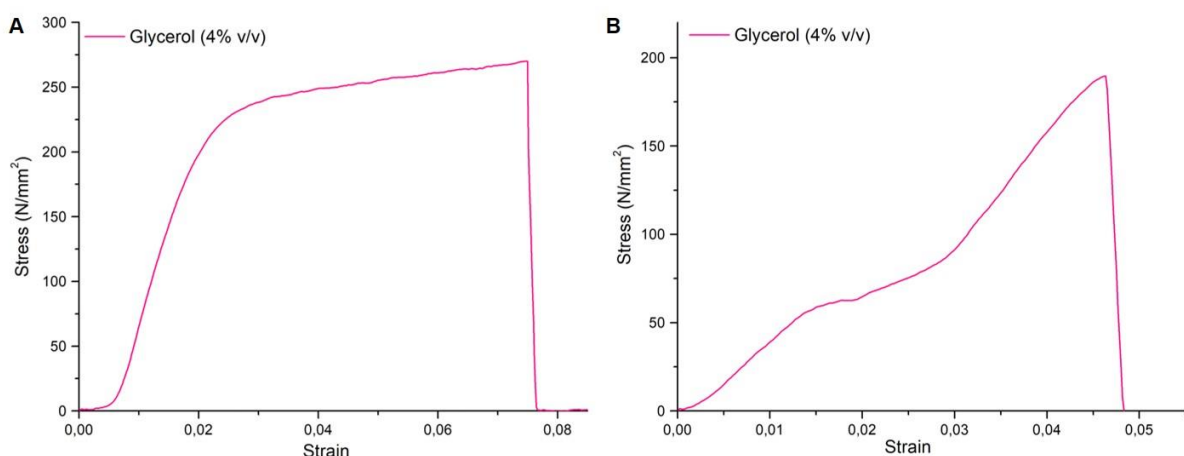


Figure 3.16: Stress-strain curves of biosutures containing 4% v/v glycerol in the straight (A) and knotted (B) configuration.

Toughness, as mentioned earlier, can be a very useful tensile parameter for sutures and can give an indication of the material's ability to balance tensile strength and ductility. The highest toughness, in both the straight and knotted configuration, was achieved with 4% v/v glycerol which displayed a toughness of 18.524 and 2.558 J.mm⁻³, respectively (shown in bold in Table 3.10). This suggests that, when 4% glycerol is added to the formulation, the ductility can be increased without sacrificing too much of the material's tensile strength. Hence, 4% v/v glycerol, was selected for inclusion in the biosuture formulation. This plasticizer concentration also resulted in the highest knot pull tensile strength, an important factor considering the knot is the weakest point of any suture material and confirms the selection of 4% v/v glycerol for inclusion in the biosuture formulation.

3.5.4.3 Addition of pectin as reinforcing agent

Pectin was the first polymer investigated for its ability to improve the mechanical properties of the biosuture. In line with the low concentration of reinforcing agents that are normally used, we first studied the effect of 0.5, 1 and 2% w/v pectin and then later evaluated the effect of even lower concentrations, i.e., 0.1, 0.2, 0.3 and 0.4% w/v pectin. With the addition of even the smallest quantity of pectin to the alginate solution, the behaviour and flow of the polymer solution instantly changed. The solution was notably less viscous and shot out of the needle tip in a linear fashion which led to straighter and more suture-like fibres, than when alginate was used on its own (Figure 3.15 A). Additionally, when pectin was added to the polymer solution, the resulting dried biosutures were thinner, with a diameter of 0.08 mm which corresponds with a 7-0 suture size, compared to the 0.10 mm diameter of pure alginate biosutures which corresponds with a 6-0 suture size (Figure 3.15. B). This substantial improvement in morphology provides ample incentive for the inclusion of pectin in the biosuture formulation and can be ascribed to the great synergy that is known to exist between the two polymers (as described in detail in Section 2 of this chapter).

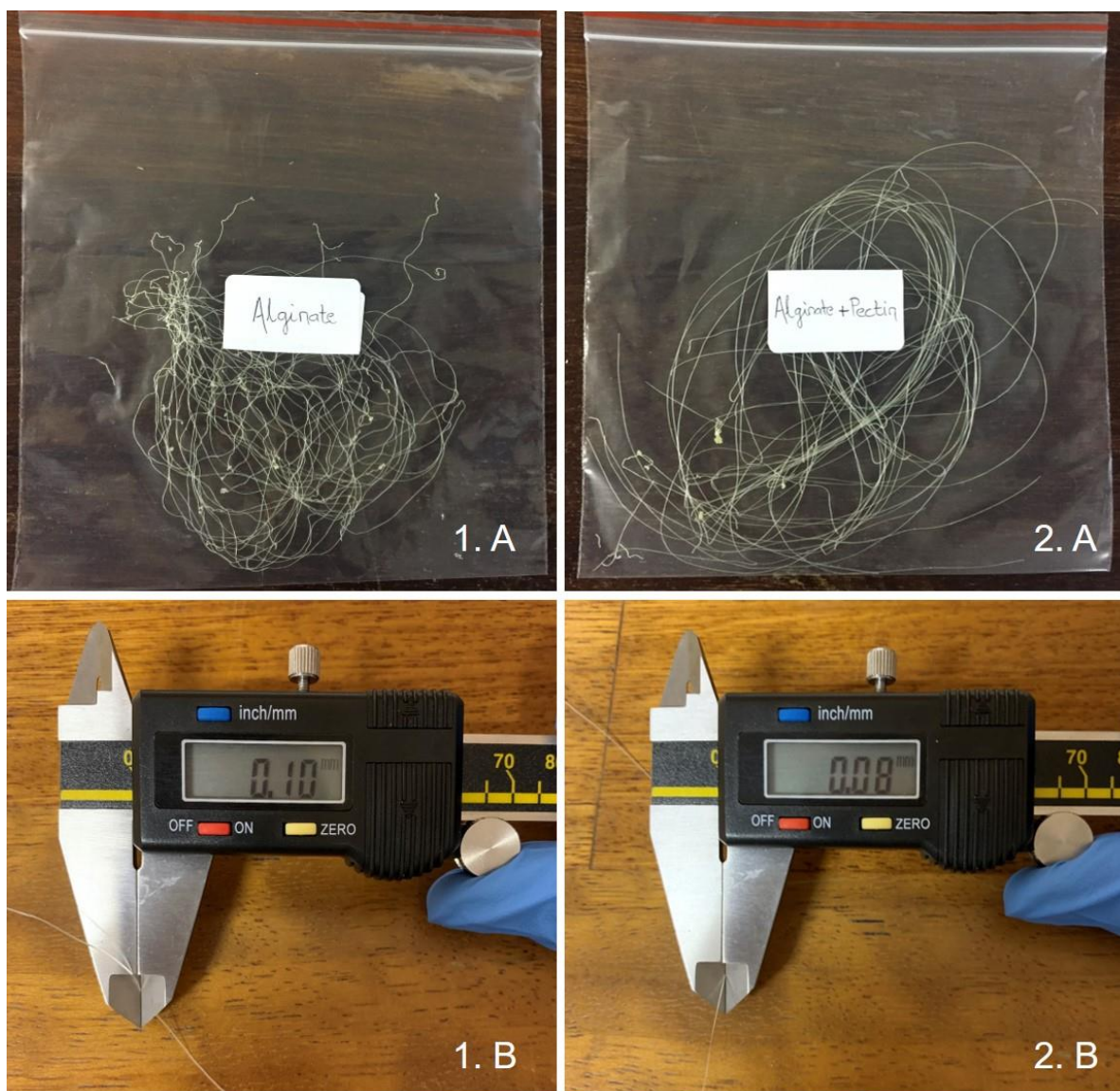


Figure 3.17: Morphology of biosutures consisting of alginate alone (1. A) and alginate plus pectin (1. A) and the corresponding diameter of each biosuture fibre – alginate alone (2. A) and alginate plus pectin (2. B).

The decrease in diameter of an alginate fibre or film, after the addition of pectin, has been observed by several authors, including Bierhalz *et al.*, and Walkenström *et al.*, who found a change in the microstructure (more compact molecular packing) of a pectin-alginate blend, compared to pure polymer networks, that resulted in smaller pore sizes and thinner films (Bierhalz *et al.*, 2012; Gohil, 2011; Islan *et al.*, 2012; Walkenström *et al.*, 2003). According to Lambrech *et al.*, the addition of pectin to an alginate network, increases the amount of molecular interactions and leads to a denser, more compact network that ultimately results in a thinner fibre or film, as they proved with SEM and TEM micrographs (Lambrech *et al.*, 2009). Yet, the influence of these interactions and the synergy between alginate and pectin, on the extrudability of polymer solutions and the mechanical properties of the resulting biomaterials,

has not been widely investigated. Figure 3.17 shows the force that is needed to extrude an alginate and alginate-pectin solution, from a 23G needle into a crosslinker bath. The alginate-pectin solution required a lower force (95 N) than the pure alginate solution (107 N), proving that pectin improves the extrudability of the biosuture formulation, possibly because of the increased interactions and synergistic molecular arrays that form within the polymer blend.

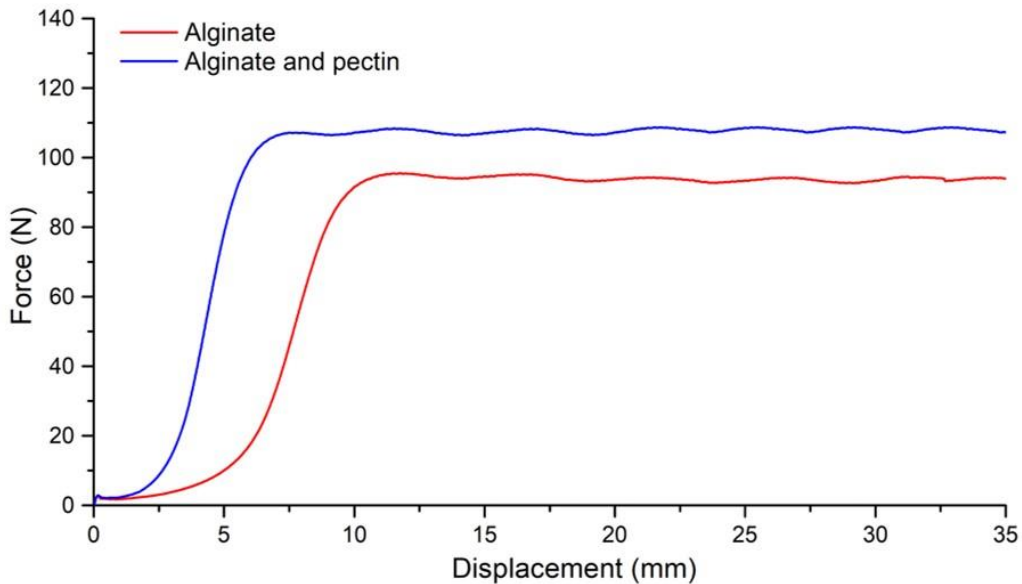


Figure 3.18: The force required to extrude the alginate (blue) and alginate – pectin (red) solutions through a 23G needle into a crosslinker solution as measured with the Texture Analyser (T.A.X.T Plus).

As expected, the synergy between alginate and pectin also improved the mechanical properties of the biosuture, which displayed higher load failure, tensile strength, and elongation at break values than the pure alginate biosutures. Upon analysis of Figure 3.18, which shows the load failure and tensile strength of biosutures containing increasing concentrations of pectin, two features become undeniably apparent. The first observation that was made, was that pectin had a much more profound impact on the mechanical properties of the biosuture when it is in the knotted configuration, compared to the straight configuration. Particularly in the low concentration range (0.1 – 0.5 % w/v pectin) the load failure only varied by one or two decimal points in the straight configuration, while in the knotted configuration more substantial differences were seen. This can be ascribed to the greater sensitivity of the knotted configuration to changes in the biosuture formulation. The knotted configuration considers handling, bending, and tying of the biosutures and probably provides a more accurate picture of the influence that pectin has on the mechanical properties thereof. The second observation that was made from Figure 3.18, are that the mechanical properties were better at lower concentrations of pectin, suggesting that the synergy between alginate and pectin has a threshold, above which a further increase in pectin concentration leads to a

decrease in mechanical performance, as was shown in previous studies (Gohil, 2011; Walkenström *et al.*, 2003). The highest load failure and tensile strength values were found with the addition of only 0.1% w/v pectin, where the load failure for the knotted configuration reached 2.024 ± 0.5 N, which exceeds the minimum value (1.76 N) required by the USP.

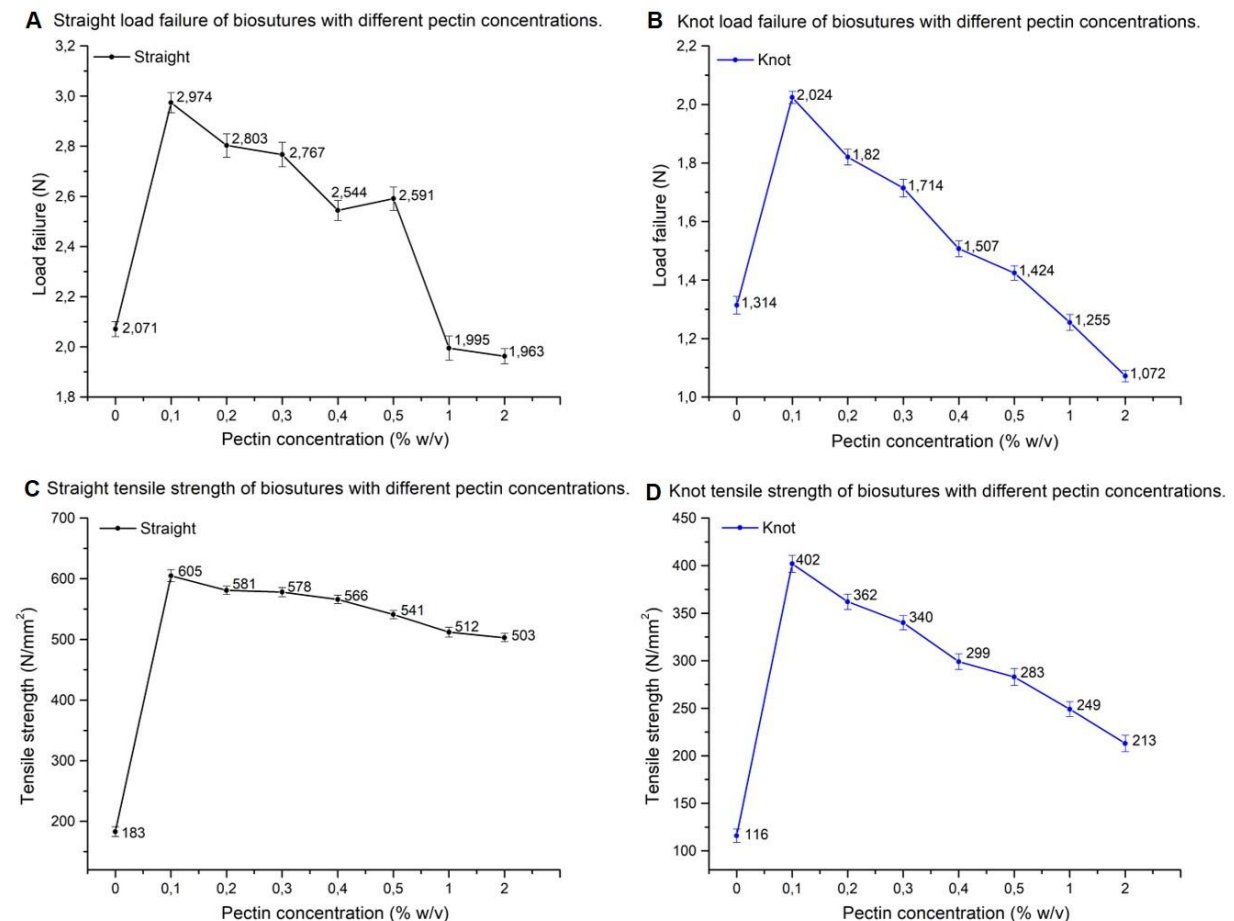


Figure 3.19: Load failure (N) and tensile strength (N/mm²) of biosuture samples containing different concentrations of pectin in the straight (A & C) and knot (B & D) configuration.

When studying the elongation at break of biosutures containing different concentrations of pectin, it was again observed that the knotted configuration was impacted to a greater extent than the straight configuration (Figure 3.19). Contrary to what is expected of a crystalline polymer like pectin, the elongation at break actually increased with the addition of low concentrations of pectin (0.1 – 0.5 % w/v). However, when pectin was included in concentrations of 1 and 2 % w/v, the elongation at break started to decrease. According to Gohil, increasing the concentration of pectin in alginate-pectin blends, increases the crystallinity of the blend and results in fragile, brittle polymer films when the pectin concentration exceeds 10% of the total polymer concentration (Gohil, 2011). When pectin is % w/v added to the biosuture formulation, it comprises 14.29% of the total polymer concentration, which suggests that pectin has increased the crystallinity of the biosutures to

the point where they have become brittle and less elastic, as shown by the low elongation at break values observed with high pectin concentrations.

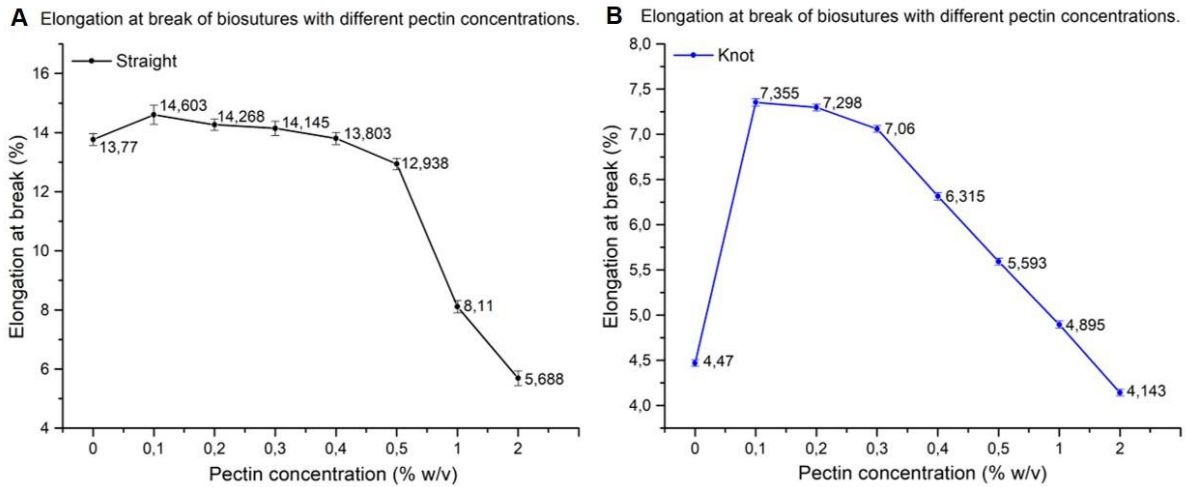


Figure 3.20: Elongation at break (%) of biosuture samples containing different concentrations of pectin in the straight (A) and knotted (B) configuration.

The increase in elongation at break at low concentrations is a very interesting occurrence that has also been observed by other authors, including Gohil who ascribed it to the slippage of alginate and pectin chains past one another (Audebrand *et al.*, 2006; Galus & Lenart, 2013; Gohil, 2011). Yet, the most probable reason for the high elongation at break observed with the inclusion of pectin in this study, is the high degree of esterification (DE) of the pectin sample that was used. According to Walkenström *et al.*, gels of pectin with a high DE show highly branched strands that are more flexible than low methoxy pectin gels where the strands are stiff and rigid (Walkenström *et al.*, 2003). Chan *et al.*, also showed that high methoxy pectin gels display a broader range of elastic behaviour in strain sweep tests than low methoxy pectin (Chan *et al.*, 2017). According to Fang *et al.*, the random distribution of ester groups along the pectin chain hinders the lateral association of dimers and induces defects into the formation of egg-box dimers, resulting in negligible chain – chain association and greater elasticity (Fang *et al.*, 2008). Yet, Chan *et al.*, proved that the large amount of hydrogen bonds and hydrophobic forces between methyl groups of high methoxy pectin, is stronger than the ionic bonding of low methoxy pectin, which could explain the high tensile strength seen with high methoxy pectin in this study (Chan *et al.*, 2017).

The ability of pectin to improve the extrudability of the biosuture hydrogel and subsequently the morphology of the biosuture fibre, provided ample motivation for its inclusion in the biosuture formulation. Yet, the benefits of pectin transcended to include the improvement of the mechanical properties of the biosutures, in terms of both strength and elasticity. The greatest improvement was seen with 0.1% w/v pectin, which was subsequently selected for

inclusion in the biosuture formulation. The inclusion of such a low concentration reinforcing agent is further substantiated by the work of Serrano-Aroca *et al.*, who found that a miniscule amount of graphene oxide (also 0.1% w/v) had a substantial impact on the mechanical properties of a crosslinked alginate film and was able to increase its compressive modulus than four times (Serrano-Aroca *et al.*, 2017).

3.5.4.2 Addition of nanocellulose as reinforcing agent

Low concentrations of the reinforcing agent NCF, i.e., 1, 0.5 and 0.25% w/v, were studied. The diameter of the biosutures (± 0.10 mm) remained the same, before and after the addition of NCF, but the surface morphology changed considerably. The fibres changed from smooth, linear, and uniform to irregular and uneven with rugged edges (Figure 3.20). At each of the concentrations investigated, the load failure, tensile strength and elongation at break dramatically decreased, for both the straight and knotted configuration, as shown in Table 3.11. With the addition of only 0.25% w/v NCF, the load failure and elongation at break were more than halved, while the elongation at break decreased by over 30% for both the straight and knotted configuration. When the NCF concentration was increased to 0.5% w/v, the load failure was similarly low in the straight configuration but dropped a further 19% in the knotted configuration, while the elongation at break also dramatically declined. With the use of 1% w/v NCF, the biosutures became notably brittle and difficult to handle. In attempts to tie a knot with these biosutures, they would instantly break without forming a proper knot. Subsequently, no data could be collected for the knot-pull tensile strength of biosutures containing 1% w/v NCF.

Table 3.11: The load failure, tensile strength, and elongation at break of biosutures containing different concentrations of CNF, in the straight and knot configuration.

Nano-cellulose (% w/v)	Straight-pull			Knot-pull		
	Load failure (N)	Tensile strength (N/mm ²)	Elongation at break (%)	Load failure (N)	Tensile strength (N/mm ²)	Elongation at break (%)
0	2.07 \pm 0.9	183.11 \pm 0.9	13.77 \pm 0.4	1.30 \pm 0.6	114.94 \pm 0.6	4.47 \pm 0.5
0.25	1,35 \pm 0.8	119,54 \pm 0.8	4,83 \pm 0.5	0,89 \pm 0.1	79,41 \pm 0.1	1,39 \pm 0.7
0.5	1,58 \pm 0.9	140,41 \pm 0.9	3,70 \pm 0.8	0,64 \pm 0.3	57,38 \pm 0.3	1,59 \pm 0.8
1	0,87 \pm 0.7	77,10 \pm 0.7	3,86 \pm 0.7	-	-	-

The complete inability of CNF to improve the mechanical properties of the biosutures can be ascribed to agglomeration of the nanoparticles within the biosuture. One of the greatest challenges, with the use of nanoparticles as reinforcing agents, is to obtain proper particle dispersion (Zare, 2016). Despite a vast amount of research on the subject, agglomeration of nanoparticles remains a significant problem and the obtainment of a completely homogeneous dispersion of individual particles is remarkably difficult (Kargarzadeh *et al.*, 2017).

Researchers employ different techniques to overcome agglomeration, including chemical modification, sonification and physical coating (Jiang *et al.*, 2009). Several authors have shown that nanocellulose materials are highly segregated in an aqueous environment and that ultrasonication of nanocellulose in water is an efficient method of obtaining a homogeneous dispersion (Deepa *et al.*, 2020; Shen *et al.*, 2017; Zhou *et al.*, 2018). Hence, in the current study, nanocellulose was ultrasonicated in an aqueous medium for 15 minutes, before addition to the polymer solution, and again after blending with alginate to obtain a homogenous, well dispersed polymer blend.

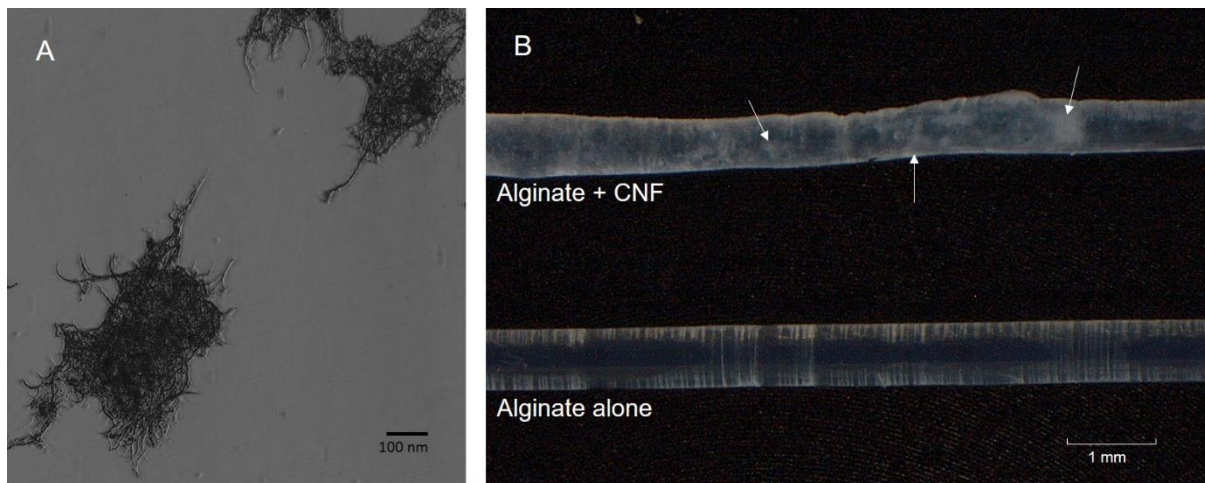


Figure 3.21: A) Microscopic image of the cellulose nanofibrils (CNF), illustrating their tendency to entangle and agglomerate. B) Microscopic image of biosutures consisting of alginate and CNF (top) and alginate alone (bottom). Arrows indicate CNF agglomerates. Note that fibres are in the wet, swollen state and diameters do not correlate with the final dry biosuture fibre diameter.

Even though a seemingly homogenous polymer solution was obtained with no particles visible within the solution, light microscope images revealed CNF aggregates within the biosuture fibre after extrusion (Figure 3.20). This can be due to the method of biosuture fabrication namely, extrusion, which takes place under high pressure and increases the tendency of particles to aggregate. It can also be ascribed to the morphology of CNF (Figure 3.20), which is more prone to entanglement than CNC because of their high aspect ratio and the length of the fibres (Siqueira *et al.*, 2019). According to Kargarzadeh *et al.*, the extrusion parameters are of critical importance and excess loads or high stress can lead to a heterogeneous suspensions that will ultimately affect the physical properties of the composite (Kargarzadeh *et al.*, 2017). This is in line with work done by Alloin *et al.*, who found significant differences in the mechanical properties of CNF-alginate films produced by different methods, i.e., extrusion, casting and evaporation (Alloin *et al.*, 2011). In fact, several other authors have also found that CNF can actually degrade the mechanical properties of the composite, due to

agglomeration and stronger filler-filler interactions than filler-polymer interactions (De Castro *et al.*, 2016; Kargarzadeh *et al.*, 2017; Lemahieu *et al.*, 2011). Wang *et al.*, showed that alginate-CNF composite films had a rough surface with cracks, holes and aggregated fibres compared to the smooth, homogeneous surface of pure alginate films, similar to what was seen in the current study (Wang *et al.*, 2017).

Due to the high degree of agglomeration of the CNF particles in the biosutures that cannot be avoided, the rough surface properties of fibres containing CNF and especially the diminutive effect of CNF on the mechanical properties of the biosutures, we decided not to include this polymer into the biosuture formulation.

3.5.4.3 Addition of gelatin as reinforcing agent

Gelatin proved to be an effective reinforcing material and similar to pectin, had a profound impact on the biosuture as a whole. The diameter remained the same as without the addition of gelatin, but the load failure, tensile strength, elasticity, and general handling properties vastly improved, as shown in Table 3.13. The maximum load that the biosuture could withstand increased with increasing concentrations of gelatin, reached a maximum at 3% w/v, and then started to decrease again. The same trend was seen for the tensile strength and elongation at break in both the straight and knotted configurations. The increased tensile strength can be ascribed to electrostatic interactions between sodium alginate and gelatin, as well as the greater amount of hydrogen bonds in the network due to the addition of gelatin (Xiao *et al.*, 2001b).

Table 3.12: Mechanical properties of biosutures containing different concentrations of gelatin.

Alginate content (% w/v)	Gelatin content (% w/v)	Load failure (N)	Tensile strength (N/mm ²)	Elongation at break (%)
Straight configuration				
6	0	2.071 ± 0.91	183.116 ± 0.91	13.77 ± 0.43
6	0.75	2.115 ± 0.72	187.007 ± 0.72	14.26 ± 1.04
6	1.5	2.253 ± 0.81	199.208 ± 0.81	17.31 ± 0.72
6	3	3.439 ± 0.67	304.074 ± 0.67	20.52 ± 0.64
6	6	2.721 ± 0.77	240.589 ± 0.77	15.19 ± 0.97
Knotted configuration				
6	0	1.314 ± 0.62	116.183 ± 0.62	4.47 ± 0.51
6	0.75	1.359 ± 0.81	120.161 ± 0.81	7.05 ± 0.63
6	1.5	1.439 ± 0.89	127.235 ± 0.89	9.19 ± 0.78
6	3	1.923 ± 0.78	170.031 ± 0.78	10.06 ± 0.85
6	6	1.541 ± 0.91	136.254 ± 0.91	7.79 ± 0.65

Yet, most authors report the same trend that is seen in the current study where the tensile strength initially increases with higher gelatin concentrations and then suddenly decreases again (Distler *et al.*, 2021; Dong *et al.*, 2006; Fan *et al.*, 2005). According to Wang *et al.*, there exists a very specific optimal additive amount of gelatin for each alginate-based platform at which the mechanical properties of the material will reach a peak. The authors suggest that gelatin and alginate are highly compatible at this point, but once gelatin is added in an excessive amount, the compatibility is lost and the mechanical properties of the material deteriorates (Wang *et al.*, 2019). Similarly, Fan *et al.*, showed that if gelatin exceeds 30% of the total polymer concentration of a gelatin-alginate blend, the alginate solution becomes destabilized and phase separation occurs (Fan *et al.*, 2005). In the current study, the combination of 6% w/v alginate with 3% w/v gelatin resulted in the highest load failure (3.4 and 1.9 N), tensile strength (304 and 170 N/mm²) and elongation at break (20 and 10 %) in the straight and knotted configuration respectively, suggesting that this is the sweet spot for maximum compatibility between alginate and gelatin. This is in accordance with the work of Fadnavis *et al.*, who found that maximum reinforcement of sodium alginate can be achieved with 3% gelatin as well as that of Dong *et al.*, who advised the inclusion of 20 – 50% gelatin to alginate-gelatin films for optimal mechanical performance (Dong *et al.*, 2006; Fadnavis *et al.*, 2003).

The weighty effect that gelatin had on the elasticity of the biosutures can clearly be seen in the stress – strain curves of biosutures containing different concentrations of gelatin (Figure 3.21). The increase in the elongation at break and the strain that the biosutures could withstand, can be ascribed to the recognized plasticizing effect of gelatin which stems from its hygroscopic nature and tendency to absorb water molecules, which then act as plasticizers within the polymeric system. The elongation at break also reached a maximum with the use of 3% w/v gelatin and thereafter decreased, suggesting that the blend has weakened and is no longer able to withstand the same amount of strain. Hence, 3% w/v gelatin was the clear choice for inclusion in the biosuture formulation.

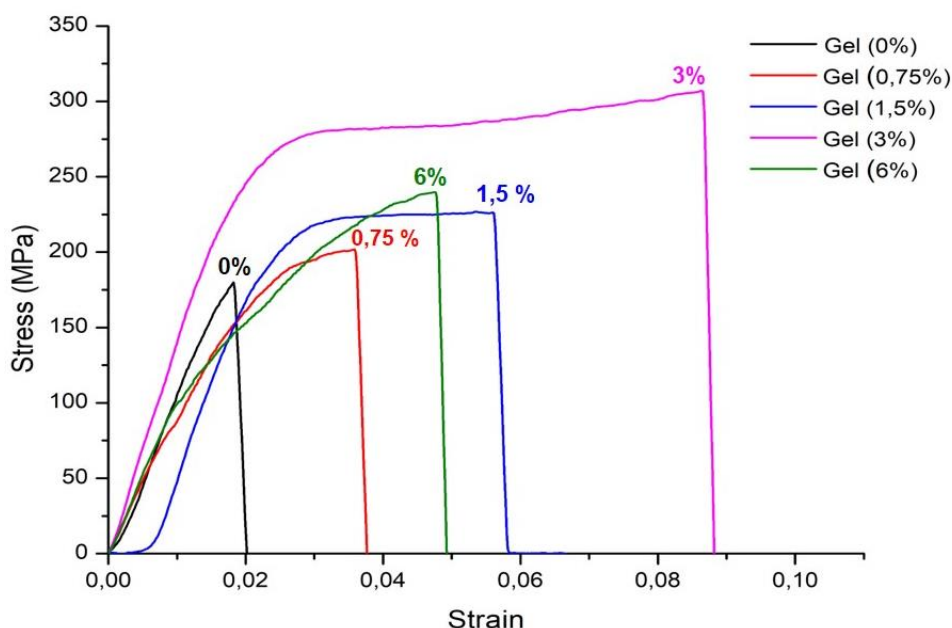


Figure 3.22: Representative stress-strain graphs (straight configuration) of biosutures containing different concentrations of gelation.

3.4.5.6 Selection of the appropriate crosslinker concentration.

In order to find the best crosslinker concentration and ratio, we studied the combination of BaCl₂ and epichlorohydrin (ECH), by varying the concentration of the crosslinkers, one at a time, keeping the concentration of the other crosslinker constant. The biosuture formulation contained not only alginate (6%), but also glycerol (4%), pectin (0.1%) and gelatin (3%), to ensure effective crosslinking of the system as a whole. The load failure, tensile strength and elongation at break results are provided in Table 3.13 and Table 13.14. It became clear early on that, as was the case with the plasticizer concentration, the ideal crosslinker concentration will be the result of a compromise between the tensile strength and elasticity of the biosutures.

Table 3.13: Mechanical properties of biosutures crosslinked with different BaCl₂ concentrations.

BaCl ₂ (% w/v)	ECH (% v/v)	Straight configuration			
		Load failure (N)	Tensile strength (N/mm ²)	Young's modulus (MPa)	Elongation at break (%)
1	0.5	2.692 ± 0.6	238.02 ± 0.6	1.16 ± 1.1	18.49 ± 0.68
2	0.5	3.118 ± 0.7	275.69 ± 0.7	2.32 ± 0.9	6.34 ± 0.84
4	0.5	2.854 ± 0.6	252.35 ± 0.6	2.74 ± 0.9	4.84 ± 0.75
Knotted configuration					
1	0.5	1.719 ± 0.9	151.99 ± 0.9	1.01 ± 1.2	9.82 ± 0.96
2	0.5	1.896 ± 0.7	167.64 ± 0.7	1.34 ± 1.0	7.99 ± 0.87
4	0.5	1.652 ± 0.8	146.06 ± 0.8	1.36 ± 1.1	5.12 ± 0.97

We first studied the effect of different BaCl₂ concentrations (1, 2 and 4% w/v) on the mechanical properties of the biosutures. Fibres that were crosslinked by 1% BaCl₂ and 0.5% ECH, had the lowest tensile strength (238.025 and 151.993 MPa), but the highest elongation at break (15.497 and 9.82%), in both the straight and knotted configuration. According to Cuadros *et al.*, the ionic crosslinker concentration must exceed the stoichiometric requirements of the carboxylate groups of alginate, several times, before maximum tensile strength can be observed (Cuadros *et al.*, 2012). They, and other authors, suggest that the carboxylic-binding sites throughout the entire alginate matrix, is only saturated once the CaCl₂ concentrations exceeded 1.4 % w/v (Li *et al.*, 2016; Oh *et al.*, 2020). The addition of pectin to the current polymer blend, increases the amount of available crosslinking sites and suggests that an even higher crosslinker concentration is needed to fully crosslink the biosutures and obtain maximum tensile strength. The high elongation at break also suggests a very low degree of crosslinking with 1% BaCl₂, where the polymer chains are not as closely packed but have a greater mobility and where more space is available for water molecules to adhere and plasticize the polymer fibres (Seixas *et al.*, 2013). This high measure of elongation at break is not desirable in suture materials where too flexible materials have been linked to gaping wounds and hernia formation (Greenberg & Clark, 2009).

Biosutures crosslinked with 4% BaCl₂ and 0.5% ECH, displayed both lower tensile strength (252.349 and 146.068 MPa) and lower elongation at break (4.84 and 5.122%) in the straight and knotted configurations, than the other biosutures. It is possible that the high crosslinker concentration lead to rapid crosslinking of the carboxylate groups on the surface of the fibres and prevented further penetration of the crosslinker molecules to the matrix of the fibre (Liling *et al.*, 2016). However, the high aspect ratio of the biosutures make this an unlikely possibility as there is very little matrix for the molecules to penetrate. Alternatively, the low elongation at break and particularly high young's modulus of the biosutures crosslinked with 4% BaCl₂ suggest a high degree of crosslinking that lead to stiff, brittle, and weak fibres (Park *et al.*, 2018). It is also possible that some of the salt molecules, that were in excess, got trapped within the crosslinked matrix leading to weak points and uneven crosslink distribution as was described by Kim *et al.*, (Kim *et al.*, 2000).

Crosslinking with 2% BaCl₂ and 0.5% ECH, resulted in biosutures with a higher tensile strength (275.691 and 167.643 MPa), than the BaCl₂ concentrations discussed above, and a medium to low elongation at break (6.347 and 7.99%), again in the straight and knotted configuration. This suggests that with the use of 2% BaCl₂, there is sufficient barium molecules available to saturate the crosslinking sites of the polymer matrix and form a stable, thoroughly crosslinked egg-box structure (Costa *et al.*, 2018). The higher tensile strength also suggests efficient crosslinking of both alginate and pectin that could lead to a stronger, more cohesive fibre

(Seixas *et al.*, 2013). The denser packing of the polymer chains, after full crosslinking, would naturally inhibit their movement and is well known to result in a lower elongation at break and ductility (Ibrahim *et al.*, 2019).

Table 3.14: Mechanical properties of biosutures crosslinked with varying concentrations of ECH, in the straight and knotted configuration.

BaCl ₂ (% w/v)	ECH (% v/v)	Straight configuration			
		Load failure (N)	Tensile strength (N/mm ²)	Young's modulus (MPa)	Elongation at break (%)
2	0	3.408 ± 0.9	301.3 ± 0.9	1.99 ± 1.1	10.77 ± 0.57
2	0.25	2.929 ± 0.8	258.98 ± 0.8	2.29 ± 1.2	7.32 ± 0.75
2	0.5	3.195 ± 0.6	282.5 ± 0.6	2.93 ± 1.1	5.85 ± 0.77
2	1	2.204 ± 0.8	194.87 ± 0.8	3.64 ± 1.0	3.84 ± 68
Knotted configuration					
2	0	2.071 ± 0.8	184.61 ± 0.8	0.73 ± 0.9	9.37 ± 0.82
2	0.25	1.638 ± 0.6	144.83 ± 0.6	1.43 ± 1.1	8.37 ± 0.95
2	0.5	1.619 ± 0.7	143.15 ± 0.7	1.47 ± 0.8	7.75 ± 0.81
2	1	0.760 ± 0.4	67.19 ± 0.4	1.85 ± 0.9	4.84 ± 0.83

Next, we studied different concentrations of ECH (0, 0.25, 0.5 and 1% v/v) while keeping the BaCl₂ constant at 2% w/v, since this concentration produced biosutures with the highest tensile strength thus far. We also studied 2% BaCl₂ on its own without the addition of ECH (0% v/v), in order to analyse the effect of ECH on the mechanical properties of the biosutures. Surprisingly, the 2% BaCl₂ on its own provided biosutures with the highest tensile strength (301.334 and 184.619 MPa) and greatest elongation at break (8.77 and 9.372%) in both the straight and knotted configuration, as show in Table 3.14 and Figure 3.22. The use of increasing concentrations of ECH, lead to a subsequent decrease in the tensile strength and elongation at break of the biosutures, with the lowest values observed with 1% ECH. The young's modulus of the biosutures also drastically increased with the use of ECH, which suggests that the formation of covalent bonds in the biosutures (as proved by FTIR) lead to greater crystallinity and stiffness. This is in accordance with the work of other researchers, such as Pan *et al.*, who found that the use of glutaraldehyde as a chemical crosslinker, in addition to CaCl₂ as a physical crosslinker, dramatically effected the stiffness of alginate scaffolds and eventually lead to a decrease in tensile strength (Pan *et al.*, 2016). When BaCl₂ (2% w/v) is used on its own, it provides a good balance between tensile strength and ductility that could not be achieved at lower concentrations of BaCl₂ or with the addition of ECH, as

seen in Figure 3.22. Therefore, we selected 2% w/v BaCl₂ as the optimal crosslinker concentration for the current study.

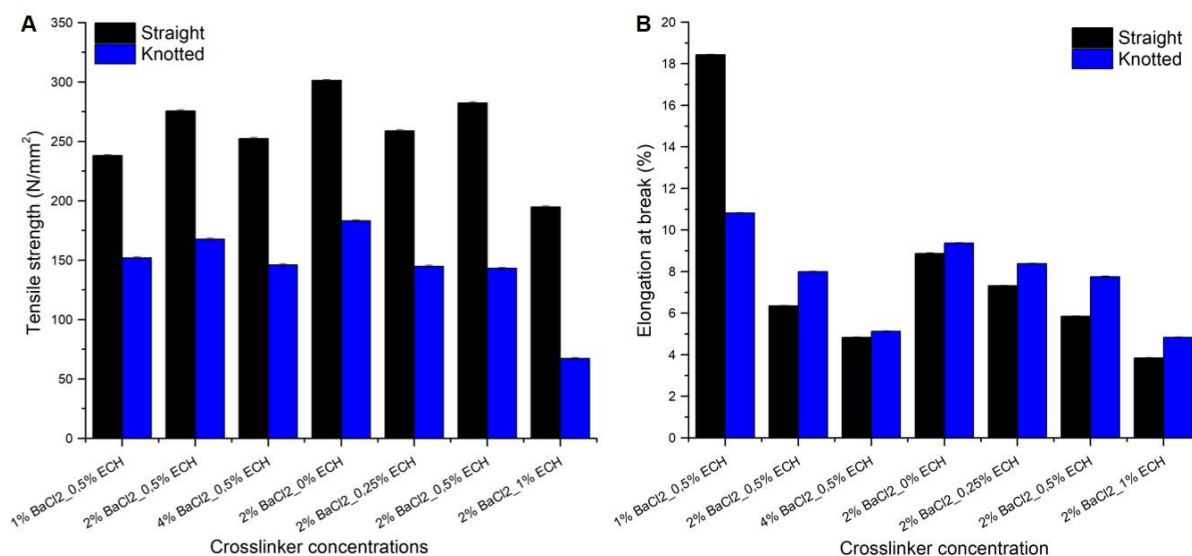


Figure 3.23: A) Tensile strength and B) Elongation at break of biosutures crosslinked with different concentrations of the crosslinkers, Barium chloride (BaCl₂) and Epichlorohydrin (ECH), in the straight and knotted configuration.

3.5.4.4 Selection of the optimal drying method

According to Bagheri *et al.*, drying conditions have a profound impact on the physical characteristics, and especially the mechanical properties, of glycerol-plasticized alginate films (Bagheri *et al.*, 2019). Drying, which is the process of simultaneous mass and heat transfer, is accompanied by different factors, such as temperature and air flow rate, that can have a direct impact on the characteristics of the biosutures. Temperature may influence and alter the physiochemical properties of the polymers, while air flow may change the moisture content of the biosutures, both of which can affect the final product properties. Hence, we studied the mechanical properties of biosutures produced under different drying conditions namely, normal air drying at room temperature ($22 \pm 2^\circ\text{C}$) and 50% relative humidity, under lamellar flow in a fume hood, and in an oven at 35°C , in order to select the optimal method.

Table 3.15 shows the load failure, tensile strength, young's modulus, and elongation at break of biosutures produced under different drying conditions in the straight and knotted configuration. The lowest straight and knotted load failure was seen in biosutures dried at room temperature (2.756 and 1.393 N), followed by those dried at 35°C in the oven (3.150 and 1.743 N) and the highest load failure was seen in biosutures dried under lamellar flow (3.824 and 1.819 N). The same trend was also seen in the tensile strength, young's modulus,

and elongation at break of the biosutures, despite slight differences in the diameter of the biosutures dried under different conditions, as shown in Table 3.15.

Table 3.15: Diameter and mechanical properties of biosutures dried under different drying conditions, in the straight and knotted configuration.

Drying method	Diameter (mm)	Load failure (N)	Tensile strength (N/mm ²)	Young's modulus (MPa)	Elongation at break (%)
Straight configuration					
Airdried (25°C)	0.15	2.75 ± 0.51	243.68 ± 0.51	0.53 ± 0.72	18.5 ± 0.87
Lamellar flow	0.10	3.82 ± 0.55	338.12 ± 0.55	0.85 ± 1.03	16.37 ± 0.97
Oven dried (35°C)	0.07	3.15 ± 0.43	278.52 ± 0.43	2.86 ± 1.41	4.92 ± 0.91
Knotted configuration					
Airdried (25°C)	0.15	1.39 ± 0.61	123.16 ± 0.61	0.64 ± 1.07	12.25 ± 0.78
Lamellar flow	0.10	1.82 ± 0.52	160.83 ± 0.76	1.31 ± 1.39	9.88 ± 0.73
Oven dried (35°C)	0.07	1.74 ± 0.63	154.12 ± 0.65	2.17 ± 1.01	4.43 ± 0.94

The elongation at break and young's modulus, which both refer to the elasticity and bendability of the biosutures, was greatly impacted by the drying method used. Figure 3.23 shows the stress-strain curve of the biosutures dried in different conditions, in the straight configuration, and provides a good visual representation of the impact that drying conditions have on the mechanical properties of the biosutures.

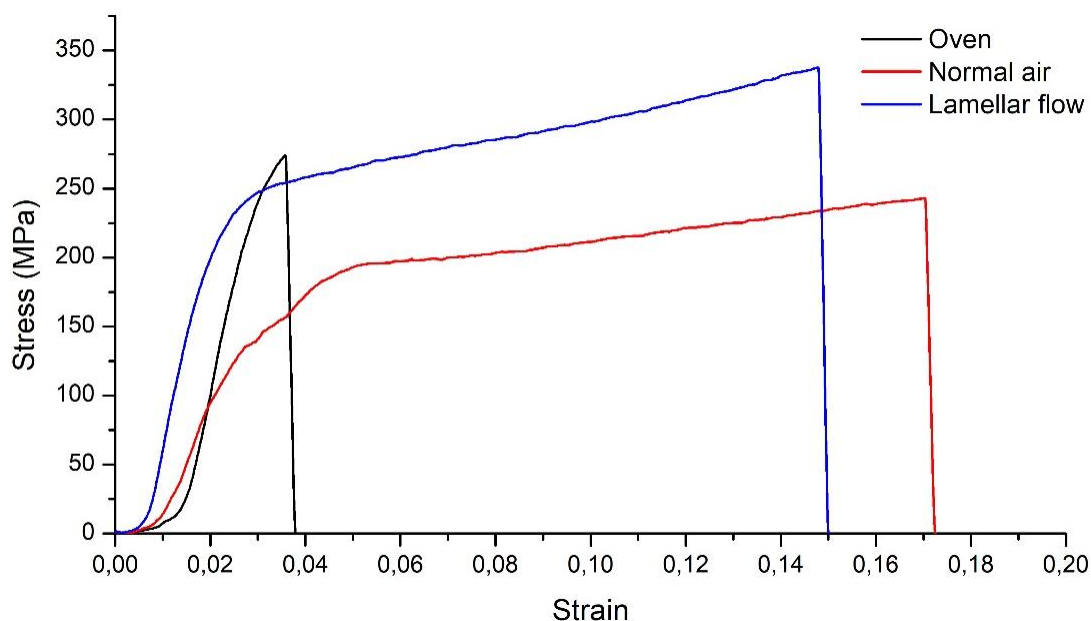


Figure 3.24: Stress-strain curves of biosutures dried under different drying conditions, as evaluated in the straight configuration.

Biosutures dried in normal air had the highest elongation at break, in both the straight and knot configuration (18.5% and 12.25%, respectively), as well as the lowest young's modulus (0.537 and 0.64), which is normally associated with high levels of elasticity (Gu *et al.*, 2005). This may be due to a higher moisture content in airdried fibres, compared to those produced by other drying methods, that resulted in a higher level of plasticity. This was also seen by other researchers such as Homez-Jara *et al.*, who showed that films dried at low temperatures (2 and 25°C), had greater moisture content and elasticity than films dried at high temperatures (40°C) (Homez-Jara *et al.*, 2018). The diameter of airdried fibres was also larger than the rest, which again points to a greater moisture content and less effective evaporation of water from the biosutures. A high moisture content will also explain the poor mechanical properties of the fibres as the polymer matrix is still hydrated, with more space between the polymer chains and weaker interactions between the molecules (Smyth *et al.*, 2018).

On the other hand, biosutures that were dried in the oven at 35°C, tended to break early on in the tensile test and displayed low elongation at break values in both the straight and knotted configuration (4.918% and 2.685%, respectively), despite the load failure being relatively high. The young's modulus of these fibres was particularly high (2.869 compared to the 0.537 and 0.853 MPa of airdried and lamellar flow dried fibres), indicating that the fibres were particularly stiff and difficult to bend. This can be ascribed to over drying of the biosutures or evaporation of glycerol from the formulation, which would naturally have left the fibres brittle and inelastic. Bagheri *et al.*, found that glycerol content of alginate films decrease with increasing drying temperature and time (Bagheri *et al.*, 2019). Similarly, da Silva *et al.*, showed that considerable glycerol evaporation can already occur from 30°C and subsequently influence the mechanical properties of alginate films. As was seen in the current study, da Silva *et al.*, also reported a lower tensile strength in oven dried films, compared to other drying methods, which they ascribed to significant water loss and glycerol evaporation (da Silva *et al.*, 2012).

Biosutures that were dried under lamellar flow in a fume hood displayed surprisingly favourable elongation at break values in both the straight and knotted configuration. The elongation at break in the straight configuration was slightly lower (16.373%) than that of fibres airdried at room temperature (18.5%), but considerably higher than that of fibres that were dried in the oven (4.918%). The exact same pattern was witnessed in the knot configuration, with airdried fibres at 12.25 %, those under lamellar flow at 9.88 % and oven dried fibres at 4.435 %. The diameter of the biosutures was also between that of the biosutures produced by the other two drying methods, i.e., 0.10 mm compared to 0.15 mm of airdried fibres and 0.07 mm of oven dried fibres. This would suggest that lamellar flow as a drying method, removes more water from the fibre than normal air drying at room temperature, but less than drying at 35°C in an oven, and might therefore provide a good balance between tensile strength and

ductility in the biosutures. It is also possible that the increased rate of water removal and directional air movement in the lamellar flow fume hood improved the alignment of the polymer chains in the matrix, which resulted in improved mechanical properties in the biosutures (Marzec & Pietrucha, 2018). The young's modulus of biosutures dried under lamellar flow was relatively low (0.853 MPa) compared to the high load failure and tensile strength of the material. This suggests that the biosutures are easy to bend and deform but can still withstand high amounts of pressure, which is valuable combination in suture design. Hence, we selected lamellar flow in a fume hood as the optimal drying method.

3.6 Conclusion

In this chapter, we first drew a theoretical basis for the selection of key materials that are included in the study and did a thorough characterization of the four main polymers (i.e., sodium alginate, pectin, nanocellulose and gelatin) via FTIR. We confirmed the ability of sodium alginate to form suture-like fibres, that closely resemble synthetic sutures in terms of look and feel, and confirmed the best method of biosuture fabrication namely, extrusion via the Texture Analyser (TA.XTplus). Next, we set out to improve the mechanical properties of the pure sodium alginate fibres through a thorough investigation of the effect that several potential formulation components and fabrication parameters, can have on the mechanical properties of the biosutures.

We found that pectin drastically improves the extrudability, morphology and linearity of the biosutures while improving the load failure and tensile strength, if used at low enough concentrations. Nanocellulose, on the other hand, had a diminutive effect on the mechanical properties of the biosutures and resulted in rough fibres with varying diameters. This was ascribed to agglomeration of the nanofibrils during the extrusion process, despite proper dispersion and homogenization of the nanofibril solution prior to extrusion. Gelatin also had a favourable effect on the mechanical properties of the biosutures and managed to improve, not only the load failure and tensile strength of the fibres, but also the elongation at break or ductility. Glycerol was selected as the optimal plasticizer for use in the current study, due to its commendable ability to plasticize the biosutures without causing a significant decrease in tensile strength. The final optimized biosuture formulation consisted of alginate (6% w/v), pectin (0.1% w/v), gelatin (3% w/v) and glycerol (4% v/v). The crosslinker ratio and concentration also had a noteworthy impact on the mechanical properties of the biosutures and, contrary to our initial proposal of a dual crosslinking approach, we decided to only use BaCl₂ (2% w/v) as crosslinker, due to the good balance between tensile strength and elasticity that it provides. Lastly, we identified lamellar flow in a fume hood as the optimal drying method for the biosutures due to the superior mechanical properties of the fibres produced under these conditions.

CHAPTER 4: APPROACHES TO THE CONFIGURATION OF A DRUG-ELUTING BIOSUTURE WITH OPTIMAL METHOD SELECTION.

4.1 Introduction

In light of the widespread use of suture materials and their profound impact on the success of major surgical procedures, it is only logical that researchers are now focused on improving the therapeutic efficacy of sutures, in addition to their mechanical performance (Prithyani *et al.*, 2021). One of the principal methods in which this can be achieved, is by transforming suture materials into drug delivery devices. Other emerging methods include cell seeded sutures, smart self-tightening sutures and photosynthetic sutures for local delivery of oxygen and growth factors (Alshomer *et al.*, 2017; Centeno-Cerdas *et al.*, 2018). The deep-seated benefits of using sutures as drug delivery devices, as mentioned in previous chapters, suggest that drug-eluting sutures will enjoy still increasing attention in years to come. In the case of microvascular surgery (MVS), drug-eluting sutures can provide a long-awaited solution to several troubling complications, such as ischemic reperfusion injury (IRI) and thrombosis, which cannot be successfully or safely overcome through traditional systemic drug administration.

In this study, dexamethasone will be employed as a model drug to study and evaluate different methods of drug loading. Dexamethasone is a potent glucocorticoid with very limited mineralocorticoid activity and well-known immunosuppressant and anti-inflammatory activity, that is achieved through various genomic and nongenomic mechanisms (Johnson *et al.*, 2018). Dexamethasone is particularly valuable in cases of leuko-embolization, which often occurs during IRI and the no-reflow phenomenon, as the drug sequesters polymorphonuclear neutrophils (PMN) in the microvasculature, by simply altering the surface properties of PMNs, which in turn affects their adherence and aggregation in the vasculature (Takahira *et al.*, 2001). Through this action, dexamethasone is also able to suppress superoxide production and release, prevent neutrophil degranulation and hence limit the amount of harmful or toxic metabolites that can be released once reperfusion is initiated (Concepcion & Zhang, 2018). Yet, the full mechanism of action of glucocorticoids, in the context of IRI, is not well understood. According to Kumar *et al.*, dexamethasone significantly ameliorates acute IRI injury, if it is administered at the onset of reperfusion, but they suggest a neutrophil-independent, receptor-dependant, nongenomic mechanism of action that involves the inhibition of caspase-9 and caspase-3 (Kumar *et al.*, 2009). On the other hand, dexamethasone, has also been found to reduce apoptosis and necrosis of proximal cells during the no-reflow phenomenon,

supposedly through the inhibition of phospholipase A2 and the improvement of blood flow (Dolan *et al.*, 1995b).

Regardless of the mechanism of action, several authors have illustrated that dexamethasone can be useful in the clinical setting of MVS, if administered at high concentrations, from the onset of reperfusion until the risk of no-reflow has subsided (approximately 1 week) (Carroll & Esclamado, 2000; Rezkalla, 2002; Sayed & Sayed, 2020; Speir *et al.*, 2015; Ummat & Zells, 1980). However, continued systemic administration of high dosages dexamethasone can cause undesired immunosuppression and place patients at risk for nosocomial or other infections. Additionally, significant drug amounts must be administered continually in order to achieve and maintain therapeutic drug levels at the site of action, which is unnecessarily costly and places additional stress on the body's elimination systems (Lei *et al.*, 2018). Hence, in this study we will strive to transform the newly developed biosuture material into a drug delivery device that can release dexamethasone immediately upon implantation and continue to release the drug for approximately 7 days, whereafter the risk of the no-reflow phenomenon will have subsided. This form of localised drug delivery can provide high local drug levels without the risk of systemic side effects and will not require additional time and effort from the surgeon and nursing staff.

A last reinforcing argument for the use of dexamethasone as model drug in this study, is its availability in both a water-soluble salt form (dexamethasone 21-phosphate disodium salt) and the original lipid-soluble form. This provides us with the opportunity to study different methods of drug loading that are suitable for either hydrophilic or hydrophobic drug molecules and thereby extends the scope and applicability of this study. Four methods of drug loading will be investigated in this chapter – two using the water-soluble form of the drug (method A and B) and two using the lipid soluble form (method C and D). For the first method (method A), the drug will be added to the biopolymer solution before extrusion into the crosslinker solution for incorporation of the drug into the biosuture matrix. This is a simple and common method of drug loading that has previously been used with great success in the preparation of alginate beads and nanoparticles (Hasnain *et al.*, 2020; Nguyen *et al.*, 2021). Method B will be performed by immersion of the already crosslinked biosuture in a drug-saline solution for absorption of the drug molecule onto the biosuture. This is a more indirect method of drug loading that is less often used. For the methods employing the lipid-soluble drug form, the biosutures will be coated with a lipid-drug layer. Soy phosphatidylcholine (SPC) will be used for method C and palmitic acid for method D. Both these lipids are of natural origin and play very distinct physiological roles in the human body which safeguards their excellent biocompatibility (Carta *et al.*, 2017; Drescher & van Hoogevest, 2020). SPC has ensured numerous commendable accomplishments in the field on drug delivery and displays several

favourable attributes as a drug carrier, i.e., high loading capacity, controlled release abilities and flexible physiochemical and biophysical properties (Le *et al.*, 2019). Palmitic acid is the most widely encountered fatty acid in the human body and is commonly used as a drug carrier in the fabrication of micelles, nanoparticles and microspheres for drug delivery (Gong *et al.*, in press; Sethi *et al.*, 2021). These two lipids, however, have very different chemical structures and physiochemical properties and should, therefore, provide distinctly different drug release profiles.

In this chapter, the different drug loading methods will be thoroughly investigated by studying the drug loading capacity and drug release profile, provided by each method. The influence of the different drug loading methods on the degradation and mechanical properties of the biosutures will also be studied. After careful consideration of all these parameters, the most appropriate method of drug loading for this study will be identified and carried through to subsequent chapters.

4.2 Materials and methods

4.2.1 Materials

Sodium alginate, pectin from citrus peel, and gelatine was purchased from Sigma-Aldrich (St. Louis, MO, USA). Barium chloride 2-hydrate and glycerol (Mw=92.1g/mol) was purchased from LabChem (Founder's hill, Johannesburg, SA). Phosphate buffered saline (PBS) tablets and methanol were purchased from Rochelle Chemicals (Electron, Johannesburg, SA). Dexamethasone (392,46 g/mol) and dexamethasone 21-phosphate disodium salt (516,40 g/mol) were also procured from Sigma-Aldrich (St. Louis, MO, USA). Palmitic acid and Soy Phosphatidylcholine (PDC) with 95% purity were obtained from Avanti Polar Lipids (Alabaster, AL, USA).

4.2.2 Methods of drug loading

A) Direct addition of dexamethasone to the biopolymer solution

Biosutures were prepared as described in the previous chapter, with small alterations. Briefly, the biopolymers were separately dissolved in deionized water and combined with the plasticizer to obtain a solution containing 6% w/v alginate, 0.1% w/v pectin, 3% w/v gelatin and 4% w/v glycerol. For drug loading method A, dexamethasone 21-phosphate disodium salt, was also dissolved separately in deionized water and combined with the biopolymer solution to obtain a final drug concentration of 25 mg/mL. The biopolymer solution was homogenised and sonicated to remove unwanted air bubbles and then extruded, using the Texture Analyser (TA. *XT plus*, Stable Micro Systems, England), into a crosslinker solution (BaCl₂, 2% w/v) for biosuture fabrication. The drug-loaded biosutures were washed to remove excess crosslinker,

dried in a fume hood for approximately 40 minutes, and stored in airtight zip lock bags until further characterization.

B) Immersion of the biosuture in a drug-saline solution

Biosutures were prepared exactly as described in the previous chapter, followed by immersion of the dried biosutures in a drug-saline solution. The biopolymer solution was prepared to contain alginate (6% w/v), pectin (0.1% w/v), gelatin (3% w/v) and glycerol (4% w/v). The solution was homogenised, sonicated, and extruded, using the Texture Analyser (TA. *XT plus*, Stable Micro Systems, England), into a crosslinker solution (BaCl₂, 2% w/v) for biosuture fabrication. After the biosutures were washed and dried as previously described, the biosutures were immersed in a solution of dexamethasone 21-phosphate disodium salt (25 mg/mL) and phosphate buffered saline (pH 7.4), for one hour. After the biosutures had swelled and absorbed the drug-saline solution, they were removed and repeatedly washed with deionised water to remove any excess drug or salt. The drug-loaded biosutures were then again dried in a fume hood, until they reached a constant diameter (approximately 40 minutes) and stored in airtight zip lock bags until further characterization.

C) Coating of the biosuture with a lipid-drug layer using soy phosphatidylcholine

Biosutures were fabricated exactly as described in the previous chapter and then coated with a lipid-drug coating, using a drop coating method. In brief, the biopolymer solution was prepared to contain alginate (6% w/v), pectin (0.1% w/v), gelatin (3% w/v) and glycerol (4% w/v). The solution was homogenised, sonicated, and extruded, using the Texture Analyser (TA. *XT plus*, Stable Micro Systems, England), into a crosslinker solution (BaCl₂, 2% w/v) for biosuture fabrication. The biosutures were washed with deionised water and dried in a fume hood as previously described. A lipid-drug solution (5% w/w) was prepared with soy phosphatidylcholine and dexamethasone in a 60:40 ratio, using methanol as solvent. The biosutures were placed on an ointment tile and the lipid-drug solution dropped over the biosutures, using a 1 mL syringe, and allowed to spread along the length of the biosuture. The coated biosutures were immediately placed under a fume hood for rapid evaporation of methanol and formation of a thin lipid-drug layer on the biosuture surface. This specific method of drop coating, rather than soaking of the biosutures in the lipid-drug solution, as was done by Obermeier *et al.*, was adopted to prevent a solvent exchange process, between water in the biosuture and methanol in the lipid-drug solution, which could interfere with the mechanical properties of the biosutures as was seen by Psimadas *et al.*, (Obermeier *et al.*, 2015; Psimadas *et al.*, 2012). The original soaking method described by Obermeier *et al.*, was first investigated and found to cause a significant decrease in diameter and elasticity in the biosutures (presumably because of the removal of water from the biosuture matrix) which left

the biosutures brittle and unable to tie proper knots. The drop coating method, however, did not alter the diameter of the biosutures nor did it make a startling or immediately discernible difference to the elasticity thereof, and was therefore investigated further.

D) Coating of the biosuture with a lipid-drug layer using palmitic acid

The same process described above, for coating with a lipid-drug layer, was used for method D with the only difference that palmitic acid was used as the lipid component instead of soy phosphatidylcholine. Table 4.1 below provides the composition of the lipid-drug solutions that were used in the respective methods.

Table 4.1: Composition of lipid-drug solutions used for coating the biosuture material.

Method	Mass content % (w/w)	Lipid used	Lipid weight (mg)	Drug used	Drug weight (mg)	Solvent used	Solvent weight (mg)
C	5	Soy PDC	237	DEX	158	Methanol	7900
D	5	Palmitic acid	237	DEX	158	Methanol	7900

4.2.3 Evaluation of the drug loading capacity of the different drug-loaded biosutures

The amount of drug loaded, using methods A – D, were determined spectrophotometrically at $\lambda_{\max} = 241$, which was determined as the wavelength of maximum absorbance of the drug, using the nanophotometer (Implen GmbH, München, Germany). Two calibration curves were constructed – one for dexamethasone 21-phosphate disodium salt, dissolved in PBS (pH=7.4), and another for dexamethasone dissolved in methanol and topped up with PBS (pH=7.4) and their respective linear regression equations determined as shown in Figure 4.1. To estimate the amount of drug loaded, using the different methods, three biosuture segments (5 cm in length) of each drug loading method, was prepared and placed into separate vials (Eppendorf tubes) containing 20 mL PBS (pH=7.4). The vials were kept at 37°C for 30 days and subjected to vigorous stirring, centrifuging and sonication to achieve full release of the loaded drug and disintegration of the biosuture material. Absorbance ($\lambda=241$) of the resulting solutions were measured in triplicate and the respective linear equations, from the constructed calibration curves, were used to determine the amount of drug loaded using the respective methods. Drug loading capacity was normalised to the amount of drug (μg) per cm biosuture.

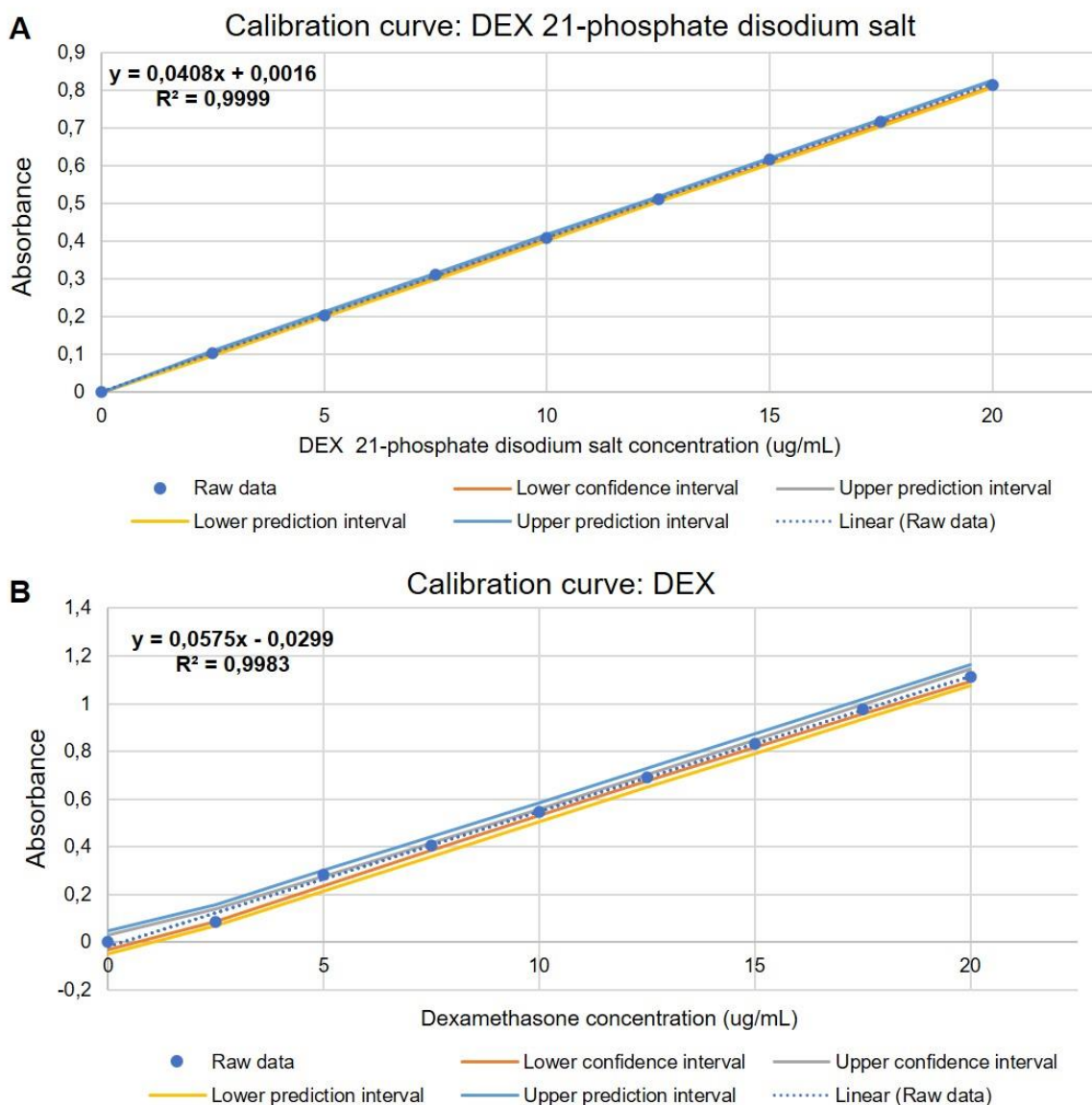


Figure 4.1: Calibration curve of (A) dexamethasone 21-phosphate disodium salt and (B) dexamethasone, indicating the linear regression equation and R^2 values, as well as the confidence and prediction intervals for each curve.

4.2.4 Evaluation of the drug release behaviour of the different drug-loaded biosutures

To determine the drug release profile of the different drug-loaded biosutures, three 2 cm segments of the biosutures, prepared using methods A – D, were placed in Eppendorf tubes containing 10 mL of PBS (pH 7.4). The samples were kept in a shaker incubator (Orbital shaker incubator, LM-530, Lasec Scientific equipment, Johannesburg, South Africa) rotating at 25 rpm at a temperature of 37°, to mimic the expected *in vivo* conditions. At predetermined time intervals (0.5, 1.5, 3, 6, 12, 24, 48, 72, 96, 120, 144 and 168 hours), 2 mL was removed from each Eppendorf tube and replaced with fresh PBS in order to maintain sink conditions. The amount of drug released at each time point was determined by measuring the absorbance

of the solution at $\lambda=241$ and substituting the value into the respective linear regression equations. The experiment was performed in triplicate in order to minimize the error variation and the average values used for further data treatment and plotting. The cumulative drug release was determined using Equation 4.1.

$$\text{Cumulative release (\%)} = \frac{C_t}{C_i} \times 100 \quad \text{Equation 4. 1}$$

Where C_t is the amount of DEX released at time t , and C_i is the amount of DEX loaded onto the biosuture sample. The cumulative drug release profiles were normalized to amount or percentage of drug ($\mu\text{g/mL}$ or %) released from 1 cm biosuture.

4.2.5 Determination of the degradation profiles of the different drug-loaded biosutures

The degradation profiles of biosutures before drug loading and of those prepared with method A – D, were evaluated in terms of weight loss over time. Pre-weighed samples were incubated in 10 mL fresh PBS (pH = 7.4) at 37°C, rotating at 25 rpm. Samples were removed every day, placed on absorbent filter paper and allowed to dry under lamellar flow in a fume hood. Once the samples were dry and achieved a constant diameter, they were accurately weighed on a precision microbalance and the percentage weight loss (i.e., degradation) calculated using Equation 4.2.

$$\text{Percentage degradation} = \frac{W_o - W_t}{W_i} \times 100 \quad \text{Equation 4. 2}$$

Where W_o is the original, starting weight of the sample and W_t is the weight at time t , after incubation in PBS. All experiments were performed in triplicate and expressed as the mean, \pm standard deviation. Sample removal and weighing was performed once a week for the first four weeks and thereafter every day to determine the exact time of 100% weight loss.

4.2.6 Evaluation of the mechanical properties of each drug loaded biosuture

The mechanical properties of the biosuture can easily be altered by the drug-loading process. Hence, we investigated the maximum force at break (N), tensile strength (N/mm^2), elongation at break (%) and young's modulus (MPa) of each drug-loaded biosuture. First, the average diameter of the biosutures were determined by measuring the diameter at three points along the length of each biosuture (the middle and each end), with digital vernier callipers, as described in the USP guidelines for suture diameter measurement (NF24, s.a.). The mechanical properties of the biosutures were measured with the Texture Analyser, fitted with the mini tensile grips (A/MTG, Stable Micro Systems, England) and set to the tensile mode. Biosuture samples were secured in the middle of the grips, with an active gauge length of 4cm and the test performed at a constant rate of 80 mm/min, as specified by the USP standards for tensile testing (*Tensile Strength. United States Pharmacopeia and National Formulary*

(USP 29-NF 24). Rockville, MD: United States Pharmacopeial Convention, 2006). Each drug-loaded biosuture was evaluated in the straight (n=10) and knot (n=10) configuration, where a single overhand throw knot was placed in the centre of the biosuture sample. The average was calculated and presented as the mean, \pm standard error, for all ten readings of each configuration. Load-displacement and stress-strain curves were generated, and the data used to determine the above-mentioned tensile properties. The maximum load at failure is the highest value of the load-displacement curve while young's modulus is defined as the slope of the stress-strain curve. The tensile strength and elongation at break were calculated using Equations 4.3 and 4.4.

$$\text{Tensile strength} = \frac{\text{load failure}}{\text{CSA}} \quad \text{Equation 4. 3}$$

Where load failure is the maximum load (N) at failure (i.e., where the biosuture breaks) and CSA is the cross-sectional area (mm²) of the biosuture.

$$\text{Elongation at break} = \frac{l_1 - l_0}{l_0} \times 100 \quad \text{Equation 4. 4}$$

Where l_0 is the initial length of the biosuture, and l_1 is the final length of the biosuture.

4.2.7 Selection of the optimal drug loading method for the specific study

The optimal method of drug loading, which best suits the developed biosuture material and the specific needs of the study, was selected based on the investigated properties, i.e., drug loading capacity, drug release profile and mechanical properties. It is important that the drug loading methods allows for an adequate amount of drug to be incorporated into/onto the biosuture so that a clinically relevant dosage can be achieved *in vivo*. Ideally, the drug-loaded biosuture should rapidly release the drug upon implantation (i.e., burst release) so that the effects of IRI can be addressed immediately. Additionally, the drug release process should ideally continue for approximately 7 days, so that the late occurring no-reflow phenomenon can be evaded. The drug loading method should ideally not interfere with the optimised mechanical properties of the biosuture nor significantly alter its degradation profile.

4.3 Results and discussion

4.3.1 Drug loading capacity of the different drug-loaded biosutures

The drug loading capacity of any drug delivery device is of critical importance, as it can determine whether sub-therapeutic, therapeutic, or toxic dosages are achieved, upon release of the drug *in vivo*. Each of the drug loading methods provided a different loading capacity to the biosutures as shown in Table 4.2. The specific loading capacity of each biosuture can largely be ascribed to the drug loading method that was used, as well as the various parameters and factors, such as immersion time or the drug-lipid ratio, that accompany each

method. These parameters are not set in stone and can often be altered to obtain a slightly different loading capacity. Yet, certain inherent properties of the biosuture itself, such as the hydrophilicity of the biopolymers it is made of, also contribute to the drug loading capacity, and should not be altered if the initial mechanical performance of the biosuture is to be maintained.

Table 4.2: The drug loading capacity of biosutures prepared using methods A – D.

Drug-loading method	A) Addition to the polymer matrix	B) Immersed in a drug-saline solution	C) Lipid-drug coating: SPC	D) Lipid-drug coating: PA
Amount of drug loaded (ug/cm)	14.94 ± 2.8	93.5 ± 2.7	53 ± 1.8	20.57 ± 2.1
Amount of drug loaded in 20 cm biosuture (ug)	298.8 ± 2.8	1870 ± 2.7	1060 ± 1.8	411.4 ± 2.1

In general, the large surface-area-to-volume ratio of sutures, allows for relatively high drug amounts to be loaded onto the surface of sutures, compared to other biomaterials. On the other hand, the bulk volume of a suture material is normally very low due to the small diameter and size of sutures and cannot accommodate large amounts of drug (Parikh *et al.*, 2021). This was reflected in our work, where method A (direct addition of the drug to the biopolymer matrix), resulted in the lowest drug loading capacity (14.94 ug/cm) of all the methods that were investigated. This low loading capacity of method A, can also be ascribed to the high biopolymer concentrations that were used to prepare the biosutures, which could have resulted in a dense matrix with little space available for the incorporation of a high molecular weight drug such as dexamethasone 21-phosphate disodium salt, that was used in this study (Champeau *et al.*, 2017).

In contrast, method B, where the biosutures were immersed in a drug-saline solution, resulted in the highest loading capacity (93.5 ug/cm), even though the same initial drug concentration (25 mg/mL) was used for both method A and B. The high loading capacity seen with method B, can be ascribed to the high swelling capacity of the biosutures upon incubation in an ionic medium, which is the result of the hydrophilic nature of the biopolymers as well as the crosslinking mechanism that was used to fabricate the biosutures (Pilipenko *et al.*, 2019). Alginate and gelatin, which are extremely hydrophilic, immediately absorbed large amounts of the aqueous drug-saline solution, which allowed the bulk volume of the biosuture to expand and accommodate a greater amount of drug (Pilipenko *et al.*, 2019). Additionally, during the immersion process, ionic exchanges could have occurred between the sodium ions in the drug-saline solution and the barium ions in the biosuture matrix, which could have allowed pores to open up and water to flux in (Liling *et al.*, 2016). The high loading capacity of method B, was also visually observed by a change in colour in the biosutures from slightly yellow, to

white after immersion, which confirms the presence of a high amount of drug/salt molecules in the biosutures produced with method B.

The loading capacity achieved with method C and D, lay between that of method A and B, and differed considerably, despite the close similarity of the two methods. Method C resulted in a higher loading capacity than method D, which can be ascribed to the difference in affinity of the drug for the specific lipid that was used, or the compatibility between the lipid and the biosuture surface. Soy phosphatidylcholine (SPC), that was used in method C, has a hydrophilic head group, in addition to the hydrophobic fatty acid tail, which would have made it more compatible with the hydrophilic surface of the biosuture, than palmitic acid which consist only of a hydrophobic, saturated long chain fatty acid. Additionally, it is possible that dexamethasone has a greater affinity for SPC, which is a much larger and more polar molecule (zwitterion at pH 7.4) than palmitic acid (Figure 4.2) which would have resulted in a higher loading capacity for method C, as seen in the results.

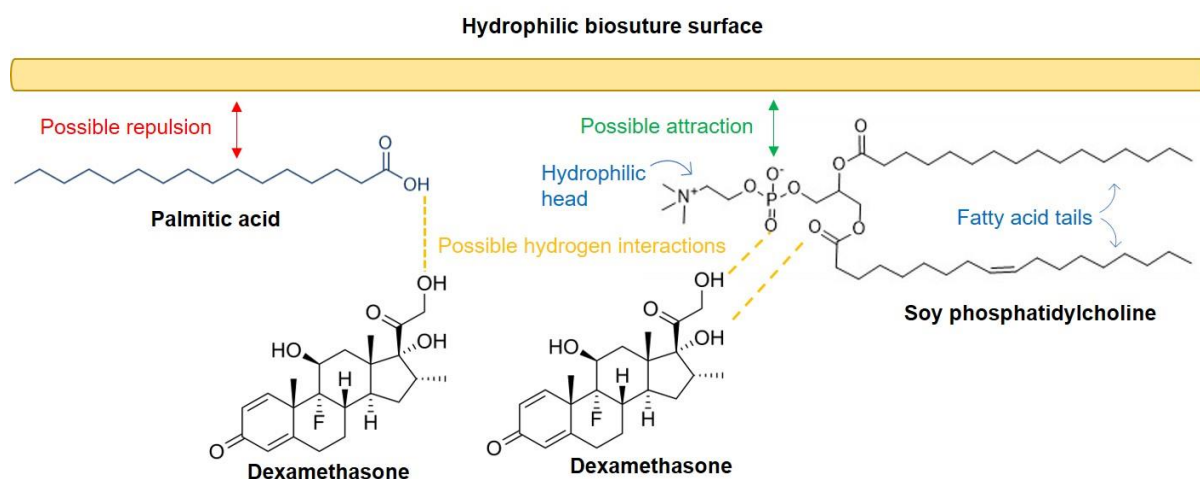


Figure 4.2: Chemical structures of the drug and lipids used in the study and possible interactions and attractive/repulsive forces that may occur.

4.3.2 Drug release behaviour of biosutures prepared with drug loading methods A – D.

For optimal prevention of ischemic reperfusion injury (IRI) and no-reflow in MVS, continued drug release for a period of 7 days is necessary. Hence, the drug release profile from the different drug loaded biosutures was evaluated over 7 days, at 37°C in PBS (pH 7.4) with continuous rotation at 25 rpm, to simulate physiological conditions. As expected, each of the drug loading methods resulted in their own unique drug release profile, with a similar pattern only observed for method A and D, while major differences were seen in the cumulative percentage drug released over the period of one week, for all biosutures (Figure 4.3).

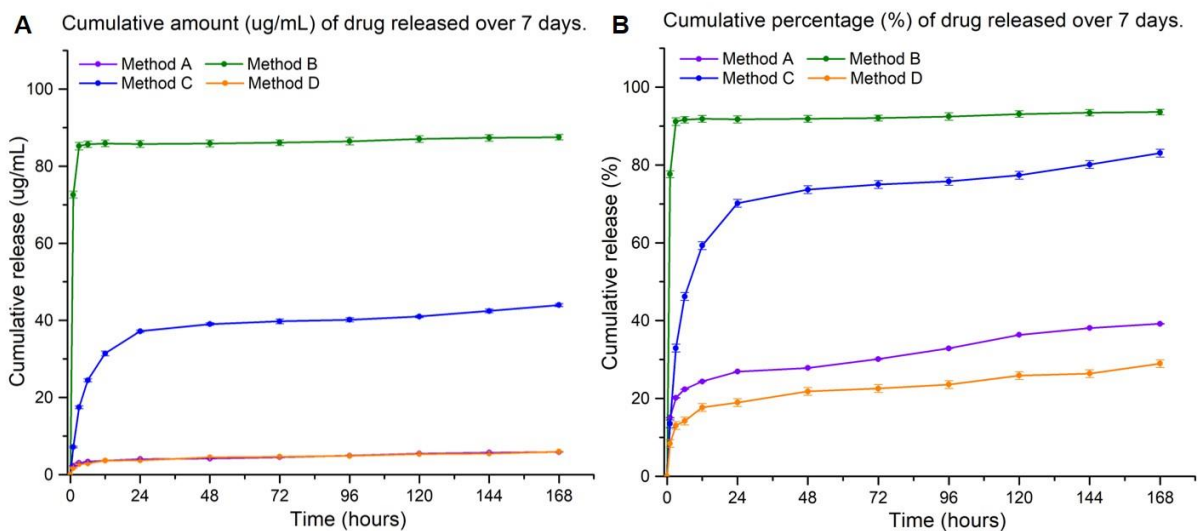


Figure 4.3: Cumulative drug release over 7 days in A) amount (ug/mL) and B) percentage (%) from biosutures prepared with method A – D.

Method A, where the drug was directly incorporated into the biopolymer matrix, released on average $39.2 \pm 0.8\%$ of the loaded drug at the end of the 7-day period (Figure 4.4 B). The drug release profile, showed an initial small burst release, which probably reflects the immediate release of the drug from the biosuture surface, as graphically represented in Figure 4.4 C. At this point in time, there is a large concentration gradient present, between the high concentration of drug on the biosuture surface, and the lack of drug in the release media, which explains this sudden burst effect. During the burst phase, drug release mechanisms, such as swelling and osmotic pressure may also play a role, as water penetrates the biopolymer matrix and causes the hydrophilic drug to diffuse out. After this initial phase, the drug release becomes more gradual and is controlled by the degradation of the biosuture material, i.e., as the biosuture degrades, new surfaces are exposed to the release medium, allowing drug molecules buried within the biopolymer matrix, to diffuse out and be released (Figure 4.4 C). This form of degradation dependant, controlled release is well-known and common among biodegradable polymer devices, but the specific released profile remains a function of the physiochemical properties of the particular polymers and drug used (Lee *et al.*, 2010). The degradation profiles of the biosutures, prepared with methods A – D, are provided and discussed in Section 4.3.4 of this chapter. Briefly, the biosutures prepared using method A, reflected an average degradation of $38 \pm 0.4\%$, after 7 days of incubation under simulated physiological conditions, which correlates well with the $39.2 \pm 0.8\%$ drug release that was recorded after 7 days of incubation for method A (Figure 4.4 D). This supports the hypothesis that drug release from the biosutures prepared with method A, is dependent on the degradation of the biosuture and suggests that 100% drug release can only be achieved after 33 days of incubation.

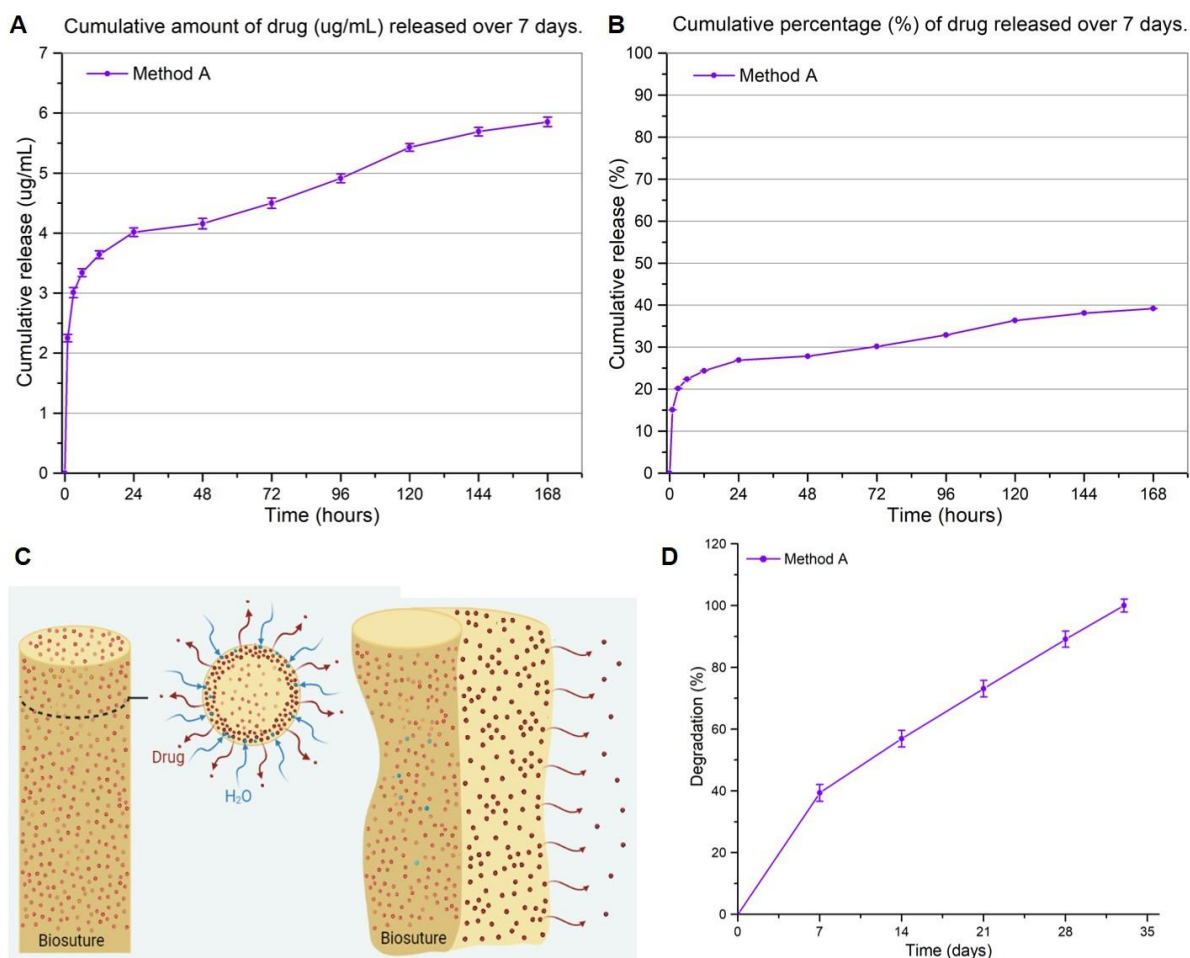


Figure 4.4: Cumulative drug release over 7 days in A) amount (ug/mL) and B) percentage (%) for biosutures prepared with method A. C) Graphical representation of the proposed drug release mechanism and D) the degradation profile of biosutures prepared with method A.

For method B, where the biosutures were immersed in a drug-saline solution, the drug release profile looked considerably different, with $91.1 \pm 0.9\%$ of the drug released within the first 3 hours of incubation (Figure 4.5 B). This form of immediate burst release, is also common, although not widely applicable within the clinical setting. A burst release of the drug from a biomaterial can be the result of several factors including, processing conditions (e.g., drying and storage), sample geometry and material-drug interactions (surface adsorption) (Son *et al.*, 2017). It is possible that, during the immersion process, the drug molecules only adsorbed to the surface of the biosuture, and then easily released upon submersion in PBS, with the hydrophilic nature of the drug further amplifying the burst effect (Yoo & Won, 2020). Yet, the significant swelling of the biosuture, that was observed during the immersion process, suggests that the dissolved drug was absorbed into the biopolymer matrix and hence evenly distributed throughout it. However, in contrast with method A, and the non-drug loaded biosuture, method B has an additional drying step in the fabrication process which, according to Yeo *et al.*, could cause migration of the drug to the surface of the biopolymer matrix which

will in turn lead to burst release (Yeo & Park, in press). During the drying process, water will have moved to the surface of the biosuture and evaporated, which could have caused the drug to diffuse by convection with the water, leaving a high drug concentration on the biosuture surface (Figure 4.5) which would have released in a burst fashion upon incubation in the release media, as shown in the drug release profile. The burst release phase was responsible for the release of more than 90% of the loaded drug, leaving very little to be released over the following days.

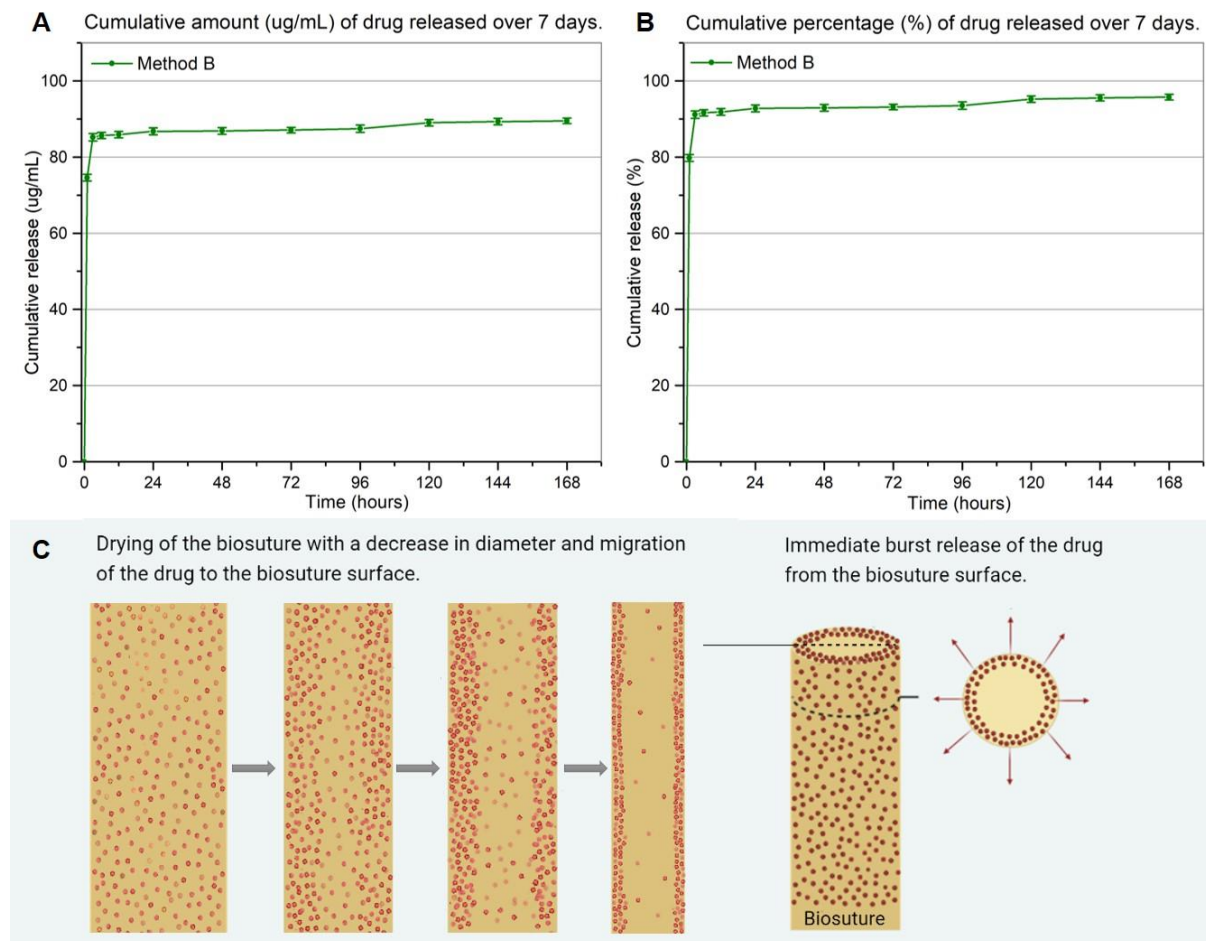


Figure 4.5: Cumulative drug release over 7 days in A) amount (ug/mL) and B) percentage (%) for biosutures prepared with method B. C) Graphical representation of drug migration to the surface of the biosuture during drying and subsequent burst release from the surface.

Method C provided a more appropriate and expected drug release profile, which consisted of an initial small burst phase, followed by a lag phase and finally a linear release phase (Figure 4.6). The controlled release, achieved with method C, is a result of the poor solubility of both the lipid and the drug in water (Obermeier *et al.*, 2015). The initial burst release, which is a common phenomenon among all drug delivery devices, including fibres, films and nanoparticles (Son *et al.*, 2017) can be ascribed to the close proximity of the drug to the biosuture surface, which resulted in direct exposure of the drug to the large volume of drug-

free release medium. This, in turn, created a large concentration gradient for the drug across a very short diffusion layer which encouraged immediate burst release (Figure 4.6). During this initial burst phase, the higher solubility of dexamethasone in aqueous media (0.1 mg/mL) compared to that of the lipid, SPC (2.1×10^{-5} mg/mL), might have played a considerable role by allowing a certain amount of drug to be released before segregation of the lipid layer from the biosuture surface. This would also play a role in the subsequent lag phase, where the release medium has become more saturated, resulting in a lower concentration gradient and decrease in the solubility of the drug, which would now prefer to remain within the hydrophobic lipid layer where it is most comfortable. Yet, after 5 days of incubation, the lipid layer begins to dissociate and move away from the biosuture surface, as was observed macroscopically during the drug release study, possibly due to the increased swelling of the biosuture that caused the surface to become more hydrophilic and less favourable for the hydrophobic lipid layer. At this point, drug release becomes more linear as the lipid-drug layer distributes throughout the release medium and exposes more of the drug molecules to fresh medium. By the end of the 7-day release period, more than 80% of the drug was released, which is ideal within the context of IRI and the no-reflow phenomenon in MVS.

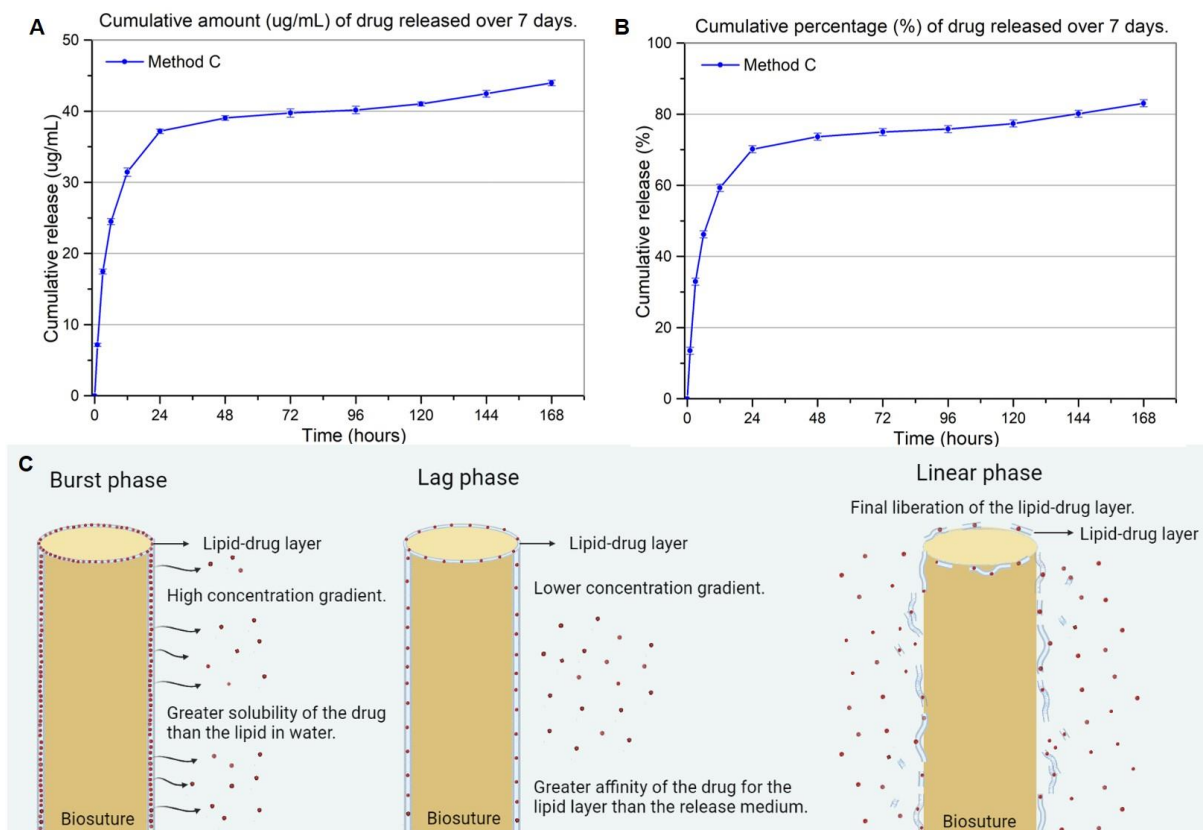


Figure 4.6: Cumulative drug release over 7 days in A) amount (ug/mL) and B) percentage (%) for biosutures prepared with method C and C) Graphical representation of the proposed drug release mechanism from biosutures prepared with method C.

The drug release profile of method D, was very similar in shape to that of method C but achieved a lower cumulative release of only $29 \pm 0.53\%$, after 7 days of incubation (Figure 4.7). Similar results have been recorded by Obermeier *et al.*, who found that palmitic acid provided extremely slow sustained release of chlorhexidine, with only 26% of the loaded drug released after 5 days of incubation (Obermeier *et al.*, 2014). This slower release from palmitic acid compared to SPC, can be ascribed to the poor solubility of palmitic acid in water, which is even lower than that of SPC, due to the complete lack of a polar or hydrophilic group in the fatty acid (van der Veen *et al.*, 2017). The drug release process, was however very similar to that of method C and also showed an initial burst release, followed by a lag phase which turned into a linear phase, once the lipid layer is liberated from the biosuture surface (Figure 4.7). Liberation of the lipid layer took place earlier for palmitic acid (96 hours) than for SPC (120 hours), presumably also because of the greater hydrophobicity of palmitic acid, that would have led to an earlier dissociation away from the hydrophilic biosuture surface.

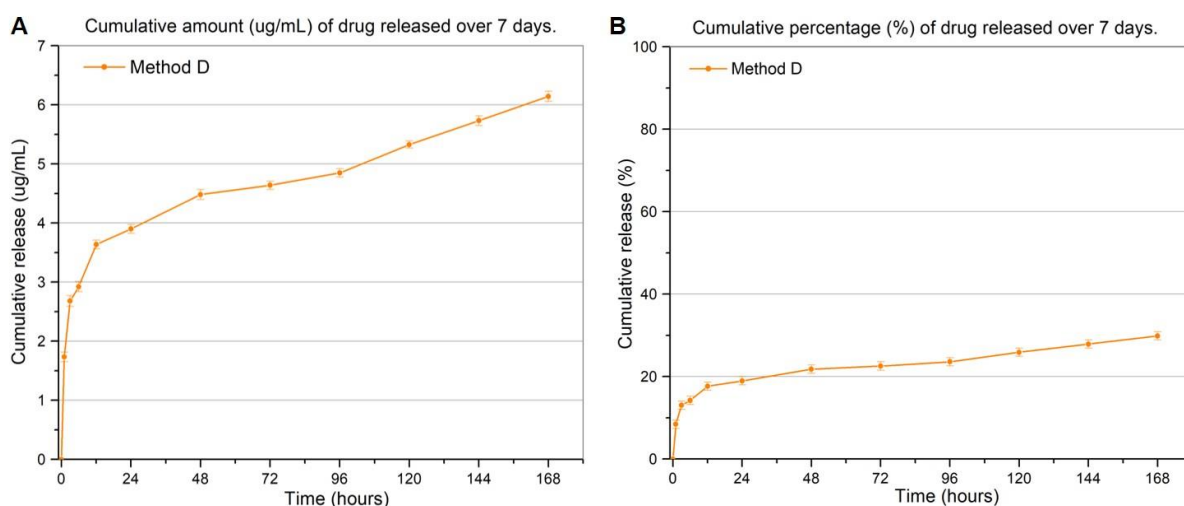


Figure 4.7: Cumulative drug release over 7 days in A) amount (ug/mL) and B) percentage (%) for biosutures prepared with method D.

4.3.3 Degradation profile of the different drug-loaded biosutures

Degradation *in vivo* is a very important property of absorbable biomaterials and can easily be influenced by processes such as drug loading and storage due to changes in intra- and intermolecular interactions, matrix density and hydrophilicity of the biomaterial, that may occur during drying or heating (Annan *et al.*, 2008). Hence, we studied the degradation profile of the biosutures, prepared with method A – D, before selecting the optimal drug loading method. Figure 4.8 provides the degradation profiles of the original biosuture before drug loading, and the degradation profiles of the biosutures prepared with drug loading methods A – D. In general, all the biosutures displayed a favourable degradation profile with gradual weight loss that took place over roughly 5 weeks. The exact method of degradation will be further studied

and elaborated on in a future chapter. Here, however, we are only concerned with the influence of drug loading methods on the degradation profile of the biosutures. The biosutures prepared with method A and B, degraded at a slightly faster rate than the original biosuture, or those prepared with method C and D. This can be ascribed to the presence of the drug within the biopolymer matrix, where it can interfere with the strong intramolecular interactions between the biopolymers, resulting in faster degradation of the biosuture. It is also possible that, during the immersion process used in method B, some of the intramolecular bonds were broken, through ionic interaction with salt ions in the immersion solution (Mndlovu *et al.*, 2019a). This would have dramatically decreased the biosuture tensile strength and matrix density, which would in turn have led to a more rapid degradation. However, this could not have taken place at a very pronounced degree, as the drug loading process had a very small effect on the degradation rate of the biosutures prepared with method B, which deviated even less from that of the original than those prepared with method A.

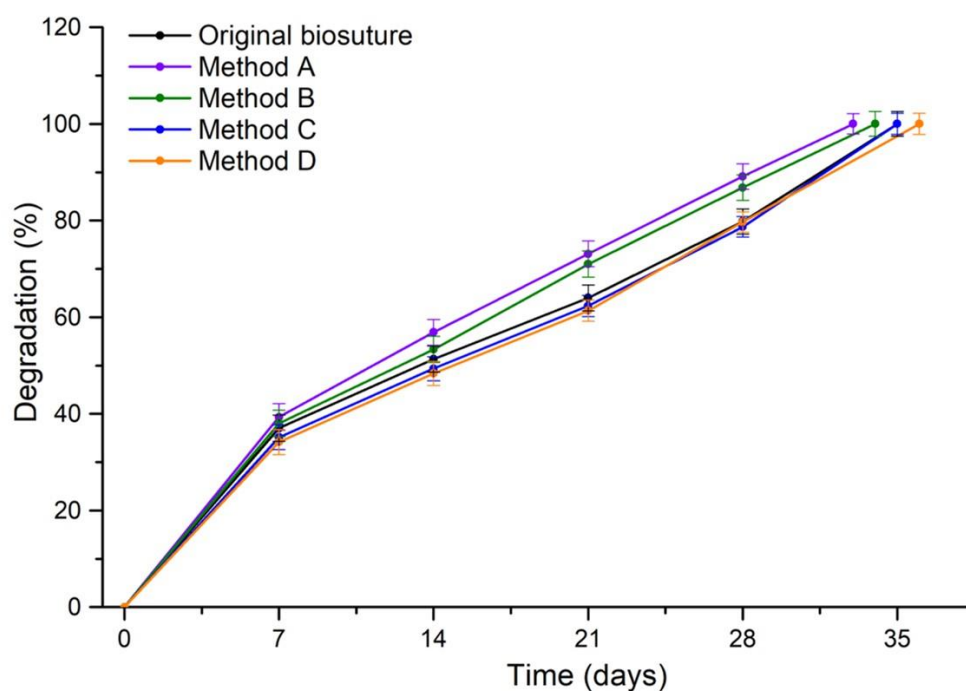


Figure 4.8: *In vitro* degradation profile of the original biosuture and of biosutures prepared with different methods (A – D) of drug loading.

The biosutures prepared with method C and D, degraded slightly slower than the original biosuture, or those prepared with method A and B. This is most likely due to the shielding effect of the hydrophobic lipid-drug layer, that temporarily prevented water from entering the biopolymer matrix, and thereby delayed the degradation process as a whole (Obermeier *et al.*, 2014). None of the drug loading methods, however, had a dramatic influence on the degradation profile of the biosutures, which followed more or less the same pattern regardless of the drug loading method that was employed.

4.3.4 Mechanical properties of the different drug-loaded biosutures

Even more important than the impact on the degradation profile of the biosutures, is the impact that drug loading has on the mechanical properties of the biosuture, which has been optimized with great effort in the previous chapter. The mechanical properties of the drug loaded biosutures could have a very decisive influence on the selection of the optimal drug loading method, as even a perfect drug loading and release profile is worthless without satisfactory mechanical properties. Hence, we studied the key mechanical properties, i.e., maximum load (N), tensile strength (N/mm²), elongation at break (%) and young's modulus (MPa), of the original and drug loaded biosutures. The average values of these parameters, for the original biosuture and the drug loaded biosutures, are provided in Table 4.3.

Table 4.3: The average values of key parameters used to study the mechanical properties of the original and drug loaded biosutures.

Biosuture	Load failure (N)	Tensile strength (N/mm ²)	Elongation at break (%)	Young's modulus (MPa)
<i>Straight configuration</i>				
Original	4.08 ± 0.4	360.39 ± 0.4	18.55 ± 0.9	2.04 ± 0.4
Method A	5.43 ± 0.5	480.83 ± 0.5	6.25 ± 0.8	2.52 ± 0.5
Method B	4.49 ± 0.3	397.93 ± 0.3	16.73 ± 0.4	2.38 ± 0.7
Method C	4.14 ± 0.7	366.23 ± 0.7	18.57 ± 0.5	2.06 ± 0.5
Method D	4.12 ± 0.6	391.69 ± 0.6	18.48 ± 0.7	2.10 ± 0.6
<i>Knot configuration</i>				
Original	2.44 ± 0.3	216.09 ± 0.3	9.47 ± 0.4	1.51 ± 0.4
Method A	1.64 ± 0.4	145.00 ± 0.4	4.59 ± 0.6	1.13 ± 0.6
Method B	2.57 ± 0.8	227.85 ± 0.8	6.75 ± 0.8	1.36 ± 0.5
Method C	2.59 ± 0.4	229.27 ± 0.4	12.26 ± 0.7	1.56 ± 0.3
Method D	2.45 ± 0.5	217.78 ± 0.5	12.14 ± 0.5	1.54 ± 0.5

Even though the drug loading processes did affect the mechanical properties of the biosutures, the effect was less pronounced than what was expected. Method A and B showed the greatest deviation and the biosutures prepared with method A could withstand a higher load (5.43 ± 0.5 N) than the original biosutures (4.08 ± 0.4) in the straight configuration. These biosutures, however, broke much earlier than the rest of the biosutures, as was signified in the considerably lower elongation at break (6.25 ± 0.8%) of the biosutures prepared with method A, than the original biosutures (18.55 ± 0.9%). This can be attributed to the incorporation of the drug into the polymer matrix, which might have increased the density and crystallinity of the biosuture material, making it stronger but also more brittle and less elastic (Li, Han, *et al.*,

2020). This loss in elasticity had a profound impact on the mechanical properties of the biosutures prepared with method A, in the knotted configuration where all the measured parameters decreased in comparison with the original biosuture, as shown in Table 4.3. Hence, the addition of a large drug molecule, such as dexamethasone 21-phosphate, directly to the polymer matrix, had a profound and undesirable influence on the biosuture's mechanical performance, which can clearly be observed in the representative stress – strain curves of the various biosutures (Figure 4.9). However, it should be noted that the addition of other drug molecules, such as proteins or low molecular weight drugs, might not have a significant influence on the mechanical properties of the biosuture, or could even improve the mechanical performance, depending on the specific setting and application. The knot stress – strain curves are bimodal due to the tightening of the knot that takes place (first mode) before the biosuture itself deforms (second mode).

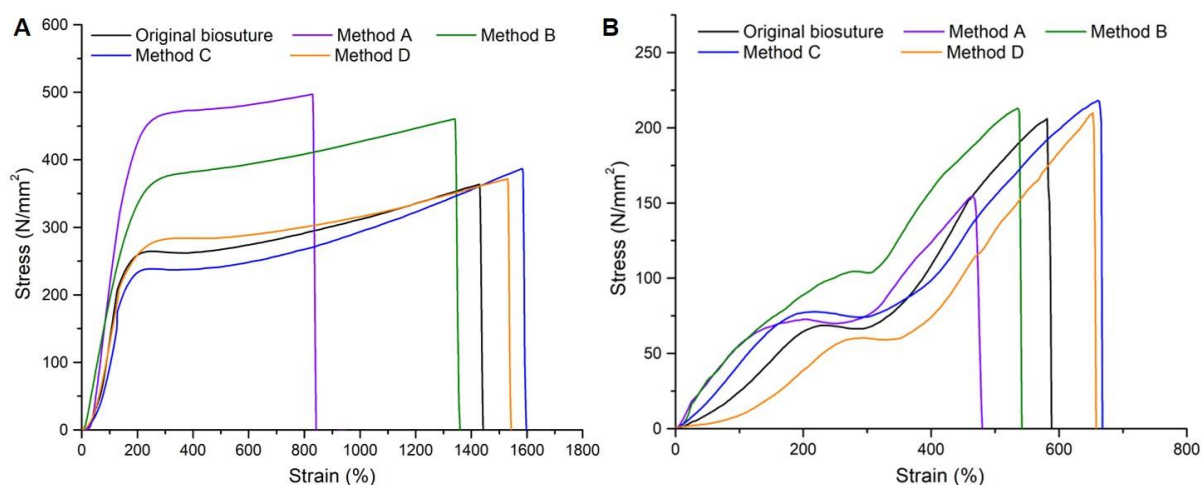


Figure 4.9: Representative stress – strain curves of the original and drug loaded biosutures in the (A) straight configuration and (B) knotted configuration.

The biosutures prepared with method B, on the other hand, displayed excellent mechanical properties with a slightly higher load failure in both the straight and knotted configuration (4.49 ± 0.3 N and 2.57 ± 0.8 N) compared to the original biosuture (4.08 ± 0.4 N and 2.44 ± 0.3). The elongation at break decreased slightly in the straight configuration (16.73 ± 0.4 %) and more profoundly in the knotted configuration (6.75 ± 0.8 %) but remained within an acceptable range. All the other parameters in the straight and knotted configuration were higher for the biosuture prepared with method B, than the original biosutures which suggests that the immersion process had a favourable influence on the mechanical properties of the biosutures. It is plausible that during the immersion process, drug molecules filled any available pores in the matrix, which would have slightly increased the density and hence the tensile strength of the biosutures, without interfering with existing molecular bonds (Mndlovu *et al.*, 2019b). The decrease in elongation at break is less pronounced than with method A, as the drug molecules

are only adsorbed to the matrix and not effectively intertwined between the polymers as evidenced by the burst drug release profile of the biosutures that were prepared with method B. In terms of mechanical properties, method B can therefore be presumed as a favourable method of drug loading.

The biosutures prepared with method C and D displayed very similar mechanical properties, and also did not deviate drastically from that of the original biosuture. This was expected as the lipid-drug coatings used in method C and D, do not directly affect the biosuture matrix and therefore should not significantly alter its mechanical performance. Coating, however, does change the surface of the material and can change the handling properties, knot security and slippage of the biosuture (Rethinam *et al.*, 2020). The load failure of the biosutures prepared with method C and D, was slightly higher than that of the original biosuture, in both the straight and knotted configuration (Table 4.3). This slight increase in load failure and tensile strength can be ascribed to the additional drying and water removal that transpired during the coating process. Yet, the elongation at break of the biosutures prepared with method C and D, were also higher than that of the original biosuture – especially in the knotted configuration (12.26 ± 0.7 N and 12.14 ± 0.5 % compared to 9.47 ± 0.4 %). This is most likely due to the lubricating effect of the lipid-drug layer on the surface of the biosutures, which allowed the biosuture to form a tighter, more secure knot, which in turn allowed the biosuture to elongate for longer before breaking (Matl *et al.*, 2009). Hence, the lipid-drug coatings, used in method C and D, improved the mechanical performance of the biosutures, especially in the knotted configuration, by improving the knot security of the biosutures.

4.3.5 Selection of the optimal drug loading method for the specific study

In selecting the optimal drug loading method, all the properties studied in this chapter, i.e., loading capacity, drug release, degradation, and mechanical performance, should be considered. Yet, the drug release profile and mechanical performance of the biosuture are the most critical properties and will carry the most weight in selecting the ideal method. Still, each of the properties must be appropriate within the context and application of the study, i.e., the prevention of IRI and no-reflow in MVS through the sustained release of dexamethasone from an absorbable biosuture material.

In terms of the loading capacity, the method should provide a realistic value, that can result in therapeutic drug levels after release *in vivo*. In the case of dexamethasone, which is a fast-acting glucocorticoid with 26 times the anti-inflammatory potency of hydrocortisone, relatively low dosages of 500 – 2500 ug is normally used for localized administration (e.g., dexamethasone eye drops or intracranial inserts) (Brooks *et al.*, 2020). Within the context of MVS applications, it is important to consider the length of suture that will be administered in

order to ensure that on average, the amount of released drug is within a safe and therapeutic range. Depending on the surgeon, 8 – 12 interrupted sutures are normally used to achieve microvascular anastomosis, with each knot comprising around 2 cm of suture material (Blanchaert., 2012). Hence, on average 20 cm of suture material is implanted at the site of anastomosis and can be used to achieve localized drug delivery.

Method A provided biosutures with a drug loading capacity of 298.8 ± 2.8 ug per 20 cm biosuture (Table 4.2) which is considerably lower than the dosage normally used for localized dexamethasone administration. The biosutures prepared with method B and C, on the other hand, displayed favourable drug loading capacities of 1870 ± 2.7 ug and 1060 ± 1.8 ug per 20 cm biosuture, respectively. These values are within an acceptable range and can provide clinically relevant drug dosages after implantation of the biosutures, without the risk of reaching toxic drug concentrations. Method D again resulted in biosutures with a low drug loading capacity (411.4 ± 2.1 ug per 20 cm biosuture) that will not be able to produce therapeutic drug levels *in vivo*. Yet, these drug loading capacities have not been optimized and small alterations, such as increasing the drug concentration used for method A and B or changing the lipid-drug ratio of method C and D, could significantly improve the loading capacity achieved with these methods. Hence, drug loading capacity is not used as a decisive factor for selecting the most appropriate drug loading method, but method B and C are highlighted as the most suitable amongst the methods that were investigated.

The drug release profiles of the biosutures prepared with the different methods, were all valuable in their own right, but not necessarily all suitable for the goal of this study. Biosutures prepared with method A, released the drug slowly and gradually as the biosuture itself degraded. This meant that 100% drug release could only be achieved after 33 days, when the biosuture was fully degraded. This form of slow, controlled drug release is ideal for treating chronic conditions such as glaucoma or rheumatoid arthritis, where long-term drug administration is necessary but not in the case of more acute conditions such as IRI and no-reflow where the risk subsides within a week after surgery. Additionally, with immunosuppressant drugs such as dexamethasone, the time of drug administration must be kept to a minimum in order to limit the risk of infections or similar complications. Method A is therefore not the ideal method of drug loading for this particular study.

In contrast to the slow release achieved with method A, the biosutures prepared with method B, released the drug in an immediate burst fashion that represented more than 90% of the loaded drug. Burst release is a very common and troublesome occurrence in the field of pharmaceutical sciences and controlled drug delivery. The biggest concern with burst release is the risk of reaching drug concentrations near or above toxic levels *in vivo* (Abbasnezhad *et*

al., 2021). However, even if no harm is caused by the immediate high drug release rates, it does result in therapeutic and economical waste as a large amount of the released drug will be metabolised and excreted before it can produce any therapeutic effect. Burst release also reduces the lifespan of the drug delivery device as it leaves it practically empty with no further drug to release (Huang & Brazel, 2001). Hence, method B is also not the optimal method of drug loading for this study.

The biosutures prepared with method C, however, displayed a favourable drug release profile that consisted of an initial small burst release phase followed by more controlled and gradual release phase over the next 7 days. This is ideal in the case of MVS, where the initial burst release can immediately reduce the damage caused by IRI, at the onset of reperfusion, while the prolonged drug release will limit the risk of the no-reflow phenomenon setting in. The biosutures prepared with method C also released more than 80% of the drug that was loaded by day 7, making this a very good drug loading method to employ in this study.

The biosutures prepared with method D displayed a similar drug release profile to that of the biosutures prepared with method C, with the exception that only 30% of the loaded drug was released after 7 days of incubation. This suggests that longer time periods are necessary to achieve 100% drug release from the biosutures prepared with method D, making it a less than ideal for the prevention of IRI and no-reflow in MVS.

The degradation profiles of the biosutures prepared with method A – D were very similar and did not deviate significantly from that of the original biosuture. All the biosutures degraded within 5 weeks, which falls within the USP guidelines for classification of a suture material as absorbable and places all the methods of drug loading on equal footing in terms of degradation.

The different drug loading methods also had a very interesting influence on the mechanical properties of the biosutures. The biosutures prepared with method C and D, displayed the best mechanical performance with higher load failure, tensile strength, and elongation at break, in both the straight and knotted configuration, than the original biosuture. However, the mechanical properties of the biosutures prepared with method C were also acceptable, with only the elongation at break decreasing slightly. Hence, based on mechanical performance alone, either method B, C or D could be employed as drug loading method in this study.

Table 4.4 summarises the methods that performed best in each of the categories that were evaluated in this chapter. From this table and the above discussion, it is clear that method C, where the biosutures were coated with a lipid-drug layer consisting of SPC and dexamethasone, is the most appropriate drug loading method for this study.

Table 4.4: Summary of the methods that performed best in the investigated categories.

Property	Method(s)	Comment
Drug loading capacity	B and C	Methods could provide clinically relevant and therapeutic drug concentrations
Drug release	C	Method displayed the most appropriate drug release profile with near 100% drug release after 7 days of incubation.
Degradation	A, B, C, D	All methods had favourable degradation profiles.
Mechanical performance	C and D	Methods improved the mechanical performance of the biosuture on all accounts.

4.3.6 Conclusion

In this chapter, different methods of transforming the newly developed biosuture into a drug delivery device, were investigated. These methods were A) addition of the drug directly to the biopolymer matrix, B) immersion of the biosuture in a drug-saline solution, C) coating of the biosuture with a lipid-drug layer consisting of soy phosphatidylcholine and dexamethasone and D) coating of the biosuture with a lipid-drug layer consisting of palmitic acid and dexamethasone. The biosutures prepared with each of these methods were studied in terms of drug loading capacity, drug release, degradation behaviour and mechanical performance.

The drug loading capacity achieved with method A and D were disappointing and too low to provide therapeutic drug concentrations *in vivo*. The drug loading capacities of biosutures prepared with method B and C, on the other hand were within an acceptable range and high enough to provide clinically relevant dosages, without a significant risk of reaching toxic drug concentrations. The best drug release profile was achieved with method C, which provided slow, controlled release of the drug with near 100% drug release after 7 days of incubation. Method B, on the other hand, did not control the drug release effectively and resulted in an immediate burst release of nearly all the loaded drug within the first day of incubation. The biosutures prepared with method A and D, released the drug in a highly controlled fashion and did not reach depletion early enough to be applicable in this study. The degradation profile of the biosutures prepared with method A – D did not deviate significantly from each other or from the original, non-drug loaded biosuture. The biosutures prepared with method C and D displayed the best mechanical performance, with overall improvement of all the mechanical properties, and especially the knot security of the biomaterials.

Hence, method C was selected as the optimal method of drug loading within the context of this study and the biosutures prepared with this method will be further discussed in subsequent chapters.

CHAPTER 5: PHYSIOCHEMICAL AND PHYSICOMECHANICAL CHARACTERIZATION OF THE OPTIMIZED MONOFILAMENT, ABSORBABLE, DRUG-ELUTING BIOSUTURE.

5.1 Introduction

In the previous chapters, the concept for a new biosuture was constructed, studied, reviewed and then executed through the meticulous development and optimization of a new biosuture material with appropriate production and drug loading methods. However, all these efforts are pointless if not followed up by thorough characterization of the physiochemical and physicomechanical properties of the newly developed biosuture. According to De Jong *et al.*, knowledge of the material properties of alginate fibres, as well as the properties that govern and influence them, such as chemical structure, purity, and stability, is necessary to effectively use these systems (De Jong *et al.*, 2019). Likewise, evaluation of the *in vitro* behaviour of biomaterials is critical in forecasting its success *in vivo*. Hence, this chapter will be focussed on elucidating key properties of both the pristine biopolymers and that were used to produce the biosutures, and that of the uncoated and coated biosutures themselves.

5.2 Materials and methods

5.2.1 Materials

Sodium alginate (M/G ratio, 1.45), pectin from citrus peel (degree of esterification, 86.44%), gelatin (pharmaceutical grade, no. 48723, type B), and dexamethasone (bioreagent, suitable for cell culture, $\geq 97\%$), were purchased from Sigma-Aldrich (St. Louis, Missouri, USA). Barium chloride 2-hydrate and glycerol (MW=92.1 g/mol) was purchased from LabChem (Founder's hill, Johannesburg, SA). Phosphate buffered saline (PBS) tablets and ethanol were purchased from Rochelle Chemicals (Electron, Johannesburg, SA). Phosphatidyl choline (from soybean, <99% TLC) was procured from Avanti Polar Lipids Inc (Alabaster, Alabama, USA).

5.2.2 Preparation of the optimized biosutures

The biosutures were prepared using the optimized formulation and methods, developed in the previous chapters. First, the biopolymers were individually dissolved in deionized water and then combined, together with the plasticizer, to obtain the final concentrations as shown in Table 5.1. The biopolymer solution was sonicated in a bath ultrasonicator (Labotec, Midrand, SA), until a homogenous, bubble-free solution was obtained (± 5 minutes). The solution was aspirated with a 3 mL luer-lock syringe and loaded onto the specialized universal syringe rig of the Texture Analyser (TA, XT plus, Stable Micro Systems, England). The syringe was fitted with a 23G needle and the biopolymer solution extruded into a crosslinker solution of BaCl₂ (2% w/v). The Texture Analyser was set in the compression mode with the standard 'return to

start' sequence, a target of 50 mm distance and 'button' as the trigger type. An initial high-speed setting of 2 mm/sec was used to prevent clogging of the needle tip. Once a proper flow was established, a lower speed setting of 0.6 mm/sec was used and the crosslinker bath moved in a circular direction. After crosslinking, the biosutures were removed from the crosslinker bath and washed repeatedly with deionised water to remove any excess crosslinker from the biosuture surface. The washed biosutures were placed on a large ointment tile and left to dry in a fume hood with constant circulating air for 40 minutes.

Table 5.1: Composition of the optimised biosuture formulation

Component	Sodium alginate	Pectin	Gelatin	Glycerol
Concentration	6% (w/v)	0.1% (w/v)	3% (w/v)	4% (v/v)

Half of the prepared biosutures were coated with a lipid-drug layer to achieve drug loading. The lipid-drug solution was prepared by dissolving soy phosphatidylcholine (SPC) and dexamethasone in a 40:60 ratio, in 7.9 g (10 mL) of ethanol to obtain a final 8.5% w/w solution. The lipid-drug solution was dropped over the biosutures with a syringe and allowed to spread along the length of the biosutures. The coated biosutures were again placed under the fume hood for rapid evaporation of the solvent and formation of a thin lipid-drug layer on the biosuture surface.

5.2.3 Evaluation of vibrational transitions within the biosuture by means of Fourier Transform Infrared Spectroscopy (FTIR)

FTIR is a valuable, non-destructive analytical technique that is often used as the first step in material analysis. It's a highly sensitive method and can indicate any changes in a material's composition, the formation or breaking of bonds or the introduction of impurities amongst others. These changes can be observed as the appearance or disappearance of infrared absorption bands that are characteristic of certain functional groups or as shifts in these vibrational frequencies. In the current study, FTIR spectroscopy was used to study the interactions between the different natural polymers, plasticizer, crosslinking salt, and drug-coating of the newly developed biosuture material. Specifically, the goal was to confirm the compatibility of the polymers in the suture formulation, crosslinking of the polymer blend and effective coating of the biosuture material with the drug-lipid layer. All formulation components were run individually and compared to that of the biosuture material before crosslinking, after crosslinking and after coating with the drug-lipid layer. FTIR parameters were set as follows; 75 scans at a wavenumber range of 4000 – 650 cm^{-1} using a PerkinElmer Spectrum 2000 FTIR spectrometer (PerkinElmer 100, Llantrisant, Wales, UK) fitted with a single reflection diamond MIRTGS detector.

5.2.4 Evaluation of the relative crystallinity of materials by means of Powder X-ray Diffraction (XRD)

X-ray diffraction (XRD) is a valuable, non-destructive method that provides information on the crystallographic structure of materials. In the current study, XRD was used to determine the degree of crystallinity of the individual polymers and gain insight into the different phases present within the polymers, i.e., their chemical composition. XRD was also performed on the biosutures to study the influence that the combination and crosslinking of the selected biopolymers had on the crystallinity of the final biosuture material, bearing in mind that it needs to be strong, yet elastic. A high degree of crystallinity would result in brittleness which is not desirable in the case of suture materials. The XRD spectra of the biopolymers, the biosutures and the lipid-drug coated biosutures were recorded using a benchtop Miniflex 600 diffractometer (Rigaku, Japan) with CuK α radiation at 40 kV and 15 mA. The 2 θ scan range was selected between 10–90 degrees at a scan rate of 10 degrees/minute.

5.2.5 Thermal evaluation of the biosutures by means of Thermogravimetric analysis (TGA) and Differential Scanning Calorimetry (DSC)

Thermal analysis of the biosuture material, before and after coating, and of the individual biopolymer constituents, were conducted via Thermogravimetric Analysis (TGA), Differential Scanning Calorimetry (DSC), and melting point analysis. The thermal analysis of biomaterials is typically conducted at wide temperature ranges (0 – 500 °C) that far exceed the normal temperature encountered by the materials *in vivo* or during distribution and storage. Hence, it can seem like a fatuous study but, if properly analysed, thermo-analytical techniques can provide valuable information on the physical and chemical properties of the material such as its thermodynamic behaviour, heating capacity, stability and interactions between macromolecules or other chemical reactions and/or structural changes that take place at high temperatures, which might even be encountered during production, storage, or transport.

TGA measures the change in weight that occurs as a sample is heated at a constant rate and is useful for studying the thermal stability, decomposition temperature and fraction of volatile components of the material. The first derivative of the TGA data (DTG) can also be useful as it indicates the exact temperature at which weight changes occur, as well as the rate of weight loss at each temperature point. DSC is a popular technique that measures the heat flow into or out of a sample as a function of time or temperature, while the sample is exposed to a controlled temperature range. This enables the measurement of specific transitions in the material such as the glass transition, melting and crystallization point. Melting point analysis, with a digital melting apparatus, does not provide any additional information on the thermal

properties of the investigated material, but can confirm TGA and DSC data while providing a visual understanding of the changes that occur in the material during the heating process.

For the TGA analysis, samples of the biosuture material (uncoated and coated) and the pristine biopolymers, were heated at a rate of 10 °C/min from 0 – 900 °C under continuous nitrogen purging, using a thermogravimetric analyser (TGA 4000, PerkinElmer, Llantrisant, Wales, UK). TGA data was used to plot both the TGA and DTG curve of the materials. For the DSC analysis, samples of 3 – 10 mg were sealed in aluminium crucibles and heated over a temperature range of 0 – 400 °C at a heating rate of 5 °C/min under N₂ atmosphere, using a differential scanning calorimeter (DSC 1, STARe System, Mettler Toledo, Schwerzenbach, ZH, Switzerland). The melting point analysis was performed on biosuture samples that were loaded into glass capillary tubes and heated from 0 – 250 °C using a digital melting point apparatus (Electrothermal, Stone, Staffordshire, UK).

5.2.6 Evaluation of the surface morphology of biosutures by means of light microscopy and Scanning Electron Microscope (SEM) imaging

Scanning electron microscope (SEM) imaging is a key part of material characterization as it provides high-resolution, magnified images that can reveal detail about the material topography that is not visible to the naked eye (Sun, Lux, *et al.*, 2020). Microscopy can reveal important information such as the texture, porosity and size of the studied material and allows us to conclude whether the material will be suitable for its purpose. It can also provide information on the compatibility of the constituting elements and uniformity of the final formulation (Brodusch, N., Demers, H. and Gauvin, 2017). In the current study, a CKX 53 light microscope (Olympus, Tokyo, Japan) was initially used to study the ability of the biosutures to tie secure knots and to confirm the diameter of the biosutures. Hereafter, SEM images were taken with a Phenom™ Scanning Electron Microscope (FEI, OR, USA), to get more detailed information on the surface morphology of the biosutures, before and after coating. Before SEM analysis, biosuture samples (approximately 1 cm in length) were mounted onto aluminium stubs, secured with carbon adhesive tape, and coated with carbon and palladium/gold in a 2:1 ratio.

5.2.7 Evaluation of the mechanical properties of the biosutures

The mechanical properties of the biosutures were re-evaluated to ensure the accuracy and reproducibility of the results. The same method and equations described in Chapter 3 and 4 were employed here and again used to construct the stress-strain curves of the uncoated and coated biosutures.

5.2.8 Evaluation of the *in vitro* drug loading and release behaviour of the biosutures

Dexamethasone loading and release were again evaluated by means of ultra-violet (UV) spectroscopy using the nanophotometer (Implen GmbH, München, Germany). The same wavelength ($\lambda=241$), calibration curve, linear regression equation ($y = 0.0575x - 0.0299$; $R^2 = 0.9983$) and methodology described in Chapter 4, was employed here. The only exception is that data points were recorded until the cumulative drug release no longer increased, i.e., until complete drug release was achieved.

5.2.9 Evaluation of the *in vitro* swelling and degradation behaviour of the biosutures

The ability of the uncoated and coated biosutures to absorb water was evaluated by incubation of pre-weighed samples in 10 mL of PBS (pH = 7.4) at 37°C. Samples were removed from the PBS solution at frequent time points (10, 20, 30 and 50 minutes and 1, 2, 3, 4, 8, 12, 24 hours) to determine the swelling rate and time point of equilibrium swelling. Surface water was gently removed using filter paper and the samples weighed on a precision microbalance (A&D Instruments Limited, Oxfordshire, OX14 1DY, United Kingdom). The swelling ration (SR) was calculated using Equation 5.2.

$$SR = \frac{W_s - W_d}{W_d} \quad \text{Equation 5. 1}$$

Where W_s is the weight of the swollen sample and W_d the original weight of the dry sample.

The degradation profiles of the coated and uncoated biosutures were evaluated in terms of weight loss over time. Pre-weighed samples were again incubated in 10 mL fresh PBS (pH = 7.4) at 37°C, rotating at 25 rpm. Samples were removed after 1, 2, 3, 4 and 5 weeks of incubation, placed on absorbent filter paper and allowed to dry under lamellar flow in a fume hood. Once the samples were dry and achieved a constant diameter, they were accurately weighed on a precision microbalance and the percentage weight loss (i.e., degradation) calculated using Equation 5.3.

$$\text{Percentage degradation} = \frac{W_o - W_t}{W_i} \times 100 \quad \text{Equation 5. 2}$$

Where W_o is the original, starting weight of the sample and W_t is the weight at time t , after incubation in PBS. All experiments were performed in triplicate and expressed as the mean, \pm standard deviation. The appearance of the biosutures during the degradation process was studied by imaging the dried, weighed samples with a scanning electron microscope (Phenom™ Scanning Electron Microscope, FEI Company, OR, USA).

5.3 Results and discussion

5.3.1 Preparation of the optimized biosutures

The uncoated and coated biosutures were successfully prepared according to the formulation and methods there were optimised in the previous chapters. Figure 5.1 provides pictures taken at different stages of the biosuture fabrication and coating process and represents the following:

- A) The biopolymer solution, that consist of alginate (6% w/v), pectin (0.1% w/v), gelatin (3% w/v) and glycerol (4% v/v), after the removal of air bubbles via sonication.
- B) The extrusion process where the biopolymer solution is extruded at a constant rate into the crosslinker solution (BaCl_2 , 2% w/v) using the Texture Analyser (T.A.X.T Plus).
- C) Drying of the biosutures in a fume hood, after they have been washed repeatedly in deionised water baths.
- D) Drop coating of the dried biosutures with a lipid-drug solution (8.5% w/w) consisting of soy phosphatidylcholine and dexamethasone in a 40:60 ratio.
- E) Drying of the coated biosutures in a fume hood for rapid evaporation of the solvent.
- F) The final biosutures, prepared and ready for analyses.

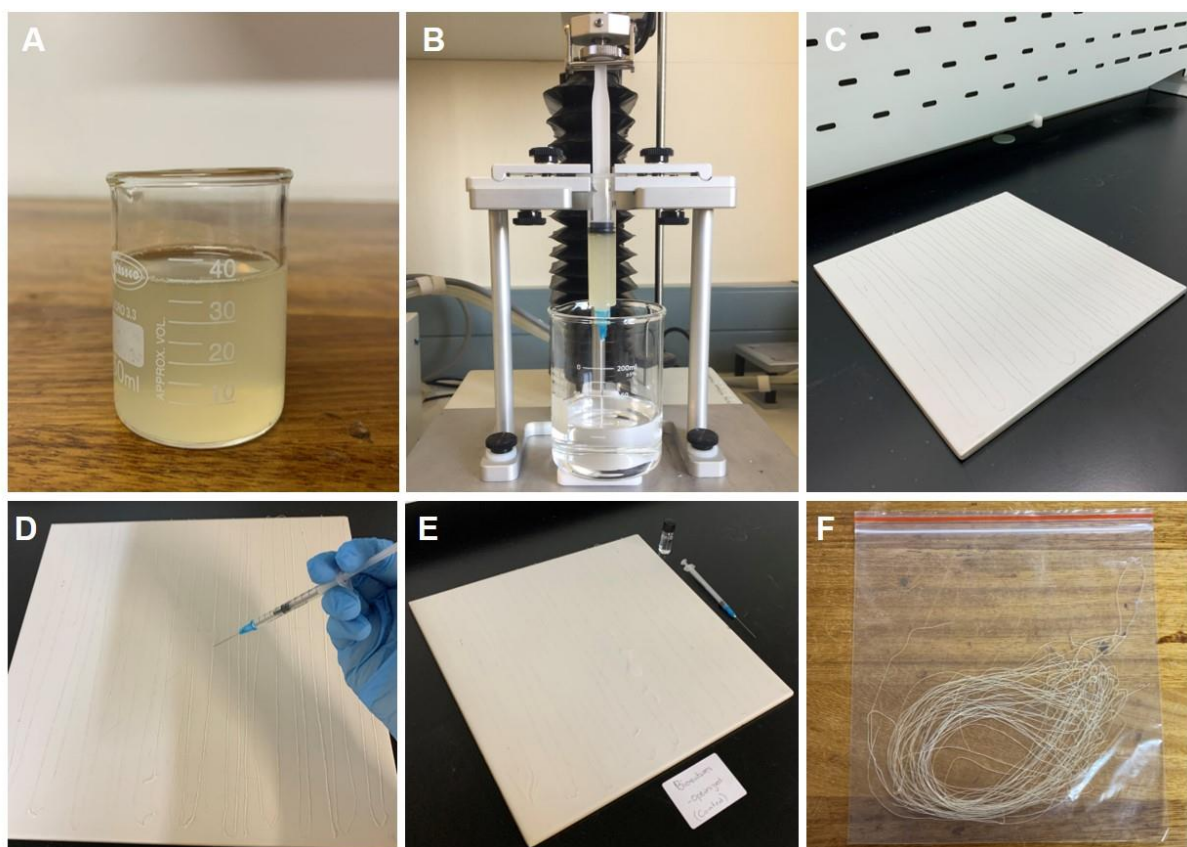


Figure 5.1: Images taken during the biosuture fabrication process; A) biopolymer solution, B) extrusion into the crosslinker, C) drying in a fume hood, D) coating with lipid-drug layer, E) drying of the coated biosutures F) final coated biosutures.

5.3.2 Evaluation of vibrational transitions within the biosuture by means of Fourier Transform Infrared Spectroscopy (FTIR)

In order to make a comparative study of the FTIR spectra of the newly developed biosutures, we first analysed the spectra of the individual formulation components, which was then used as a reference for the biosuture spectra. The FTIR spectra of the biopolymers also helped us to confirm the composition and structure of the biopolymers that were employed in this study. Figure 5.2 shows the FTIR spectra of the biopolymers and plasticizer that was used in the biosuture formulation.

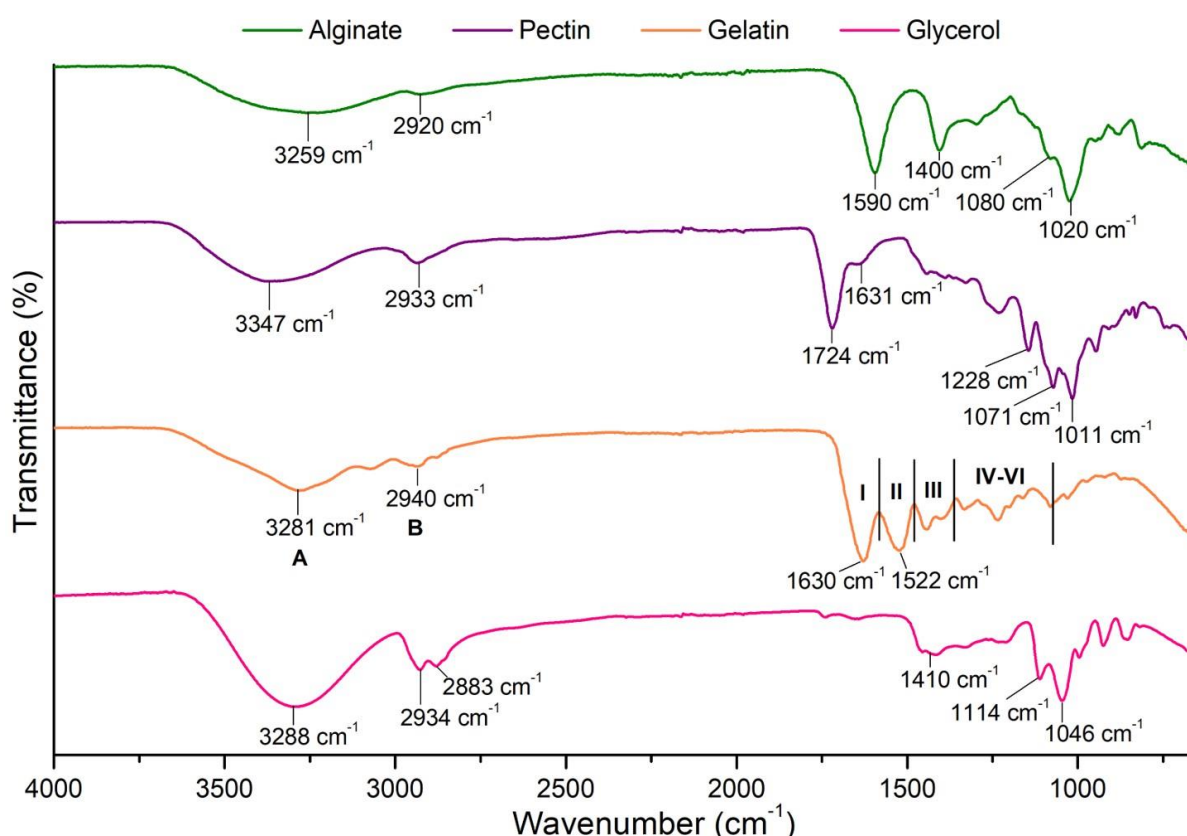


Figure 5.2: FTIR spectra of the biosuture formulation components in their pristine form, top to bottom: alginate, pectin, gelatin and glycerol.

The FTIR spectrum of alginate, gives a clear indication of all the functional groups found in the molecule and correlates well with the spectra found in literature (Merakchi *et al.*, 2019; De Moraes & Beppu, 2013). The broad absorption band in the range of 3600 – 3000 cm^{-1} , represents the stretching vibrations of the -OH groups attached to the tetrahydropyran ring, while the -CH vibration was observed as a small absorption band at 2930 – 2840 cm^{-1} , as previously reported by Fenoradosoa *et al.*, (Fenoradosoa *et al.*, 2010). The two characteristic bands at 1590 and 1400 cm^{-1} , can be ascribed to the symmetric and asymmetric stretching vibrations of the -COO groups. This is the site where any ionic interaction, such as crosslinking

by means of Ba^{2+} , can potentially take place which will cause a shift and/or change in intensity of these bands (Badita *et al.*, 2020). There is also a shoulder at 1080 cm^{-1} which, according to Badita *et al.*, can be ascribed to C-C and C-O stretching vibrations (Badita *et al.*, 2020) while the strong, sharp peak at 1020 cm^{-1} is reflective of the pyranosyl ring with its C-C and C-O stretching vibrations (Fenoradosoa *et al.*, 2010; Nastaj *et al.*, 2016). In the fingerprint region, stretching vibrations of the uronic acid residues are encountered, as was discussed in Chapter 3 (Daemi & Barikani, 2012). The IR spectrum of alginate, therefore, clearly indicates all the functional groups present in the molecule without any traces of impurities.

Pristine pectin also delivered an expected IR spectrum that corresponds well with literature (Fracasso *et al.*, 2018; Nisar *et al.*, 2019). The broad band around 3347 cm^{-1} , can safely be ascribed to the stretching vibrations of the hydroxyl groups of pectin while the less intense peak at 2933 cm^{-1} can be related to CH (CH, CH_2 and CH_3) vibrations (Mishra *et al.*, 2008). According to Assifaoui *et al.*, the CO groups of pectin normally present as three peaks in the $1750 - 1200$ region of the IR spectrum, as was observed in the current study (Assifaoui *et al.*, 2010). The first and most intense CO peak is found at 1724 cm^{-1} and relates to the carbonyl group of the methyl ester, while the other two CO peaks (at 1631 and 1228 cm^{-1} respectively) can be allocated to the stretching vibrations of free carboxylate groups (Chaharbaghi *et al.*, 2017). The later bands at 1071 and 1011 cm^{-1} is indicative of a pyran sugar in the pectin sample and can be interpreted to be caused by neutral sugars, such as arabinose or xylose, as was seen in a study done on pectin quality and yield (Baum *et al.*, 2017).

Compared to the previous two polymers, gelatin has a much larger and slightly more complex molecular structure that is comprised of amino acids joined together by amide bonds, which give rise to characteristic IR absorption bands (Das *et al.*, 2017). The peak observed at 3281 cm^{-1} , can be attributed to the presence of hydrogen bonds but is also representative of the amide A band which arises from N-H stretching, while the C-H stretching at 2940 cm^{-1} , is representative of amide B as was described by Hossan *et al.*, (Hossan *et al.*, 2014). According to Sancakli *et al.*, the strong absorption band at 1630 cm^{-1} is due to C=O stretching and hydrogen coupling with COO, which is representative of amide I. In turn, the peak at 1522 cm^{-1} is thought to be representative of amide II and caused by bending vibrations of N-H groups and stretching vibrations of C-N groups (Sancakli *et al.*, 2021). Amide III often presents as several small peaks, which can be seen at $1443 - 1358\text{ cm}^{-1}$ and is related to in plane vibrations of C-N groups as well as N-H groups of bound amines (Irfanita *et al.*, 2017). Furthermore, an intensive study done by Rahman *et al.*, showed that the peaks observed in the region of $1235 - 1080\text{ cm}^{-1}$ belong to amide IV, V and VI (Al-Saidi *et al.*, 2012). Hence, the IR spectrum obtained for gelatin in this study is well defined and in-line with the spectra found in literature.

The last component of the biosuture formulation is the plasticizer, glycerol, which can have a profound impact on the final composition and properties of the biosuture material (Barbut & Harper, 2020). In the IR spectrum of glycerol, a characteristic deep peak can be observed at 3288 cm^{-1} , which corresponds with O-H stretching, followed by a bimodal peak at 2934 and 2883 cm^{-1} , due to C-H symmetric and asymmetric stretching (Salehpour & Dubé, 2012). The rest of the spectrum also correlates well with literature and displays five peaks in the region from $800 - 1150\text{ cm}^{-1}$, which is typical of glycerol and corresponds with the vibrations of the C-C and C-O linkages. The peaks at 854 , 925 and 995 cm^{-1} , can be ascribed to the vibration of the C-C skeleton, the absorption band at 1046 cm^{-1} to the C-O bond in C1 and C3, and the band at 1114 cm^{-1} to the C-O stretching in C2 (Guerrero *et al.*, 2010). According to Turney *et al.*, the peak around 1410 cm^{-1} is due to C-OH in plane bending and the IR spectrum of glycerol therefore correlates well with previous studies and shows no sign of impurities (Turney *et al.*, 2013).

Next, we studied the FTIR spectra of the biosuture formulation, before and after crosslinking to confirm the presence of the biopolymers and observe any vibrational changes that occurred (Figure 5.3). The IR spectrum of the biosuture closely resembles the spectrum of the main component, i.e., sodium alginate, with clear contributions from the second most abundant component, i.e., glycerol. The presence of the other two biopolymers, i.e., pectin and gelatin, is less prominent but can safely be deduced. This points to good compatibility and effective incorporation of the low concentration biopolymers into the alginate matrix. The broad band around 3269 cm^{-1} was observed in the IR spectra of all the pristine polymers, but its intensity is greatly increased in the combined biosuture formulation spectrum. This can be due to the combined contribution of all the hydroxyl groups in the various biopolymers which will increase the absorption in this region, as was seen in a study done by Majidi *et al.*, (Majidi *et al.*, 2018). This peak, even though broad, is narrower than in the case of the pristine polymers and resembles the deep absorption band of glycerol in this region, pointing towards its presence in the formulation. The peak also shifted from 3259 cm^{-1} (where it was observed in the alginate spectrum, as shown in Figure 5.2) to 3269 cm^{-1} , which suggests that hydrogen bonds have formed between the different polymers and confirms their compatibility.

The small peak in the 2900 cm^{-1} region, was observed for all of the individual components and were ascribed to the stretching vibrations of the C-H groups of the polymers. In the biosuture spectrum, however, the peak is bimodal which reveals both the symmetric and asymmetric stretching vibrations of the C-H groups, and confirms the presence of glycerol, which displayed a similar small bimodal peak in this region (Figure 5.2). In the region of $1550 - 1200\text{ cm}^{-1}$, significant overlapping of absorption bands occurs, making the assignment of individual peaks more difficult. The two peaks at 1604 and 1405 cm^{-1} can be ascribed to the symmetric and

asymmetric stretching vibrations of the -COO^- groups found in alginate. Yet, the 1604 cm^{-1} peak has a shoulder at 1560 cm^{-1} which can be ascribed to the free carboxylate groups of pectin. The strong peak at 1026 cm^{-1} can be ascribed to the C-C and C-O stretching vibrations of the pyranosyl ring which is found in both alginate and pectin. The small peaks observed in the region $1330 - 1080\text{ cm}^{-1}$ could be representative of amide III – VI but is less clear due to interference and overlapping of the carbohydrate functional groups in the same region.

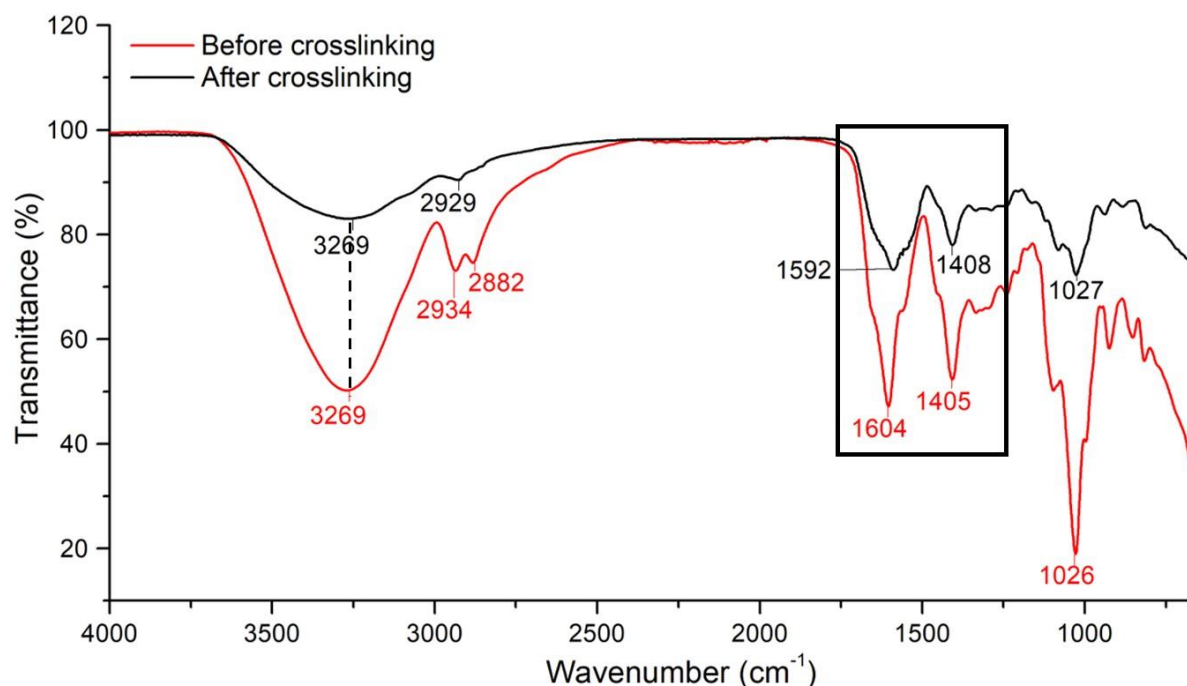


Figure 5.3: FTIR spectra of the biosuture before (black) and after crosslinking (red) with BaCl_2 .

Upon comparison of the biosuture formulation before and after crosslinking, it is clear that some change did occur on a molecular level during the crosslinking process. The most significant difference between the two spectra can be seen at the strong absorption bands that represent the -COO^- groups, which have shifted from 1604 to 1595 cm^{-1} and from 1405 to 1408 cm^{-1} , while broadening and lowering their intensity (outlined in Figure 5.3). This undoubtedly indicates a strong interaction between Ba^{2+} and the -CO^- of the carboxyl group in the polymer chains and confirms crosslinking of the biosuture. Similar results were found by Awasthi *et al.*, after they crosslinked an alginate-pectin network with Ca^{2+} for the sustained release of repaglinide (Awasthi *et al.*, 2017). Yet, there is no indication of the presence of Ba-Cl in the IR spectrum (which would have revealed a characteristic peak around 1450 cm^{-1}) and confirms that the washing process was effective in removing any excess crosslinker from the biosuture surface.

The IR spectra of the lipid-drug coating (Figure 5.4) displays three very sharp peaks in the $3000 - 2800\text{ cm}^{-1}$ region (outlined in black), which is characteristic of soy phosphatidyl choline

and can be ascribed to the different C-H stretching vibrations of the molecule. These absorption bands also overlap with the stretching vibrations of the methyl groups in dexamethasone, which could account for the high intensity of the peaks. The other three sharp peaks, found at 1742, 1665 and 1622 cm^{-1} , (circled in green) are characteristic of dexamethasone and can be ascribed to the $\nu\text{C}=\text{O}$ (aliphatic-C20), $\nu\text{C}=\text{O}$ (cyclic (conjugated) C3), and $\nu\text{C}=\text{C}$ (cyclic) of the drug molecule, while the absorption at 1242 cm^{-1} (circled in red) is due to the stretching vibrations of the C-F bonds in dexamethasone.

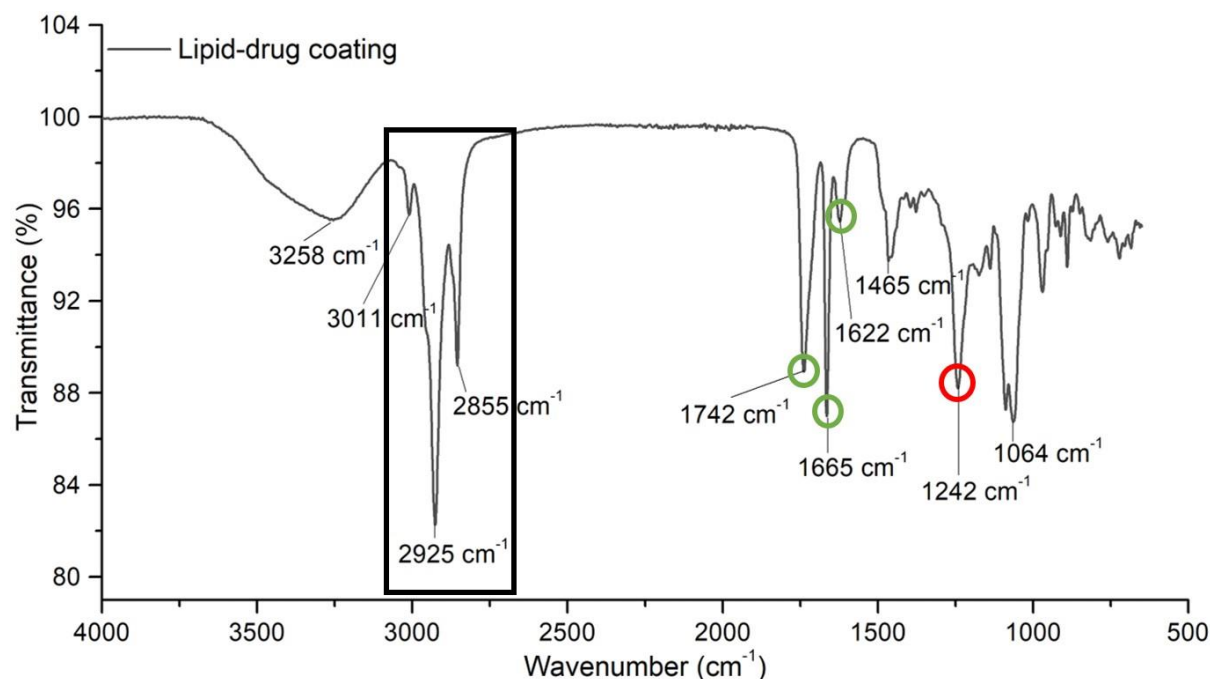


Figure 5.4: FTIR spectra of the lipid-drug coating that consists of soy phosphatidyl choline and dexamethasone.

The IR spectrum of the coated biosuture (Figure 5.5) resembled the spectrum of the uncoated biosuture but with distinct additional absorption bands that confirm effective coating of the biosutures with the lipid-drug layer. Similar to the spectrum of the coating material, three sharp peaks can be observed in the 3000 – 2800 cm^{-1} region (outlined in black), which were absent in the uncoated biosuture spectrum. These peaks have not shifted significantly, even though their intensity slightly decreased (presumably because of the small quantity present on the suture surface), indicating no unwanted interaction between the coating material and the biosuture and confirming that dexamethasone should maintain its bioactivity. The sharp peak that can be observed at 1663 cm^{-1} , (circled in green) as well as the important C-F indicating peak at 1242 cm^{-1} , (circled in red) are characteristic of dexamethasone and confirm the presence of the drug on the surface of the coated biosuture (Figure 5.5).

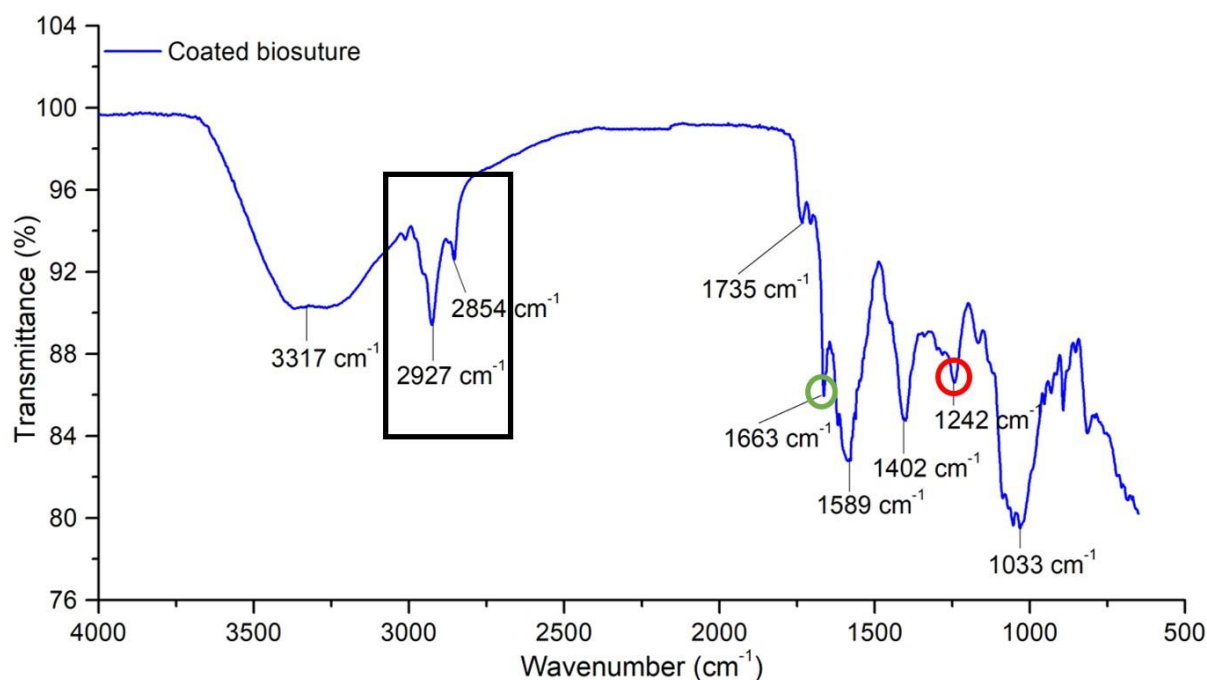


Figure 5.5: FTIR spectra of the lipid-drug coated biosuture.

5.3.3 Evaluation of the relative crystallinity of materials by means of Powder X-ray Diffraction (XRD)

XRD analysis was used to determine the crystallographic structure of the newly fabricated biosuture, before and after coating with the lipid-drug layer. As with FTIR analyses, the XRD spectra of the pristine biopolymers (Figure 5.6) were first analysed and then compared to that of the biosuture spectra. The diffraction pattern of sodium alginate revealed a semi-crystalline structure with two peaks at 2θ equal to 22.12° and 38.42° . The diffraction pattern of pectin, on the other hand, contained mostly sharp, narrow peaks that clearly pointed to a more crystalline nature. These sharp peaks were found at 2θ equal to 8.48° , 11.92° , 18.96° , 24.88° , 27.78° , 38.54° , 46.48° and 50.92° . Gelatin, in turn, displayed a highly amorphous diffraction pattern with a single, slightly pronounced peak at 2θ equal to 21.92° . After combining the semi-crystalline alginate, with the crystalline pectin and more amorphous gelatin, the produced biosuture displayed a semi-crystalline diffraction pattern (Figure 5.6). Similar to the FTIR spectra, the diffraction pattern mostly resembled that of the main component, i.e., alginate, and displayed two peaks at 2θ equal to 25.36° and 40.08° . The semi-crystalline structure of the biosuture material is in accordance with the good and well-balanced mechanical properties thereof. If the produced biosuture material was completely amorphous it would most likely not have displayed sufficient strength to meet the USP requirements, while high crystallinity would have resulted in a brittle biosuture that is unable to tie a successful knot. The semi-crystalline structure, however, ensured a good balance between strength and elasticity in the biosuture and supports the notion that the newly developed biosutures will be suitable for clinical use.

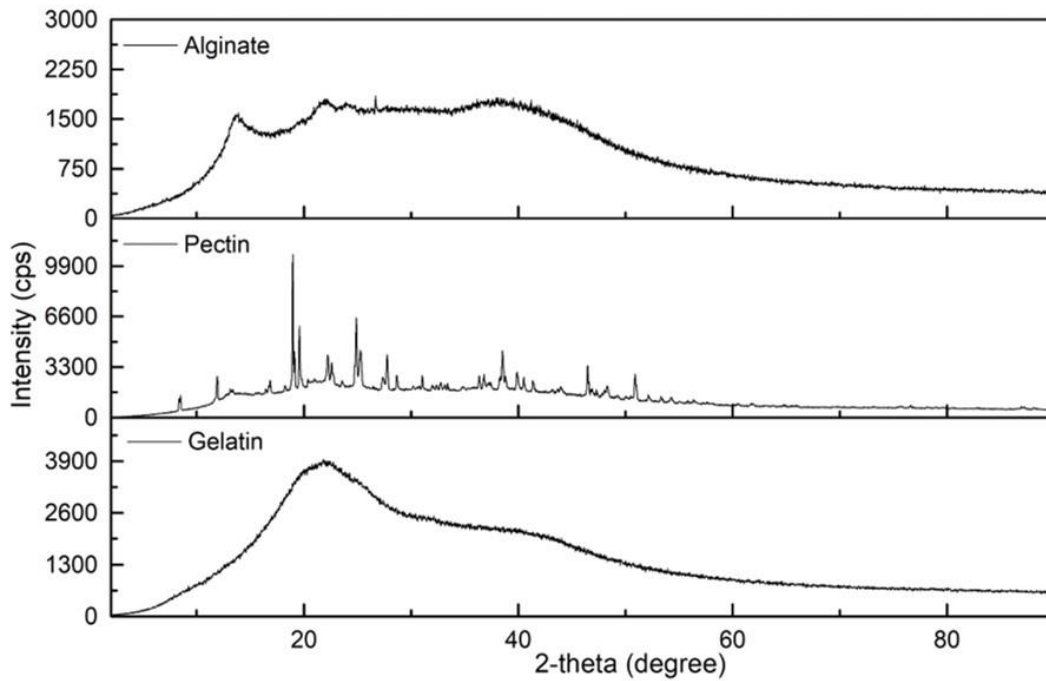


Figure 5.6: XRD spectra of the biopolymers; top to bottom: alginate, pectin and gelatin.

The diffraction pattern of the coated biosuture correlates well with that of the uncoated biosuture except for a very sharp, intense peak at 2θ equals to 2.54° and a second less intense, sharp peak at 2θ equal to 15.26° (Figure 5.7). These sharp peaks in the low 2θ region are characteristic of dexamethasone, which has a crystalline structure and confirms the presence of the drug in the coated biosuture. Soy phosphatidyl choline is amorphous and its contributing peaks are most likely masked by that of the semi-crystalline biosuture.

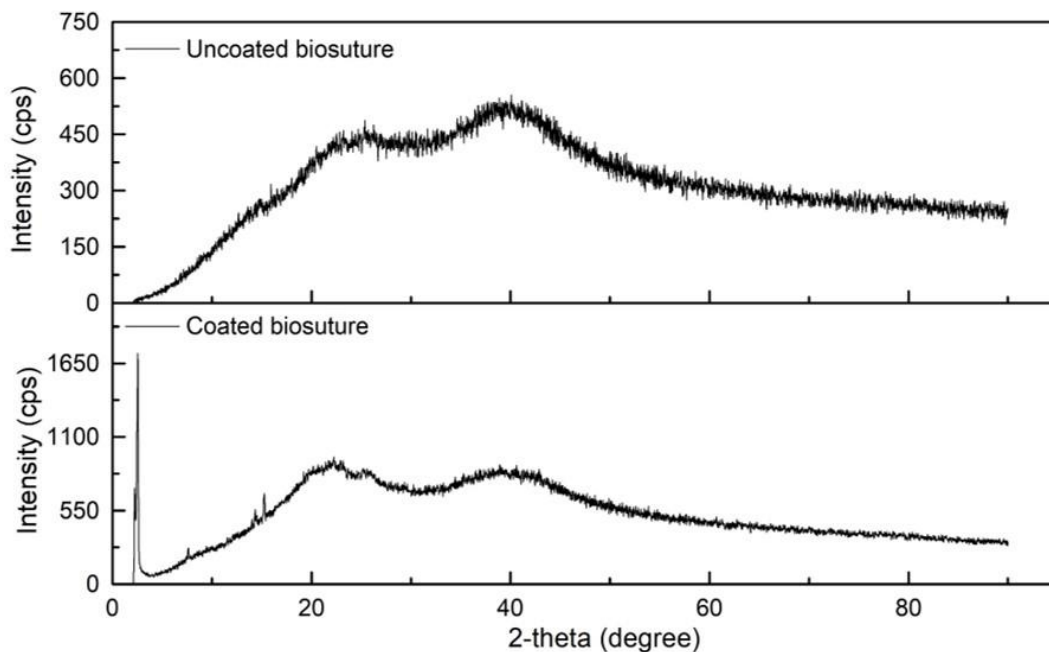


Figure 5.7: XRD spectra of the uncoated (top) and coated (bottom) biosutures, showing additional sharp peaks in the coated biosuture spectrum that are indicative of dexamethasone.

5.3.4 Thermal evaluation of the biosutures by means of Thermogravimetric analysis (TGA) and Differential Scanning Calorimetry (DSC)

TGA was performed in order to analyse the thermal stability and decomposition behaviour of the newly developed biosuture material. In addition to the TGA curve, the differential thermogravimetry (DTG) curve, which reports the degradation velocity, was obtained for all the pristine polymers and for the coated and uncoated biosuture. Alginate revealed a three-stage decomposition (Figure 5.8 A), which has also been observed by other researchers (Nadeem & Datta, 2014; Salisu *et al.*, 2015). The first stage, which can be seen from 50°C – 150°C, resulted in a 17% weight loss and is ascribed to the evaporation of water bound to the hygroscopic alginate molecules (Zhao *et al.*, 2018). The second stage of decomposition occurred around 240°C and led to the greatest decrease in weight (46%). This can be ascribed to the complex depolymerization process where the alginate backbone is ruptured, and glycosidic bonds broken (Vincent *et al.*, 2020). This stage of degradation initially took place at a very rapid rate, which can be deduced from the steep slope in the TGA curve, and then slowed down, presumably as the amount of available bonds decreased. Decomposition reached a maximum rate at 252°C, as shown by the strong peak or inflection point of the DTG curve (Figure 5.8 B). The final stage of decomposition, which can be seen around 800°C, involves the carbonization of the remaining material, with the release of Na_2 and CO_3 , and resulted in a further 27% weight loss. This stage peaked at 853°C and left a char residue that accounted for 10% of the initial sample weight, and is in accordance with the work of Soares *et al.* (Soares *et al.*, 2004).

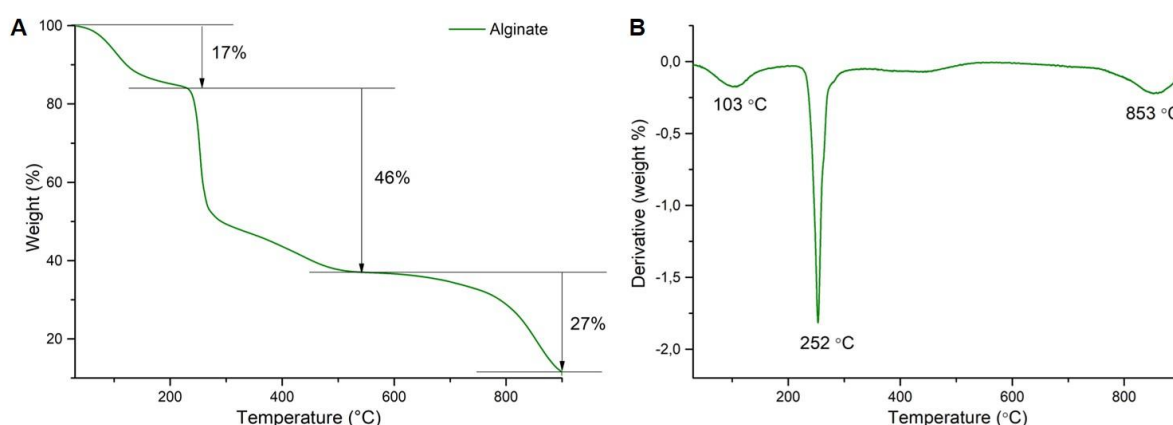


Figure 5.8: A) TGA and B) DTG curves of pristine sodium alginate.

The DSC results of the pristine polymers and the uncoated and coated biosuture is provided in Figure 5.9 A. The DSC curve of alginate revealed two thermodynamic events that correspond well with the TGA data of the polymer. The first event is an endotherm at 50°C – 150°C, which represents the evaporation of water from the sample and was also observed in the TGA graph within the same temperature range. The second event is a sharp exotherm,

with its peak at 242°C and reflects the decomposition of alginate with the release of energy as bonds break. No additional thermal events, such as melting or crystallization peaks, were observed for alginate and is in line with its low crystallinity, as shown by XRD studies. The results corresponds well with literature and have been reported by several other authors including Hou *et al.*, Kataria *et al.*, and Iswandana *et al.*, (Hou *et al.*, 2014; Iswandana *et al.*, 2018; Kataria *et al.*, 2017).

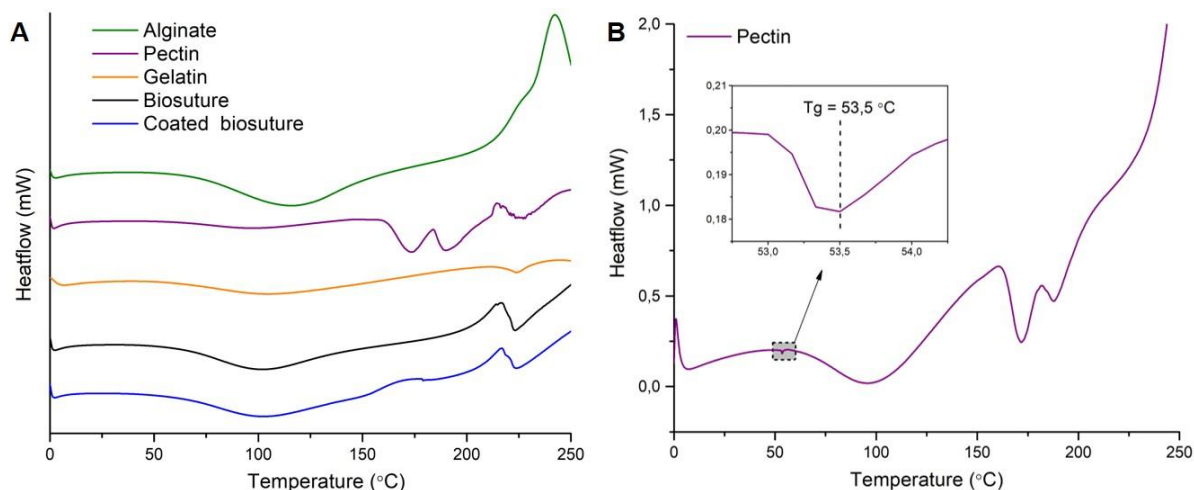


Figure 5.9: A) DSC curve of the pristine polymers and the uncoated and coated biosuture. B) Enlarged DSC curve of pectin, showing its glass transition (Tg) temperature.

Pectin displayed a two-step degradation (Figure 5.10 A), which was confirmed by the DTG data, which also revealed two separate thermal events (Figure 5.10 B). The first step is found from 40°C to 170°C and accounts for the evaporation of molecular water from the sample. This first degradation step only lead to a 10% decrease in weight, which is less than what was seen with alginate, and coincides with the less hygroscopic nature of pectin compared to alginate (Sun *et al.*, 2020). The second weight loss step took place from 200°C to 880°C with a maximum rate of decomposition at 252°C, as evidenced by the inflection point of the DTG curve. The main decomposition peak of the DTG curve, however, displayed two shoulders at 208°C and 310°C respectively, which reflects different degradation rates and coincides with changes on the slope of the TGA curve at these temperatures. It has been reported that degradation in these temperature ranges is primarily derived from pyrolytic decomposition which consists of primary and secondary decarboxylation of the acid side group and the carbon in the ring. These processes take place at different rates and accounts for the change of slope in the TGA curve and the peak shoulders of the DTG curve (Ruano *et al.*, 2020). From about 340°C decomposition takes place at a much slower rate and the polymer material continues to gradually degrade, leaving a final char yield of 18%.

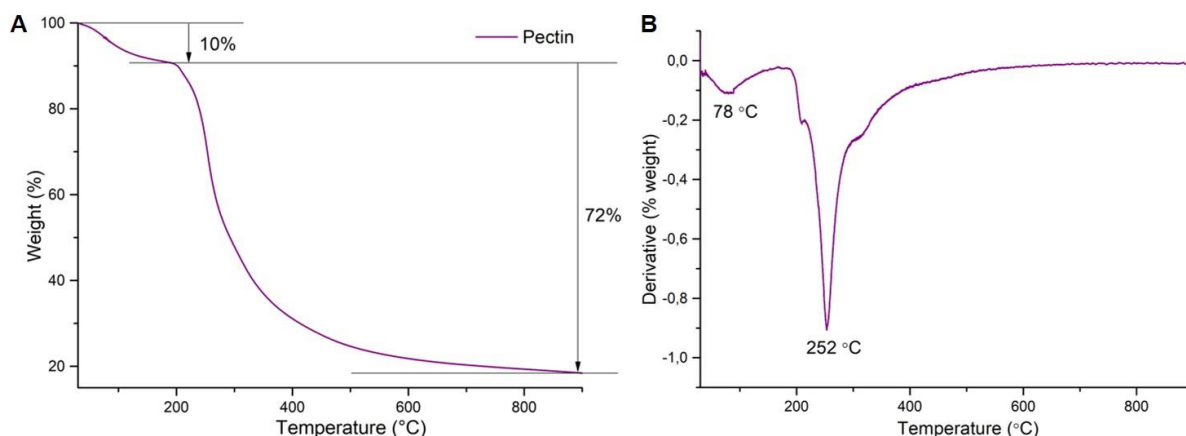


Figure 5.10: A) TGA and B) DTG curves of pristine pectin.

The DSC curve of pectin (Figure 5.9 A) revealed several interesting events, the first of which is an endotherm that peaks at 97°C and corresponds with the release of water, that was also seen in the TGA curve. There is a characteristic small endotherm at 53.5°C, that can clearly be observed when the graph is enlarged and is representative of the glass transition temperature (T_g) of pectin (Figure 5.9 B). This confirms the presence of an amorphous portion within the pectin matrix, that was also indicated by the crystallinity index and XRD results. Similar T_g values have been reported for other high methoxyl pectin samples, especially in the dry state where the low water content of the polymer limited the normal plasticizing and T_g depressing effect of moisture effect and its poor plasticizing effect did not succeed in depressing the T_g temperature (Jahromi *et al.*, 2020; Perez *et al.*, 2009). Additionally, two consecutive melting point (T_m) endotherms can clearly be seen on the pectin DSC graph at 172°C and 190°C, respectively. This points to the presence of two different crystal structures within the pectin matrix, each with their own specific melting temperature, as previously been described by Ajaz *et al.*, (Ajaz *et al.*, 2020; Auriemma *et al.*, 2020). These two separate melting temperatures points to polymorphism and suggests that two different polymorphs are present within the sample, the one with the highest melting point being more stable (Giri *et al.*, 2013). The last thermal event, on pectin's DSC curve, is an exotherm that peaks at 214°C and corresponds with the decomposition weight loss seen in the TGA curve.

The TGA graph of gelatin, is very similar to that of pectin and also displays a two-step decomposition profile (Figure 5.11) that starts with a small decrease in weight (12%), due to the evaporation of molecular water. The second weight loss step, accounts for the decomposition of gelatin, which starts at around 225°C with the loss of intermolecular interactions and the destruction the 3D protein structure, and ends at around 520°C, where the peptide chain is fully ruptured. The DTG graph also reflects two peaks, one representing water loss and the other decomposition of the polymer which reaches a maximum rate at 323°C.

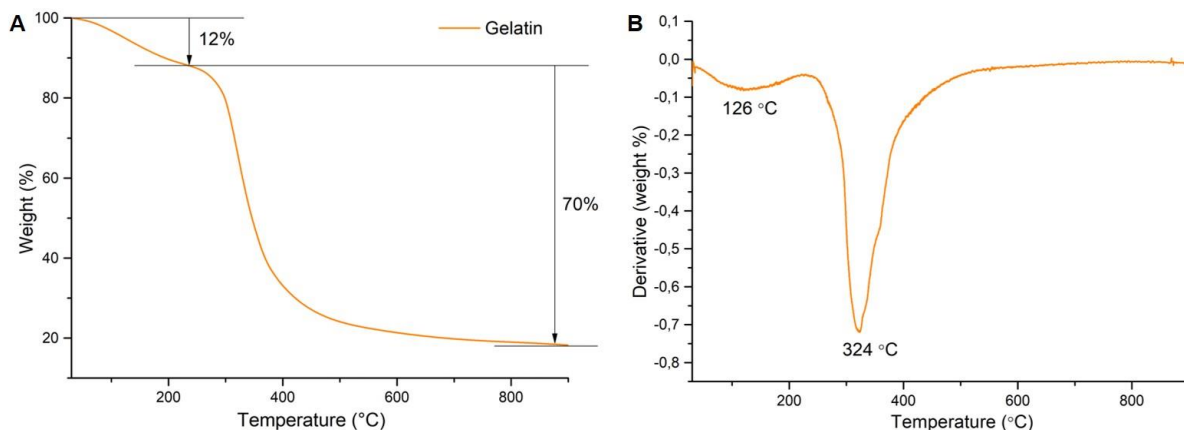


Figure 5.11: A) TGA and B) DTG curves of pristine gelatin

The DSC curve of gelatin shows two endotherms at 105°C and 222°C respectively and an exotherm at 300°C, which corresponds well with the TGA data. The first endotherm is found in the same temperature region as the boiling point of water and is, therefore, attributed to moisture evaporation, as described by Sahraee *et al.*, (Sahraee *et al.*, 2017). It has been widely shown that this peak overlaps with the glass transition temperature of gelatin, which is usually at a low temperature due to the amorphous nature of the polymer (Al-Saidi *et al.*, 2011; Lau, Y W. Tan, 2010; Parvez *et al.*, 2012). The second endotherm corresponds well with the start of the second weight loss step in the TGA data and reflects a phase change in the sample. According to Shehap *et al.*, this endotherm represents the melting temperature of gelatin ($T_m=222^\circ\text{C}$) and is the temperature at which the triple-helix crystalline structure of the polymer melts, as was suggested by the TGA data (Shehap *et al.*, 2015). The exotherm at 300°C represents the decomposition of gelatin and is the temperature at which the peptide chains disintegrate, as was found by Salem *et al.*, and others (Salem *et al.*, 2015; Shehap *et al.*, 2015; Subramanian & Vijayakumar, 2013).

The TGA graph of the biosuture, looks a lot like that of alginate at first glance, yet there are several significant differences that become apparent when comparing the DTG graphs of the pristine polymer and the biosuture (Figure 5.12 A and B). The TGA data suggests that the biosuture undergoes a three-phase decomposition process, which according to the DTG graph includes several different steps during the second decomposition phase. The first weight loss phase can be observed from 40°C to 143°C according to the DTG graph, which provides the most accurate reflection of the temperature range at which the weight loss took place. This first phase can be ascribed to the evaporation of water but can potentially include water from the original hydrogel that was left in the biosuture sample after drying, in addition to the molecular water found in the pristine polymers. This would explain both the low temperature and high rate at which the weight loss occurs, since this entrapped moisture can escape much easier than the tightly bound molecular water found in the polymers. This also accounts for the

relatively high amount of weight loss (16%) compared to that of the constituting polymers, of which only alginate had a similar amount of weight loss due to water evaporation (17%). Yet, alginate makes out less than half of the biosuture sample weight and its molecular water could not account for this great and rapid weight loss due to water evaporation.

In the biosuture fabrication process, there are two factors that could affect the thermal stability of the final biosuture material. The first is the addition of the plasticizer, glycerol, which interferes with the intermolecular interactions and decreases the thermal stability and the other is crosslinking, which leads to the formation of new ionic interactions and increases the thermal stability of the material (Azucena Castro-Yobal *et al.*, 2021). The second weight loss phase of the TGA curve, represents the decomposition of the biosuture with rupturing of the polymer backbones. This process initiates at 223°C, which is very similar to the starting decomposition temperature of the pristine polymers (i.e., 224°C for alginate, 200°C for pectin and 225°C for gelatin). This suggests that the thermal stability of the biosuture is not significantly different from that of the pristine polymers and that the decreasing effects of the plasticizer and increasing effects of the crosslinker, potentially work at different timescales or events due to stress. Another good measure of the thermal stability of materials is the temperature at which 50% of the material is decomposed. The biosuture material reached a 50% weight loss at 403°C, which is considerably higher than the 291°C, 292°C and 346°C of alginate, pectin and gelatin respectively. This confirms that the crosslinking process improved the thermal stability of the biosuture material, despite the addition of a plasticizer, which has also been reported previously by Thomas-Busani *et al.*, (Thomas-Busani *et al.*, 2020).

The DTG curve of the biosuture also reflected a higher rate of water evaporation from the biosuture sample, than from the pristine polymers as exemplified by the greater intensity of the first peak at 72°C. In the temperature range of the second weight loss phase, the DTG curve of the biosuture displays a bimodal peak at 236°C and 273°C and a broad shoulder from 330°C (Fig 5.12 B). This clearly illustrates that the constituents of the biosuture material decomposed at different rates, albeit at within the same temperature range. In the pristine form, alginate and pectin displayed similar degradation rates at exactly the same temperature (252°C). It is, therefore, possible that these two peaks are overlapping in the DTG curve of the biosuture and collectively represent the one mode, while the decomposition of gelatin, which takes place at a higher temperature than the carbohydrates, represents the second mode. The shoulder of the peak corresponds well with the slight change in slope (i.e., decomposition rate) of the TGA graph during the same second phase of decomposition. Similar to alginate, the third and final weight loss phase is also reflected in the DTG curve as a small broad peak near 800°C.

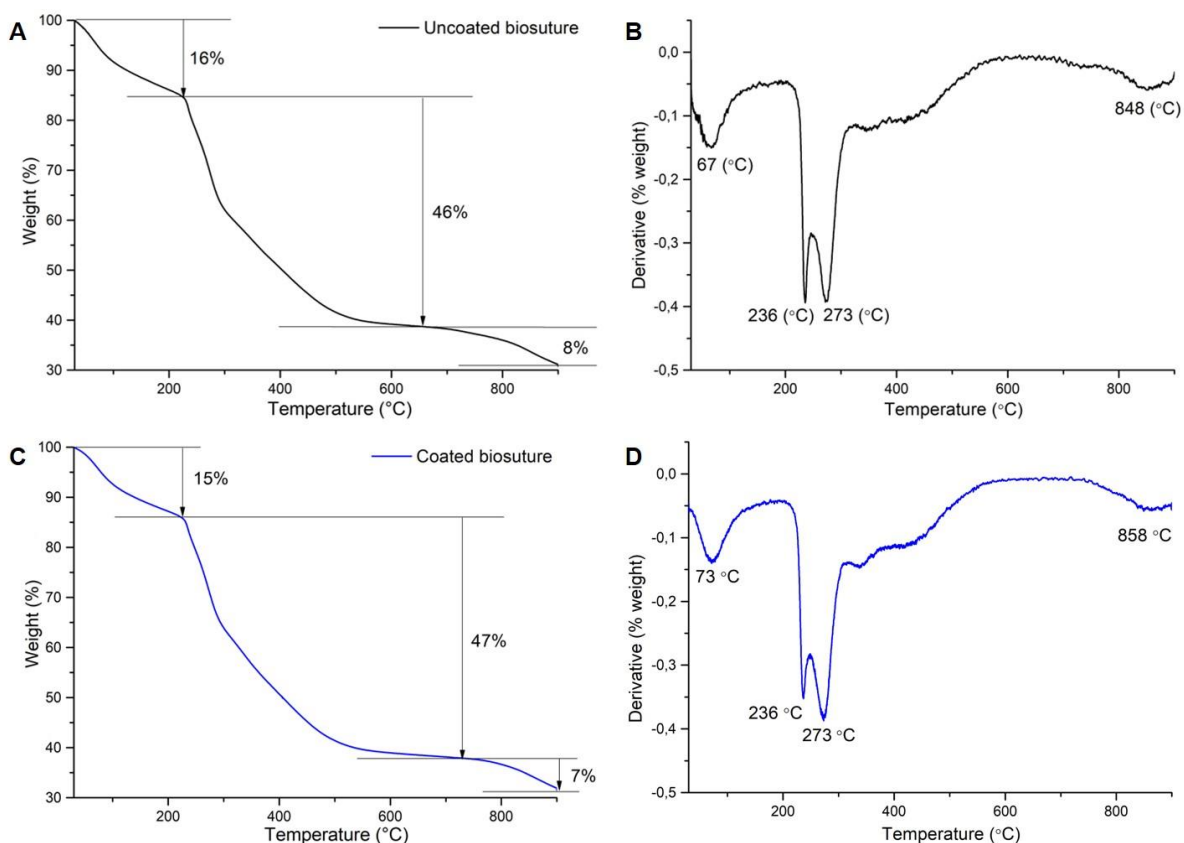


Figure 5.12: A) TGA and B) DTG curves of the uncoated biosuture and C) TGA and D) DTG curves of the coated biosuture.

The DSC curve of the biosuture again corresponds well with its TGA curve and shows a big endotherm around 100°C, which represents the removal of water from the sample. The next thermodynamic event, that can be observed on the DSC curve, is an exotherm that peaks at 222°C, which again aligns closely with the TGA data where decomposition was seen at 223°C. In harmony with the low crystallinity index of the biosuture seen in the XRD results, no melting or crystallization peaks could be observed for the biosuture sample. It is possible that a T_g event did occur but was hidden by the great water evaporation endotherm in the same temperature range. After the decomposition peak, the DSC curve does not return to a proper baseline but continues upwards which is in agreement with the ongoing decomposition that is witnessed in the TGA curve. According to Saunders *et al.*, DSC data should not be interpreted beyond the decomposition temperature as erroneous results are very likely at these temperatures where several endothermic and exothermic events occur in association with the decomposition process (Saunders *et al.*, 2008). Hence, no further deductions were made from the DSC curve of the biosuture.

The TGA and DTG graphs of the coated biosuture is nearly identical to that of the uncoated biosuture, indicating that the coating process did not dramatically affect the thermal stability of the material (Figure 5.12 A – D). The TGA graph again showed a three-stage decomposition

profile with weight loss percentages that are exactly 1% less than that of the uncoated biosuture for each material. This could indicate a slight increase in thermal stability of the biosuture after coating, but more likely indicates that the lipid-drug coating shielded the biosuture against the effects of heating. However, the temperature at which 50% weight loss occurred in the coated biosuture sample, was exactly the same as without the coating (403°C), which confirms that the coating process did not have a noteworthy effect on the thermal stability of the biosuture. The DSC results of the coated biosuture also aligned precisely with that of the uncoated biosuture and revealed no new thermal events. The normal melting endotherm that is expected for a lipid such as soy phosphatidylcholine, was not observed in DSC curve of the coated biosuture. This is probably due to the small quantity of the coating material present in the sample in relation to the biosuture material and confirms that it had a negligible effect in terms of thermal properties.

Since DSC data is extremely difficult to analyse, and requires a high level of expertise and experience, additional melting point analysis was conducted on the suture material to ensure that a potential melting peak was not overlooked or misinterpreted in the DSC curves of the biosuture materials. The melting apparatus allowed for visual inspection of the physical changes that occur in the biosuture sample as the temperature increased. As shown in Figure 5.13 B, the suture material changed from the original transparent colour to slightly yellow at 220°C, which signals the onset of decomposition, and stands in agreement with the TGA and DSC data. The suture material turned black and became carbonized around 264°C, which is again in line with the decomposition temperature seen in the TGA and DSC data. There was no signs of melting or phase changes during the temperature ramp and the biosuture maintained its original morphology surprisingly well. Interestingly, early on around 80°C – 100°C, small water droplets formed on the capillary tube, confirming the evaporation of moisture from the biosuture at this temperature range.

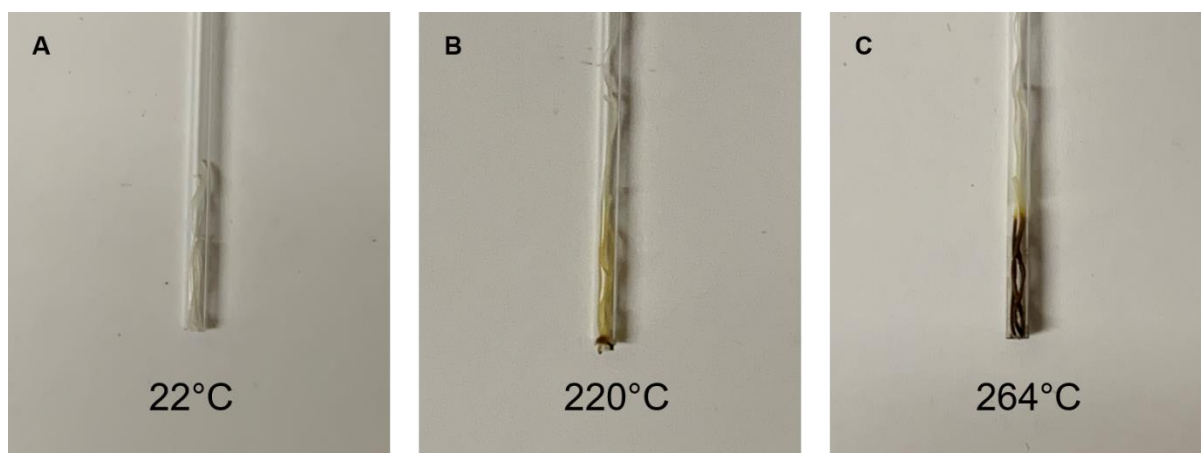


Figure 5.13: Macroscopic appearance of the biosuture at different temperature points (x3 magnification).

5.3.6 Evaluation of the surface morphology of biosutures by means of light microscopy and Scanning Electron Microscope (SEM) imaging

SEM images (Figure 5.14) revealed a smooth, uniform biosuture surface that should easily glide through tissues without causing significant damage. The uniform appearance of the biosuture also confirms the compatibility and good distribution of the biopolymers that make up the material. The long fibre-like lines on the surface of the uncoated biosuture can be attributed to the extrusion process during manufacturing and can also be a consequence of the long polymeric chains of alginate and pectin that form during crosslinking. The average diameter of the uncoated and coated biosuture samples (n=10) were both $100 \pm 1.5 \mu\text{m}$, as calculated from light microscope images, shown in Figure 5.14 H. This suggests that the lipid-drug layer is extremely thin and does not affect the biosuture diameter. Additionally, it confirms the diameter measurements taken with a digital vernier calliper in previous chapters and reaffirms that the biosutures belong to the 6-0 suture size (100 – 149 μm), as specified by the USP monograph for absorbable surgical sutures. Figure 5.14 B shows the coated biosuture, which unfortunately cracked under the focussed electron beam of the microscope, but still confirms the successful coating of the biosuture. The lipid-drug coating looks like a silk draping that covers the biosuture surface in a dramatic fashion. The fact that the coating remained on the biosuture even after extensive handling and sample preparation, points to a good affinity of the coating material for the biosuture surface and suggests that it will also remain on the biosuture during suturing, which has previously been reported for similar coatings (Guambo *et al.*, 2020). The SEM and light microscope images also confirmed the good elasticity of the biosutures and their ability to tie secure knots (Figure 5.14 E – G) without any sign of fracturing or breaking at the bends where the strain is at its highest.

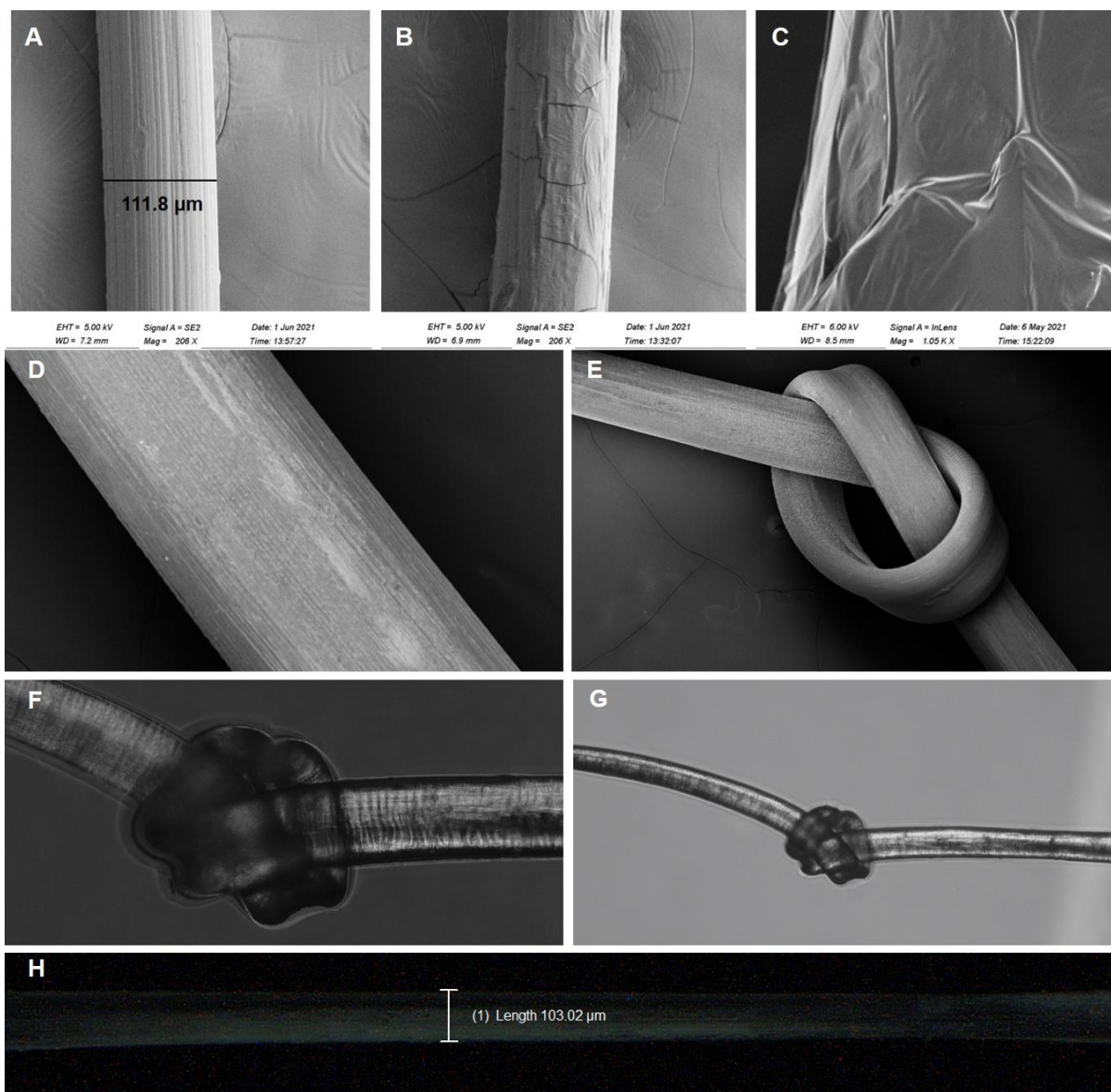


Figure 5.14: SEM images of the uncoated biosuture (A) and coated biosuture (B). Image (C) provides an enlarged (1.05K magnification) image of the coated biosuture without damage by the electron beam. Image (D) and (E) show in lens SEM images of the biosuture in the straight and knotted configuration, respectively. Light microscope images (F) and (G) show the morphology of tightened knots made with biosutures and (H) the diameter (103.02 μm) of a coated biosuture.

5.3.7 Evaluation of the mechanical properties of the biosutures

The mechanical properties of the uncoated and coated biosutures were again studied in detail to ensure acceptable performance for clinical use. Table 5.2 provides the average values of the studied mechanical properties and confirms that there was not a significant deviation from the results found in the previous chapters.

Table 5.2: Mechanical properties of the uncoated and coated biosutures.

Biosuture	Load failure (N)	Tensile strength (N/mm²)	Elongation at break (%)	Young's modulus (MPa)	Toughness (J.mm⁻³)
<i>Straight configuration</i>					
Uncoated	4.09 ± 0.3	361.64 ± 0.3	18.35 ± 0.7	2.04 ± 0.4	10.52 ± 0.5
Coated	4.17 ± 0.6	368.71 ± 0.6	18.58 ± 0.5	2.06 ± 0.5	10.85 ± 0.4
<i>Knot configuration</i>					
Uncoated	2.42 ± 0.3	213.97 ± 0.3	9.45 ± 0.4	1.51 ± 0.5	2.61 ± 0.4
Coated	2.59 ± 0.4	229.27 ± 0.4	12.28 ± 0.7	1.56 ± 0.3	2.79 ± 0.6

As can be seen in Figure 5.15, the stress-strain curves of the uncoated and coated biosutures are very similar, with the coated biosutures reaching slightly higher tensile stress before fracturing. The Young's modulus of the biosutures is more or less the same before and after coating, while the toughness slightly increased. This suggests that the stiffness of the material was not drastically altered by the coating process, but that the coated biosuture is able to undergo a greater amount of plastic deformation and absorb more energy than the uncoated biosuture before breaking. This is a highly desirable quality in any suture material and suggests that the biosuture will tend to bend rather than break during handling and knot tying. The stress-strain curves of the biosutures in the knotted configuration, display a typical bimodal shape where the first mode represents the tightening of the knot and the second mode reflects the inherent properties of the material. It is widely accepted that the knot is the weakest point of a suture and the primary position where the material will fracture, and the same observation was made in the current study. Yet, as can be deduced from Figure 5.15 B, the biosutures were able to withstand an impressive amount of stress and strain after tightening of the knot, before finally rupturing at the knot site. The minimum requirement for knot strength, as specified by the USP for 6-0 sutures is 1.76 N for an individual strand and 0.98 N on average. Hence, both the uncoated and coated biosutures produced in this study meet the minimum requirements set by the USP for mechanical performance, which again suggests that the biosutures suitable for *in vivo* clinical use.

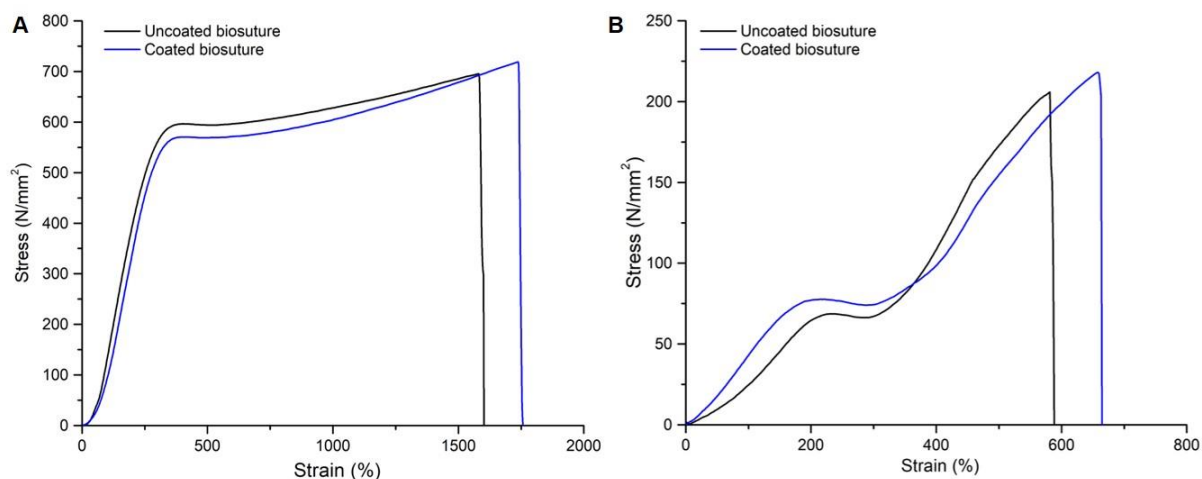


Figure 5.15: Stress – strain curves of the uncoated and coated biosutures in the (A) straight configuration and (B) knotted configuration.

5.2.8 Evaluation of the *in vitro* drug loading and release behaviour of the biosutures

In the previous chapter, coating of the biosutures with lipid-drug layer consisting of soy phosphatidylcholine and dexamethasone was identified as the most appropriate method of drug loading for this study. This method provided a suitable drug loading capacity but since ischemic reperfusion injury (IRI) might require high local drug dosages, we decided to increase the concentration of the lipid-drug layer from 5% w/w to 8.5% w/w to see if a higher drug loading capacity could be achieved. This change in concentrations caused the loading capacity of the biosutures to increase from 53 ug/cm to 101 ug/cm with a practical loading capacity of 2020 ug per 20 cm biosuture. This dosage is still within the acceptable dosage range for localized dexamethasone administration (500 – 2500 ug) and will not result in toxic drug levels *in vivo* but might improve the therapeutic effect achieved with the biosutures. The lipid-drug ratio was kept the same to avoid any unwanted changes in the drug release profile.

As can be seen in Figure 5.16, the drug release profile did not change significantly from what was achieved in the previous chapter and the lipid-drug layer still provided controlled drug release. In contrast with Chapter 4, we continued the drug release study until the cumulative release no longer increased, i.e., the drug release process was complete. The highest cumulative release (%) value was achieved after 10 days of incubation with 98.44 ± 1.05 % of the loaded drug released at this timepoint. Drug release over the last 3 – 4 timepoints reflected linear drug release kinetics, as was discussed and predicted in Chapter 4. It can be concluded that the drug release method employed in this study provides favourable and reliable controlled drug release with almost 100% of the loaded drug released after 10 days of simulated physiological conditions. Naturally, there is a chance that the drug release behaviour might change *in vivo*, and this will have to be confirmed in future studies.

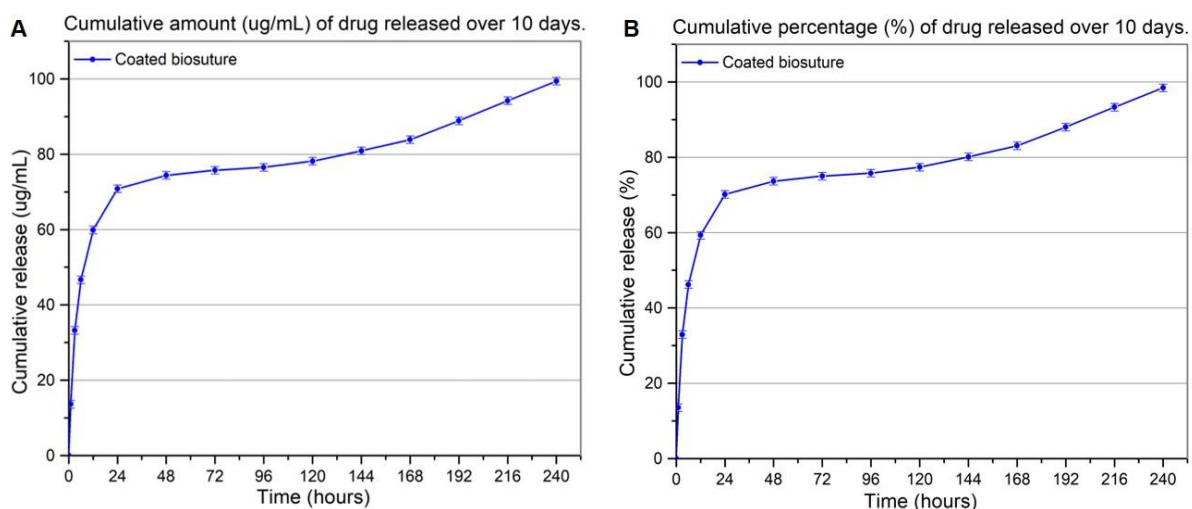


Figure 5.16: Cumulative drug release from coated biosutures expressed as (A) amount (ug/cm) and B) percentage (%) of drug released over a period of 12 days.

5.2.9 Evaluation of the *in vitro* swelling and degradation behaviour of the biosutures

After crosslinking, polymeric hydrogels tend to no longer dissolve in aqueous media but rather swell upon immersion in ionic buffers. The swelling behaviour is dependent on the inherent properties (e.g. hydrophilicity) and concentration of the polymers as well as crosslinker factors, such as degree of crosslinking and the type of crosslinker used (Li *et al.*, 2016). In the current study, the uncoated and coated biosutures gradually swelled to reach an equilibrium swelling ratio of 9.213 and 8.741, respectively. It should be noted that the biosutures revealed no swelling upon immersion in pure distilled water, which indicates that the swelling behaviour is governed by ionic interactions with ions, such as sodium (Na^+) in the employed buffer. As can be seen in Figure 5.17 A, the coated biosutures swelled at a considerably slower pace than the uncoated biosutures, even though they both had similar final swelling ratios. This can be ascribed to the hydrophobic lipid-drug layer that covers the coated biosuture and delays water absorption. The ends of the biosutures, where the samples were cut during preparation, are however not covered by the hydrophobic layer, and allows water to freely penetrate the system, albeit at a much slower rate due to the small surface area that is exposed.

Overall, the swelling profiles of the biosutures are more gradual than what previously reported for other physically crosslinked alginate systems. Giz *et al.*, for example, found that crosslinked alginate films swelled rapidly within the first 5 minutes of immersion in an aqueous media and reached equilibrium swelling after 50 – 60 minutes (Giz *et al.*, 2020). Similarly, alginate-pectin films prepared by Shahzad *et al.*, swelled within 15 minutes and reached their swelling limit after 2 hours (Shahzad *et al.*, 2019). Yet, these systems were all crosslinked with calcium as crosslinking ion, while in the current study we employed barium as crosslinking agent. According to Bajpai & Sharma, the barium ion, which has a larger radius than calcium, fits

securely in the polymer chain and does not undergo ion exchange as readily as other, smaller divalent cations (Bajpai & Sharma, 2004). This has been confirmed by Valentin *et al.*, who found that alginate hydrogels that were crosslinked with Ba^{2+} , swelled and degraded at a slower rate than those that were crosslinked with Ca^{2+} or Mg^{2+} (Valentin *et al.*, 2017). The gradual swelling of the biosutures in the current study can, therefore, safely be ascribed to the large size of the barium ions that are tightly bound to the carboxyl groups of alginate and do not readily participate in the ion-exchange process.

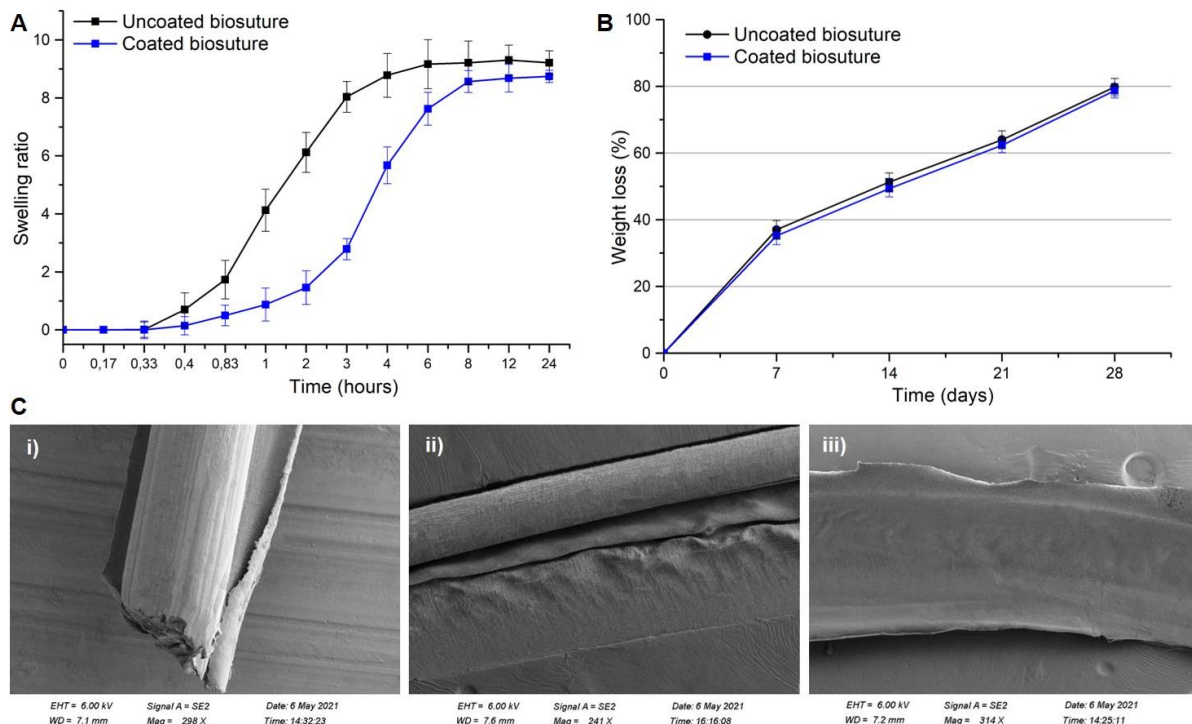


Figure 5.17: Swelling ratio (A) and degradation expressed as percentage weight loss (B) of the uncoated (black) and coated (blue) biosutures as a function of time immersed in phosphate buffered saline (pH = 7.4) at 37°C. C) SEM images of biosuture samples after 7 (i), 14 (ii) and 28 (iii) days of degradation.

Additionally, the moderate swelling ratio of the coated and uncoated biosutures (9.213 and 8.699, respectively) is most probably a result of the type and concentration of both the biopolymers and crosslinkers employed. According to Li *et al.*, crosslinking with 1.5% w/v calcium results in a fully crosslinked alginate system that provides significant resistance to swelling (Li *et al.*, 2016). In the current study, barium, which has a greater ionic strength than calcium, was employed at 2% w/v, suggesting that the biosuture system has a high crosslinking density and is aptly able to resist water penetration. Yet, alginate and gelatin are extremely hydrophilic polymers that are known to have high water absorption capacities, especially at the concentrations used in the current study (Shahzad *et al.*, 2019). Pectin, however, has been found to dramatically decrease the swelling capacity of gelatin films by

forming strong electrostatic interactions with the polymer, which hinders the penetration of water molecules (Farris *et al.*, 2011). Hence, the specific combination of polymers and crosslinker used in the study, possibly resulted in equidistant swelling behaviour where the high level of crosslinking largely prevented and stalled water penetration, but the hygroscopicity of the biopolymers ensured that sufficient swelling did take place. Furthermore, it should be noted that the swollen biosutures maintained their structural integrity with no signs of cracking or fracturing during the swelling process and remained easy to handle, even at their maximum swelling capacity.

The degradation of the biosutures were studied over a period of 35 days, through incubation in PBS (pH = 7.4) at 37°C, rotating at 25 rpm to mimic physiological conditions. The results were near identical to what was found in Chapter 4, with only the initial value being slightly higher, as can be seen in Figure 5.17 B. The degradation of alginate, pectin and gelatin systems are primarily based on hydrolysis and erosion mechanisms (Wang *et al.*, 2019). The human body does not produce the enzyme necessary to enzymatically degrade alginate and even though it does produce proteases (e.g. collagenase) that can degrade gelatin, several authors have found similar degradation rates for gelatin with or without collagenase, confirming a mainly hydrolytic degradation process for gelatin based systems (Van Den Bosch & Gielens, 2003; Rosellini *et al.*, 2009). In the current study, the uncoated and coated biosutures revealed similar degradation profiles, with the coated biosutures undergoing slightly less degradation, which is in accordance with the TGA results described earlier. The degradation profiles revealed an initial rapid weight loss within the first week, followed by a more gradual weight loss over the following weeks. The first rapid weight loss phase corresponds well with literature and can be ascribed to loss of the lipid-drug layer from the biosuture surface, leaching of the plasticizer out of the system as well as the easier removal of trapped water molecules after the swelling process (Li *et al.*, 2012).

After the initial rapid weight loss in the first week, the biosutures continued to gradually degrade at a constant pace which can be ascribed to surface erosion due to hydrolytic degradation. In general, swellable polymer systems undergo one of two types of degradation processes – bulk erosion or surface erosion. Surface erosion occurs when the diffusion of water into the system is slower than the hydrolytic reactions and the water is used before it can reach the bulk of the system. This results in gradual and continuous degradation from the surface of the system, while bulk erosion is characterized by a period of no erosion followed by a sudden and spontaneous loss of weight and strength (Schedl, 2002). In the current study, SEM images of the biosutures during different time points of degradation, confirm surface degradation as the primary mechanism of degradation (Figure 5.17 C). This form of degradation is ideal in suture materials where a sudden, rapid loss of suture material can lead

to wound dehiscence and failure of the wound to heal (Goel, 2016). However, gradual removal of the material from the biosuture surface will provide continuous, diminishing support to the wound as it heals and regains its own strength. Both the uncoated and coated biosutures were fully degraded after 5 weeks of incubation. This suggests that the biosuture will remain in the body long enough to support the healing wound (healing usually takes 2 – 3 weeks) and will be fully removed from the body shortly after the wound healing process is complete, thereby preventing unwanted irritation caused by the lengthy presence of a foreign body in the wound.

5.4 Conclusion

In order to determine if the newly developed biosuture material was at all suitable for clinical application, characterization, and analyses of the physiochemical and physicomachanical properties of the starting materials and biosutures, were necessary. The chemical structures and purity of the pristine biopolymers were confirmed with Fourier Transform Infrared Spectroscopy (FTIR). The FTIR spectrum of crosslinked sutures depicted $\Delta 9 \text{ cm}^{-1}$ downward shift for the carboxyl stretching band which was indicative of ionic interactions between barium ions and sodium alginate, while the characteristic C-F bond, observed as a vibration at 1242 cm^{-1} , confirmed the presence of the drug on the coated biosutures. X-ray diffraction (XRD) spectra revealed a semi-amorphous c structure in the biosuture, which aligned well with the mechanical properties thereof. Thermogravimetric analysis (TGA) and Differential Scanning Calorimetry (DSC) revealed good thermal stability in the biosutures, which was increased by the crosslinking process. Surface analyses by means of Scanning Electron Microscopy (SEM) revealed a smooth, uniform surface morphology that will allow the biosuture to easily glide through tissues without causing unwanted sawing or damage. Imaging also confirmed the average diameter of the biosutures ($100 \pm 0.5 \mu\text{m}$) and their ability to tie secure knots.

The mechanical properties of the biosutures remained unchanged and again exceeded the minimum requirements specified out by the United States Pharmacopoeia for absorbable suture materials. The lipid-drug coating provided an effective loading capacity of 101 ug/cm , that should provide effective drug concentrations *in vivo*. The drug release profile was very similar to what was obtained in the previous chapter, which confirms the accuracy and reproducibility of the results. Near 100% drug release was achieved after 10 days of incubation under simulated physiological conditions, which is a suitable time frame for the prevention of ischemic reperfusion injury and no-reflow in microvascular surgery. The biosutures displayed a near ideal degradation profile with gradual weight loss, that was confirmed to be the result of surface erosion. The biosutures were fully degraded after 5 weeks, which is also suitable within the context of wound healing and revascularization. The results were overall very encouraging and warrants further investigation of the biosutures in terms of biocompatibility and *in vivo* activity.

CHAPTER 6: ANALYSIS OF THE *IN VITRO* BIOCOMPATIBILITY OF THE NEWLY DEVELOPED BIOSUTURES

6.1 Introduction

Biocompatibility is arguably the most important property of any biomaterial and even though the individual components of the newly developed biosuture are well established in terms of safety and biocompatibility, it's crucial to confirm the biocompatibility of the biosuture itself (Tan *et al.*, 2020). *In vitro* biocompatibility studies are invaluable in predicting the potential safety of a biomaterial *in vivo* and have the added benefit of not requiring animal sacrifice. Additionally, a wide array of studies, that evaluate different aspects of biocompatibility such as cytotoxicity, cellular attachment, migration or even secretion of inflammatory markers, can be evaluated *in vitro* (Przekora, 2019).

In this chapter cell viability in the presence of the biosuture material will be evaluated using two different cell lines, namely Human Embryonic Kidney cells (HEK 293) and Mouse fibroblasts cells (3T3), to ascertain any possible cytotoxic effects that the biosutures might have. The selection of these cell lines is based on their reputable performance, widespread use to evaluate cytotoxicity and availability in the cell bank of our laboratory (Bhavsar *et al.*, 2019). Additionally, HEK 293 cells are specifically used because of their human origin, which should provide an accurate picture of the influence of the biosutures on human cells. Fibroblast cells are found in connective tissue all over the body and play a critical role not only in wound healing, but also angiogenesis, which serves as motivation for their employment in this study (Desjardins-Park *et al.*, 2018). It should be noted that another cell line, namely Human Umbilical Vein Endothelial Cells (HUVEC) was precured specifically for this study. Regrettably, the first batch got contaminated soon after revival and the second batch showed very low cell viability after revival and did not reach confluence even after many weeks of care and coaxing. In this chapter, cell viability will be quantified with a colorimetric assay (based on the XTT, 2,3-bis-(2-methoxy-4-nitro-5-sulfophenyl)-2H-tetrazolium-5-carboxanilide, reagent) using an indirect method, described in ISO 10993-5, which outlines how biomaterials should be evaluated for biocompatibility (2009).

One of the key differences between the newly developed biosuture, and other synthetic sutures, is its natural origin and the presence of specific amino acids, such as the tripeptide Arg-Gly-Asp (RDG), in the biosuture material which could mediate cell attachment or adhesion to the biosuture surface (Wu *et al.*, 2020). Hence, a cell attachment experiment will be performed in this chapter to confirm the ability of cells to adhere to the biosuture surface, which might improve cell proliferation and even support wound healing *in vivo*.

Hemocompatibility is another critical component of biocompatibility, which often limits the clinical applicability of blood-contacting biomaterials, such as the biosutures developed in this study. The biosutures will be in direct contact with blood, which is a complex 'organ' consisting of plasma, erythrocytes, leukocytes and platelets, from the moment of implantation, until it is degraded (Nalezinková, 2020). Hence, it is imperative to ensure that the biosutures do not cause any adverse interactions that could trigger the activation and destruction of the blood components. If erythrocytes or platelets are activated, thrombosis will immediately ensue which, in the case of microvascular surgery, could lead to vascular occlusion and surgical failure. Moreover, the thrombus can dislodge and cause additional serious complications, such as pulmonary embolism, myocardial infarction, or stroke (Siedlecki, 2018). Erythrocytes are the most abundant and most rigid cells in the blood, which makes them extremely prone to rupture (haemolysis) when exposed to hypotonic solutions or cationic and toxic materials. Platelets are the smallest and second most abundant cell in the blood and can swiftly recognize foreign substances and activate blood coagulation (Picone *et al.*, 2019). According to Weber *et al.*, *in vitro* models of hemocompatibility evaluation of biomaterials are more reliable and accurate than *in vivo* models, since they allow analysis under well controlled conditions and eliminate disturbing factors such as flow obstruction, surgery and tissue effects that can occur *in vivo* (Weber *et al.*, 2018). Hence, we will perform the two most common *in vitro* blood compatibility tests, namely haemolysis and platelet activation, to confirm the biocompatibility of the biosutures.

6.2 Materials and methods

6.2.2 Materials

Human embryonic kidney cells (HEK 293) and mouse embryonic fibroblast cells (NIH-3T3) were purchased from Cellonex (Johannesburg, South Africa). Dulbecco's minimal essential medium (DMEM), foetal calf serum (FCS), antibiotics (100 IU/mL penicillin and 100 IU/mL streptomycin), collagen, Triton X-100 and a cell proliferation kit (XTT), were obtained from Sigma-Aldrich (St. Louis, Missouri, USA). Anticoagulated sheep's blood was graciously provided by the National Health Laboratory Services of South Africa and human whole blood was collected into sodium citrate anticoagulation tubes, from healthy volunteers (ethical clearance number: M180978).

6.2.2 Evaluation of the *in vitro* cytotoxicity of the biosutures

Cytotoxicity evaluation was performed on two cell lines, namely a human embryonic kidney cells (HEK 293) and mouse embryonic fibroblast cells (NIH-3T3). Cells were revived from cryogenic freezing by placing a 1.5 mL vial with the cells into a water bath set to 37 °C, with extreme care to ensure the water level does not reach the cap of the vial. Once defrosted, the cells were carefully aspirated and transferred to a T-75 cell culture flask supplemented with

Dulbecco's minimal essential medium (DMEM), containing 10% foetal calf serum (FCS) and antibiotics (100 IU/mL penicillin and 100 IU/mL streptomycin). Culture flasks were kept in a controlled incubator (37 °C, 95% humidity and 5% CO₂). Once 80% confluency was reached, the cells were seeded into 96-well plates (3 x 10³ cells/well) and incubated for 24 hours.

An XTT cytotoxicity assay was performed as outlined by ISO 10993-5, using an indirect extract method previously employed by Baygar *et al.* (Baygar *et al.*, 2019). Extracts were prepared by incubating the uncoated and coated biosutures (5cm/mL) in fresh culture media for 5 days. High extract concentrations were used so as to exaggerate the clinical use conditions and determine any potential toxicological hazard. After the seeded cells were incubated for 24 hours, the 96-well plates were treated by removing the culture media and replacing it with 100 µl of either the uncoated or coated extract medium. All treatments were performed in triplicate across a concentration range of 1.25 cm/mL, 2.5 cm/mL and 5 cm/mL. Some cells were also treated with drug solutions, at concentrations equal to what was loaded on the biosutures (i.e., 126 µg/mL, 252.5 µg/mL and 505 µg/mL. Normal culture medium was used as negative control and 5-flurouracil (0.1% w/v) as positive control. The 96-well plates were incubated for 24 and 48 hours at 37°C, 5% CO₂ and at the end of the incubation period, the cell viability was determined by XTT assay according to the standard protocol. Briefly, 100uL of the electron coupling reagent (ECR) was added to 5 mL of the XTT labelling reagent and 50uL of the XTT mixture immediately added to each well (final concentration, 0.3 mg/mL) followed by incubation for 4 hours. The spectrophotometric absorbance of each sample was measured with a multiplate reader (VICTOR™ X Multilabel Plate Reader, Perkin Elmer, SA) at 450 nm, with 650 nm as reference wavelength. The percentage cell viability was calculated according to equation 6.1:

$$\text{Cell viability (\%)} = \frac{Abs_s}{Abs_c} \times 100 \quad \text{Equation 6. 1}$$

6.2.3 Evaluation of cellular attachment to the biosutures

Segments (0.5 cm in length) of the uncoated and coated biosutures were placed on the bottom of a 96-well plate and 100 µL of HEK 293 cells in fresh culture medium (7500 cells/well) seeded on top of the biosutures. The cellular adhesion to the biosuture surface was evaluated qualitatively at different time points (1, 24 and 48 hours after incubation) with a CKX53 light microscope (Olympus, Tokyo, Japan).

6.2.4 Evaluation of the haemolytic activity of the biosutures

The haemolytic activity of the uncoated and coated biosutures were evaluated on both sheep and human blood according to the indirect method, as outlined in practice F619-03 and described by Sunitha *et al.*, (Sunitha *et al.*, 2017). Anticoagulated whole blood was centrifuged

at 3000 rpm for 15 minutes to separate the blood constituents. The top layer of platelets and leucocytes were removed, and the erythrocyte pellet washed twice with isotonic phosphate buffered saline (PBS). The erythrocytes were diluted with PBS to obtain an 8% v/v suspension. Small 2 mL Eppendorf tubes were filled with 1 mL erythrocyte suspension and 0.5 mL biosuture extract (5 cm/mL), which was prepared by incubating the uncoated and coated biosutures in PBS for 5 days at 37°C. The Eppendorf tubes were incubated for 24 hours at 37°C with constant agitation (25 rpm) to mimic *in vivo* conditions. After incubation, the erythrocyte suspensions were again centrifuged at 3000 rpm for 15 minutes and 100 uL of the supernatants transferred to a 96-well plate. The absorbance of the supernatants was measured at 540 nm using a multiplate reader (VICTOR™ X Multilabel Plate Reader, Perkin Elmer, SA). Triton X-100 (1% v/v) was used as positive control and PBS as negative control. All experiments were performed in triplicate and the average percentage haemolysis calculated according to equation 6.2:

$$\% \text{ Haemolysis} = \frac{OD_s - OD_n}{OD_p - OD_n} \times 100 \quad \text{Equation 6. 2}$$

Where OD_s, OD_n, and OD_p are the absorbance values of the sample, negative control, and positive control, respectively.

6.2.5 Evaluation of the platelet activation ability of the biosutures

Platelet activation was evaluated microscopically, by studying the change in platelet shape as a function of incubation with uncoated and coated biosuture extracts (Okpalugo *et al.*, 2004). Both sheep and human blood was again centrifuged, this time at 1200 rpm for 15 minutes to obtain platelet rich plasma (PRP) which formed at the top of the centrifuge tube. Platelets were transferred to a 48-well plate (406 x 10⁴ platelets/mL for sheep blood and 67.5 x 10⁴ platelets/mL for human blood). Due to the small amount of human blood that was available, a much lower concentration of human platelets had to be used. Extracts of the uncoated and coated biosutures (5 cm/mL) were prepared by incubation of the biosutures in PBS for 5 days at 37°C and 100 µl of each extract added to the wells in triplicate. Collagen (100 ug/mL) served as positive control and PBS and negative control. After static incubation for 1 hour at room temperature, the treated wells were visualized with a CKX53 light microscope (Olympus, Tokyo, Japan) and the morphology of the platelets studied.

Statistical analysis

All data values are presented as mean ± standard deviation. Differences were assessed using Student's t-tests (GraphPad Prism 2021) and the data in figures marked by (*) for p<0.05 and (**) for p<0.01.

6.3 Results and discussion

6.3.1 Evaluation of the *in vitro* cytotoxicity of the biosutures

Good biocompatibility is one of the basic requirements of any implantable biomaterial. We assessed the cytotoxicity of the biosutures, firstly by treating cells with a series of biosuture extracts, that were prepared by incubating increasing amounts of biosuture in cell culture media, and secondly by directly adding biosuture segments of increasing length to the cell seeded wells. Cell viability was evaluated at 24 and 48 hours using two cell lines, HEK 293 and NIH-3T3, and a colorimetric XTT method to establish the metabolic activity of the cells. Normal culture medium was used as negative control and taken to provide 100% cell viability. According to ISO 10993-5 a biomaterial is considered cytotoxic if it reduces the cell viability by more than 30% (2009). As can be seen in Figure 6.1. and 6.2., all of the tested samples displayed good biocompatibility, with none displaying more than 5% decrease in cell viability. Increasing biosuture concentrations correlated with greater suppression of cell growth, in both cell lines. Yet even the highest concentration of 5 cm/mL (which is considerably higher than the 1 cm/mL reported in similar previous studies) was not cytotoxic.

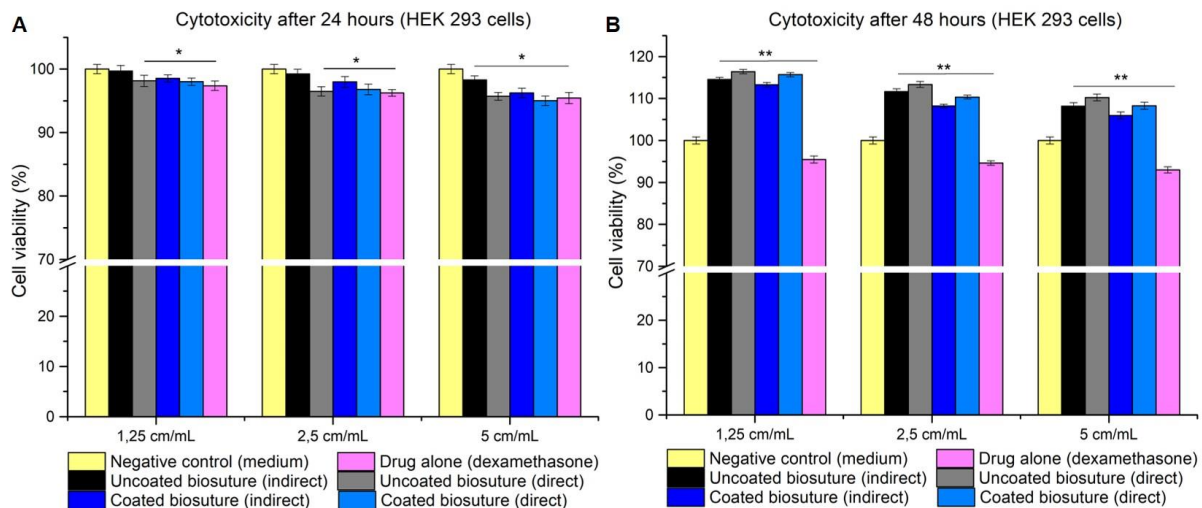


Figure 6.1: Percentage cell viability of HEK 293 cells after A) 24 hours and B) 48 hours, with $p < 0.05$ indicated as (*) and $p < 0.01$ as (**).

After 24 hours of incubation with HEK 293, extracts of the uncoated biosutures, resulted in cell viability values very similar to that of the negative control, i.e., 99.6%, 99.2% and 98.3% for increasing extract concentrations (Figure 6.1). The direct method, however, resulted in slightly lower values of 98.1%, 96.4% and 95.7%, possibly due to initial shock from exposure to the large unfamiliar biosuture surface. Extracts of the coated biosutures, also suppressed cell growth to a greater extent than extracts of the uncoated biosutures, with cell viability values of 98.5%, 97.9% and 96.2%, which is still indicative of good biocompatibility. Direct incubation with coated biosuture segments, again resulted in a lower cell viability, and provided the lowest

values seen with the biosuture samples, i.e., 97.3%, 96.2% and 95.4%. The lower cell viability seen with the coated biosutures, can be ascribed to the initial burst release of dexamethasone from the lipid-drug coating. Dexamethasone is known to be selectively cytotoxic to certain cell types, such as osteoblasts, and was found to lower the viability of both HEK 293 and NIH-3T3 cells, compared to the negative control, in the current study (Zhu *et al.*, 2019).

After 48 hours, the picture changed considerably and all the biosuture samples provided significantly higher ($p < 0.01$) cell viability than the negative control. Extracts of the uncoated biosutures increased the cell viability to 114.5%, 111.6% and 108.1%, while extracts of the coated biosutures again provided slightly lower cell viability values of 113.2%, 108.2% and 105.9%, respectively. Contrary to after 24 hours, the direct method resulted in higher cell viability after 48 hours, than the indirect method for both the uncoated and coated biosutures, with values of 116.4%, 113.3% and 110.2%, for the uncoated samples and 115.6%, 110.3% and 108.2%, for the coated samples. This suggest that, even though the biosuture segments initially had an inhibiting effect on cell growth, their surfaces later supported and even encouraged cell proliferation.

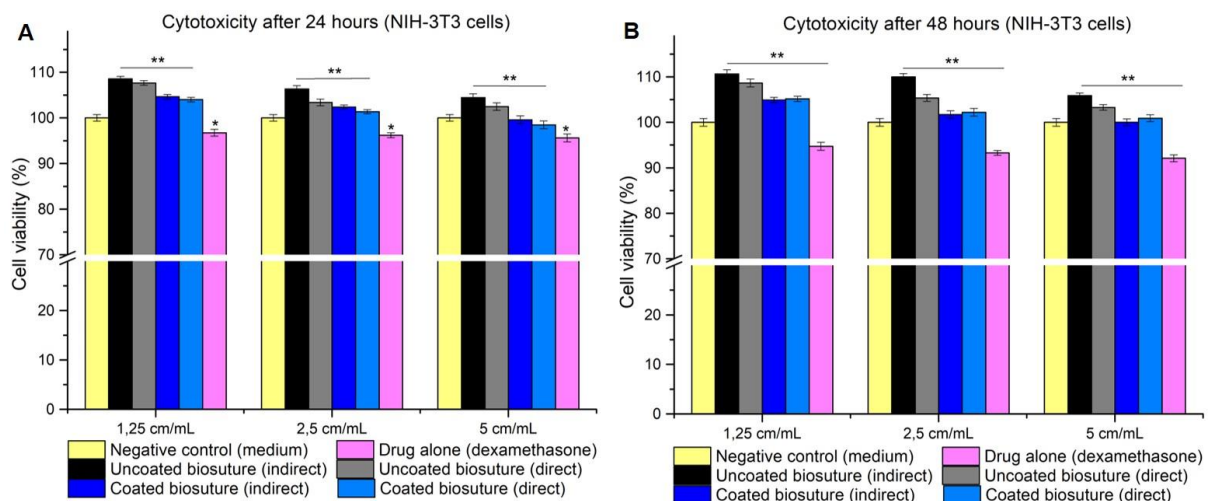


Figure 6.2: Percentage cell viability of NIH-3T3 cells after A) 24 hours and B) 48 hours, with $p < 0.05$ indicated as (*) and $p < 0.01$ as (**).

As can be seen in Figure 6.2., the NIH-3T3 cells did not show the initial decrease in cell viability 24 hours after treatment with the biosuture extracts or segments, as was observed with HEK 293 cells. Instead, all of the samples, i.e., both the uncoated and coated biosutures tested in the indirect and direct method, significantly ($p < 0.01$) increased the cell viability, compared to the negative control. It is possible that the mouse fibroblast cells are more robust and not affected by the treatment process, or they required less time to acclimatize to the new extract growth medium and presence of the biosutures, than the human cells. The rest of the NIH-3T3 cell viability results, however, correspond very well with that of the HEK 293 results, with

the coated biosutures resulting in lower viability than the uncoated biosutures and the direct method initially showing lower viability than the direct method, but higher values as time progresses. Also similar to the HEK 293 cells, the cell viability of the NIH-3T3 cells were significantly higher after 48 hours, compared to 24 hours, which suggests that the biosutures are able to support viability and proliferation over extended time periods without causing cytotoxicity.

The *in vitro* cell viability results are very encouraging and point to excellent biocompatibility of both the uncoated and coated biosutures. The general increase in cell viability is often seen with natural polymers such as gelatin and alginate, which mimics the native extracellular matrix (ECM). Mohammadi *et al.*, for example showed that nylon sutures coated with chitosan/hyaluronic acid could increase cell viability to nearly 140%, compared to the 100% achieved with culture media (Mohammadi *et al.*, 2020). Similarly, Li *et al.*, showed that combinations of natural polysaccharides, such as alginate and collagen, with proteins such as gelatin and collagen, significantly increases cell viability by providing the same proteoglycan structures found in the ECM, and thereby supporting both cell attachment and viability (Li *et al.*, 2005). Earlier this year, Deng *et al.*, also illustrated the value of including natural polymers to suture formulations and concluded that, this kind of suture materials that are able to enhance cell proliferation, might aid wound healing *in vivo* and thereby become invaluable once translated to clinical practise. However, in the case increased cell proliferation, the risk of carcinogenicity must always be kept in mind. In the current study, the highest cell viability (116.4%) was achieved with the direct treatment of HEK 293 cells with 1.25 cm/mL of the uncoated biosuture segments. Similar and higher results have been reported for natural polymer-based biomaterials, which did not show any signs of carcinogenicity *in vivo*. Moreover, according to ISO 10993, only permanent biomaterials that are intended to remain in the body indefinitely, can pose a carcinogenic risk and should be evaluated accordingly.

6.3.2 Evaluation of cellular attachment to the biosutures

Good cellular adhesion is characterized by an elliptical, stretched cellular morphology, while a spherical morphology is indicative of poor attachment (Yang *et al.*, 2010). One hour after incubation of the cells on the biosutures, their morphology was round and spherical but after 24 hours, there were clear signs of spreading and adoption of the normal cellular morphology (indicated by arrows in Figure 6.3). After 48 hours, there was a clear increase in cell number with proliferation of the cells on the biosuture surface. In contrast, only debris could be detected on the surface of a synthetic suture (Prolene®, Polypropylene suture) after 48 hours of incubation. It should be noted that it is extremely difficult to bring the synthetic braided suture into focus due to the different planes of the swollen multifilaments.

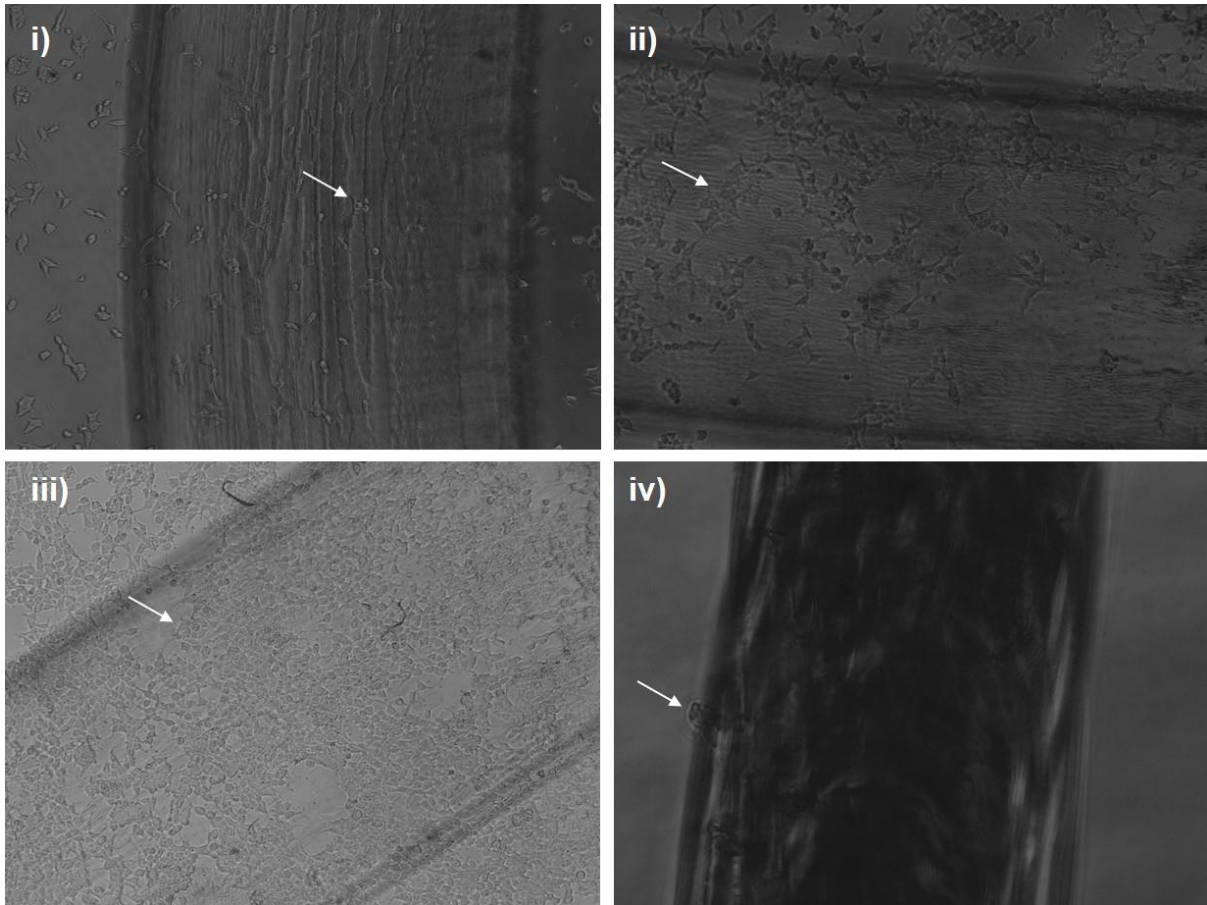


Figure 6.3: Light microscope images (60x magnification) of the biosutures, showing cell attachment after i) 1 hour, ii) 24 hours and iii) 48 hours of incubation; iv) synthetic polypropylene suture (Prolene®) after incubation with cells for 48 hours.

Several properties of a biomaterial, such as surface topography, stiffness and hydrophilicity, determine, firstly how it will interact with cells and secondly, its potential to promote physiological functions such as signal transduction and cellular migration, proliferation and differentiation. According to Nishida *et al.*, “the hydrated water content of the biomaterials will be a predominant factor affecting the cell adhesion strength and behaviour” (Nishida *et al.*, 2021). Several other authors have also argued that surface wettability has a direct influence on cell adhesion, with hydrophilic surfaces supporting better cellular adhesion than hydrophobic surfaces (Amani *et al.*, 2019; Arango *et al.*, 2021; Metwally & Stachewicz, 2019). Hence, it is probable that the hydrophilicity of the biosuture, and its ability to absorb water had a positive impact on its ability to support cell adhesion and behaviour. Additionally, water absorption and swelling have a profound effect on the stiffness of a material and would have made the biosuture considerably more elastic and, therefore, more favourable for cellular attachment. Furthermore, surface roughness and topographies such as microgrooves, have been found to boost and localize cell adhesion and differentiation (Naganuma, 2017). The lines observed on the surface of the biosutures during SEM imaging, are also clearly visible

on the light microscope images and seem to have been enhanced by the swelling process, increasing the surface roughness, and creating long grooves on the biosuture surface, which could potentially have supported cellular adhesion and spreading.

Another important factor, that is known to facilitate cell adhesion and induce cell differentiation, is the presence of amino acid sequences such as arginine-glycine-aspartate (Arg-Gly-Asp; RDG) on biomaterials. Gelatin is abundant in RGD sequences and could have contributed to the good adhesion of cells to the biosuture surface (Klimek & Ginalska, 2020). Several other authors have also shown that gelatin-based biomaterials encourage cell adhesion and differentiation, while Deng *et al.*, found that biocompatible sutures create a comfortable environment for cells to attach, spread and proliferate, thereby supporting cell growth and potentially improving wound healing (Bello *et al.*, 2020; Deng *et al.*, 2021; Liu *et al.*, 2019).

6.3.3 Evaluation of the haemolytic activity of the biosutures

Haemolysis is a universal method of evaluating the blood compatibility of biomaterials. According to international standards (ASTM F756-00) a biomaterial should not cause more than 5% haemolysis for it to be considered safe for clinical use (Zheng *et al.*, 2021). Figure 6.4., provides the haemolysis results for sheep blood and shows images of the erythrocyte suspensions, treated with the different controls and samples, after centrifugation. The positive control, the powerful surfactant Triton-X 100, caused profound lysis of the erythrocytes with the release of haemoglobin that can clearly be seen in the deep red colour of the supernatant. The supernatants obtained with the uncoated and coated biosutures, on the other hand, was clear, colourless, and resembled that of the negative control, where no haemolysis was detected. The drug, dexamethasone, also caused negligible haemolysis as confirmed by the clear appearance of the supernatant and quantified by the optical density therefor. The quantitative results (Figure 6.4 A), confirmed that all the tested samples caused near 0% haemolysis. The direct method, however, resulted in slightly higher percentages compared to the indirect method, used for the coated and coated biosutures (0.05% vs. 0.15% for the uncoated biosutures, and 0.07% vs. 0.23% for the coated sutures). Yet, these values remained well below the permissible degree of haemolysis and was considerably lower than what has previously been reported for commercial PLLA sutures (4.75%) (Hu *et al.*, 2009). The coated biosutures also displayed slightly higher haemolysis degrees than the uncoated biosutures. This was unexpected, since the zwitterionic phosphatidylcholine in the lipid-drug layer is known to have excellent hemocompatibility and is often used to improve the hemocompatibility of other biomaterials. The drug, however, displayed the highest haemolysis degree (0.43%) of all the samples that were tested, and even though this value is still very low, might be the reason for the slightly higher haemolysis observed with the coated biosutures, compared to the uncoated biosutures.

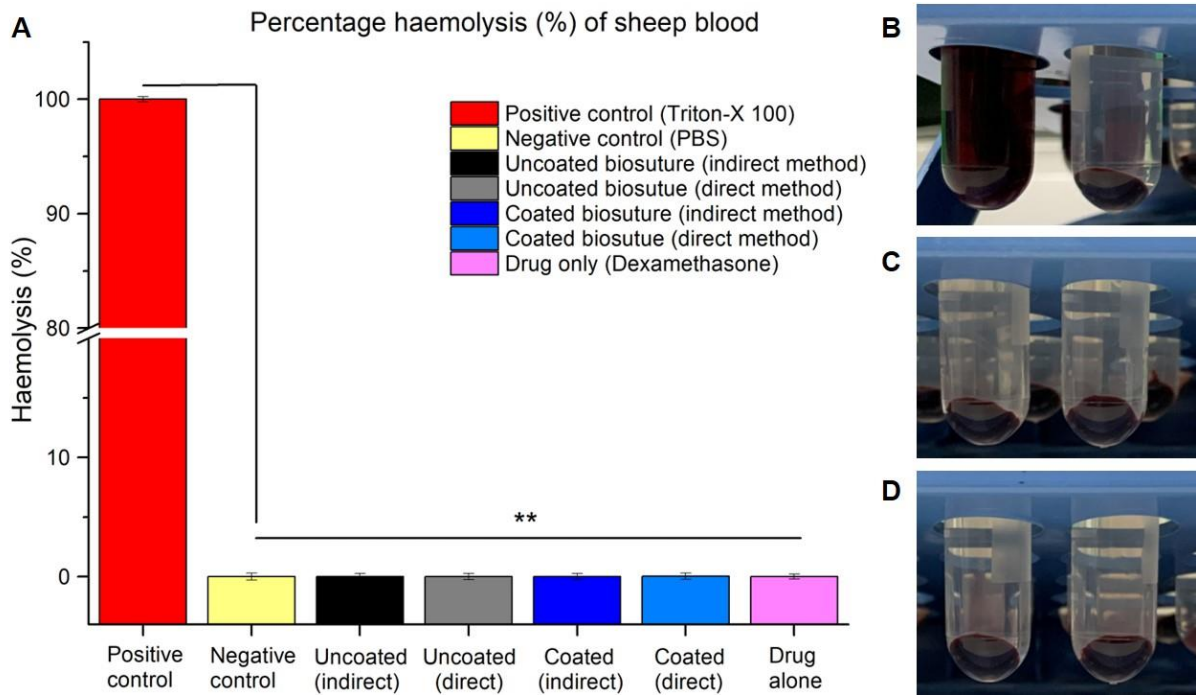


Figure 6.4: A) Percentage haemolysis of sheep blood and images indicating the respective supernatants of the erythrocyte suspensions after centrifugation, as treated with B) the positive and negative control, C) the uncoated biosuture (indirect and direct method) and D) the coated biosuture (indirect and direct method).

Henkelman *et al.*, who did an in-depth study on the “Standardization of incubation conditions for haemolysis testing for biomaterials”, found that the most accurate haemolysis results can be obtained by 24-hour incubation of a biomaterial sample at 37°C in diluted human blood (Henkelman *et al.*, 2009). Hence, we repeated the study using human erythrocytes as shown in Figure 6.5. Interestingly, the human blood displayed even lower haemolysis degrees, than what was observed with sheep blood, even though the same trends were followed, i.e., the direct method caused higher haemolysis (0.009% vs. 0.011% for the uncoated biosutures and 0.017% vs. 0.03% for the coated biosutures) and the drug displayed the greatest haemolysis (0.045%). The slightly higher haemolysis, observed for the direct method, is interesting as the biosuture surface is expected to be neutral and not cause haemolysis of any degree. It is possible, however, that the little haemolysis observed for these samples, was the result of the treatment process itself, where tweezers were used to add the biosutures to the erythrocyte suspension. The direct method of treatment could have been more traumatic to the erythrocytes, as the biosutures had to be pushed to the bottom of the vial to ensure full submersion in the erythrocyte suspension, compared to the simple addition of the extracts with a pipette, in the indirect method.

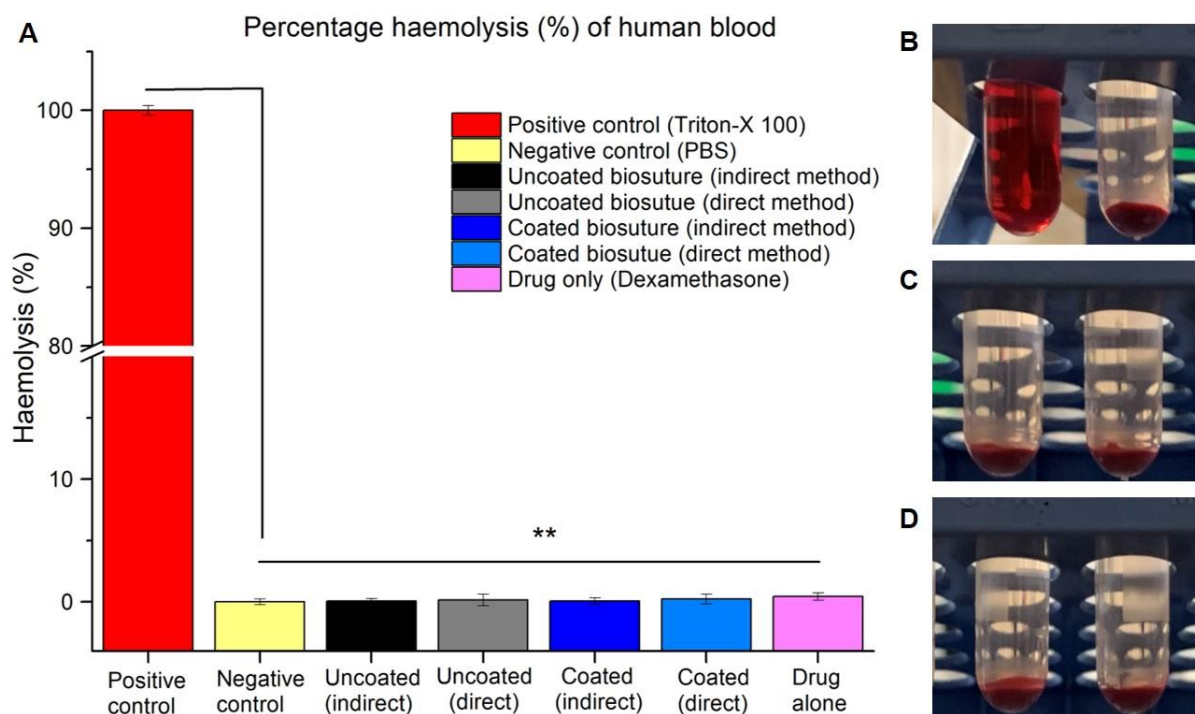


Figure 6.5: A) Percentage haemolysis of human blood and images indicating the respective supernatants of the erythrocyte suspensions after centrifugation, as treated with B) the positive and negative control, C) the uncoated biosuture (indirect and direct method) and D) the coated biosuture (indirect and direct method).

The haemolysis results, therefore, suggest that the biosutures have good hemocompatibility. This was expected as the individual biopolymers, that make up the biosutures, have all been found to not cause erythrocyte lysis (Konovalova *et al.*, 2017; Notara *et al.*, 2009). Yet, the biomaterial itself, or extracts thereof, could still cause haemolysis through interaction with or alteration of the erythrocyte membrane. Haemolysis usually occurs due to changes in the isotonicity of the surrounding solution that alters the osmotic pressure inside the erythrocytes, or due to interactions between a cationic material and the negatively charged blood cells or through particles or degradation products that induce prominent deformation of the erythrocyte membrane, leading to haemolysis (Klajnert *et al.*, 2010). Hydrophobic surfaces have also been found to cause significant haemolysis (> 7%) through nonpolar interaction with the erythrocyte membrane while hydrophilic surfaces show less intense adsorption of blood proteins and better hemocompatibility (Notara *et al.*, 2009). The hydrophilicity and lack of positive charges on the biosuture surface, can therefore be considered as contributing factors to the good hemocompatibility of the biosutures, observed so far. The indirect method, where extracts of the biosutures were used, also confirms that degradation/erosion products of the biosutures did not distort or significantly interact with the erythrocyte membrane. This can be due to the negative charge on the biopolymer surfaces, (i.e., alginate, pectin and gelatin – with an isoelectric point of 5.198, as determined in Chapter 3, are negatively charged in solution)

which would have resulted in repulsive forces between the biopolymer surfaces and the erythrocyte membranes, and hence a lack of interaction and good hemocompatibility (Jhong *et al.*, 2014).

6.3.4 Evaluation of the platelet activation ability of the biosutures

Platelet activation is a critical step in the thrombus formation process and a key mechanism that confers biomaterial thrombogenicity. Platelets attach to foreign body surfaces through a complex series of events that involves different receptors (i.e., glycoproteins) and depends on several factors including the nature of the material and the prevailing rheological conditions (Ye *et al.*, 2019). The most prevalent criteria for evaluating platelet activation on a qualitative basis, is morphological changes. Inactivated platelets are round or discoid in shape and have diameters in range of 2 – 3 μm . Once activated, platelets initially develop small pseudopodia which at a further stage of activation become fully spread pseudopodia with irregular shapes and larger diameters (Li *et al.*, 2017). In the late 1990's, Goodman categorized platelets into five distinct morphological shapes, based on increasing stages of activation, which is still used today to classify the degree of platelet activation (Braune *et al.*, 2019; Goodman, 1999). These shapes are, in order of increasing activation, discoid (round), dendritic (early pseudopodia), spread dendritic (intermediate pseudopodia), spread, and fully spread, as shown in Figure 6.6.

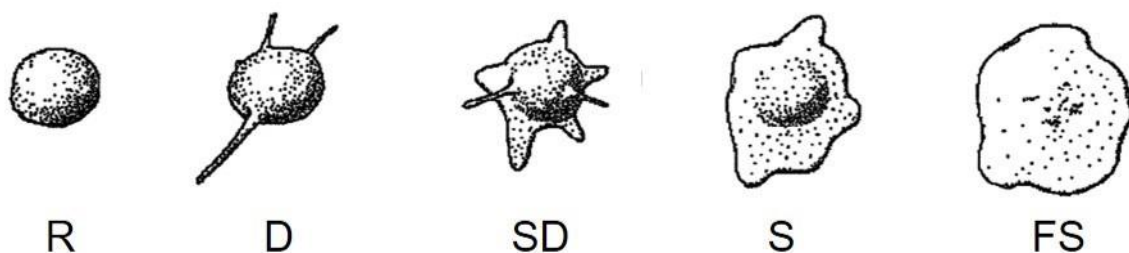


Figure 6.6: Platelet morphology according to increasing degrees of activation, (R) round, (D) dendritic, (SD) spread dendritic, (S) spread and (FS) fully spread.

As with haemolysis, we first investigate the degree of platelet activation in sheep blood. The anticoagulated blood was centrifuged to obtain platelet rich plasma (PRP), which was incubated with the positive control, negative control, and uncoated and coated biosuture samples and extracts. The positive control immediately activated the platelets, which were fully spread and aggregated in large clusters after one hour of incubation (Figure 6.7 A). After incubation with the negative control, the platelets remained round or discoid and showed no signs of activation, as expected. Both the uncoated and coated biosutures, as tested in the indirect and direct method, did not activate the platelets, which displayed a similar morphology to the negative control, as can be seen in Figure 6.7 B – F. This preliminarily suggests that the biosutures do not interact with blood platelets to a significant degree, but needs to be

confirmed as Goodman has previously found sheep platelets to be less sensitive to activation than human platelets (Goodman, 1999).

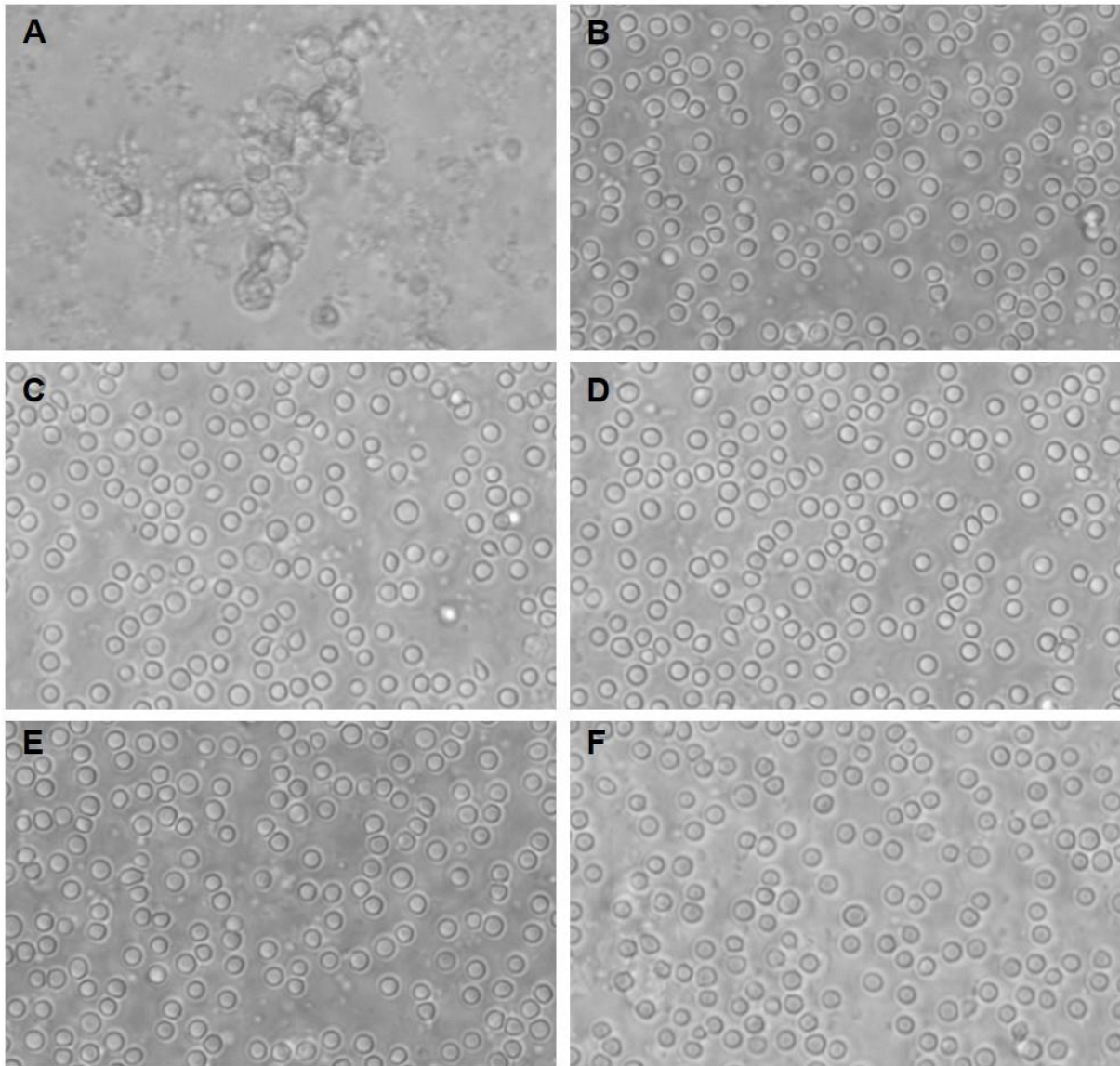


Figure 6.7: Sheep platelet morphology after incubation with A) the positive control, B) the negative control, C) uncoated biosutures (indirect method), D) uncoated biosutures (direct method), E) coated biosutures (indirect method) and F) coated biosutures (direct method).

The platelet activation results obtained with human blood, however, were very similar to results of sheep blood, as can be seen in Figure 6.8. Yet, the degree of activation, achieved with the positive control was lower, and the platelets displayed a 'spread pseudopodia' morphology, instead of the fully spread shape seen in Figure 6.7 A. This suggests that the human platelets were less sensitive to the positive control or that they did not activate at the same rapid rate as sheep platelets. The negative control showed the same lack of activation, with the platelets maintaining a round, discoid morphology. The uncoated and coated biosutures, again, caused little to no platelet activation, with the exception of one or two platelets showing early

pseudopodia formation (indicated with arrows in Figure 6.8). Slight platelet activation is expected as platelets usually become activated upon exposure to foreign materials. Yet, the activation is very low, and the results still point to the good hemocompatibility of the biosutures.

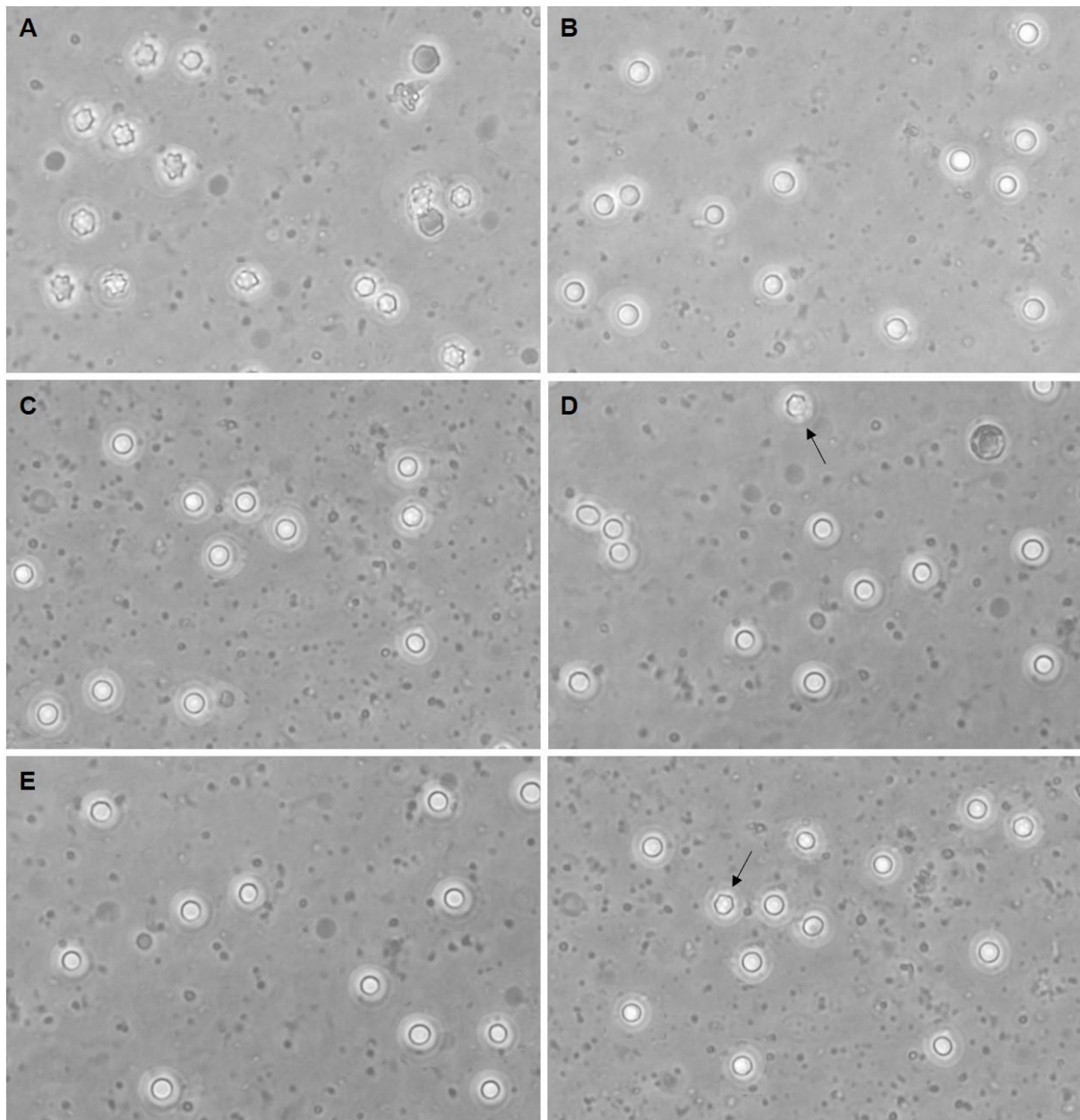


Figure 6.8: Human platelet morphology after incubation with A) the positive control, B) the negative control, C) uncoated biosutures (indirect method), D) uncoated biosutures (direct method), E) coated biosutures (indirect method) and F) coated biosutures (direct method).

The very low platelet activation properties of the biosutures can again be ascribed to the favourable characteristics and excellent biocompatibility of the biopolymers that the biosutures are made of. In a recent study on polysaccharide-based vascular patches, de Souza *et al.*, found that pectin-containing materials displayed better hemocompatibility with lower platelet adhesion and activation, presumably because of the higher elastic modulus that pectin

conveyed to the material. The study also found that human smooth muscle cells (HSMC) adhere, spread and proliferate better on the materials made with pectin, compared to alginate-based matrices (de Souza *et al.*, 2019). Similarly, it is very likely that pectin significantly contributes to the good cell viability and hemocompatibility of the biosutures seen in this study by improving the elasticity and structural properties of the biosutures. Gelatin, on the other hand, is well-known and widely used for its ability to control and prevent platelet activation, and most likely also contributes significantly to the good hemocompatibility of the biosutures. According to Li *et al.*, who showed that increasing gelatin content improves the antithrombogenicity of biomaterials, gelatin is able to avert platelet activation and thrombin generation by crippling the functioning of plasma von Willebrand factor. Apte *et al.*, in turn, recently showed that gelatin reduces surface induced platelet activation, primarily by increasing the hydrophilicity of the biomaterial, which limits the adsorption of proteins that are responsible for platelet adhesion and activation, thereby also reducing the latter (Apte *et al.*, 2021). Hence, it is possible that the good hydrophilicity of the biosutures, as conveyed by gelatin and alginate, again secured the good hemocompatibility of the material.

As can be seen in Figure 6.9, very few platelets were observed on the biosuture surface after incubation in platelet rich plasma (direct method), and the platelets that did adhere were round and inactivated. This is in line with the results of Apte *et al.*, as discussed above, and the characteristics of the biopolymers themselves, which do not necessarily encourage platelet adhesion. Another likely reason for the limited platelet adhesion and activation on the biosuture surface, is the specific surface topography and curvature of the biosutures.

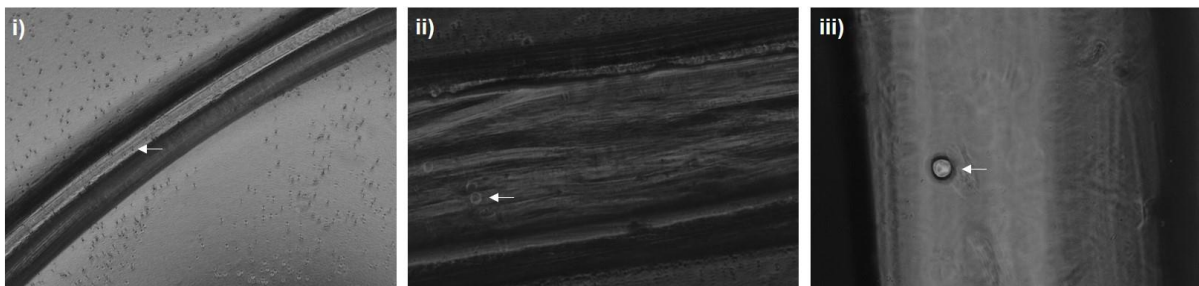


Figure 6.9: Adhesion of human platelets to the biosuture surface.

Studies have showed that surface topography plays a very distinct role in platelet adhesion, to the extent that it can even overcome the influence of chemical properties. The size, shape and distance between surface features will affect the area available for platelets to adhere and also the amount of energy they will require to maintain surface adhesion. According to Lui *et al.*, interspacing dimensions of less than 200 nm, significantly reduces platelet adhesion, while Xu and Siedlecki, reported a 65.5% decrease in platelet adhesion to textured polymer surfaces (400 x 400 nm dimensions), relative to smooth surfaces (Liu *et al.*, 2016; Xu & Siedlecki,

2017). Several authors have also found that surface topography can directly affect the degree of activation of platelets, with low aspect ratios resulting in greater circularity and less activation, than high aspect ratios, despite similar levels of platelet adhesion (Firkowska-Boden *et al.*, 2020; Koh *et al.*, 2010; Liu *et al.*, 2019; Xu *et al.*, 2019). The specific surface topography of the biosutures, which consists of long, narrowly spaced grooves that run along the length of the biosutures, could potentially have made the surface less favourable for platelet adhesion and activation and improved the hemocompatibility of the biomaterial. The round, 3D structure of the biosuture, and its specific curvature could also have affected the adsorption, orientation, and functionality of specific proteins, such as fibrinogen (the protein that facilitates platelet adhesion and activation) and made the receptor ligands less available to platelets. This was illustrated by Xu *et al.*, who found that platelets, adhered to fibrinogen-textured surfaces, display greater circularity than platelets adhered to smooth surfaces, indicating that textured surfaces reduce platelet activation (Xu *et al.*, 2014).

6.4 Conclusion

In this chapter we performed a detailed analysis of the *in vitro* biocompatibility of the biosutures, to determine their potential *in vivo* safety and suitability for clinical use. Biocompatibility was evaluated in terms of cell viability, using two cell lines (i.e., HEK 293 and NIH-3T3), while hemocompatibility was evaluated by means of haemolysis and platelet activation assays, using both sheep and human blood.

The HEK 293 cell viability results, reflected increased cell growth after 48 hours, with the highest concentration of the uncoated and coated biosutures respectively resulting in 108.1% and 105.9% cell viability, using the indirect method and 110.2% and 108.2% cell viability, using the direct method. The NIH-3T3 cell viability results, was very similar to that of HEK 293, with the uncoated and coated biosutures respectively providing 105.8% and 102.1% cell viability, using the indirect method, and 103.2% and 102.1% cell viability, using the direct method. The coated biosutures, in general, provided lower cell viability results than the uncoated biosutures, presumably due to the presence of dexamethasone in the coating. Yet, the coated biosutures still managed to increase the cell viability, indicating that the encouraging effect of the biosuture material on cell growth, outweighs any negative impact that the drug might have. The cell viability results, therefore, confirm the biocompatibility of the biosutures but also suggests that the biosutures support and encourage cell proliferation, which might accelerate wound healing *in vivo*. Light microscope images also confirmed that HEK 293 cells attach to and proliferate on the surface of the biosuture, indicating that the biosutures create a comfortable environment for the cells to grow.

The haemolysis assay results, of both sheep and human blood, revealed that the uncoated and coated biosutures caused near 0% haemolysis, when tested with both the direct and indirect method. This confirms that the biosutures, and their degradation products, do not negatively interact with the erythrocyte membranes or disrupt the structure of the cells and suggests that the biosutures have good hemocompatibility. This is confirmed by the platelet activation assays, which indicated limited adhesion of platelets to the biosuture surface and little to no activation of the platelets, as indicated by their round, discoid morphology that was similar to the morphology of platelets that were treated with the negative control.

The results of this chapter, therefore, confirm that the newly developed biosutures are biocompatible with excellent cytocompatibility and hemocompatibility, and provide incentive for further clinical evaluation and possible commercialization of the biosuture material.

Fabrication, Mechanical Properties, and Biocompatibility of a novel monofilament, absorbable, drug-eluting biosuture for potential microvascular surgery applications. de la Harpe, K.M., Marimuthu, T., Kondiah, P.P., P. Kumar, Ubanako, P. and Choonara, Y.E. Submitted to the Journal of Biomedical Materials Research: Part B.

CHAPTER 7: CONCLUSIONS, RECOMMENDATIONS, AND FUTURE PROSPECTS

7.1 Conclusions

Sutures, unquestionably, have the power to influence a vast range of surgical and reconstructive procedures. Equally clear, is the dire need for more advanced suture materials that can create an environment conducive to wound healing, instead of contributing to the tissue damage (Wang *et al.*, 2021). This is underscored by the large and diverse series of studies, that have recently been published, on new methods to improve the biocompatibility and performance of suture materials (Czapka *et al.*, 2021; Deng *et al.*, 2021; Hu *et al.*, 2020; Hui *et al.*, 2020; Lee *et al.*, 2021; Link *et al.*, 2019; Richard & Verma, 2021; Syukri *et al.*, 2021; Zhou *et al.*, 2021). Yet most of these studies are focussed on the improvement of current, synthetic suture materials and only a select few have looked at the exclusive use of natural polymers to develop novel biosuture materials. This theme is, however, enjoying increasing attention together with the idea of employing sutures for localized delivery of bioactive moieties such as drugs, cells, and growth factors (Hakim *et al.*, 2020; Parikh *et al.*, 2021).

The ultimate goal of this research was to develop a new 3D monofilament biosuture material, with expert safety and biocompatibility as well as mechanical properties that meet the USP requirements and render it suitable for clinical use. An additional aim was to transform the newly developed biosuture into a localized drug delivery device that can help prevent common complications, such as ischemic reperfusion injury (IRI) and no-reflow, during microvascular surgery (MVS).

After a thorough review of the literature, several natural polymers, that showed potential for biosuture material development, were identified and investigated. Different methods of biosuture fabrication, such as extrusion by hand, 3D printing and extrusion with the Texture Analyser (*TA.XT plus*), were also explored. Additionally, in the process of optimizing the biosuture formulation, the influence of various formulation components and fabrication parameters on the mechanical properties of the biosuture was evaluated. The optimized biosuture formulation consisted of alginate (6% w/v), pectin (0.1% w/v), gelatin (3% w/v) and glycerol (4% v/v) and concluded the achievement of objective 1, as described in Chapter 1. Extrusion of the biopolymer solution into a crosslinker bath of BaCl₂ (2% w/v), using the Texture Analyser (*TA.XT Plus*) and a universal syringe rig, was selected as the most suitable method for biosuture fabrication, and speaks to objective 2 of the study. Different methods of drug loading were investigated, i.e., direct addition of the drug to the biopolymer solution, immersion of the biosuture in a drug-saline solution and coating of the biosuture with different lipid-drug layers. The drug loading methods were evaluated in terms of loading capacity, drug

release profile and their influence on the degradation and mechanical properties of the biosutures. Coating of the biosutures with a lipid-drug layer, that consists of soy phosphatidyl choline and dexamethasone in a 40:60 ratio, was selected as the best method of drug loading within the context of preventing IRI and no-reflow in MVS and represents the achievement of objective 3.

Appropriate physicochemical and physicomachanical analysis of the newly developed biosuture was performed, as proposed by objectives 4 and 5, and underscored the mechanisms that underline the fabrication and functioning of the biomaterial. Critical processes, such as effective crosslinking and coating of the biosutures, were confirmed and the mechanical properties reaffirmed to meet the minimum requirements set out by the USP. Detailed *in vitro* analysis revealed favourable swelling, degradation and drug release behaviour, and highlighted the appropriateness of the newly developed biosuture for clinical use. In line with objectives 6 and 7, the biocompatibility and hemocompatibility of the biosutures were established through extensive evaluation of the cytotoxic, haemolytic and platelet activating properties of the biosutures. The results indicated that the newly developed biosutures support and encourage cell attachment, migration and proliferation and suggests that they could potentially improve wound healing *in vivo*. Furthermore, the biosutures caused in near 0% haemolysis and very limited platelet activation, which again suggests that the biosutures will display excellent safety, if future *in vivo* or clinical evaluations are undertaken.

7.2 Recommendations and future prospects

The results of this research, indicate the immense potential of the newly developed biosuture to function as a safe and effective drug-eluting biosuture. Although it is not a defined objective of the research, further *in vivo* characterization of the biosuture is advised. *In vitro* studies of the degradation and drug release behaviour of the biosutures under simulated conditions, provide valuable information and a good indication of how the biosuture might behave in the body, but cannot wholly simulate *in vivo* conditions or the *in vivo* performance of the biosuture (Bernard *et al.*, 2018). Hence, *in vivo* studies are imperative to accurately define the pharmacokinetic parameters and to establish a correlation between the *in vitro* and *in vivo* results. Moreover, *in vivo* animal testing and histological analysis must be performed to corroborate the *in vitro* biocompatibility and safety of the biosutures before further steps can be taken towards clinical trials or commercialization of the product. A Sprague-dawley rat model with ligation of the femoral artery is a suitable method to evaluate the ability of the biosuture to prevent IRI and no-reflow and is recommended (Pruthi *et al.*, 2021). It might also be valuable to evaluate the influence of the biosuture on the rate of wound healing, wound strength, and scar formation, compared to commercial synthetic sutures.

The newly developed biosuture provides an innovative way of preventing deleterious complications during surgical procedures. The benefits of employing suture materials as drug delivery devices are profuse and deep-seated, as was aptly discussed in this study. Dexamethasone, the model anti-inflammatory drug that was used in this study, can be beneficial in several surgical settings, over and above MVS, including allografts and organ transplants where immunosuppressants can help lower the risk of rejection. The biosuture and lipid-drug coating are also highly adaptable, and dexamethasone can easily be replaced by another drug with a similar solubility profile, and the properties of the biosuture, such as diameter and strength, adapted to fit the requirements of the specific clinical setting. Moreover, Chapter 4 provides several drug loading methods, for both hydrophilic and hydrophobic drugs, that can be employed to obtain different drug release profiles. For example, if slow, sustained drug release over a period of 4 – 5 weeks is required, the drug can be incorporated into the biopolymer matrix for continued release as the biosuture erodes and degrades. Alternatively, drug loading method B, where the biosutures are immersed in a drug-saline solution, can be employed if rapid burst release is required, e.g., for the immediate prevention of infection and eradication of microbes. The lipid-drug coating can also be experimented with and different lipids evaluated to obtain a drug-release profile that suits a specific situation expertly. Therefore, the biosuture described in this study, can in future be used to develop wide range of specialized biosutures, each with a singular or more focused field of application, as was suggested in Chapter 2.

Although the newly developed biosuture requires further evaluation and pruning, this research undoubtably provides a valuable contribution to field of biomaterial sciences and drug delivery and could potentially pioneer the way for the development of more bioabsorbable, drug-eluting, natural polymer-based biosutures with more focussed fields of application.

REFERENCES

- Abbasnezhad, N., Kebdani, M., Shirinbayan, M., Champmartin, S., Tcharkhtchi, A., ... Bakir, F. 2021. Development of a model based on physical mechanisms for the explanation of drug release: Application to diclofenac release from polyurethane films. *Polymers*. 13(8).
- Abhari, R.E., Martins, J.A., Morris, H.L., Mouthuy, P.A. & Carr, A. 2017. Synthetic sutures: Clinical evaluation and future developments. *Journal of Biomaterials Applications*. 32(3):410–421.
- Açan E, Hapa O, B.F. 2018. Mechanical properties of suture materials. *Knots in Orthopedic Surgery*. Springer. 21–31.
- Ajaz, N., Khalid, I., Minhas, M.U., Barkat, K., Khan, I.U., ... Aslam, F. 2020. Pectin-based hydrogels with adjustable properties for controlled delivery of nifedipine: development and optimization. *Polymer Bulletin*. 77(11):6063–6083.
- Ajmeri, J.R. & Ajmeri, C.J. 2006. *Surgical sutures: the largest textile implant material. Medical Textiles and Biomaterials for Healthcare*. Woodhead Publishing Limited.
- Akgun, U., Karahan, M., Randelli, P.S. & Espregueira-Mendes, J. 2018. Knots in orthopedic surgery: Open and arthroscopic techniques. *Knots in Orthopedic Surgery: Open and Arthroscopic Techniques*. 1–193.
- Al-Mubarak, L. & Al-Haddab, M. 2013. Cutaneous wound closure materials: An overview and update. *Journal of Cutaneous and Aesthetic Surgery*. 6(4):178.
- Al-Saidi, G., Rahman, M.S., Al-Alawi, A. & Guizani, N. 2011. Thermal characteristics of gelatin extracted from shaari fish skin Effects of extraction conditions. *Journal of Thermal Analysis and Calorimetry*. 104(2):593–603.
- Al-Saidi, G.S., Al-Alawi, A., Rahman, M.S. & Guizani, N. 2012. Fourier transform infrared (FTIR) spectroscopic study of extracted gelatin from shaari (*Lithrinus microdon*) skin: Effects of extraction conditions. *International Food Research Journal*. 19(3):1167–1173.
- Alamgir, A.N.M. 2017. Fibers, surgical dressings, and bandages of natural origin. *Therapeutic Use of Medicinal Plants and Their Extracts*. 1:295–353.
- Alfieri S, Di DM, Menghi R, Quero G, Cina C, Pericoli MR, D.G. 2011. Role of oxidized regenerated cellulose in preventing infections at the surgical site: prospective, randomized study in 98 patients affected by a dirty wound. *Minerva chirurgica*. 66(1):55–62.
- Alizadeh Sardroud, H., Nemati, S., Baradar Khoshfetrat, A., Nabavinia, M. & Beygi Khosrowshahi, Y. 2017. Barium-cross-linked alginate-gelatine microcapsule as a potential platform for stem cell production and modular tissue formation. *Journal of Microencapsulation*. 34(5):488–497.
- Alloin, F., D'Aprèa, A., Dufresne, A., Kissi, N. El & Bossard, F. 2011. Poly(oxyethylene) and ramie whiskers based nanocomposites: Influence of processing: Extrusion and casting/evaporation. *Cellulose*. 18(4):957–973.
- Almeida, P., Silva Lannes, S., Calarge, F., Brito Farias, T. & Santana, J.C.. 2012. FTIR characterization of gelatin from chicken feet. *J. Chem. Chem Eng*. 6(February 2018):1029–1032.
- Alsarhan, M., Alnofaie, H., Ateeq, R. & Almahdy, A. 2018. The effect of chlorhexidine and listerine® mouthwashes on the tensile strength of selected absorbable sutures: An in vitro study. *BioMed Research International*. 2018.
- Alshomer, F., Madhavan, A., Pathan, O. and Song, W. 2017. Bioactive sutures: a review of advances in surgical suture functionalisation. *Current medicinal chemistry*. 24(2):215–223.
- Altomare, L., Bonetti, L., Campiglio, C.E., De Nardo, L., Draghi, L., ... Farè, S. 2018. Biopolymer-based strategies in the design of smart medical devices and artificial organs. *International Journal of Artificial Organs*. 41(6):337–359.
- Amani, H., Arzaghi, H., Bayandori, M., Dezfuli, A.S., Pazoki-Toroudi, H., ... Moradi, L. 2019. Controlling cell behavior through the design of biomaterial surfaces: A focus on surface

- modification techniques. *Advanced Materials Interfaces*. 6(13):1–30.
- Annan, N.T., Borza, A.D. & Hansen, L.T. 2008. Encapsulation in alginate-coated gelatin microspheres improves survival of the probiotic *Bifidobacterium adolescentis* 15703T during exposure to simulated gastro-intestinal conditions. *Food Research International*. 41(2):184–193.
- Apte, G., Lindenbauer, A., Schemberg, J., Rothe, H. & Nguyen, T.H. 2021. Controlling surface-induced platelet activation by agarose and gelatin-based hydrogel films. *ACS Omega*. 6(16):10963–10974.
- Aramwit, P., Jaichawa, N., Ratanavaraporn, J. & Srichana, T. 2015. A comparative study of type A and type B gelatin nanoparticles as the controlled release carriers for different model compounds. *Materials Express*. 5(3):241–248.
- Arango, M.C., Montoya, Y., Peresin, M.S., Bustamante, J. & Álvarez-López, C. 2021. Silk sericin as a biomaterial for tissue engineering: a review. *International Journal of Polymeric Materials and Polymeric Biomaterials*. 70(16):1115–1129.
- Arora, A., Aggarwal, G., Chander, J., Maman, P. & Nagpal, M. 2019. Drug eluting sutures: A recent update. *Journal of Applied Pharmaceutical Science*. 9(7):111–123.
- Asghari, F., Samiei, M., Adibkia, K., Akbarzadeh, A. & Davaran, S. 2017. Biodegradable and biocompatible polymers for tissue engineering application: a review. *Artificial Cells, Nanomedicine and Biotechnology*. 45(2):185–192.
- Askar, I. & Bozkurt, M. 2002. Protective effects of immunosuppressants and steroids against ischemia-reperfusion injury in cremaster muscle flap at microcirculatory level. *Microsurgery*. 22(8):361–366.
- Askari, M., Fisher, C., Weniger, F.G., Bidic, S. & Lee, W.P.A. 2006. Anticoagulation therapy in microsurgery: A review. *Journal of Hand Surgery*. 31(5):836–846.
- Asnani, G.P. & Kokare, C.R. 2018. In vitro and in vivo evaluation of colon cancer targeted epichlorohydrin crosslinked Portulaca-alginate beads. *Biomolecular Concepts*. 9(1):190–199.
- Assifaoui, A., Loupiac, C., Chambin, O. & Cayot, P. 2010. Structure of calcium and zinc pectinate films investigated by FTIR spectroscopy. *Carbohydrate Research*. 345(7):929–933.
- Audebrand, M., Kolb, M. & Axelos, M.A.V. 2006. Combined rheological and ultrasonic study of alginate and pectin gels near the sol-gel transition. *Biomacromolecules*. 7(10):2811–2817.
- Auriemma, G., Cerciello, A., Aquino, R.P., Del Gaudio, P., Fusco, B.M. & Russo, P. 2020. Pectin and zinc alginate: The right inner/outer polymer combination for core-shell drug delivery systems. *Pharmaceutics*. 12(2).
- Avoine, X., Lussier, B., Brailovski, V., Inaekyan, K. & Beauchamp, G. 2016. Evaluation of the effect of 4 types of knots on the mechanical properties of 4 types of suture material used in small animal practice. *Canadian Journal of Veterinary Research*. 80(2):162–170.
- Awasthi, R., Kulkarni, G.T., Ramana, M.V., de Jesus Andreoli Pinto, T., Kikuchi, I.S., ... Dua, K. 2017. Dual crosslinked pectin–alginate network as sustained release hydrophilic matrix for repaglinide. *International Journal of Biological Macromolecules*. 97:721–732.
- Azeredo, H.M.C. & Waldron, K.W. 2016. Crosslinking in polysaccharide and protein films and coatings for food contact - A review. *Trends in Food Science and Technology*. 52:109–122.
- Azhahia Manavalan, R. & Mukhopadhyay, A. 2008. Surgical sutures: Performance, development and use. *Journal of Biomimetics, Biomaterials, and Tissue Engineering*. 1:1–36.
- Azucena Castro-Yobal, M., Contreras-Oliva, A., Saucedo-Rivalcoba, V., Rivera-Armenta, J.L., Hernández-Ramírez, G., ... Herrera-Corredor, A. 2021. Evaluation of physicochemical properties of film-based alginate for food packing applications. *E-Polymers*. 21(1):82–95.
- Bacakova, L., Pajorova, J., Bacakova, M., Skogberg, A., Kallio, P., ... Svorcik, V. 2019. Versatile application of nanocellulose: From industry to skin tissue engineering and

- wound healing. *Nanomaterials*. 9(2).
- Badita, C.R., Aranghel, D., Burducea, C. & Mereuta, P. 2020. Characterization of sodium alginate based films. *Romanian Journal of Physics*. 65(1–2):1–8.
- Badwan, A.A., Rashid, I., Al Omari, M.M.H. & Darras, F.H. 2015. Chitin and chitosan as direct compression excipients in pharmaceutical applications. *Marine Drugs*. 13(3):1519–1547.
- Bagheri, F., Radi, M. & Amiri, S. 2019. Drying conditions highly influence the characteristics of glycerol-plasticized alginate films. *Food Hydrocolloids*. 90(November 2018):162–171.
- Bajpai, S.K. & Sharma, S. 2004. Investigation of swelling/degradation behaviour of alginate beads crosslinked with Ca²⁺ and Ba²⁺ ions. *Reactive and Functional Polymers*. 59(2):129–140.
- Balani, K., Verma, V., Agarwal, A. & Narayan, R. 2015. Physical, thermal, and mechanical properties of polymers. *Biosurfaces*. 329–344.
- Barbut, S. & Harper, A. 2020. Influence of relative humidity on dried Ca⁺⁺-alginate films and composites made with soy and pectin. *Italian Journal of Food Science*. 32(1):195–208.
- Barrows TH. 2017. Synthetic bioabsorbable polymers. In: 1st ed. *High performance biomaterials*. Routledge. pp. 243–254.
- Baum, A., Dominiak, M., Vidal-Melgosa, S., Willats, W.G.T., Søndergaard, K.M., ... Mikkelsen, J.D. 2017. Prediction of pectin yield and quality by FTIR and carbohydrate microarray analysis. *Food and Bioprocess Technology*. 10(1):143–154.
- Baybekov, I., Kartashev, V. & Ibadov, B. 2018. Features of surgical suture material. *Economic and Social Development: Book of Proceedings*. (October):926–929.
- Baygar, T., Sarac, N., Ugur, A. & Karaca, I.R. 2019. Antimicrobial characteristics and biocompatibility of the surgical sutures coated with biosynthesized silver nanoparticles. *Bioorganic Chemistry*. 86(November 2018):254–258.
- Bekhit, M., Sánchez-González, L., Ben Messaoud, G. & Desobry, S. 2016. Encapsulation of *Lactococcus lactis* subsp. *lactis* on alginate/pectin composite microbeads: Effect of matrix composition on bacterial survival and nisin release. *Journal of Food Engineering*. 180:1–9.
- Bello, A.B., Kim, D., Kim, D., Park, H. & Lee, S.H. 2020. Engineering and functionalization of gelatin biomaterials: From cell culture to medical applications. *Tissue Engineering - Part B: Reviews*. 26(2):164–180.
- Ben Amar Cheba. 2011. Chitin and chitosan: Marine biopolymers with unique properties and versatile applications. *Global Journal of Biotechnology & Biochemistry*, 6(3), pp.149–153.
- Benesch, J. & Tengvall, P. 2002. Blood protein adsorption onto chitosan. *Biomaterials*. 23(12):2561–2568.
- Benlier, E., Top, H., Aygit, A.C., Usta, U. & Unal, Y. 2007. Microvascular anastomosis with minimal suture and arista: An experimental study. *Journal of Reconstructive Microsurgery*. 23(6):311–315.
- Beppu, M.M., Vieira, R.S., Aimoli, C.G. & Santana, C.C. 2007. Crosslinking of chitosan membranes using glutaraldehyde: Effect on ion permeability and water absorption. *Journal of Membrane Science*. 301(1–2):126–130.
- Bernard, M., Jubeli, E., Pungente, M.D. & Yagoubi, N. 2018. Biocompatibility of polymer-based biomaterials and medical devices-regulations,: In vitro screening and risk-management. *Biomaterials Science*. 6(8):2025–2053.
- Bhavsar, D., Patel, V. & Sawant, K. 2019. Systemic investigation of in vitro and in vivo safety, toxicity and degradation of mesoporous silica nanoparticles synthesized using commercial sodium silicate. *Microporous and Mesoporous Materials*. 284(January):343–352.
- Bier, J.M., Verbeek, C.J.R. & Lay, M.C. 2013. Using synchrotron FTIR spectroscopy to determine secondary structure changes and distribution in thermoplastic protein. *Journal of Applied Polymer Science*. 130(1):359–369.
- Bierhalz, A.C.K., Da Silva, M.A. & Kieckbusch, T.G. 2012. Natamycin release from alginate/pectin films for food packaging applications. *Journal of Food Engineering*.

- 110(1):18–25.
- Bissett, D.L. 2006. Glucosamine: An ingredient with skin and other benefits. *Journal of Cosmetic Dermatology*. 5(4):309–315.
- Blanchaert., R.. 2012. Principles of microvascular surgery. In: *Current Therapy In Oral and Maxillofacial Surgery 2*. pp. (pp. 63-67).
- Bloom, B.S. & Goldberg, D.J. 2007. Suture material in cosmetic cutaneous surgery. *Journal of Cosmetic and Laser Therapy*. 9(1):41–45.
- Bombaldi de Souza, F.C., Bombaldi de Souza, R.F., Drouin, B., Popat, K.C., Mantovani, D. & Moraes, Â.M. 2019. Polysaccharide-based tissue-engineered vascular patches. *Materials Science and Engineering C*. 104(March):109973.
- Bortolini, C., Jones, N.C., Hoffmann, S. V., Wang, C., Besenbacher, F. & Dong, M. 2015. Mechanical properties of amyloid-like fibrils defined by secondary structures. *Nanoscale*. 7(17):7745–7752.
- Bouleti, C., Newton, N. & Germain, S. 2015. The no-reflow phenomenon: State of the art. *Archives of Cardiovascular Diseases*. 108(12):661–674.
- Braune, S., Latour, R.A., Reinthaler, M., Landmesser, U., Lendlein, A. & Jung, F. 2019. In vitro thrombogenicity testing of biomaterials. *Advanced Healthcare Materials*. 8(21).
- Breitbart, G.B., Dillon, P.K., Suval, W.D., Padberg, F.T., FitzPatrick, M. & Durán, W.N. 1989. Dexamethasone attenuates microvascular ischemia-reperfusion injury in the rat cremaster muscle. *Microvascular Research*. 38(2):155–163.
- Brigham, C.J. 2017. Chitin and chitosan: sustainable, medically relevant biomaterials. *International Journal of Biotechnology for Wellness Industries*. 6(2):41–47.
- Brinsko, K.M. 2010. Optical characterization of some modern “eco-friendly” fibres. *Journal of Forensic Sciences*. 55(4):915–923.
- Brodusch, N., Demers, H. and Gauvin, R. 2017. Field emission scanning electron microscopy: New perspectives for materials characterization. Springer.
- Brooks, C.C., Jabbehdari, S. & Gupta, P.K. 2020. Dexamethasone 0.4mg sustained-release intracanalicular insert in the management of ocular inflammation and pain following ophthalmic surgery: Design, development and place in therapy. *Clinical Ophthalmology*. 14:89–94.
- Brown, E., Suh, H.P., Han, H.H., Pak, C.J. & Hong, J.P. 2020. Best new flaps and tips for success in microsurgery. *Plastic and Reconstructive Surgery*. 796E-807E.
- Bt Ibrahim, S.F., Mohd Azam, N.A.N. & Amin, K.A.M. 2019. Sodium alginate film: The effect of crosslinker on physical and mechanical properties. *IOP Conference Series: Materials Science and Engineering*. 509(1).
- Burkhardt, R. and Lang, N.P. (in press). Influence of suturing on wound healing. *Periodontology 2000*. 68(1):pp.270-281.
- Byrne, M. & Aly, A. 2019. The surgical suture. *Aesthetic Surgery Journal*. 39:S67–S72.
- Cai, S. & Singh, B.R. 1999. Identification of β -turn and random coil amide III infrared bands for secondary structure estimation of proteins. *Biophysical Chemistry*. 80(1):7–20.
- Caiazzo, G., Musci, R.L., Frediani, L., Umińska, J., Wanha, W., ... Navarese, E.P. 2020. State of the art: No-reflow phenomenon. *Cardiology Clinics*. 38(4):563–573.
- Campbell, A.L., Patrick, D.A., Liabaud, B. & Geller, J.A. 2014. Superficial wound closure complications with barbed sutures following knee arthroplasty. *Journal of Arthroplasty*. 29(5):966–969.
- Carroll, W.R. & Esclamado, R.M. 2000. Ischemia/reperfusion injury in microvascular surgery. *Head and Neck*. 22(7):700–713.
- Carta, G., Murru, E., Banni, S. & Manca, C. 2017. Palmitic acid: Physiological role, metabolism and nutritional implications. *Frontiers in Physiology*. 8(NOV):1–14.
- Cassimjee, H., Kumar, P., Choonara, Y.E. & Pillay, V. 2020. Proteosaccharide combinations for tissue engineering applications. *Carbohydrate Polymers*. 235(November 2019):115932.
- Cebi, N., Durak, M.Z., Toker, O.S., Sagdic, O. & Arici, M. 2016. An evaluation of Fourier transforms infrared spectroscopy method for the classification and discrimination of bovine, porcine and fish gelatins. *Food Chemistry*. 190:1109–1115.

- Centeno-Cerdas, C., Jarquín-Cordero, M., Chávez, M.N., Hopfner, U., Holmes, C., ... Egaña, J.T. 2018. Development of photosynthetic sutures for the local delivery of oxygen and recombinant growth factors in wounds. *Acta Biomaterialia*. 81(September):184–194.
- Cernencu, A.I., Lungu, A., Stancu, I.C., Serafim, A., Heggset, E., ... Iovu, H. 2019. Bioinspired 3D printable pectin-nanocellulose ink formulations. *Carbohydrate Polymers*. 220(May):12–21.
- Chaharbaghi, E., Khodaiyan, F. & Hosseini, S.S. 2017. Optimization of pectin extraction from pistachio green hull as a new source. *Carbohydrate Polymers*. 173:107–113.
- Chaichi, M., Hashemi, M., Badii, F. & Mohammadi, A. 2017. Preparation and characterization of a novel bionanocomposite edible film based on pectin and crystalline nanocellulose. *Carbohydrate Polymers*. 157:167–175.
- Champeau, M., Thomassin, J.M., Tassaing, T. & Jérôme, C. 2017. Current manufacturing processes of drug-eluting sutures. *Expert Opinion on Drug Delivery*. 14(11):1293–1303.
- Chan, S.Y., Choo, W.S., Young, D.J. & Loh, X.J. 2017. Pectin as a rheology modifier: Origin, structure, commercial production and rheology. *Carbohydrate Polymers*. 161:118–139.
- Chandra, P.K., Soker, S. & Atala, A. 2020. Tissue engineering: current status and future perspectives. *Principles of Tissue Engineering*. INC.
- Chang, J.J., Lee, Y.H., Wu, M.H., Yang, M.C. & Chien, C.T. 2012. Preparation of electrospun alginate fibers with chitosan sheath. *Carbohydrate Polymers*. 87(3):2357–2361.
- Cheba, B.A., 2011. Chitin and chitosan: marine biopolymers with unique properties and versatile applications. *Global Journal of Biotechnology & Biochemistry*, 6(3), pp.149-153.
- Chen, C., Li, D., Yano, H. & Abe, K. 2019. Bioinspired hydrogels: Quinone crosslinking reaction for chitin nanofibers with enhanced mechanical strength via surface deacetylation. *Carbohydrate Polymers*. 207(December 2018):411–417.
- Chen, L.E., Silver, W.P., Seaber, A. V., Korompilias, A. V. & Urbaniak, J.R. 1996. Effects of dexamethasone on the contractile function of reperfused skeletal muscle. *Microsurgery*. 17(6):313–320.
- Chen, R., Liu, J., Yang, C., Weitz, D.A., He, H., ... Bai, H. 2019. Transparent impact-resistant composite films with bioinspired hierarchical structure. *ACS Applied Materials and Interfaces*. 11(26):23616–23622.
- Chen, S., Liu, B., Carlson, M.A., Gombart, A.F., Reilly, D.A. & Xie, J. 2017. Recent advances in electrospun nanofibers for wound healing. *Nanomedicine*. 12(11):1335–1352.
- Chen, X., Hou, D., Wang, L., Zhang, Q., Zou, J. & Sun, G. 2015. Antibacterial surgical silk sutures using a high-performance slow-release carrier coating system. *ACS Applied Materials and Interfaces*. 7(40):22394–22403.
- Chen, X., Wells, G. & Woods, D.M. 2001. Production of Yarns and Fabrics from Alginate Fibres for Medical Applications. *Medical Textiles*. The Bolton Institute.
- Chiaoprakobkij, N., Seetabhawang, S., Sanchavanakit, N. & Phisalaphong, M. 2019. Fabrication and characterization of novel bacterial cellulose/alginate/gelatin biocomposite film. *Journal of Biomaterials Science, Polymer Edition*. 30(11):961–982.
- Chu, C.C. 2018. Classification and general characteristics of suture materials. *Wound Closure Biomaterials and Devices*. CRC Press. 39–63.
- Chu CC. 2013. Biotextiles as medical implants: 10. Types and properties of surgical sutures. Elsevier Inc.
- Concepcion, K.R. & Zhang, L. 2018. Corticosteroids and perinatal hypoxic-ischemic brain injury. *Drug Discovery Today*. 23(10):1718–1732.
- Conn, J., Oyasu, R., Welsh, M. & Beal, J.M. 1974. Vicryl (polyglactin 910) synthetic absorbable sutures. *The American Journal of Surgery*. 128(1):19–23.
- Cooke, F.W., Lemons, J.E. and Ratner, B.D. 1996. Properties of materials. In: *Biomaterials science*. Academic Press. pp. 11–35.
- Coseri, S., Biliuta, G., Simionescu, B.C., Stana-Kleinschek, K., Ribitsch, V. & Harabagiu, V. 2013. Oxidized cellulose - Survey of the most recent achievements. *Carbohydrate*

- Polymers*. 93(1):207–215.
- Costa-Almeida, R., Domingues, R.M.A., Fallahi, A., Avci, H., Yazdi, I.K., ... Khademhosseini, A. 2018. Cell-laden composite suture threads for repairing damaged tendons. *Journal of Tissue Engineering and Regenerative Medicine*. 12(4):1039–1048.
- Costa, M.J., Marques, A.M., Pastrana, L.M., Teixeira, J.A., Sillankorva, S.M. & Cerqueira, M.A. 2018. Physicochemical properties of alginate-based films: Effect of ionic crosslinking and mannuronic and guluronic acid ratio. *Food Hydrocolloids*. 81:442–448.
- Costa Da Silva, M., Silva, H.N. Da, Holanda, S.A., Silva, A.R.O. & Fook, M.V.L. 2020. Biodegradable polymeric wires: monofilament and multifilament. *Materials Research Innovations*. 24(3):166–170.
- Cruz, R. de C.A.L., Diniz, L.G.M., Lisboa, H.M. & Fook, M.V.L. 2016. Effect of different carboxylic acids as solvent on chitosan fibers production by wet spinning. *Revista Materia*. 21(2):525–531.
- Cuadros, T.R., Skurtys, O. & Aguilera, J.M. 2012. Mechanical properties of calcium alginate fibers produced with a microfluidic device. *Carbohydrate Polymers*. 89(4):1198–1206.
- Czaja, W., Krystynowicz, A., Bielecki, S. & Brown, R.M. 2006. Microbial cellulose - The natural power to heal wounds. *Biomaterials*. 27(2):145–151.
- Czapka, T., Maliszewska, I. & Winkler, A. 2021. Decontamination of polymeric surgical sutures covered with bacterial biofilms using nonthermal plasma. *Plasma Chemistry and Plasma Processing*. 41(1):227–243.
- D'souza, A.A. & Shegokar, R. 2016. Polyethylene glycol (PEG): a versatile polymer for pharmaceutical applications. *Expert Opinion on Drug Delivery*. 13(9):1257–1275.
- Daemi, H. & Barikani, M. 2012. Synthesis and characterization of calcium alginate nanoparticles, sodium homopolymannuronate salt and its calcium nanoparticles. *Scientia Iranica*. 19(6):2023–2028.
- Das, M.K. and Senapati, P.C., 2008. Furosemide-loaded alginate microspheres prepared by ionic cross-linking technique: Morphology and release characteristics. *Indian journal of pharmaceutical sciences*, 70(1), p.77.
- Das, M.P., R., S.P., Prasad, K., Jv, V. & M, R. 2017. Extraction and characterization of gelatin: a functional biopolymer. *International Journal of Pharmacy and Pharmaceutical Sciences*. 9(9):239.
- Dash, S., Murthy, P.N., Nath, L. & Chowdhury, P. 2010. Kinetic modeling on drug release from controlled drug delivery systems. *Acta Poloniae Pharmaceutica - Drug Research*. 67(3):217–223.
- da Silva, M.A., Bierhalz, A.C.K. & Kieckbusch, T.G. 2012. Influence of drying conditions on physical properties of alginate films. *Drying Technology*. 30(1):72–79.
- da Silva, M.C., da Silva, H.N., Cruz, R. de C.A.L., Amoah, S.K.S., Silva, S.M. de L. & Fook, M.V.L. 2019. N-Acetyl-D-glucosamine-loaded chitosan filaments biodegradable and biocompatible for use as absorbable surgical suture materials. *Materials*. 12(11).
- Debbabi, F., Gargoubi, S., Hadj Ayed, M.A. & Abdessalem, S. Ben. 2017. Development and characterization of antibacterial braided polyamide suture coated with chitosan-citric acid biopolymer. *Journal of Biomaterials Applications*. 32(3):384–398.
- De Castro, D.O., Bras, J., Gandini, A. & Belgacem, N. 2016. Surface grafting of cellulose nanocrystals with natural antimicrobial rosin mixture using a green process. *Carbohydrate Polymers*. 137:1–8.
- Deepa, B., Abraham, E., Cordeiro, N., Faria, M., Primc, G., ... Pothan, L.A. 2020. Nanofibrils vs nanocrystals bio-nanocomposites based on sodium alginate matrix: An improved-performance study. *Heliyon*. 6(2).
- De Jong, W.H., Carraway, J.W. & Geertsma, R.E. 2019. In vivo and in vitro testing for the biological safety evaluation of biomaterials and medical devices. Second Edition. *Biocompatibility and Performance of Medical Devices*. Elsevier Ltd.
- de la Harpe, K.M., Kondiah, P.P., Marimuthu, T., Du Toit, L.C., Kumar, P., Choonara, Y.E. and Pillay, V. (in press). An advanced 3D monofilament biosuture. *South African Pharmaceutical Journal*. 87(1):pp.45-48.
- de la Harpe, K.M., Kondiah, P.P.D., Marimuthu, T. & Choonara, Y.E. 2021. Advances in

- carbohydrate-based polymers for the design of suture materials: A review. *Carbohydrate Polymers*. 261(February):117860.
- de Moraes, M.A. and Beppu, M.M., 2013. Biocomposite membranes of sodium alginate and silk fibroin fibers for biomedical applications. *Journal of Applied Polymer Science*, 130(5), pp.3451-3457.
- Deng, X., Qasim, M. & Ali, A. 2021. Engineering and polymeric composition of drug-eluting suture: A review. *Journal of Biomedical Materials Research - Part A*. (June 2020):1–17.
- Deng, X., Gould, M. & Ali, M.A. 2021. Fabrication and characterisation of melt-extruded chitosan/keratin/PCL/PEG drug-eluting sutures designed for wound healing. *Materials Science and Engineering C*. 120(October 2020):111696.
- Deng X, Qasim M, A.A. 2021. Engineering and polymeric composition of drug-eluting suture: A review. *Journal of Biomedical Materials Research Part A*.
- Dennis, C., Sethu, S., Nayak, S., Mohan, L., Morsi, Y. & Manivasagam, G. 2016. Suture materials - Current and emerging trends. *Journal of Biomedical Materials Research - Part A*. 104(6):1544–1559.
- Desjardins-Park, H.E., Foster, D.S. & Longaker, M.T. 2018. Fibroblasts and wound healing: An update. *Regenerative Medicine*. 13(5):491–495.
- Devick IF, H.D. 2021. Complications Associated with Sutures. *Complications in Equine Surgery*. 70–78.
- Distler, T., Kretschmar, L., Schneidereit, D., Girardo, S., Goswami, R., ... Budday, S. 2021. Mechanical properties of cell- And microgel bead-laden oxidized alginate-gelatin hydrogels. *Biomaterials Science*. 9(8):3051–3068.
- Dolan, R.W., Kerr, D.C. & Arena, S. 1995b. Improved reflow and viability in reperfused ischemic rat island groin flaps using dexamethasone. *Microsurgery*. 16(2):86–9.
- Domnick, E.D. 2014. Suture material and needle options in oral and periodontal surgery. *Journal of Veterinary Dentistry*. 31(3):204–211.
- Dong, Z., Wang, Q. & Du, Y. 2006. Alginate/gelatin blend films and their properties for drug controlled release. *Journal of Membrane Science*. 280(1–2):37–44.
- Doppalapudi, S., Katiyar, S. & Domb, A.J. 2015. *Advanced Polymers in Medicine. Advanced Polymers in Medicine*.
- Drescher, S. & van Hoogevest, P. 2020. The phospholipid research center: Current research in phospholipids and their use in drug delivery. *Pharmaceutics*. 12(12):1–36.
- Drive, I.L. 1993. Temperature on crystallinity , permeability and mechanical properties of Methylcellulose Films. 247–257.
- Duarah, R., Singh, Y.P., Gupta, P., Mandal, B.B. & Karak, N. 2018. Smart self-tightening surgical suture from a tough bio-based hyperbranched polyurethane/reduced carbon dot nanocomposite. *Biomedical Materials (Bristol)*. 13(4).
- Dungani R, Aditiawati P, Aprilia S, Yuniarti K, Karliati T, Suwandhi I, S.I. 2018. Biomaterial from oil palm waste: properties, characterization and applications. In: V. Waisundara, ed. *Palm Oil*. pp. 31–34.
- Eichhorn, S.J., Dufresne, A., Aranguren, M., Marcovich, N.E., Capadona, J.R., ... Peijs, T. 2010. Review: Current international research into cellulose nanofibres and nanocomposites. Vol. 45. *Journal of Materials Science*.
- Escorihuela, J., Marcelis, A.T.M. & Zuilhof, H. 2015. Metal-free click chemistry reactions on surfaces. *Advanced Materials Interfaces*. 2(13):1–42.
- Fadnavis, N.W., Sheelu, G., Kumar, B.M., Bhalerao, M.U. & Deshpande, A.A. 2003. Gelatin blends with alginate: Gels for lipase immobilization and purification. *Biotechnology Progress*. 19(2):557–564.
- Fahma, F., Iwamoto, S., Hori, N., Iwata, T. & Takemura, A. 2010. Isolation, preparation, and characterization of nanofibers from oil palm empty-fruit-bunch (OPEFB). *Cellulose*. 17(5):977–985.
- Fan, L., Du, Y., Huang, R., Wang, Q., Wang, X. & Zhang, L. 2005. Preparation and characterization of alginate/gelatin blend fibers. *Journal of Applied Polymer Science*. 96(5):1625–1629.
- Fan, S., Chen, K., Yuan, W., Zhang, D., Yang, S., ... Zhang, Y. 2020. Biomaterial-based

- scaffolds as antibacterial suture materials. *ACS Biomaterials Science and Engineering*. 6(5):3154–3161.
- Fan M, Dai D, H.B. 2012. Fourier transform infrared spectroscopy for natural fibres. In: *Fourier transform-materials analysis*. pp. 3:45-68.
- Fang, Y., Al-Assaf, S., Phillips, G.O., Nishinari, K., Funami, T. & Williams, P.A. 2008. Binding behavior of calcium to polyuronates: Comparison of pectin with alginate. *Carbohydrate Polymers*. 72(2):334–341.
- Farris, S., Schaich, K.M., Liu, L.S., Cooke, P.H., Piergiovanni, L. & Yam, K.L. 2011. Gelatin-pectin composite films from polyion-complex hydrogels. *Food Hydrocolloids*. 25(1):61–70.
- Fenoradosoa, T.A., Ali, G., Delattre, C., Laroche, C., Petit, E., ... Michaud, P. 2010. Extraction and characterization of an alginate from the brown seaweed *Sargassum turbinarioides* Grunow. *Journal of Applied Phycology*. 22(2):131–137.
- Filippov, M.P., Shkolenko, G. a & Kohn, R. 1978. Determination of esterification degree of pectin of different origin and composition by method of infrared spectroscopy. *Chemicke Zvesti*. 32(2):218–222.
- Firkowska-Boden, I., Jandt, K.D., Helbing, C., Dauben, T.J. & Pieper, M. 2020. How nanotopography-induced conformational changes of fibrinogen affect platelet adhesion and activation. *Langmuir*. 36(39):11573–11580.
- Flynn, C.N., Byrne, C.P. & Meenan, B.J. 2013. Surface modification of cellulose via atmospheric pressure plasma processing in air and ammonia-nitrogen gas. *Surface and Coatings Technology*. 233:108–118.
- Fracasso, A.F., Perussello, C.A., Carpiné, D., Petkowicz, C.L. de O. & Haminiuk, C.W.I. 2018. Chemical modification of citrus pectin: Structural, physical and rheological implications. *International Journal of Biological Macromolecules*. 109:784–792.
- Fu, S., Thacker, A., Sperger, D.M., Boni, R.L., Buckner, I.S., ... Block, L.H. 2011. Relevance of rheological properties of sodium alginate in solution to calcium alginate gel properties. *AAPS PharmSciTech*. 12(2):453–460.
- Fundeanu, G., Nastruzzi, C., Carpov, A., Desbrieres, J. & Rinaudo, M. 1999. Physico-chemical characterization of Ca-alginate microparticles produced with different methods. *Biomaterials*. 20(15):1427–1435.
- Gabrielli, F., Potenza, C., Puddu, P., Sera, F., Masini, C. and Abeni, D. 2001. Suture materials and other factors associated with tissue reactivity, infection, and wound dehiscence among plastic surgery outpatients. *Plastic and reconstructive surgery*. 107(1):38-45.
- Galus, S. & Lenart, A. 2013. Development and characterization of composite edible films based on sodium alginate and pectin. *Journal of Food Engineering*. 115(4):459–465.
- Gao, C., Pollet, E. & Avérous, L. 2017. Properties of glycerol-plasticized alginate films obtained by thermo-mechanical mixing. *Food Hydrocolloids*. 63:414–420.
- Garavand, F., Rouhi, M., Razavi, S.H., Cacciotti, I. & Mohammadi, R. 2017. Improving the integrity of natural biopolymer films used in food packaging by crosslinking approach: A review. *International Journal of Biological Macromolecules*. 104:687–707.
- Gartti-Jardim, E.C., de Souza, A.P., de Souza Carvalho, A.C.G., Pereira, C.C.S., Okamoto, R. & Filho, O.M. 2013. Comparative study of the healing process when using Vicryl®, Vicryl Rapid®, Vicryl Plus®, and Monocryl® sutures in the rat dermal tissue. *Oral and Maxillofacial Surgery*. 17(4):293–298.
- Gatenholm, P., BC GENESIS LLC. 2013. *Patent No. U.S. Patent Application 13/983,709*.
- Gatenholm, P. & Klemm, D. 2010. Bacterial nanocellulose as a renewable material for biomedical applications. *MRS Bulletin*. 35(3):208–213.
- Gazivoda, D., Pelemiš, D., Vujašković, G. & Djurdjević, S. 2015. Influence of suturing material on wound healing – An experimental study on dogs. *Vojnosanitetski Pregled*. 72(5):397–404.
- Gazivoda, D., Pelemiš, D. & Vujašković, G. 2015. A clinical study on the influence of suturing material on oral wound healing. *Vojnosanitetski Pregled*. 72(9):765–769.
- Geiger, D., Debus, E.S., Ziegler, U.E., Larena-Avellaneda, A., Frosch, M., ... Dietz, U.A.

2005. Capillary activity of surgical sutures and suture-dependent bacterial transport: A qualitative study. *Surgical Infections*. 6(4):377–383.
- Ghorbani, M., Roshangar, L. & Soleimani Rad, J. 2020. Development of reinforced chitosan/pectin scaffold by using the cellulose nanocrystals as nanofillers: An injectable hydrogel for tissue engineering. *European Polymer Journal*. 130(February):109697.
- Giammalva, G.R., Maugeri, R., Graziano, F., Guli, C., Giugno, A., ... Iacopino, D.G. 2017. White cord syndrome after non-contiguous double-level anterior cervical decompression and fusion (ACDF): A “no reflow phenomenon”? *Interdisciplinary Neurosurgery: Advanced Techniques and Case Management*. 7:47–49.
- Gierek, M., Kuśnierz, K., Lampe, P., Ochała, G., Kurek, J., ... Majewski, J. 2018. Absorbable sutures in general surgery - Review, available materials, and optimum choices. *Polski Przegląd Chirurgiczny/ Polish Journal of Surgery*. 90(2):34–37.
- Giri, T.K., Thakur, D., Alexander, A., Ajazuddin, A., Badwaik, H., ... Tripathi, D.K. 2013. Biodegradable IPN hydrogel beads of pectin and grafted alginate for controlled delivery of diclofenac sodium. *Journal of Materials Science: Materials in Medicine*. 24(5):1179–1190.
- Giz, A.S., Berberoglu, M., Bener, S., Aydelik-Ayazoglu, S., Bayraktar, H., ... Catalgil-Giz, H. 2020. A detailed investigation of the effect of calcium crosslinking and glycerol plasticizing on the physical properties of alginate films. *International Journal of Biological Macromolecules*. 148:49–55.
- Gnanasambandam, R., Proctor, A. 2000. Determination of pectin degree of esterification by diffuse reflectance. *Food Chemistry*. 68:327–332.
- Goel, A. 2016. Surgical Sutures - A Review. *Delhi Journal of Ophthalmology*. 26(3):159–162.
- Gohil, R.M. (in press). Synergistic blends of natural polymers, pectin and sodium alginate. *Journal of Applied Polymer Science*. 120(4):pp.2324-2336.
- Gong, T., Tan, T., Zhang, P., Li, H., Deng, C., Huang, Y., Gong, T. and Zhang, Z. (in press). Palmitic acid-modified bovine serum albumin nanoparticles target scavenger receptor-A on activated macrophages to treat rheumatoid arthritis. *Biomaterials*. 258:p.120296.
- Goodman, S.L. 1999. Sheep, pig, and human platelet-material interactions with model cardiovascular biomaterials. *Journal of Biomedical Materials Research*. 45(3):240–250.
- Gopinathan, J. & Noh, I. 2018. Recent trends in bioinks for 3D printing. *Biomaterials Research*. 1–15.
- Grant, G.T., Morris, E.R., Rees, D.A., Smith, P.J. and Thom, D. 1973. Biological interactions between polysaccharides and divalent cations: the egg-box model. *FEBS letters*. 32(1):195–198.
- Greenberg, J.A. & Clark, R.M. 2009. Advances in suture material for obstetric and gynecologic surgery. *Reviews in obstetrics & gynecology*. 2(3):146–58.
- Gu, S.Y., Wu, Q.L., Ren, J. & Vancso, G.J. 2005. Mechanical properties of a single electrospun fiber and its structures. *Macromolecular Rapid Communications*. 26(9):716–720.
- Guambo, M.P.R., Spencer, L., Vispo, N.S., Vizquete, K., Debut, A., ... Alexis, F. 2020. Natural cellulose fibers for surgical suture applications. *Polymers*. 12(12):1–20.
- Guerrero, P., Retegi, A., Gabilondo, N. & De La Caba, K. 2010. Mechanical and thermal properties of soy protein films processed by casting and compression. *Journal of Food Engineering*. 100(1):145–151.
- Guo, H., Cao, R.H., Zheng, Y.F., Bai, J., Xue, F. & Chu, C.L. 2019. Diameter-dependent in vitro performance of biodegradable pure zinc wires for suture application. *Journal of Materials Science and Technology*. 35(8):1662–1670.
- Gupta, K.C. & Ravi Kumar, M.N.V. 2000. Overview on chitin and chitosan applications with an emphasis on controlled drug release formulations. *Journal of Macromolecular Science - Reviews in Macromolecular Chemistry and Physics*. 40.
- Guyette, J.P., Fakhrazadeh, M., Burford, E.J., Tao, Z.W., Pins, G.D., ... Gaudette, G.R. 2013. A novel suture-based method for efficient transplantation of stem cells. *Journal of Biomedical Materials Research - Part A*. 101 A(3):809–818.
- Hadlock, T. & Varvares, M. 2002. Microvascular and microneural surgery new horizons in

- facial plastic and reconstructive surgery. *Facial Plastic Surgery Clinics*. 10(2):167–174.
- Hakim, M.L., Nahar, N., Saha, M., Islam, M.S., Reza, H.M. & Sharker, S.M. 2020. Local drug delivery from surgical thread for area-specific anesthesia. *Biomedical Physics and Engineering Express*. 6(1).
- Hakkarainen, T., Koivuniemi, R., Kosonen, M., Escobedo-Lucea, C., Sanz-Garcia, A., ... Kavola, H. 2016. Nanofibrillar cellulose wound dressing in skin graft donor site treatment. *Journal of Controlled Release*. 244:292–301.
- Halepas, S., Chen, X.J. & Ferneini, E.M. 2020. Thread-Lift Sutures: Anatomy, Technique, and Review of Current Literature. *Journal of Oral and Maxillofacial Surgery*. 78(5):813–820.
- Halib, N., Perrone, F., Cemazar, M., Dapas, B., Farra, R., ... Grassi, M. 2017. Potential applications of nanocellulose-containing materials in the biomedical field. *Materials*. 10(8):1–31.
- Harris JJ, Serafica G, Damien CJ, Nonnenmann HR, Xylos Corp, A. 2010.
- Hasnain MS, Nayak AK, Kurakula M, H.M. 2020. Alginate nanoparticles in drug delivery. *Alginates in Drug Delivery*. 129–152.
- Hassan, M.E., Bai, J. & Dou, D.Q. 2019. Biopolymers; Definition, classification and applications. *Egyptian Journal of Chemistry*. 62(9):1725–1737.
- Hastuti, N., Kanomata, K. & Kitaoka, T. 2018. Hydrochloric acid hydrolysis of pulps from oil palm empty fruit bunches to produce cellulose nanocrystals. *Journal of Polymers and the Environment*. 26(9):3698–3709.
- Haug AR, S.O. 1965. The effect of divalent metals on the properties of alginate solutions. *Acta chem. scand*. 19(2):341–51.
- He, W., Ma, Z.W., Yong, T., Teo, W.E. & Ramakrishna, S. 2005. Fabrication of collagen-coated biodegradable polymer nanofiber mesh and its potential for endothelial cells growth. *Biomaterials*. 26(36):7606–7615.
- He, Y., Zhang, N., Gong, Q., Qiu, H., Wang, W., ... Gao, J. 2012. Alginate/graphene oxide fibers with enhanced mechanical strength prepared by wet spinning. *Carbohydrate Polymers*. 88(3):1100–1108.
- Henkelman, S., Rakhorst, G., Blanton, J. & van Oeveren, W. 2009. Standardization of incubation conditions for hemolysis testing of biomaterials. *Materials Science and Engineering C*. 29(5):1650–1654.
- Hermes, H., 1991. Nilpotent and high-order approximations of vector field systems. *SIAM review*, 33(2), pp.238-264.
- Homez-Jara, A., Daza, L.D., Aguirre, D.M., Muñoz, J.A., Solanilla, J.F. & Vázquez, H.A. 2018. Characterization of chitosan edible films obtained with various polymer concentrations and drying temperatures. *International Journal of Biological Macromolecules*. 113:1233–1240.
- Hong, S.H., Kim, S., Park, J.P., Shin, M., Kim, K., ... Lee, H. 2018. Dynamic bonds between boronic acid and alginate: hydrogels with stretchable, self-healing, stimuli-responsive, remoldable, and adhesive properties. *Biomacromolecules*. 19(6):2053–2061.
- Hossan, J., Gafur, M.A., Kadir, M.R. & Mainul, M. 2014. Preparation and characterization of gelatin- hydroxyapatite composite for bone tissue engineering. *Material Sciences and Engineering C*: 57(01):113–122.
- Hosseini, R., Mansoorli, S., Pirjani, R., Eslamian, L. and Rabiee, M., 2021. A comparison of the effects of Two suture materials on isthmocele formation: A cohort study. *Journal of Gynecology Obstetrics and Human Reproduction*, 50(4), p.101933.
- Hou, A., Zhou, M. and Wang, X., 2009. Preparation and characterization of durable antibacterial cellulose biomaterials modified with triazine derivatives. *Carbohydrate Polymers*, 75(2), pp.328-332.
- Hou, J.Y., Gao, L.N., Meng, F.Y. & Cui, Y.L. 2014. Mucoadhesive microparticles for gastroretentive delivery: Preparation, biodistribution and targeting evaluation. *Marine Drugs*. 12(12):5764–5787.
- Hu, J., Song, Y., Zhang, C., Huang, W., Chen, A., ... Wu, J. 2020. Highly aligned electrospun collagen/polycaprolactone surgical sutures with sustained release of

- growth factors for wound regeneration. *ACS Applied Bio Materials*. 3(2):965–976.
- Hu, W., Huang, Z.M., Meng, S.Y. & He, C.L. 2009. Fabrication and characterization of chitosan coated braided PLLA wire using aligned electrospun fibers. *Journal of Materials Science: Materials in Medicine*. 20(11):2275–2284.
- Huang, X. & Brazel, C.S. 2001. On the importance and mechanisms of burst release in matrix-controlled drug delivery systems. *Journal of Controlled Release*. 73(2–3):121–136.
- Hui, X., Geng, X., Jia, L., Xu, Z., Ye, L., ... Feng, Z.G. 2020. Preparation and in vivo evaluation of surface heparinized small diameter tissue engineered vascular scaffolds of poly(ϵ -caprolactone) embedded with collagen suture. *Journal of Biomaterials Applications*. 34(6):812–826.
- Im, J.N., Kim, J.K., Kim, H.K., In, C.H., Lee, K.Y. & Park, W.H. 2007. In vitro and in vivo degradation behaviors of synthetic absorbable bicomponent monofilament suture prepared with poly(p-dioxanone) and its copolymer. *Polymer Degradation and Stability*. 92(4):667–674.
- Ioelovich, M. 2017. Characterization of Various Kinds of Nanocellulose. *Handbook of Nanocellulose and Cellulose Nanocomposites*. (June):51–100.
- Irfanita, N., Jaswir, I., Mirghani, M.E.S., Sukmasari, S., Ardini, Y.D. & Lestari, W. 2017. Rapid detection of gelatin in dental materials using attenuated total reflection fourier transform infrared spectroscopy (ATR-FTIR). *Journal of Physics: Conference Series*. 884(1).
- Islam, S., Bhuiyan, M.A.R. & Islam, M.N. 2017. Chitin and chitosan: structure, properties and applications in biomedical engineering. *Journal of Polymers and the Environment*. 25(3):854–866.
- Islan, G.A., De Verti, I.P., Marchetti, S.G. & Castro, G.R. 2012. Studies of ciprofloxacin encapsulation on alginate/pectin matrixes and its relationship with biodisponibility. *Applied Biochemistry and Biotechnology*. 167(5):1408–1420.
- “ISO 10993-5 Biological evaluation of medical devices. Part 5: Tests for in vitro cytotoxicity.” 2009.
- Iswandana, R., Putri, K.S.S., Wulandari, F.R., Najuda, G., Sari, S.P. & Djajadisastra, J. 2018. Preparation of calcium alginate-tetrandrine beads using ionic gelation method as colon-targeted dosage form. *Journal of Applied Pharmaceutical Science*. 8(5):68–74.
- Jahromi, M., Niakousari, M., Golmakani, M.T. & Mohammadifar, M.A. 2020. Physicochemical and structural characterization of sodium caseinate based film-forming solutions and edible films as affected by high methoxyl pectin. *International Journal of Biological Macromolecules*. 165:1949–1959.
- Jamróz, E., Kulawik, P. & Kopel, P. 2019. The effect of nanofillers on the functional properties of biopolymer-based films: A review. *Polymers*. 11(4):1–43.
- Jantrawut, P., Chaiwarit, T., Jantanasakulwong, K., Brachais, C.H. & Chambin, O. 2017. Effect of plasticizer type on tensile property and in vitro indomethacin release of thin films based on low-methoxyl pectin. *Polymers*. 9(7).
- Jejurikar, A., Lawrie, G., Martin, D. & Grøndahl, L. 2011. A novel strategy for preparing mechanically robust ionically cross-linked alginate hydrogels. *Biomedical Materials*. 6(2).
- Jhong, J.F., Venault, A., Liu, L., Zheng, J., Chen, S.H., ... Chang, Y. 2014. Introducing mixed-charge copolymers as wound dressing biomaterials. *ACS Applied Materials and Interfaces*. 6(12):9858–9870.
- Jiang, J., Oberdörster, G. & Biswas, P. 2009. Characterization of size, surface charge, and agglomeration state of nanoparticle dispersions for toxicological studies. *Journal of Nanoparticle Research*. 11(1):77–89.
- Jindal, M., Kumar, V., Rana, V. & Tiwary, A.K. 2013. Aegle marmelos fruit pectin for food and pharmaceuticals: Physico-chemical, rheological and functional performance. *Carbohydrate Polymers*. 93(2):386–394.
- Johnson, D.B., Lopez, M.J. and Kelley, B. 2018. Dexamethasone. StatPearls Publishing, Treasure Island (FL).

- Joseph, B., George, A., Gopi, S., Kalarikkal, N. & Thomas, S. 2017. Polymer sutures for simultaneous wound healing and drug delivery – A review. *International Journal of Pharmaceutics*. 524(1–2):454–466.
- Kaczmarek, B., Nadolna, K. & Owczarek, A. 2019. The physical and chemical properties of hydrogels based on natural polymers. *Hydrogels Based on Natural Polymers*. Elsevier Inc.
- Kanagaraj, S., Varanda, F.R., Zhil'tsova, T. V., Oliveira, M.S.A. & Simões, J.A.O. 2007. Mechanical properties of high density polyethylene/carbon nanotube composites. *Composites Science and Technology*. 67(15–16):3071–3077.
- Karaman, K., Bal, A., Aziret, M., Ercan, M., Bostanci, E.B. & Akoglu, M. 2017. Which suture material is optimal for pancreaticojejunostomy anastomosis? An In Vitro Study. *Journal of Investigative Surgery*. 30(4):277–284.
- Kargarzadeh, H., Mariano, M., Huang, J., Lin, N., Ahmad, I., ... Thomas, S. 2017. Recent developments on nanocellulose reinforced polymer nanocomposites : A review. *Polymer*. 132:368–393.
- Kataria, P., Katara, R., Sahoo, P.K. & Sachdeva, S. 2017. Dorzolamide in situ gel forming system: Characterization and evaluation for glaucoma treatment. *Madridge Journal of Pharmaceutical Research*. 1(1):13–21.
- Kaygusuz, H., Evingür, G.A., Pekcan, Ö., von Klitzing, R. & Erim, F.B. 2016. Surfactant and metal ion effects on the mechanical properties of alginate hydrogels. *International Journal of Biological Macromolecules*. 92:220–224.
- Kazi, G.A.S. & Yamamoto, O. 2019. Effectiveness of the sodium alginate as surgical sealant materials. *Wound Medicine*. 24(1):18–23.
- Khan, M.K., Rahman, M.M., Nesa, B., Nasrin, R., Molla, S., Islam, M.M., Rashid, T.U., Haque, P., Mustafa, A.I. and Khan, M.A., 2013. Preparation and characterization of poly (ethylene glycol) grafted Ca-alginate fibers by-irradiation for biomedical applications. *Journal of Adhesion Science and Technology*, 27(2), pp.216-226.
- Khor, E. 2014. *Chitin: fulfilling a biomaterials promise*. 2nd ed. Elsevier.
- Kildeeva, N., Chalych, A., Belokon, M., Petrova, T., Matveev, V., ... Sazhnev, N. 2020. Influence of genipin crosslinking on the properties of Chitosan-based films. *Polymers*. 12(5).
- Kim, J.C., Lee, Y.K., Lim, B.S., Rhee, S.H. & Yang, H.C. 2007. Comparison of tensile and knot security properties of surgical sutures. *Journal of Materials Science: Materials in Medicine*. 18(12):2363–2369.
- Kim, J.H., Shim, B.S., Kim, H.S., Lee, Y.J., Min, S.K., ... Kim, J. 2015. Review of nanocellulose for sustainable future materials. *International Journal of Precision Engineering and Manufacturing - Green Technology*. 2(2):197–213.
- Kim, Y.J., Yoon, K.J. & Ko, S.W. 2000. Preparation and properties of alginate superabsorbent filament fibers crosslinked with glutaraldehyde. *Journal of Applied Polymer Science*. 78(10):1797–1804.
- Klajnert, B., Pikala, S. & Bryszewska, M. 2010. Haemolytic activity of polyamidoamine dendrimers and the protective role of human serum albumin. *Proceedings of the Royal Society A: Mathematical, Physical and Engineering Sciences*. 466(2117):1527–1534.
- Klemm, D., Schumann, D., Udhardt, U. & Marsch, S. 2001. Bacterial synthesized cellulose - Artificial blood vessels for microsurgery. *Progress in Polymer Science (Oxford)*. 26(9):1561–1603.
- Klemm, D., Schumann, D., Kramer, F., Heßler, N., Hornung, M., ... Marsch, S. 2006. Nanocelluloses as innovative polymers in research and application. *Advances in Polymer Science*. 205(1):49–96.
- Klimek, K. & Ginalska, G. 2020. Proteins and peptides as important modifiers of the polymer scaffolds for tissue engineering. *Polymers*. 12(844):1–38.
- Koh, L.B., Rodriguez, I. & Venkatraman, S.S. 2010. The effect of topography of polymer surfaces on platelet adhesion. *Biomaterials*. 31(7):1533–1545.
- Kong, M., Chen, X.G., Xing, K. & Park, H.J. 2010. Antimicrobial properties of chitosan and mode of action: A state of the art review. *International Journal of Food Microbiology*.

- 144(1):51–63.
- Konovalova, M. V., Markov, P.A., Durnev, E.A., Kurek, D. V., Popov, S. V. & Varlamov, V.P. 2017. Preparation and biocompatibility evaluation of pectin and chitosan cryogels for biomedical application. *Journal of Biomedical Materials Research - Part A*. 105(2):547–556.
- Koshy, S.T., Desai, R.M., Joly, P., Li, J., Bagrodia, R.K., ... Mooney, D.J. 2016. Click-crosslinked injectable gelatin hydrogels. *Advanced Healthcare Materials*. 5(5):541–547.
- Kucharska, M., Sikora, M., Brzoza-Malczewska, K. & Owczarek, M. 2019. Antimicrobial properties of chitin and chitosan. *Chitin and Chitosan: Properties and Applications*. 169–187.
- Kukreja, K., Chennubhotla, S., Bhandari, B., Arora, A. & Singhal, S. 2018. Closing the gaps: Endoscopic suturing for large submucosal and full-thickness defects. *Clinical Endoscopy*. 51(4):352–356.
- Kulkarni, V., Butte, K. & Rathod, S. 2012. Natural polymers – a comprehensive review. *International Journal of Research in Pharmaceutical and Biomedical Sciences*. 3(4):1597–1613.
- Kumar, M., Mishra, R.K. & Banthia, A.K. 2010. Development of pectin based hydrogel membranes for biomedical applications. *International Journal of Plastics Technology*. 14(2):213–223.
- Kumar, S., Allen, D.A., Kieswich, J.E., Patel, N.S.A., Harwood, S., ... Yaqoob, M.M. 2009. Dexamethasone ameliorates renal ischemia-reperfusion injury. *Journal of the American Society of Nephrology*. 20(11):2412–2425.
- Kume, T., Nagasawa, N. & Yoshii, F. 2002. Utilization of carbohydrates by radiation processing. *Radiation Physics and Chemistry*. 63(3–6):625–627.
- Kunanopparat, T., Menut, P., Morel, M.H. & Guilbert, S. 2008. Reinforcement of plasticized wheat gluten with natural fibers: From mechanical improvement to deplasticizing effect. *Composites Part A: Applied Science and Manufacturing*. 39(5):777–785.
- Kurakula, M., Rao, G.K., Kiran, V., Hasnain, M.S. & Nayak, A.K. 2020. Alginate-based hydrogel systems for drug releasing in wound healing. *Alginates in Drug Delivery*. INC.
- Kurita, K., Kaji, Y., Mori, T. & Nishiyama, Y. 2000. Enzymatic degradation of β -chitin: Susceptibility and the influence of deacetylation. *Carbohydrate Polymers*. 42(1):19–21.
- Lambrech, M.V.P., Sorrivas, V., Villar, M.A. & Lozano, J.E. 2009. Structure and permeability of low-methoxyl pectin (LMP)-sodium alginates (NaAlg) films. *Chemical Engineering Transactions*. 17(8000):1765–1770.
- Lapointe, S., Zhim, F., Sidéris, L., Drolet, P., Célestin-Noël, S. & Dubé, P. 2015. Effect of chemotherapy and heat on biomechanical properties of absorbable sutures. *Journal of Surgical Research*. 200(1):59–65.
- Lau, Y W. Tan, B.C. 2010. Glass transition measurement of undried fish gelatin with fast scan DSC technique. *Seafood*: p.12.
- Le, N.T.T., Cao, V. Du, Nguyen, T.N.Q., Le, T.T.H., Tran, T.T. & Thi, T.T.H. 2019. Soy lecithin-derived liposomal delivery systems: Surface modification and current applications. *International Journal of Molecular Sciences*. 20(19).
- Leaper, D.J., Edmiston, C.E. & Holy, C.E. 2017. Meta-analysis of the potential economic impact following introduction of absorbable antimicrobial sutures. *British Journal of Surgery*. 104(2):e134–e144.
- Lee, E.J., Huh, B.K., Kim, S.N., Lee, J.Y., Park, C.G., ... Choy, Y. Bin. 2017. Application of materials as medical devices with localized drug delivery capabilities for enhanced wound repair. *Progress in Materials Science*. 89:392–410.
- Lee, S.S., Hughes, P., Ross, A.D. & Robinson, M.R. 2010. Biodegradable implants for sustained drug release in the eye. *Pharmaceutical Research*. 27(10):2043–2053.
- Lee, W.J., Clancy, A.J., Kontturi, E., Bismarck, A. & Shaffer, M.S.P. 2016. Strong and stiff: High-performance cellulose nanocrystal/poly(vinyl alcohol) composite fibers. *ACS Applied Materials and Interfaces*. 8(46):31500–31504.
- Lee, W.R., Park, J.H., Kim, K.H., Kim, S.J., Park, D.H., ... Park, K.K. 2009. The biological effects of topical alginate treatment in an animal model of skin wound healing. *Wound*

- Repair and Regeneration*. 17(4):505–510.
- Lee, Y., Kim, H., Kim, Y., Noh, S., Chun, B., ... Seo, J. 2021. A multifunctional electronic suture for continuous strain monitoring and on-demand drug release. *Nanoscale*.
- Lei, Y. ting, Xu, B., Xie, X. wei, Xie, J. wei, Huang, Q. & Pei, F. xing. 2018. The efficacy and safety of two low-dose peri-operative dexamethasone on pain and recovery following total hip arthroplasty: a randomized controlled trial. *International Orthopaedics*. 42(3):499–505.
- Lemahieu, L., Bras, J., Tiquet, P., Augier, S. & Dufresne, A. 2011. Extrusion of nanocellulose-reinforced nanocomposites using the dispersed nano-objects protective encapsulation (DOPE) process. *Macromolecular Materials and Engineering*. 296(11):984–991.
- Lendlein, A. & Langer, R. 2002. Biodegradable, elastic shape-memory polymers for potential biomedical applications. *Science*. 296(5573):1673–1676.
- Li, D., Li, P., Zang, J. & Liu, J. 2012. Enhanced hemostatic performance of tranexamic acid-loaded chitosan/alginate composite microparticles. *Journal of Biomedicine and Biotechnology*. 2012.
- Li, H., Cheng, F., Chávez-Madero, C., Choi, J., Wei, X., ... He, J. 2019. Manufacturing and physical characterization of absorbable oxidized regenerated cellulose braided surgical sutures. *International Journal of Biological Macromolecules*. 134:56–62.
- Li, J., Wu, F., Zhang, K., He, Z., Zou, D., ... Huang, N. 2017. Controlling molecular weight of hyaluronic acid conjugated on amine-rich surface: Toward better multifunctional biomaterials for cardiovascular implants. *ACS Applied Materials and Interfaces*. 9(36):30343–30358.
- Li, J., Wu, Y., He, J. & Huang, Y. 2016. A new insight to the effect of calcium concentration on gelation process and physical properties of alginate films. *Journal of Materials Science*. 51(12):5791–5801.
- Li, K., Qu, X., Wang, Y., Tang, Y., Qin, D., ... Feng, M. 2005. Improved performance of primary rat hepatocytes on blended natural polymers. *Journal of Biomedical Materials Research - Part A*. 75(2):268–274.
- Li, X.Y., Chen, X.G., Liu, C.S., Liu, C.G. & Xue, Y.P. 2008. Preparation of alginate-gelatin capsules and its properties. *Frontiers of Materials Science in China*. 2(3):253–260.
- Li, Y., Jiang, K., Feng, J., Liu, J., Huang, R., ... Jiang, X. 2017. Construction of small-diameter vascular graft by shape-memory and self-rolling bacterial cellulose membrane. *Advanced Healthcare Materials*. 6(11):1–10.
- Li, Y., Han, C., Yu, Y. & Xiao, L. 2020. Effect of loadings of nanocellulose on the significantly improved crystallization and mechanical properties of biodegradable poly(ϵ -caprolactone). *International Journal of Biological Macromolecules*. 147:34–45.
- Li, Y., Li, J., Sun, J., He, H., Li, B., ... Zhang, H. 2020. Bioinspired and mechanically strong fibers based on engineered non-spider chimeric proteins. *Angewandte Chemie*. 132(21):8225–8229.
- Liao, H., Zhang, H. & Chen, W. 2009. Differential physical, rheological, and biological properties of rapid in situ gelable hydrogels composed of oxidized alginate and gelatin derived from marine or porcine sources. *Journal of Materials Science: Materials in Medicine*. 20(6):1263–1271.
- Liling, G., Di, Z., Jiachao, X., Xin, G., Xiaoting, F. & Qing, Z. 2016. Effects of ionic crosslinking on physical and mechanical properties of alginate mulching films. *Carbohydrate Polymers*. 136:259–265.
- Link, A., Haag, H., Michel, T., Denzinger, M., Wendel, H.P., Schlensak, C. and Krajewski, S., 2019. Development of a Novel Polymer-Based mRNA Coating for Surgical Suture to Enhance Wound Healing. *Coatings*, 9(6), p.374.
- Liu, L.S., Fishman, M.L. & Hicks, K.B. 2007. Pectin in controlled drug delivery - A review. *Cellulose*. 14(1):15–24.
- Liu, S.A., Cheng, C.C., Chen, J.S., Hung, Y.W., Chen, F.J. & Chiu, Y.T. 2012. Effect of oxidized regenerated cellulose on the healing of pharyngeal wound: An experimental animal study. *Journal of the Chinese Medical Association*. 75(4):176–182.

- Liu, Y., Zhang, X. & Hao, P. 2016. The effect of topography and wettability of biomaterials on platelet adhesion. *Journal of Adhesion Science and Technology*. 30(8):878–893.
- Liu, Y., Cai, Z., Sheng, L., Ma, M., Xu, Q. & Jin, Y. 2019. Structure-property of crosslinked chitosan/silica composite films modified by genipin and glutaraldehyde under alkaline conditions. *Carbohydrate Polymers*. 215(March):348–357.
- Liu, Y., Weng, R., Wang, W., Wei, X., Li, J., ... Li, Y. 2020. Tunable physical and mechanical properties of gelatin hydrogel after transglutaminase crosslinking on two gelatin types. *International Journal of Biological Macromolecules*. 162:405–413.
- Liu, Y., Cheong NG, S., Yu, J. & Tsai, W.B. 2019. Modification and crosslinking of gelatin-based biomaterials as tissue adhesives. *Colloids and Surfaces B: Biointerfaces*. 174(September 2018):316–323.
- Liu, Y., Li, Y., Yang, G., Zheng, X. & Zhou, S. 2015. Multi-stimulus-responsive shape-memory polymer nanocomposite network cross-linked by cellulose nanocrystals. *ACS Applied Materials and Interfaces*. 7(7):4118–4126.
- Lourdin, D., Bizot, H. and Colonna, P., 1997. "Antiplasticization" in starch-glycerol films?. *Journal of Applied Polymer Science*, 63(8), pp.1047-1053.
- Lu, H.L. & Chiang, C.H. 2008. Combined therapy of pentastarch, dexamethasone, and dibutyryl-cAMP or β 2-agonist attenuates ischaemia/reperfusion injury of rat lung. *Injury*. 39(9):1062–1070.
- M. Iguchi, S. Yamanaka; & A. Budhiono; 2000. Bacterial cellulose - a masterpiece of nature's arts. *Journal of Materials Science*. 35(2):261–270.
- MacDonald, J.D. 2005. Learning to perform microvascular anastomosis. *Skull Base*. 15(3):229–240.
- Macovescu, G., Chelaru, C., Ignat, M., Albu, L. & Gurau, D. 2018. Validation of method for determining the isoelectric point of protein solutions. *Leather and Footwear Journal*. 18(1):53–66.
- Mahesh, L., Kumar, V.R., Jain, A., Shukla, S., Aragonese, J.M., ... Calvo-Guirado, J.L. 2019. Bacterial adherence around sutures of different material at grafted site: A microbiological analysis. *Materials*. 12(18):1–8.
- Maitra, J. & Shukla, V.K. 2014. Cross-linking in hydrogels - A review. *American Journal of Polymer Science*. 4(2):25–31.
- Majidi, S.S., Slemming-Adamsen, P., Hanif, M., Zhang, Z., Wang, Z. & Chen, M. 2018. Wet electrospun alginate/gelatin hydrogel nanofibers for 3D cell culture. *International Journal of Biological Macromolecules*. 118:1648–1654.
- Malafaya, P.B., Silva, G.A. & Reis, R.L. 2007. Natural-origin polymers as carriers and scaffolds for biomolecules and cell delivery in tissue engineering applications. *Advanced Drug Delivery Reviews*. 59(4–5):207–233.
- Mammarella, E.J. & Rubiolo, A.C. 2003. Crosslinking kinetics of cation-hydrocolloid gels. *Chemical Engineering Journal*. 94(1):73–77.
- Mangavel, C., Barbot, J., Guéguen, J. & Popineau, Y. 2003. Molecular determinants of the influence of hydrophilic plasticizers on the mechanical properties of cast wheat gluten films. *Journal of Agricultural and Food Chemistry*. 51(5):1447–1452.
- Mansoor, S., Kondiah, P.P.D., Choonara, Y.E. & Pillay, V. 2019. Polymer-based nanoparticle strategies for insulin delivery. *Polymers*. 11(9).
- Marturello, D.M., Mcfadden, M.S., Bennett, R.A., Ragetly, G.R. & Horn, G. 2014. Knot security and tensile strength of suture materials. *Veterinary Surgery*. 43(1):73–79.
- Marzec, E. & Pietrucha, K. 2018. Efficacy evaluation of electric field frequency and temperature on dielectric properties of collagen cross-linked by glutaraldehyde. *Colloids and Surfaces B: Biointerfaces*. 162:345–350.
- Maslova, M. V., Uspenskii, S.A., Gal'braikh, L.S. & Kil'deeva, N.R. 2016. Surgical sutures modified with polysaccharide composites. *Fibre Chemistry*. 48(3):1–5.
- Mathew, A.P., Oksman, K., Pierron, D. & Harmand, M.F. 2012. Fibrous cellulose nanocomposite scaffolds prepared by partial dissolution for potential use as ligament or tendon substitutes. *Carbohydrate Polymers*. 87(3):2291–2298.
- Mathew, A.P., Oksman, K., Pierron, D. & Harmand, M.F. 2013. Biocompatible fibrous

- networks of cellulose nanofibres and collagen crosslinked using genipin: Potential as artificial ligament/tendons. *Macromolecular Bioscience*. 13(3):289–298.
- Matl, F.D., Zlotnyk, J., Obermeier, A., Friess, W., Vogt, S., ... Kühn, K.D. 2009. New anti-infective coatings of surgical sutures based on a combination of antiseptics and fatty acids. *Journal of Biomaterials Science, Polymer Edition*. 20(10):1439–1449.
- Matsuzaki, S., Jitsumori, M., Hara, T., Matsuzaki, S., Nakagawa, S., ... Kimura, T. 2019. Systematic review on the needle and suture types for uterine compression sutures: A literature review. *BMC Surgery*. 19(1):1–6.
- Meneguim, A.B., Ferreira Cury, B.S., dos Santos, A.M., Franco, D.F., Barud, H.S. & da Silva Filho, E.C. 2017. Resistant starch/pectin free-standing films reinforced with nanocellulose intended for colonic methotrexate release. *Carbohydrate Polymers*. 157:1013–1023.
- Merakchi, A., Bettayeb, S., Drouiche, N., Adour, L. & Lounici, H. 2019. Cross-linking and modification of sodium alginate biopolymer for dye removal in aqueous solution. *Polymer Bulletin*. 76(7):3535–3554.
- Mertaniemi, H., Escobedo-Lucea, C., Sanz-Garcia, A., Gandía, C., Mäkitie, A., ... Yliperttula, M. 2016. Human stem cell decorated nanocellulose threads for biomedical applications. *Biomaterials*. 82:208–220.
- Metwally, S. & Stachewicz, U. 2019. Surface potential and charges impact on cell responses on biomaterials interfaces for medical applications. *Materials Science and Engineering C*. 104(June):109883.
- Metz, S.A., Chegini, N. & Masterson, B.J. 1989. In vivo tissue reactivity and degradation of suture materials: A comparison of Maxon and PDS. *Journal of Gynecologic Surgery*. 5(1):37–46.
- MG., L. (in press). Technique of Y and T grafts. *Technical Aspects of Modern Coronary Artery Bypass Surgery*. (pp. 99-113).
- Mishra, R.K., Datt, M. & Banthia, A.K. 2008. Synthesis and characterization of pectin/pvp hydrogel membranes for drug delivery system. *AAPS PharmSciTech*. 9(2):395–403.
- Mishra, R.K., Datt, M., Pal, K. & Banthia, A.K. 2008. Preparation and characterization of amidated pectin based hydrogels for drug delivery system. *Journal of Materials Science: Materials in Medicine*. 19(6):2275–2280.
- Mndlovu, H., du Toit, L.C., Kumar, P., Marimuthu, T., Kondiah, P.P.D., ... Pillay, V. 2019b. Development of a fluid-absorptive alginate-chitosan bioplatfrom for potential application as a wound dressing. *Carbohydrate Polymers*. 222(January):114988.
- Mogoşanu, G.D. & Grumezescu, A.M. 2014. Natural and synthetic polymers for wounds and burns dressing. *International Journal of Pharmaceutics*. 463(2):127–136.
- Mohammadi, H., Alihosseini, F. & Hosseini, S.A. 2020. Improving physical and biological properties of nylon monofilament as suture by Chitosan/Hyaluronic acid. *International Journal of Biological Macromolecules*. 164:3394–3402.
- Mohite, B. V. & Patil, S. V. 2014. A novel biomaterial: Bacterial cellulose and its new era applications. *Biotechnology and Applied Biochemistry*. 61(2):101–110.
- Monsoor, M.A., Kalapathy, U. & Proctor, A. 2001. Improved method for determination of pectin degree of esterification by diffuse reflectance Fourier transform infrared spectroscopy. *Journal of Agricultural and Food Chemistry*. 49(6):2756–2760.
- Montenegro R, F.T. 2017. *Patent No. United States patent US 9,771,668*.
- Muscat, D., Adhikari, B., Adhikari, R. & Chaudhary, D.S. 2012. Comparative study of film forming behaviour of low and high amylose starches using glycerol and xylitol as plasticizers. *Journal of Food Engineering*. 109(2):189–201.
- Nadeem, U. & Datta, M. 2014. Adsorption Studies of Zinc (II) Ions on Biopolymer Composite Beads of Alginate-Fly Ash. *European Chemical Bulletin*. 3(7):682–691.
- Naganuma, T. 2017. The relationship between cell adhesion force activation on nano/micro-topographical surfaces and temporal dependence of cell morphology. *Nanoscale*. 9(35):13171–13186.
- Naghieh, S., Karamooz-Ravari, M.R., Sarker, M.D., Karki, E. & Chen, X. 2018. Influence of crosslinking on the mechanical behavior of 3D printed alginate scaffolds: Experimental

- and numerical approaches. *Journal of the Mechanical Behavior of Biomedical Materials*. 80(October 2017):111–118.
- Naleway, S.E., Lear, W., Kruzic, J.J. & Maughan, C.B. 2015. Mechanical properties of suture materials in general and cutaneous surgery. *Journal of Biomedical Materials Research - Part B Applied Biomaterials*. 103(4):735–742.
- Nalezinková, M. 2020. In vitro hemocompatibility testing of medical devices. *Thrombosis Research*. 195(May):146–150.
- Nam, S.Y. & Park, S.H. 2018. ECM based bioink for tissue mimetic 3D bioprinting. *Advances in Experimental Medicine and Biology*. 1064:335–353.
- Naqash, F., Masoodi, F.A., Rather, S.A., Wani, S.M. & Gani, A. 2017. Emerging concepts in the nutraceutical and functional properties of pectin—A Review. *Carbohydrate Polymers*. 168:227–239.
- Nastaj, J., Przewłocka, A. & Rajkowska-Myśliwiec, M. 2016. Biosorption of Ni(II), Pb(II) and Zn(II) on calcium alginate beads: Equilibrium, kinetic and mechanism studies. *Polish Journal of Chemical Technology*. 18(3):81–87.
- Nelson, M.L. & O'Connor, R.T. 1964. Relation of certain infrared bands to cellulose crystallinity and crystal lattice type. Part II. A new infrared ratio for estimation of crystallinity in celluloses I and II. *Journal of Applied Polymer Science*. 8(3):1325–1341.
- NF24, U.-. s.a. *United States Pharmacopoeia: Suture diameter*.
http://ftp.uspbpep.com/v29240/usp29nf24s0_c861.html#usp29nf24s0_c861.
- Nguyen, D.T., Nguyen, N.M., Vu, D.M., Tran, M.D. & Ta, V.T. 2021. On-demand release of drug from magnetic nanoparticle-loaded alginate beads. *Journal of Analytical Methods in Chemistry*. 2021.
- Niccoli, G., Kharbanda, R.K., Crea, F. & Banning, A.P. 2010. No-reflow: Again prevention is better than treatment. *European Heart Journal*. 31(20):2449–2455.
- Niekraszewicz, B. & Niekraszewicz, A. 2009. *The structure of alginate, chitin and chitosan fibres*. Vol. 2. *Handbook of Textile Fibre Structure*. Woodhead Publishing Limited.
- Nisar, T., Wang, Z.C., Alim, A., Iqbal, M., Yang, X., ... Guo, Y. 2019. Citrus pectin films enriched with thinned young apple polyphenols for potential use as bio-based active packaging. *CYTA - Journal of Food*. 17(1):695–705.
- Nishida, K., Anada, T., Kobayashi, S., Ueda, T. and Tanaka, M., 2021. Effect of bound water content on cell adhesion strength to water-insoluble polymers. *Acta Biomaterialia*, 134, pp.313-324.
- Notara, M., Scotchford, C.A., Grant, D.M., Weston, N. & Roberts, G.A.F. 2009. Cytocompatibility and hemocompatibility of a novel chitosan-alginate gel system. *Journal of Biomedical Materials Research - Part A*. 89(4):854–864.
- Obermeier, A., Schneider, J., Wehner, S., Matl, F.D., Schieker, M., ... Burgkart, R. 2014. Novel high efficient coatings for anti-microbial surgical sutures using chlorhexidine in fatty acid slow-release carrier systems. *PLoS ONE*. 9(7).
- Obermeier, A., Schneider, J., Föhr, P., Wehner, S., Kühn, K.D., ... Burgkart, R. 2015. In vitro evaluation of novel antimicrobial coatings for surgical sutures using octenidine. *BMC Microbiology*. 15(1):1–8.
- Obulapuram, P.K., Kondiah, P.P.D., Choonara, Y.E., Penny, C. & Pillay, V. 2020. Role of natural cellulose and hydrogel matrices in stem cell therapy of diabetic foot ulcer. *Sustainable Nanocellulose and Nanohydrogels from Natural Sources*. INC.
- Oh, G.W., Nam, S.Y., Heo, S.J., Kang, D.H. & Jung, W.K. 2020. Characterization of ionic cross-linked composite foams with different blend ratios of alginate/pectin on the synergistic effects for wound dressing application. *International Journal of Biological Macromolecules*. 156:1565–1573.
- Okpalugo, T.I.T., Ogwu, A.A., Maguire, P.D. & McLaughlin, J.A.D. 2004. Platelet adhesion on silicon modified hydrogenated amorphous carbon films. *Biomaterials*. 25(2):239–245.
- Öktem, T. 2003. Surface treatment of cotton fabrics with chitosan. *Coloration Technology*. 119(4):241–246.
- Olivas, G.I. & Barbosa-Cánovas, G. V. 2008. Alginate-calcium films: Water vapor

- permeability and mechanical properties as affected by plasticizer and relative humidity. *LWT - Food Science and Technology*. 41(2):359–366.
- Olliviere, B.J., Bosman, H.A., Bearcroft, P.W.P. & Robinson, A.H.N. 2014. Foreign body granulomatous reaction associated with polyethylene “Fiberwire®” suture material used in Achilles tendon repair. *Foot and Ankle Surgery*. 20(2):e27–e29.
- Orliac, O., Rouilly, A., Silvestre, F. & Rigal, L. 2003. Effects of various plasticizers on the mechanical properties, water resistance and aging of thermo-moulded films made from sunflower proteins. *Industrial Crops and Products*. 18(2):91–100.
- Özkan, Ö. & Özgentaş, H.E. 2005. Open guide suture technique for safe microvascular anastomosis. *Annals of Plastic Surgery*. 55(3):289–291.
- Padmakumar, S., Joseph, J., Neppalli, M.H., Mathew, S.E., Nair, S. V., ... Menon, D. 2016. Electrospun polymeric core-sheath yarns as drug eluting surgical sutures. *ACS Applied Materials and Interfaces*. 8(11):6925–6934.
- Pan, T., Song, W., Cao, X. & Wang, Y. 2016. 3D bioplotting of gelatin/alginate scaffolds for tissue engineering: Influence of crosslinking degree and pore architecture on physicochemical properties. *Journal of Materials Science and Technology*. 32(9):889–900.
- Parikh, K.S., Omiadze, R., Josyula, A., Shi, R., Anders, N.M., ... Hanes, J. 2021. Ultra-thin, high strength, antibiotic-eluting sutures for prevention of ophthalmic infection. *Bioengineering and Translational Medicine*. 6(2):1–12.
- Park, S.Y., Kim, W.J., Choi, J.B. & Kim, S. 2018. Physical and mechanical properties of alginate-based hydrogel film as carrier for release of acetylthiocholine. *International Journal of Precision Engineering and Manufacturing*. 19(1):129–135.
- Parvez, S., Rahman, M.M., Khan, M.A., Khan, M.A.H., Islam, J.M.M., ... Ahmed, B. 2012. Preparation and characterization of artificial skin using chitosan and gelatin composites for potential biomedical application. *Polymer Bulletin*. 69(6):715–731.
- Paul, W. & Sharma, C.P. 2015. Alginates: Wound dressings. *Encyclopedia of Biomedical Polymers and Polymeric Biomaterials*. (April 2014):134–146.
- Pawar, S.N. & Edgar, K.J. 2012. Alginate derivatization: A review of chemistry, properties and applications. *Biomaterials*. 33(11):3279–3305.
- Peng, X., Liu, G., Zhu, L., Yu, K., Qian, K. & Zhan, X. 2020. In vitro and in vivo study of novel antimicrobial gellan–polylysine polyion complex fibers as suture materials. *Carbohydrate Research*. 496(August):108115.
- Peng X, Liu G, Zhu L, Yu K, Qian K, Z.X. 2020. In vitro and in vivo study of novel antimicrobial gellan–polylysine polyion complex fibers as suture materials. *Carbohydrate Research*.
- Perez, C.D., Flores, S.K., Marangoni, A.G., Gerschenson, L.N. & Rojas, A.M. 2009. Development of a high methoxyl pectin edible film for retention of L-(+)-ascorbic acid. *Journal of Agricultural and Food Chemistry*. 57(15):6844–6855.
- Petersen, N. & Gatenholm, P. 2011. Bacterial cellulose-based materials and medical devices: Current state and perspectives. *Applied Microbiology and Biotechnology*. 91(5):1277–1286.
- Phelan, P.S. & Council, M.L. 2019. Ethical considerations in the use of biopolymer sutures. *Journal of Dermatological Treatment*. 30(4):350–351.
- Picone, P., Sabatino, M.A., Ajovalasit, A., Giacomazza, D., Dispenza, C. & Di Carlo, M. 2019. Biocompatibility, hemocompatibility and antimicrobial properties of xyloglucan-based hydrogel film for wound healing application. *International Journal of Biological Macromolecules*. 121:784–795.
- Pilipenko, N., Gonçalves, O.H., Bona, E., Fernandes, I.P., Pinto, J.A., ... Barreiro, M.F. 2019. Tailoring swelling of alginate-gelatin hydrogel microspheres by crosslinking with calcium chloride combined with transglutaminase. *Carbohydrate Polymers*. 223(June):115035.
- Pillai, C.K.S. & Sharma, C.P. 2010. Review paper: Absorbable polymeric surgical sutures: Chemistry, production, properties, biodegradability, and performance. *Journal of Biomaterials Applications*. 25(4):291–366.

- Pitt, C.G. and Schindler, A. 2019. Biodegradation of polymers. In: S.D. Bruck, ed. *Controlled drug delivery*. pp. 225.
- Polykandriotis, E., Besrouf, F., Arkudas, A., Ruppe, F., Zetzmann, K., ... Horch, R.E. 2019. Flexor tendon repair with a polytetrafluoroethylene (PTFE) suture material. *Archives of Orthopaedic and Trauma Surgery*. 139(3):429–434.
- Prithyani SS, Naniwadekar AU, Mitra DK, Shah RA, D.A. 2021. Comparison and evaluation of the efficacy of plain polyglactin 910 versus chlorhexidine coated polyglactin 910 sutures in periodontal flap surgery: a clinico microbiological study. *JIDA: Journal of Indian Dental Association*. 15(3):25–29.
- Pruthi, N., Tyagi, G. & Gohil, D. 2021. End-to-side microvascular anastomosis on rat femoral vessels using only 2-throw knot interrupted sutures - evaluation of feasibility and patency rates on rat femoral vessels model. *World Neurosurgery*. 148:e145–e150.
- Przekora, A. 2019. The summary of the most important cell-biomaterial interactions that need to be considered during in vitro biocompatibility testing of bone scaffolds for tissue engineering applications. *Materials Science and Engineering C*. 97(January):1036–1051.
- Psimadas, D., Georgoulis, P., Valotassiou, V. & Loudos, G. 2012. Molecular nanomedicine towards cancer: *Journal of pharmaceutical sciences*. 101(7):2271–2280.
- Qin, X., Xia, W., Sinko, R. & Keten, S. 2015. Tuning glass transition in polymer nanocomposites with functionalized cellulose nanocrystals through nanoconfinement. *Nano Letters*. 15(10):6738–6744.
- Qin Y, Jiang J, Zhao L, Zhang J, W.F.A.P. 2018. Applications of alginate as a functional food ingredient. *Biopolymers for food design*. 409–429.
- Radhakrishnan, S., 2014. Application of biotechnology in the processing of textile fabrics. In *Roadmap to Sustainable Textiles and Clothing* (pp. 277-325). Springer, Singapore.
- Rajeswari, S. 2017. Natural Polymers: a Recent Review. *World Journal of Pharmacy and Pharmaceutical Sciences*. (June):472–494.
- Razavi, S.M.A., Mohammad Amini, A. & Zahedi, Y. 2015. Characterisation of a new biodegradable edible film based on sage seed gum: Influence of plasticiser type and concentration. *Food Hydrocolloids*. 43:290–298.
- Rengasamy, R.S. & Ghosh, S. 2010. Technical sewing threads. *Technical Textile Yarns*. 495–533.
- Rethinam, S., Nallathambi, G., Vijayan, S., Basaran, B., Mert, A., ... A, W.A. 2020. A new approach for the production of multifilament suture - in vitro and in vivo analysis. *International Journal of Polymeric Materials and Polymeric Biomaterials*. 0(0):1–10.
- Rezkalla SH, K.R. 2002a. No-reflow phenomenon. *Circulation*. 105(5):656–662.
- Riaz Rajoka, M.S., Mehwish, H.M., Wu, Y., Zhao, L., Arfat, Y., ... Anwaar, S. 2020. Chitin/chitosan derivatives and their interactions with microorganisms: a comprehensive review and future perspectives. *Critical Reviews in Biotechnology*. 40(3):365–379.
- Richard, A.S. & Verma, R.S. 2021. Bioactive nano yarns as surgical sutures for wound healing. *Materials Science and Engineering C*. 128(May):112334.
- Rickard, R.F. & Hudson, D.A. 2014. A history of vascular and microvascular surgery. *Annals of Plastic Surgery*. 73(4):465–472.
- Rinaudo, M. 2006. Characterization and properties of some polysaccharides used as biomaterials. *Macromolecular Symposia*. 245–246:549–557.
- Rockville (MD): United States Pharmacopeial Convention. 1976. *The United States Pharmacopeia*.
- Rose J, T.F. 2019. Sutures and needles. StatPearls Publishing.
- Rosellini, E., Cristallini, C., Barbani, N., Vozzi, G. & Giusti, P. 2009. Preparation and characterization of alginate/gelatin blend films for cardiac tissue engineering. *Journal of Biomedical Materials Research - Part A*. 91(2):447–453.
- Roy, D., Semsarilar, M., Guthrie, J.T. & Perrier, S. 2009. Cellulose modification by polymer grafting: A review. *Chemical Society Reviews*. 38(7):2046–2064.
- Ruano, P., Lazo Delgado, L., Picco, S., Villegas, L., Tonelli, F., ... Masuelli, M. 2020. Extraction and characterization of pectins from peels of criolla oranges (*Citrus sinensis*):

- Experimental reviews . *Pectins - Extraction, Purification, Characterization and Applications*. 1–44.
- Sachan, N., Pushkar, S., Jha, A. & Bhattacharya, A. 2009. Sodium alginate: the wonder polymer for controlled drug delivery. *Journal of pharmacy research*. 2(8):1191–1199.
- Sacui, I.A., Nieuwendaal, R.C., Burnett, D.J., Stranick, S.J., Jorfi, M., ... Gilman, J.W. 2014. Comparison of the properties of cellulose nanocrystals and cellulose nanofibrils isolated from bacteria, tunicate, and wood processed using acid, enzymatic, mechanical, and oxidative methods. *ACS Applied Materials and Interfaces*. 6(9):6127–6138.
- Sahoo, C.K., Ramana, D.V., Satyanarayana, K. & Bhongir, Y. 2017. A discussion on suture and ligature. *Academia E.U.* 2(2):46–52.
- Sahraee, S., Milani, J.M., Ghanbarzadeh, B. & Hamishehkar, H. 2017. Physicochemical and antifungal properties of bio-nanocomposite film based on gelatin-chitin nanoparticles. *International Journal of Biological Macromolecules*. 97(December):373–381.
- Sakai, A., Murayama, Y., Fujiwara, K., Fujisawa, T., Sasaki, S., ... Yanagisawa, M. 2018. Increasing elasticity through changes in the secondary structure of gelatin by gelation in a micro-sized lipid space. *ACS Central Science*. 4(4):477–483.
- Sakugawa, K., Ikeda, A., Takemura, A. & Ono, H. 2004. Simplified method for estimation of composition of alginates by FTIR. *Journal of Applied Polymer Science*. 93(3):1372–1377.
- Salehpour, S. & Dubé, M.A. 2012. Reaction monitoring of glycerol step-growth polymerization using ATR-FTIR spectroscopy. *Macromolecular Reaction Engineering*. 6(2–3):85–92.
- Salem, K.S., Lubna, M.M., Rahman, A.M., Nurnabi, M., Islam, R. & Khan, M.A. 2015. The effect of multiwall carbon nanotube additions on the thermo-mechanical, electrical, and morphological properties of gelatin-polyvinyl alcohol blend nanocomposite. *Journal of Composite Materials*. 49(11):1379–1391.
- Salisu, A., Sanagi, M.M., Naim, A.A. & Abd Karim, K.J. 2015. Graft copolymerization of methyl methacrylate onto alginate using benzoyl peroxide initiator. *Research Journal of Pharmaceutical, Biological and Chemical Sciences*. 6(2):1408–1416.
- Salthouse, T.N. 1980. Biologic response to sutures. *Otolaryngology - Head and Neck Surgery*. 88(6):658–664.
- Samadian, H., Maleki, H., Allahyari, Z. & Jaymand, M. 2020. Natural polymers-based light-induced hydrogels: Promising biomaterials for biomedical applications. *Coordination Chemistry Reviews*. 420:213432.
- Samp, M.A., 2017. Sodium Alginate Toughening of Gelatin Hydrogels and Elucidation of Possible Mechanisms. *Rose Hulman Institute of Technology*.
- Sancakli, A., Basaran, B., Arican, F. & Polat, O. 2021. Effects of bovine gelatin viscosity on gelatin-based edible film mechanical, physical and morphological properties. *SN Applied Sciences*. 3(1):1–11.
- Sánchez-Hernández, C.D., Torres-Alarcón, L.A., González-Cortés, A., Peón, A.N. & Rungtatscher, A. 2020. Ischemia/reperfusion injury: Pathophysiology, current clinical management, and potential preventive approaches. *Mediators of Inflammation*. 2020.
- Sánchez-Valdes, S., Ramos-De Valle, L.F. & Manero, O. 2013. *Polymer Blends*. Vol. 1. *Handbook of Polymer Synthesis, Characterization, and Processing*.
- Sanyang, M.L., Sapuan, S.M., Jawaid, M., Ishak, M.R. & Sahari, J. 2015. Effect of plasticizer type and concentration on dynamic mechanical properties of sugar palm starch-based films. *International Journal of Polymer Analysis and Characterization*. 20(7):627–636.
- Saralegi, A., Rueda, L., Martin, L., Arbelaz, A., Eceiza, A. & Corcuera, M.A. 2013. From elastomeric to rigid polyurethane/cellulose nanocrystal bionanocomposites. *Composites Science and Technology*. 88:39–47.
- Sarika, P.R., James, N.R., Anil kumar, P.R. & Raj, D.K. 2016. Preparation, characterization and biological evaluation of curcumin loaded alginate aldehyde–gelatin nanogels. *Materials Science and Engineering C*. 68:251–257.
- Sarker, B., Singh, R., Silva, R., Roether, J.A., Kaschta, J., ... Boccaccini, A.R. 2014. Evaluation of fibroblasts adhesion and proliferation on alginate-gelatin crosslinked

- hydrogel. *PLoS ONE*. 9(9):1–12.
- Sashiwa, H. & Aiba, S.I. 2004. Chemically modified chitin and chitosan as biomaterials. *Progress in Polymer Science (Oxford)*. 29(9):887–908.
- Saunders, M. 2008. Thermal analysis of pharmaceuticals. In: P. Gabbott, ed. *Principles and applications of thermal analysis*. John Wiley & Sons. pp. 290–297.
- Saxena, S., Ray, A.R., Kapil, A., Pavon-Djavid, G., Letourneur, D., ... Meddahi-Pellé, A. 2011. Development of a new polypropylene-based suture: plasma grafting, surface treatment, characterization, and biocompatibility studies. *Macromolecular Bioscience*. 11(3):373–382.
- Sayed Zeid, A. & Sayed, S. 2020. A comparative study of the use of dexamethasone, n-acetyl cysteine, and theophylline to ameliorate renal ischemia-reperfusion injury in experimental rat models: A biochemical and immuno-histochemical approach. *Saudi Journal of Kidney Diseases and Transplantation*. 31(5):982–997.
- Schedl, L. 2002. Why degradable polymers undergo surface erosion or bulk erosion. *Biomaterials*, 23 (21):4221–4231.
- Schmid, M. 2013. Properties of cast films made from different ratios of whey protein isolate, hydrolysed whey protein Isolate and Glycerol. *Materials*. 6(8):3254–3269.
- Seitz, J.M., Wulf, E., Freytag, P., Bormann, D. & Bach, F.W. 2010. The manufacture of resorbable suture material from magnesium. *Advanced Engineering Materials*. 12(11):1099–1105.
- Seitz, J.M., Durisin, M., Goldman, J. & Drelich, J.W. 2015. Recent advances in biodegradable metals for medical sutures: A critical review. *Advanced Healthcare Materials*. 4(13):1915–1936.
- Seixas, F.L., Turbiani, F.R.B., Salomão, P.G., Souza, R.P. & Gimenes, M.L. 2013. Biofilms composed of alginate and pectin: Effect of concentration of crosslinker and plasticizer agents. *Chemical Engineering Transactions*. 32(January):1693–1698.
- Selvi, F., Cakarer, S., Can, T., Topcu, S.İ.K., Palancioglu, A., Keskin, B., Bilgic, B., Yaltirik, M. and Keskin, C. (in press). Effects of different suture materials on tissue healing. *Journal of Istanbul University Faculty of Dentistry*. 50(1):p.35.
- Serrano-Aroca, Á., Ruiz-Pividal, J.F. & Llorens-Gámez, M. 2017. Enhancement of water diffusion and compression performance of crosslinked alginate films with a minuscule amount of graphene oxide. *Scientific Reports*. 7(1):1–8.
- Sethi S, Bhatia S, Kamboj S, R. V. 2021. Exploring the feasibility of carbamoyl ethyl pullulan-g-palmitic acid polymeric micelles for the effective targeting of raloxifene to breast tumor: Optimization and preclinical evaluation. *International Journal of Pharmaceutics*. 603:120720.
- Seyid, M., Tiftikcioglu, Y., Erdem, M., Akdemir, O., Tatar, B.E., ... Ercan, G. 2021. The effect of ceruloplasmin against ischemia-reperfusion injury in epigastric island flap in rats. *Journal of Surgical Research*. 267(267):627–635.
- Shah, N., Ul-Islam, M., Khattak, W.A. & Park, J.K. 2013. Overview of bacterial cellulose composites: A multipurpose advanced material. *Carbohydrate Polymers*. 98(2):1585–1598.
- Shahidi, F. and Abuzaytoun, R. 2005. Chitin, chitosan, and co-products: chemistry, production, applications, and health effects. In: *Advances in food and nutrition research*. pp. 93-137.
- Shahzad, A., Khan, A., Afzal, Z., Umer, M.F., Khan, J. & Khan, G.M. 2019. Formulation development and characterization of cefazolin nanoparticles-loaded cross-linked films of sodium alginate and pectin as wound dressings. *International Journal of Biological Macromolecules*. 124:255–269.
- Shao, K., Han, B., Gao, J., Jiang, Z., Liu, W., ... Liang, Y. 2016. Fabrication and feasibility study of an absorbable diacetyl chitin surgical suture for wound healing. *Journal of Biomedical Materials Research - Part B Applied Biomaterials*. 104(1):116–125.
- Sharma, B.R., Naresh, L., Dhuldhoya, N.C., Merchant, S.U. & Merchant, U.C. 2006. An overview on pectins. *Times Food Processing Journal*. 51(June-July):44–51. <http://www.taiyolucid.com/pdf/pectin.pdf>.

- Shehap, A.M., Mahmoud, K.H., Abd El-Kader, M.F.H. & El-Basheer, T.M. 2015. Preparation and thermal properties of gelatin/tgs composite films. *Middle East Journal of Applied Sciences*. 5(1):157–170.
- Sheik-Ali, S. & Guets, W. 2018. Absorbable vs non absorbable sutures for wound closure. Systematic review of systematic reviews. *Wound Medicine*. 23(August):35–37.
- Shelma, R., Paul, W. & Sharma, C.P. 2008. Chitin nanofibre reinforced thin chitosan films for wound healing application. *Trends in Biomaterials and Artificial Organs*. 22(2):107–111.
- Shen, X., Shamshina, J.L., Berton, P., Gurau, G. & Rogers, R.D. 2015. Hydrogels based on cellulose and chitin: Fabrication, properties, and applications. *Green Chemistry*. 18(1):53–75.
- Shen, X.J., Huang, P.L., Chen, J.H., Wu, Y.Y., Liu, Q.Y. & Sun, R.C. 2017. Comparison of acid-hydrolyzed and TEMPO-oxidized nanocellulose for reinforcing alginate fibers. *BioResources*. 12(4):8180–8198.
- Shi, Z., Gao, X., Ullah, M.W., Li, S., Wang, Q. & Yang, G. 2016. Electroconductive natural polymer-based hydrogels. *Biomaterials*. 111:40–54.
- Shoseyov, O., Kam, D., Shalom, T.B., Shtein, Z., Vinkler, S. and Posen, Y. 2019. Nanocellulose composite biomaterials in industry and medicine. In: *Extracellular Sugar-Based Biopolymers Matrices*. Springer, Cham. pp. 693–784.
- Siburian, W.Z., Rochima, E., Andriani, Y. & Praseptiangga, D. 2020. Fish gelatin (definition, manufacture, analysis of quality characteristics, and application): A review. *International Journal of Fisheries and Aquatic Studies*. 8(4):90–95. <http://www.fisheriesjournal.com>.
- Siedlecki, C. 2018. Hemocompatibility of biomaterials for clinical applications: blood-biomaterials interactions. *Woodhead Publishing*. 108–196.
- Siew, C.K., Williams, P.A. & Young, N.W.G. 2005. New insights into the mechanism of gelation of alginate and pectin: Charge annihilation and reversal mechanism. *Biomacromolecules*. 6(2):963–969.
- Silva, M.A. da, Bierhalz, A.C.K. & Kieckbusch, T.G. 2009. Alginate and pectin composite films crosslinked with Ca²⁺ ions: Effect of the plasticizer concentration. *Carbohydrate Polymers*. 77(4):736–742.
- Silver, E., Wu, R., Grady, J. & Song, L. 2016. Knot security- how is it affected by suture technique, material, size, and number of throws? *Journal of Oral and Maxillofacial Surgery*. 74(7):1304–1312.
- Sindhu, K.A., Prasanth, R. & Thakur, V.K. 2014. Medical applications of cellulose and its derivatives: present and future. *Nanocellulose Polymer Nanocomposites: Fundamentals and Applications*. 9781118871:437–477.
- Singh, R., Shitiz, K. & Singh, A. 2017. Chitin and chitosan: biopolymers for wound management. *International Wound Journal*. 14(6):1276–1289.
- Singh, D.K. & Ray, A.R. 2000. Biomedical applications of chitin, chitosan, and their derivatives. *Journal of Macromolecular Science - Polymer Reviews*. 40(1):69–83.
- Siqueira, P., Siqueira, É. Der, Lima, A.E. De, Siqueira, G., Delia, A., ... Botaro, V.R. 2019. Three-dimensional stable alginate-nanocellulose gels for biomedical applications : towards tunable mechanical properties and cell growing. *Nanomaterials*. 9(1):1–22.
- Sirviö, J.A., Visanko, M., Ukkola, J. & Liimatainen, H. 2018. Effect of plasticizers on the mechanical and thermomechanical properties of cellulose-based biocomposite films. *Industrial Crops and Products*. 122(June):513–521.
- Smith, G.H., McEachan, J.E., McLean, A. & Huntley, J.S. 2013. Prevention of knot slippage with the use of cyanoacrylate glue: a mechanical study. *Journal of orthopaedic surgery (Hong Kong)*. 21(1):65–67.
- Smyth, M., M'Bengue, M.S., Terrien, M., Picart, C., Bras, J. & Foster, E.J. 2018. The effect of hydration on the material and mechanical properties of cellulose nanocrystal-alginate composites. *Carbohydrate Polymers*. 179(August 2017):186–195.
- Soares, J.P., Santos, J.E., Chierice, G.O. & Cavalheiro, E.T.G. 2004. Thermal behavior of alginic acid and its sodium salt. *Eclética Química*. 29(2):57–63.
- Somasekharan, L.T., Kasoju, N., Raju, R. & Bhatt, A. 2020. Formulation and characterization of alginate dialdehyde, gelatin, and platelet-rich plasma-based bioink for bioprinting

- applications. *Bioengineering*. 7(3):1–12.
- Son, G.H., Lee, B.J. & Cho, C.W. 2017. Mechanisms of drug release from advanced drug formulations such as polymeric-based drug-delivery systems and lipid nanoparticles. *Journal of Pharmaceutical Investigation*. 47(4):287–296.
- Song, R., Murphy, M., Li, C., Ting, K., Soo, C. & Zheng, Z. 2018. Current development of biodegradable polymeric materials for biomedical applications. *Drug Design, Development and Therapy*. 12:3117–3145.
- Speir, R.W., Stallings, J.D., Andrews, J.M., Gelnett, M.S., Brand, T.C. & Salgar, S.K. 2015. Effects of valproic acid and dexamethasone administration on early bio-markers and gene expression profile in acute kidney ischemia-reperfusion injury in the rat. *PLoS ONE*. 10(5):1–24.
- Sriamornsak, P., 2003. Chemistry of pectin and its pharmaceutical uses: A review. *Silpakorn University International Journal*, 3(1-2), pp.206-228.
- Subramanian, K. & Vijayakumar, V. 2013. Evaluation of isophorone diisocyanate crosslinked gelatin as a carrier for controlled delivery of drugs. *Polymer Bulletin*. 70(3):733–753.
- Sun, J. & Tan, H. 2013. Alginate-based biomaterials for regenerative medicine applications. *Materials*. 6(4):1285–1309.
- Sun, C., Lux, S., Müller, E., Meffert, M. & Gerthsen, D. 2020. Versatile application of a modern scanning electron microscope for materials characterization. *Journal of Materials Science*. 55(28):13824–13835.
- Sun, X., Cameron, R.G. & Bai, J. 2020. Effect of spray-drying temperature on physicochemical, antioxidant and antimicrobial properties of pectin/sodium alginate microencapsulated carvacrol. *Food Hydrocolloids*. 100(October 2019):105420.
- Sunitha S, Adinarayana K, Sravanthi RP, Sonia G, Nagarjun R, Pankaj T, Veerabhadra SC, S.D. 2017. Fabrication of surgical sutures coated with Curcumin loaded gold nanoparticles. *Pharm Anal Acta*. 8(529):2.
- Sutures—Diameter. United States Pharmacopeia and National Formulary (USP 29-NF 24). Rockville, MD: United States Pharmacopeial Convention. 2006.
- Suyatma, N.E., Tighzert, L., Copinet, A. & Coma, V. 2005. Effects of hydrophilic plasticizers on mechanical, thermal, and surface properties of chitosan films. *Journal of Agricultural and Food Chemistry*. 53(10):3950–3957.
- Syukri, D.M., Nwabor, O.F., Singh, S. & Voravuthikunchai, S.P. 2021. Antibacterial functionalization of nylon monofilament surgical sutures through in situ deposition of biogenic silver nanoparticles. *Surface and Coatings Technology*. 413(December 2020):127090.
- Szycher, M. 2017. High performance biomaterials: a complete guide to medical and pharmaceutical applications. *Routledge*.
- Tajirian, A.L. & Goldberg, D.J. 2010. A review of sutures and other skin closure materials. *Journal of Cosmetic and Laser Therapy*. 12(6):296–302.
- Takahira, R., Yonemura, K., Fujise, Y. & Hishida, A. 2001. Dexamethasone attenuates neutrophil infiltration in the rat kidney in ischemia/reperfusion injury: The possible role of nitroxyl. *Free Radical Biology and Medicine*. 31(6):809–815.
- Takano, Y., Kusaka, A. & Nakamura, H. 2016. Density functional study of molecular interactions in secondary structures of proteins. *Biophysics and Physicobiology*. 13(0):27–35.
- Talja, R.A., Helén, H., Roos, Y.H. & Jouppila, K. 2007. Effect of various polyols and polyol contents on physical and mechanical properties of potato starch-based films. *Carbohydrate Polymers*. 67(3):288–295.
- Tamayol, A., Najafabadi, A.H., Aliakbarian, B., Arab-Tehrany, E., Akbari, M., ... Khademhosseini, A. 2015. Hydrogel templates for rapid manufacturing of bioactive fibers and 3D constructs. *Advanced Healthcare Materials*. 4(14):2146–2153.
- Tan, H., Sun, J., Jin, D., Song, J., Lei, M., ... Liu, C. 2020. Coupling PEG-LZM polymer networks with polyphenols yields suturable biohydrogels for tissue patching. *Biomaterials Science*. 8(12):3334–3347.
- Tan, R.H.H., Bell, R.J.W., Dowling, B.A. & Dart, A.J. 2003. Suture materials: Composition

- and applications in veterinary wound repair. *Australian Veterinary Journal*. 81(3):140–145.
- Tanasă, F. & Zănoagă, M. 2011. Biocompatible and resorbable polymeric materials for surgical sutures. 7–8.
- Tensile Strength. United States Pharmacopeia and National Formulary (USP 29-NF 24). Rockville, MD: United States Pharmacopeial Convention. 2006.*
- Teo, W.Z.W., Dong, X., Yusoff, S.K.B.M., Das De, S. & Chong, A.K.S. 2021. Randomized controlled trial comparing the effectiveness of mass and spaced learning in microsurgical procedures using computer aided assessment. *Scientific Reports*. 11(1):1–6.
- Thakhiew, W., Devahastin, S. & Soponronnarit, S. 2010. Effects of drying methods and plasticizer concentration on some physical and mechanical properties of edible chitosan films. *Journal of Food Engineering*. 99(2):216–224.
- Thom D, Dea IC, Morris ER, P.D. 1982. Interchain associations of alginate and pectins. *Progress in Food and Nutrition Science*. 6(1-6):97–108.
- Thomas-Busani, C., Sarabia-Sainz, J.A., García-Hernández, J., Madera-Santana, T.J., Vázquez-Moreno, L. & Ramos-Clamont Montfort, G. 2020. Synthesis of alginate-polycation capsules of different composition: Characterization and their adsorption for [As(iii)] and [As(v)] from aqueous solutions. *RSC Advances*. 10(48):28755–28765.
- Thomas, J. 2019. United States patent US 10,196,762 5.
- Toharisman, A., Suhartono, M.T., Spindler-Barth, M., Hwang, J.K. & Pyun, Y.R. 2005. Purification and characterization of a thermostable chitinase from *Bacillus licheniformis* Mb-2. *World Journal of Microbiology and Biotechnology*. 21(5):733–738.
- Tomihata, K., Suzuki, M. & Ikada, Y. 2001. The pH dependence of monofilament sutures on hydrolytic degradation. *Journal of Biomedical Materials Research*. 58(5):511–518.
- Torres-Giner S, Pérez-Masiá R, L.J. 2016. A review on electrospun polymer nanostructures as advanced bioactive platforms. *Polymer Engineering & Science*. 56(5):500–27.
- Trentadue, F., De Tommasi, D. & Puglisi, G. 2021. A predictive micromechanically-based model for damage and permanent deformations in copolymer sutures. *Journal of the Mechanical Behavior of Biomedical Materials*. 115(August 2020):104277.
- Tritto I, Zuchi C, Vitale S, A.G. 2013. Therapy against reperfusion-induced microvascular injury. *Current pharmaceutical design*. 19(25):4586–96.
- Tu, H., Zhang, D., Wadman, M.C. & Li, Y.L. 2020. Dexamethasone ameliorates recovery process of neuromuscular junctions after tourniquet-induced ischemia-reperfusion injuries in mouse hindlimb. *European Journal of Pharmacology*. 883:173364.
- Tummalapalli, M., Anjum, S., Kumari, S. & Gupta, B. 2016a. Antimicrobial surgical sutures: recent developments and strategies. *Polymer Reviews*. 56(4):607–630.
- Tummalapalli, M., Anjum, S., Kumari, S. & Gupta, B. 2016b. Antimicrobial Surgical Sutures: Recent Developments and Strategies. *Polymer Reviews*. 56(4):607–630.
- Turney, T.W., Patti, A., Gates, W., Shaheen, U. & Kulasegaram, S. 2013. Formation of glycerol carbonate from glycerol and urea catalysed by metal monoglycerolates. *Green Chemistry*. 15(7):1925–1931.
- Ueno, H. 2001. Topical formulations and wound healing applications of chitosan 2 . Topical findings of healing with chitosan at early phase of experimental open skin wound. *Advanced Drug Delivery Reviews*. 52:105–115. www.elsevier.com/locate/drugdeliv.
- Ullah, A. & Wu, J. 2013. Feather fiber-based thermoplastics: Effects of different plasticizers on material properties. *Macromolecular Materials and Engineering*. 298(2):153–162.
- Ullah, H., Santos, H.A. & Khan, T. 2016. Applications of bacterial cellulose in food, cosmetics and drug delivery. *Cellulose*. 23(4):2291–2314.
- Ummat, A. & Zells, R. 1980. Beneficial effect of dexamethasone on the "no reflow" phenomenon in canine myocardium. *Cardiovascular research*, 14(3), pp.137-141.
- Valentin, T.M., Leggett, S.E., Chen, P.Y., Sodhi, J.K., Stephens, L.H., ... Wong, I.Y. 2017. Stereolithographic printing of ionically-crosslinked alginate hydrogels for degradable biomaterials and microfluidics. *Lab on a Chip*. 17(20):3474–3488.
- Varaprasad, K., Jayaramudu, T., Kanikireddy, V., Toro, C. & Sadiku, E.R. 2020. Alginate-

- based composite materials for wound dressing application: A mini review. *Carbohydrate Polymers*. 236(February):116025.
- Van Den Bosch, E. & Gielens, C. 2003. Gelatin degradation at elevated temperature. *International Journal of Biological Macromolecules*. 32(3–5):129–138.
- van der Veen, J.N., Kennelly, J.P., Wan, S., Vance, J.E., Vance, D.E. & Jacobs, R.L. 2017. The critical role of phosphatidylcholine and phosphatidylethanolamine metabolism in health and disease. *Biochimica et Biophysica Acta - Biomembranes*. 1859(9):1558–1572.
- Viju, S. & Thilagavathi, G. 2013. Effect of chitosan coating on the characteristics of silk-braided sutures. *Journal of Industrial Textiles*. 42(3):256–268.
- Vincent, T., Vincent, C., Dumazert, L., Otazaghine, B., Sonnier, R. & Guibal, E. 2020. Fire behavior of innovative alginate foams. *Carbohydrate Polymers*. 250(July).
- Vroman, I. & Tighzert, L. 2009. Biodegradable polymers. *Materials*. 2(2):307–344.
- Wain, R.A.J., Hammond, D., McPhillips, M., Whitty, J.P.M. and Ahmed, W. 2016. Microvascular anastomoses: suture and non-suture methods. In: *Surgical Tools and Medical Devices*. Springer, Cham. pp. 545–562.
- Walkenström, P., Kidman, S., Hermansson, A.M., Rasmussen, P.B. & Hoegh, L. 2003. Microstructure and rheological behaviour of alginate/pectin mixed gels. *Food Hydrocolloids*. 17(5):593–603.
- Wanawananon, K., Moulton, S.E., Wallace, G.G. & Liawruangrath, S. 2016. Fabrication of novel core–shell PLGA and alginate fiber for dual-drug delivery system. *Polymers for Advanced Technologies*. 27(8):1014–1019.
- Wang, W.Z., 2009. Investigation of reperfusion injury and ischemic preconditioning in microsurgery. *Microsurgery: Official Journal of the International Microsurgical Society and the European Federation of Societies for Microsurgery*. 29(1): pp.72-79.
- Wang, B., Torres-Rendon, J.G., Yu, J., Zhang, Y. & Walther, A. 2015. Aligned bioinspired cellulose nanocrystal-based nanocomposites with synergetic mechanical properties and improved hygro-mechanical performance. *ACS Applied Materials and Interfaces*. 7(8):4595–4607.
- Wang, L.F., Shankar, S. & Rhim, J.W. 2017. Properties of alginate-based films reinforced with cellulose fibers and cellulose nanowhiskers isolated from mulberry pulp. *Food Hydrocolloids*. 63:201–208.
- Wang, Q., Hu, X., Du, Y. & Kennedy, J.F. 2010. Alginate/starch blend fibers and their properties for drug controlled release. *Carbohydrate Polymers*. 82(3):842–847.
- Wang, Q.Q., Liu, Y., Zhang, C.J., Zhang, C. & Zhu, P. 2019. Alginate/gelatin blended hydrogel fibers cross-linked by Ca²⁺ and oxidized starch: Preparation and properties. *Materials Science and Engineering C*. 99(April 2018):1469–1476.
- Wang, W.Z., Baynosa, R.C. & Zamboni, W.A. 2011. Update on ischemia-reperfusion injury for the plastic surgeon: 2011. *Plastic and Reconstructive Surgery*. 128(6):685–692.
- Wang, X., Bradford, P.D., Liu, W., Zhao, H., Inoue, Y., ... Zhu, Y. 2011. Mechanical and electrical property improvement in CNT/Nylon composites through drawing and stretching. *Composites Science and Technology*. 71(14):1677–1683.
- Wang, Y., Zhang, Y. & Tian, N. 2021. Cause and management of suture-related ocular complications after buried-suture double-eyelid blepharoplasty. *Journal of Plastic, Reconstructive and Aesthetic Surgery*. (1):1–6.
- Wang, Z., Sun, Z., Luo, G., Tian, Y. & Yang, X. 2019. Treatment of urinary calculi after Yang-Monti ileal ureter reconstruction: A case report. *BMC Urology*. 19(1):1–5.
- Washington, M.A., Balmert, S.C., Fedorchak, M. V., Little, S.R., Watkins, S.C. & Meyer, T.Y. 2018. Monomer sequence in PLGA microparticles: Effects on acidic microclimates and in vivo inflammatory response. *Acta Biomaterialia*. 65:259–271.
- Weber, M., Steinle, H., Golombek, S., Hann, L., Schlensak, C., ... Avci-Adali, M. 2018. Blood-contacting biomaterials: In vitro evaluation of the hemocompatibility. *Frontiers in Bioengineering and Biotechnology*. 6(July).
- Weldon, C.B., Tsui, J.H., Shankarappa, S.A., Nguyen, V.T., Ma, M., ... Kohane, D.S. 2012. Electrospun drug-eluting sutures for local anesthesia. *Journal of Controlled Release*.

- 161(3):903–909.
- Wu, K., Ni, J., Wu, D. and Wang, L. 2021. Design and selection of surgical suturing materials. *Tutorials in Suturing Techniques for Orthopedics*, Springer, Singapor. 37–56.
- Wu, H., Williams, G.R., Wu, J., Wu, J., Niu, S., ... Zhu, L. 2018a. Regenerated chitin fibers reinforced with bacterial cellulose nanocrystals as suture biomaterials. *Carbohydrate Polymers*. 180(August 2017):304–313.
- Wu, H., Williams, G.R., Wu, J., Wu, J., Niu, S., ... Zhu, L. 2018b. Regenerated chitin fibers reinforced with bacterial cellulose nanocrystals as suture biomaterials. *Carbohydrate Polymers*. 180(August 2017):304–313.
- Wu, H.L., Bremner, D.H., Li, H.Y., Shi, Q.Q., Wu, J.Z., ... Zhu, L.M. 2016. A novel multifunctional biomedical material based on polyacrylonitrile: Preparation and characterization. *Materials Science and Engineering C*. 62:702–709.
- Wu, I.T., Kao, P.F., Huang, Y.R. & Ding, S.J. 2020. In vitro and in vivo osteogenesis of gelatin-modified calcium silicate cement with washout resistance. *Materials Science and Engineering C*. 117(February):111297.
- Wu, Z., Li, Q., Xie, S., Shan, X. & Cai, Z. 2020. In vitro and in vivo biocompatibility evaluation of a 3D bioprinted gelatin-sodium alginate/rat Schwann-cell scaffold. *Materials Science and Engineering C*. 109(October 2019):110530.
- Xiao, C., Liu, H., Lu, Y. & Zhang, L. 2001a. Blend films from sodium alginate and blend films from sodium alginate. *Journal of Macromolecular Science , Part A : Pure and Applied Chemistry*. 38:3(May 2012):317–328.
- Xiao, C., Liu, H., Lu, Y. & Zhang, L. 2001b. Blend films from sodium alginate and gelatin solutions. *Journal of Macromolecular Science - Pure and Applied Chemistry*. 38 A(3):317–328.
- Xu, L.C. & Siedlecki, C.A. 2017. Protein adsorption, platelet adhesion, and bacterial adhesion to polyethylene-glycol-textured polyurethane biomaterial surfaces. *Journal of Biomedical Materials Research - Part B Applied Biomaterials*. 105(3):668–678.
- Xu, L.C., Bauer, J.W. & Siedlecki, C.A. 2014. Proteins, platelets, and blood coagulation at biomaterial interfaces. *Colloids and Surfaces B: Biointerfaces*. 124:49–68.
- Xu, L.C., Meyerhoff, M.E. & Siedlecki, C.A. 2019. Blood coagulation response and bacterial adhesion to biomimetic polyurethane biomaterials prepared with surface texturing and nitric oxide release. *Acta Biomaterialia*. 84:77–87.
- Yadav, M., Paritosh, K., Pareek, N. & Vivekanand, V. 2019. Composites based on bioderived polymers: potential role in tissue engineering. Vol. VI. *Materials for Biomedical Engineering*. Elsevier Inc.
- Yaltirik, M., Dedeoglu, K., Bilgic, B., Koray, M., Ersev, H., ... Soley, S. 2003. Comparison of four different suture materials in soft tissues of rats. *Oral Diseases*. 9(6):284–286.
- Yang, C.Y., Huang, L.Y., Shen, T.L. & Andrew Yeh, J. 2010. Cell adhesion, morphology and biochemistry on nanotopographic oxidized silicon surfaces. *European Cells and Materials*. 20(1):415–430.
- Yang, H., Yang, S., Kong, J., Dong, A. & Yu, S. 2015. Obtaining information about protein secondary structures in aqueous solution using Fourier transform IR spectroscopy. *Nature Protocols*. 10(3):382–396.
- Yang, J.S., Xie, Y.J. & He, W. 2011. Research progress on chemical modification of alginate: A review. *Carbohydrate Polymers*. 84(1):33–39.
- Yang, Y.M., Hu, W., Wang, X.D. & Gu, X.S. 2007. The controlling biodegradation of chitosan fibers by N-acetylation in vitro and in vivo. *Journal of Materials Science: Materials in Medicine*. 18(11):2117–2121.
- Yao, J., Korotkova, T., Riboh, J., Chong, A., Chang, J. & Smith, R.L. 2008. Bioactive Sutures for tendon repair: Assessment of a method of delivering pluripotential embryonic cells. *Journal of Hand Surgery*. 33(9):1558–1564.
- Ye, S., Wang, H., Zhao, F., Yuan, T., Liang, J., ... Zhang, X. 2019. Evaluating platelet activation related to the degradation of biomaterials using molecular markers. *Colloids and Surfaces B: Biointerfaces*. 184(September):110516.
- Yeo, Y. and Park, K. (in press). Control of encapsulation efficiency and initial burst in

- polymeric microparticle systems. *Archives of pharmacal research*. 27(1):pp.1-12.
- Yoo, J. & Won, Y.Y. 2020. Phenomenology of the initial burst release of drugs from PLGA microparticles. *ACS Biomaterials Science and Engineering*. 6(11):6053–6062.
- Yoshikawa M, Kajita H, Noguchi T, K.J. 2012. *Patent No. United States patent application US 13/442,002*.
- Yu, P. 2006. Synchrotron IR microspectroscopy for protein structure analysis: Potential and questions. *IOS Publishing*. 20(5, 6):229-251.
- Yu, X., Zhang, J. & Zheng, Y. 2021. Perchlorate adsorption onto epichlorohydrin crosslinked chitosan hydrogel beads. *Science of the Total Environment*. 761:143236.
- Yunus, M., Fahma, F., Abidin, Z., Noviana, D., Mukti, R.R. and Kusumaatmaja, A. (in press). Cellulose based surgical threads from oil palm empty fruit bunches in wound healing on male wistar rats. *The Indian Veterinary Journal*. 96(06):pp.21-23.
- Zare, Y. 2016. Study of nanoparticles aggregation/agglomeration in polymer particulate nanocomposites by mechanical properties. *Composites Part A: Applied Science and Manufacturing*. 84:158–164.
- Zhang, G., Zheng, G., Ren, T., Zeng, X. & van der Heide, E. 2020. Dopamine hydrochloride and carboxymethyl chitosan coatings for multifilament surgical suture and their influence on friction during sliding contact with skin substitute. *Friction*. 8(1):58–69.
- Zhang, J., Sun, J., Li, B., Yang, C., Shen, J., ... Liu, K. 2020. Robust biological fibers based on widely available proteins: facile fabrication and suturing applications. *Small*. 16(8):1–8.
- Zhang, L.N., Zhang, B.K., Lei, H.Y., Meng, H.Y., Huang, X. & Tan, C.H. 2018. A fiber-optic refractive index sensor detects the isoelectric point of gelatin. *Cogent Chemistry*. 4(1).
- Zhang, S., Li, J., Chen, S., Zhang, X., Ma, J. & He, J. 2020. Oxidized cellulose-based hemostatic materials. *Carbohydrate Polymers*. 230:115585.
- Zhang, W., Yin, B., Xin, Y., Li, L., Ye, G., ... Yang, Q. 2019. Preparation, mechanical properties, and biocompatibility of graphene oxide-reinforced chitin monofilament absorbable surgical sutures. *Marine Drugs*. 17(4).
- Zhao, W., Qi, Y., Wang, Y., Xue, Y., Xu, P., ... Li, Q. 2018. Morphology and thermal properties of calcium alginate/reduced graphene oxide composites. *Polymers*. 10(9):1–11.
- Zhao, X., Li, Q., Ma, X., Quan, F., Wang, J. & Xia, Y. 2015. The preparation of alginate-AgNPs composite fiber with green approach and its antibacterial activity. *Journal of Industrial and Engineering Chemistry*. 24:188–195.
- Zheng, W., Chen, C., Zhang, X., Wen, X., Xiao, Y., ... Liu, X. 2021. Layer-by-layer coating of carboxymethyl chitosan-gelatin-alginate on cotton gauze for hemostasis and wound healing. *Surface and Coatings Technology*. 406(November 2020):126644.
- Zhou, Q., Kang, H., Bielec, M., Wu, X., Cheng, Q., ... Dai, H. 2018. Influence of different divalent ions cross-linking sodium alginate-polyacrylamide hydrogels on antibacterial properties and wound healing. *Carbohydrate Polymers*. 197(April):292–304.
- Zhou, Y., Saito, T., Bergström, L. & Isogai, A. 2018. Acid-free preparation of cellulose nanocrystals by TEMPO oxidation and subsequent cavitation. *Biomacromolecules*. 19(2):633–639.
- Zhou, Y.L., Yang, Q.Q., Yan, Y.Y., Zhang, L., Wang, Q.H., ... Tang, J.B. 2019. Gene-Loaded nanoparticle-coated sutures provide effective gene delivery to enhance tendon healing. *Molecular Therapy*. 27(9):1534–1546.
- Zhou, Y.L., Yang, Q.Q., Zhang, L. & Tang, J.B. 2021. Nanoparticle-coated sutures providing sustained growth factor delivery to improve the healing strength of injured tendons. *Acta Biomaterialia*. 124(January 1996):301–314.
- Zhu, C. ya, Yao, C., Zhu, L. qing, She, C. & Zhou, X. zhong. 2019. Dexamethasone-induced cytotoxicity in human osteoblasts is associated with circular RNA HIPK3 downregulation. *Biochemical and Biophysical Research Communications*. 516(3):645–652.
- Zhukovskii, V.A. 2008. Problems and prospects for development and production of surgical suture materials. *Fibre Chemistry*. 40(3):208–216.

Appendix A: Publications

1) 'The Hemocompatibility of Nanoparticles: A Review of Cell–Nanoparticle Interactions and Hemostasis'.



Review

The Hemocompatibility of Nanoparticles: A Review of Cell–Nanoparticle Interactions and Hemostasis

Kara M. de la Harpe, Pierre P.D. Kondiah, Yahya E. Choonara, Thashree Marimuthu, Lisa C. du Toit and Viness Pillay

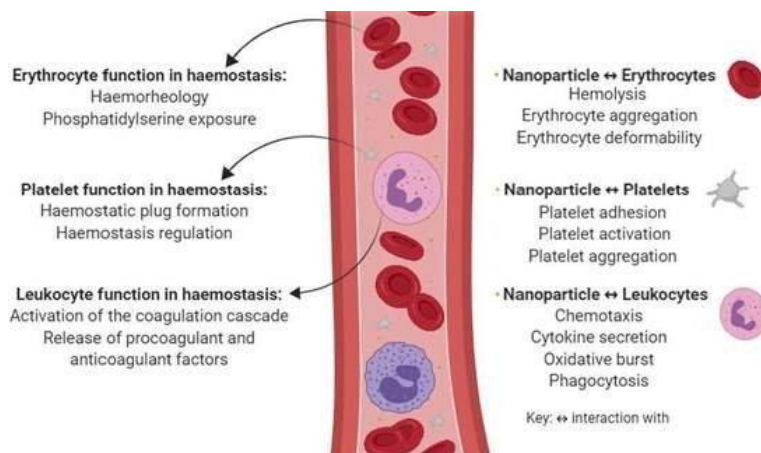
Wits Advanced Drug Delivery Platform Research Unit, Department of Pharmacy and Pharmacology, School of Therapeutic Science, Faculty of Health Sciences, University of the Witwatersrand, Johannesburg, 7 York Road, Parktown 2193, South Africa; karadelaharpe7@gmail.com (K.M.d.l.H.); pierre.kondiah@wits.ac.za (P.P.D.K.); yahya.choonara@wits.ac.za (Y.E.C.); thashree.marimuthu@wits.ac.za (T.M.); lisa.dutoit1@wits.ac.za (L.C.d.T.)
 * Correspondence: Viness.Pillay@wits.ac.za; Tel.: +11-717-2274

Received: 14 September 2019; Accepted: 3 October 2019; Published: 7 October 2019



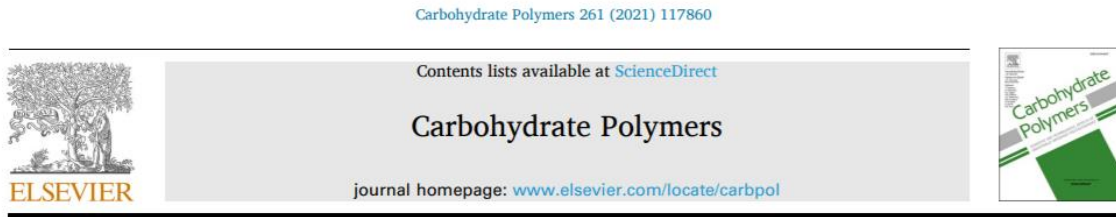
Abstract: Understanding cell–nanoparticle interactions is critical to developing effective nanosized drug delivery systems. Nanoparticles have already advanced the treatment of several challenging conditions including cancer and human immunodeficiency virus (HIV), yet still hold the potential to improve drug delivery to elusive target sites. Even though most nanoparticles will encounter blood at a certain stage of their transport through the body, the interactions between nanoparticles and blood cells is still poorly understood and the importance of evaluating nanoparticle hemocompatibility is vastly understated. In contrast to most review articles that look at the interference of nanoparticles with the intricate coagulation cascade, this review will explore nanoparticle hemocompatibility from a cellular angle. The most important functions of the three cellular components of blood, namely erythrocytes, platelets and leukocytes, in hemostasis are highlighted. The potential deleterious effects that nanoparticles can have on these cells are discussed and insight is provided into some of the complex mechanisms involved in nanoparticle–blood cell interactions. Throughout the review, emphasis is placed on the importance of undertaking thorough, all-inclusive hemocompatibility studies on newly engineered nanoparticles to facilitate their translation into clinical application.

Keywords: hemocompatibility; nanoparticles; erythrocytes; platelets; leukocytes



Appendix A: Publications

2) 'Advances in carbohydrate-based polymers for the design of suture materials: A review'.



Advances in carbohydrate-based polymers for the design of suture materials: A review

Kara M. de la Harpe, Pierre P.D. Kondiah, Thashree Marimuthu, Yahya E. Choonara *

Wits Advanced Drug Delivery Platform Research Unit, Department of Pharmacy and Pharmacology, School of Therapeutic Science, Faculty of Health Sciences, University of the Witwatersrand, Johannesburg, 7 York Road, Parktown, 2193, South Africa

ARTICLE INFO

Keywords:
Surgical suture
Natural polymers
Biocompatibility
Bioactivity
Biodegradation

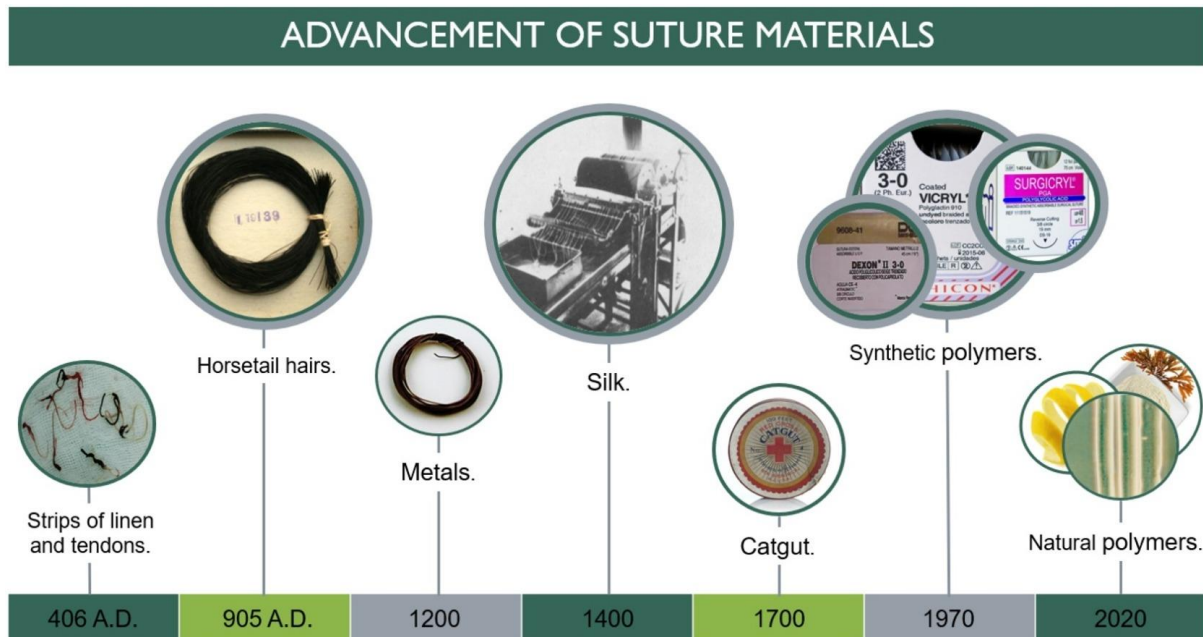
ABSTRACT

Suture materials constitute one of the largest biomedical material groups with a huge global market of \$ 1.3 billion annually and employment in over 12 million procedures per year. Suture materials have radically evolved over the years, from basic strips of linen to more advanced synthetic polymer sutures. Yet, the journey to the ideal suture material is far from over and we now stand on the brink of a new era of improved suture materials with greater safety and efficacy. This next step in the evolutionary timeline of suture materials, involves the use of natural, carbohydrate polymers that have, until recent years, never before been considered for suture material applications. This review exposes the latest and most important advancements in suture material development while digging deep into how natural, carbohydrate polymers can serve to advance this field.

1. Introduction

Since non-absorbable sutures must be removed through a second operational procedure, that is not only costly but also painful for the patient,

Graphical abstract:



Appendix A: Publications

3) 'An advanced 3D monofilament biosuture'

Cum Laude

Academy of Pharmaceutical Sciences



An advanced 3D monofilament biosuture

KM de la Harpe, PPD Kondiah, T Marimuthu, LC du Toit, P Kumar, YE Choonara, V Pillay¹

¹Wits Advanced Drug Delivery Platform Research Unit, Department of Pharmacy and Pharmacology, Faculty of Health Sciences, University of the Witwatersrand, South Africa

Kara is the winner of the Aspen Pharmacare Young Scientist competition – Laboratory Sciences category.

Introduction

Sutures are one of the most widely used medical devices with employment in over 12 million procedures per year globally.¹ Yet, the ideal suture material does not exist. Over the years scientists and surgeons alike have set out to find a suture material that is biocompatible, easy to handle, does not cause unnecessary tissue damage and creates an optimal environment for wound healing.² This has led to the discovery of numerous suture materials ranging from silk and catgut in the early 1800s to synthetic polymers such as polylactic acid and polyglycolide that are currently in use.³ Sutures on the market today are associated with distinct disadvantages that threaten the success of the procedures they are used in. For example, sutures consisting of polyglactin have been found to cause severe tissue damage and necrosis through the release of acidic degradation products that result in strong inflammatory responses.⁴ Additionally, most suture materials are multifilament or braided materials that tend to cut through tissues causing cellular damage and extending the time of wound healing.⁵ Suture-related complications have been implicated in numerous clinical problems such as hematoma formation, pulmonary embolisms and false aneurysms. A retrospective study done by Starr *et al.*, found that 26 of 39 false aneurysm cases could be directly ascribed to insufficiencies in the suture material.⁶ There is, therefore, a clear yet understated need for a superior suture material that can limit suture-related complications and improve



Kara de la Harpe

aided design (CAD) was used to obtain the monofilament suture platform with a smooth, uniform surface that allows the biosuture to easily glide through delicate tissues without causing unnecessary harm.

Materials and methods

Materials and biosuture fabrication

Sodium alginate and pectin from citrus peel was purchased from Sigma-Aldrich (St. Louis, MO, USA). The mannuronic acid and guluronic acid concentration ratio (A_{1026}/A_{1080}) of sodium alginate was calculated to be 1.52 as deduced from Fourier Transform Infrared Spectrometry (FTIR) data and described in literature.⁷ Barium chloride ($BaCl_2$) was employed as crosslinking agent and glycerol as plasticiser (LabChem, Foundershill, Johannesburg, SA).

A novel bioink was created from a homogenous hydrogel consisting of two natural polymers namely sodium alginate and pectin from citrus peel. The two polymers were dissolved separately through mechanical stirring at 35°C for one hour. The two solutions were then combined, glycerol added, and the resulting solution vigorously stirred until a homogenous hydrogel was obtained. The hydrogel was immediately transferred to a clear, sterile 3D printing syringe that was loaded onto the 3D Bioplotter® (EnvisionTEC, GmbH, Germany). The hydrogel was now used as a novel bioink by printing it, according to the intercalated architectural design, into a $BaCl_2$ solution, that allowed for *in situ* crosslinking and suture formation. The printed biosutures were left to crosslink for 24 hours after which they were washed five times with deionised water and airdried in a fume hood for six hours.

Physicochemical analysis of the biosuture material

Appendix A: Publications

4) 'Synthesis of a novel monofilament bioabsorbable suture for biomedical applications.'

Synthesis of a novel monofilament bioabsorbable suture for biomedical applications

Kara M. de la Harpe, Thashree Marimuthu, Pierre P.D. Kondiah, Pradeep Kumar, Philemon Ubanako, and Yahya E. Choonara*

Wits Advanced Drug Delivery Platform Research Unit, Department of Pharmacy and Pharmacology, School of Therapeutic Science, Faculty of Health Sciences, University of the Witwatersrand, Johannesburg, 7 York Road, Parktown, 2193, South Africa.

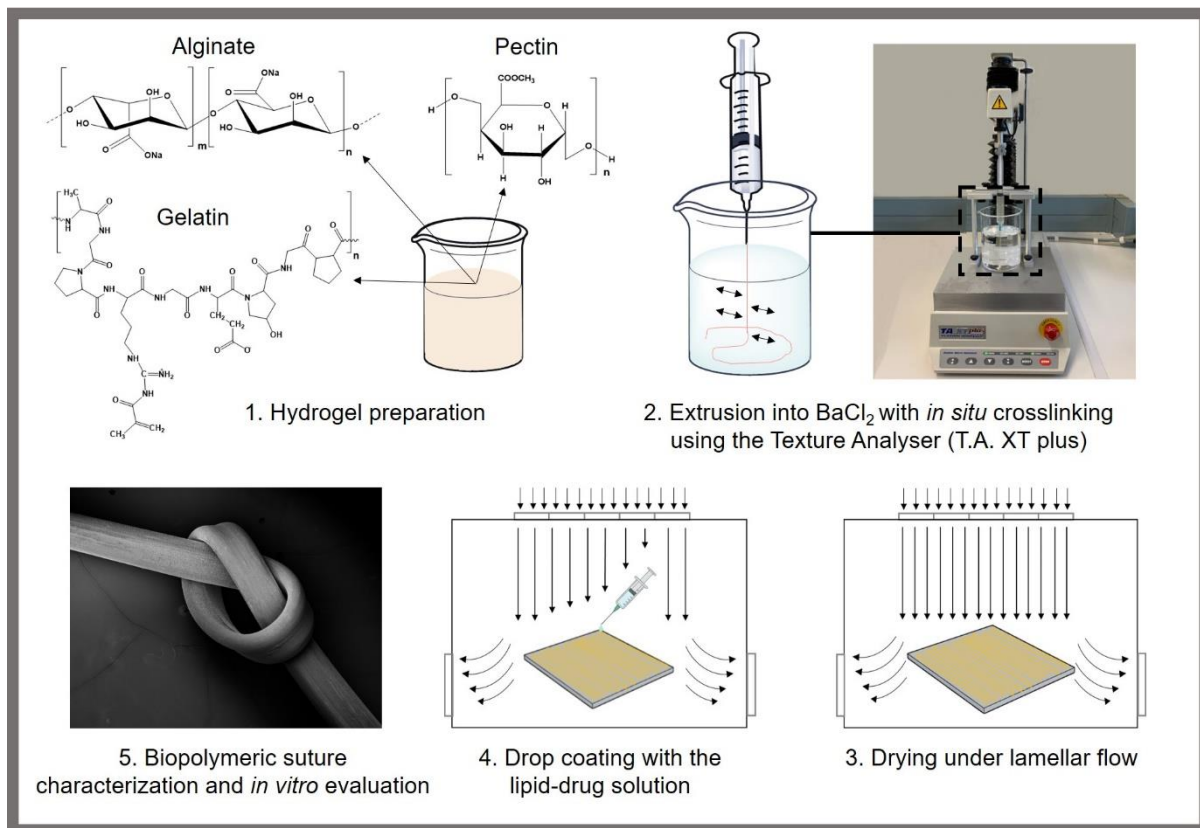
Yahya.choonara@wits.ac.za

Abstract:

In this research, a novel bioabsorbable suture that is, monofilament and capable of localized drug delivery, was developed from combination of natural biopolymers that were not previously applied for this purpose. The optimised suture formulation comprised of sodium alginate (6% w/v), pectin (0.1% w/v), and gelatin (3% w/v), in the presence of glycerol (4% v/v) which served as a plasticizer. The monofilament bioabsorbable sutures were synthesised via *in situ* ionic crosslinking in a barium chloride solution (2% w/v). The resulting suture was characterized in terms of mechanical properties, morphology, swelling, degradation, drug release, and biocompatibility, in addition to FTIR, PXRD and DSC analysis. The drug loaded and non-drug loaded sutures had a maximum breaking strength of 4.18 and 4.08 N, in the straight configuration and 2.44 N and 2.59 N in the knot configuration, respectively. FTIR spectrum of crosslinked sutures depicted $\Delta 9\text{ cm}^{-1}$ downward shift for the carboxyl stretching band which was indicative of ionic interactions between barium ions and sodium alginate. *In vitro* analysis revealed continued drug release for 7 days and gradual degradation by means of surface erosion, which was completed by day 28. Biocompatibility studies revealed excellent hemocompatibility and no cytotoxicity. These results suggest that the newly developed bioabsorbable suture meets the basic requirements of a suture material and provides a viable alternative to the synthetic polymer sutures that are currently on the market.

Keywords: sodium alginate, bioabsorbable suture; monofilament; localized drug delivery

Graphical abstract:



Appendix B: Research outputs (oral and poster presentations)

1) An advanced 3D monofilament biosuture. 10th Wits Cross-faculty Postgraduate Symposium, University of the Witwatersrand, Johannesburg, South Africa.



10th Wits Cross Faculty Postgraduate Symposium: Abstract

NAME/S: Kara de la Harpe; Dr. P Kondiah; Dr T Marimuthu; Prof Y Choonara; Prof V Pillay

FACULTY: Therapeutic Sciences

SCHOOL: Pharmacy (WADDP)

STUDENT NUMBER: 2169368

EMAIL: karadelaharpe7@gmail.com

INDICATE YOUR CHOICE: Oral presentation

TITLE: An advanced 3D monofilament biosuture

Keywords: Suture, Surgery, Wound healing

The very first reference to the use of sutures in wound closure, was found on ancient Egyptian scrolls that date back to 3500 BC (1). Since then numerous materials including hair, catgut, silk, and most recently, synthetic polymers such as polyglactin, have been explored as potentially safer and more effective suture materials. Ideally, sutures should have sufficient mechanical strength to close and support a wound while creating an optimal environment for wound healing (2). The quest for such an ideal suture material is still ongoing with suture-related complications threatening the outcome of many surgical procedures.

Just like any other implanted medical device, sutures can cause foreign body reactions and lead to excessive inflammatory tissue responses that will, not only lower the body's natural defences against infection, but also interfere with the proliferative phase of wound healing. This can ultimately lead to an inferior wound strength and detrimental scar tissue formation (3). The *in vivo* reaction to suture materials depends on the type of tissue involved as well as the chemical nature and physical properties of the suture material used. The suture materials currently on the market are all associated with distinct risks and disadvantages. For example, nonabsorbable Biofix sutures that consist of poly(L)lactic acid have been found to cause significant swelling of the soft tissue during the post-operative period (4). Sutures made of degradable synthetic polymers such as polyglactin 910, are largely considered as biocompatible, yet result in local pH shifts and debris diffusion that can induce autocatalytic reactions in adjacent tissues (5).

There is an understated need for a superior suture material that will not only improve the therapeutic efficacy of sutures but also broaden their application range (6). The current research project sets out to fabricate a novel suture material that will help fine-tune longstanding surgical procedures and improve the success rate of numerous medical interventions.

REFERENCES:

1. Kjaergard, H.K., Suture support: Is it advantageous? *The American journal of surgery*, **2001**, *182*(2), 15-20.
2. Spotnitz, W.D., Falstrom, J.K. and Rodeheaver, G.T., The role of sutures and fibrin sealant in wound healing. *Surgical Clinics*, **1997**, *77*(3), 651-669.



10th CROSS-FACULTY POSTGRADUATE SYMPOSIUM
Showcasing Postgraduate Research @WITS

WE ARE PROUD TO CONFIRM THAT

Kara de la Harpe

PRESENTED THEIR RESEARCH AT THE 10th CROSS FACULTY POSTGRADUATE SYMPOSIUM



PROFESSOR ROBERT MUPONDE



PROFESSOR ZEBLON JILIKAZI

Appendix B: Research outputs (oral and poster presentations)

2) An advanced 3D monofilament biosuture. Academy of Pharmaceutical Sciences, 2019 Conference and Young Scientist Competition, Pretoria, South Africa.

APSSA conference and Young Scientist Competition 2019

An advanced 3D monofilament biosuture

Kara M. de la Harpe¹, Pierre P.D. Kondiah¹, Yayha E. Choonara¹, Thashree Marimuthu¹, Viness Pillay¹

¹Wits Advanced Drug Delivery Platform Research Unit, Department of Pharmacy and Pharmacology, School of Therapeutic Science, Faculty of Health Sciences, University of the Witwatersrand, Johannesburg, South Africa

Purpose: Suture related complications threaten the success of numerous surgeries, yet sutures remain the most widely used medical devices for reconnecting delicate tissues. Since the inception of their use, more than 4000 years ago, researchers have set out to develop the ideal suture material that will create an optimum environment for wound healing. The ideal suture has yet to emerge and this project sets out to fabricate exactly this by utilizing advanced 3D printing technology and natural polymeric materials.

Methods: A resourceful co-polymer blend was fashioned and incorporated into an advanced bioink that was utilized to create a durable, yet elastic 3D monofilament biosuture through 3D printing of the bioink with a 3D Bioplotter® (EnvisionTEC, GmbH, Germany). The physiochemical, mechanical and morphological properties of the newly fabricated suture material was analysed using the Fourier Transform Infrared (FT-IR) spectrometer (PerkinElmer Spectrum 100), the BioTester 5000 (CellScale Biomaterials Testing) and a scanning electron microscope (FEI ESEM Quanta 400F), respectively.

Results: A 3D monofilament biosuture was created with dimensions comprising 250µm radius and total height of 300µm, consisting of three layers of 100µm each. FTIR analysis of pristine alginate showed two distinct bands at 1649 and 1460 cm⁻¹ that was ascribed to the characteristic asymmetrical and symmetrical stretching vibrations of the carboxylate salt groups. A decrease in intensity was observed in these regions after crosslinking, confirming the interaction between sodium alginate and barium chloride. Mechanical analysis revealed a peak displacement and peak force of 26.6% and 1200Pa respectively as calculated from the percentage elongation at break and Young's modulus. SEM analysis confirmed a mean diameter of 500µm and illustrated the highly condensed internal network and properly adhered layers of the suture material.

Conclusions: A promising new suture material was created, comprising an interesting co-polymer blend, through the utilization of advanced 3D printing technology. The suture material can help improve the success rate of microsurgeries as a result of fewer suture related complications.

Appendix B: Research outputs (oral and poster presentations)

3) Evolution of the suture – where to in the future? Faculty of Health Sciences, 2020 Biannual Research Day, University of the Witwatersrand, Johannesburg, South Africa.

Faculty of Health Sciences, Biannual Research Day, 2020

Abstract: Evolution of the suture – where to in the future?

Kara M. de la Harpe¹, Pierre P.D. Kondiah¹, Thashree Marimuthu¹, Yayha E. Choonara¹

¹Wits Advanced Drug Delivery Platform Research Unit, Department of Pharmacy and Pharmacology, School of Therapeutic Science, Faculty of Health Sciences, University of the Witwatersrand, Johannesburg, South Africa

With a huge global market of over 1.3 billion dollars annually, sutures are one of the most widely used medical devices of the day. Indeed, sutures find their application in nearly all surgical fields and are used in over 12 million procedures per year. Therefore, it is only logical that researchers will focus their attention on improving the therapeutic efficacy and extending the functionality of this well trusted and widely used medical device.

In recent years, there has been a staggering number of patents and innovative research studies published on new suture materials, consisting of biopolymers that have never before been used for this particular application. These natural polymers have distinct advantages that researchers have used to develop drug-eluting sutures, stem cell seeded sutures, and smart or stimuli-responsive sutures that are able to form self-tightening knots, amongst many others. Biopolymers can also have superior biocompatibility, when compared to synthetic polymers, as well as a unique balance between tensile strength and elasticity that can help improve the therapeutic efficacy of sutures as wound closure devices.

The proposed oral presentation will highlight the most significant advancements, that have recently been made in the field of suture materials and explain the potential impact of these new developments. Attention will also be given to future trends that can be expected and how this can transform our current concept of sutures as mere wound closure devices to bioactive materials that can carry a weighty role in the wound healing and tissue regeneration process.

Appendix B: Research outputs (oral and poster presentations)

4) A novel monofilament, absorbable, drug-eluting biopolymeric suture. Faculty of Health Sciences, 2021 Biannual Research Day, University of the Witwatersrand, Johannesburg, South Africa.

Faculty of Health Sciences, Biannual Research Day, 2021

Abstract: A novel monofilament, absorbable, drug-eluting biopolymeric suture.

Kara M. de la Harpe¹, Pierre P.D. Kondiah¹, Thashree Marimuthu¹, Yayha E. Choonara¹

¹Wits Advanced Drug Delivery Platform Research Unit, Department of Pharmacy and Pharmacology, School of Therapeutic Science, Faculty of Health Sciences, University of the Witwatersrand, Johannesburg, South Africa

Suture materials are one of the most popular medical devices in the global surgical market. Sutures have greatly evolved since their inception in the 1800's, with synthetic polymer sutures overtaking the market in 1970. Yet, despite the advancements made over the years, sutures continue to elicit significant foreign body responses that deter optimal wound healing. More recently, the focus has shifted towards natural polymer biosutures and bioactive drug-eluting sutures, in an attempt to develop the ideal suture material. Microvascular surgery (MVS) is one of the many procedures that relies on sutures to achieve its outcome, i.e. microvascular anastomosis. However, MVS is tainted by a high occurrence of ischemic reperfusion injury, followed by the dreaded no-reflow phenomenon that causes irreversible tissue damage. Dexamethasone has been shown to prevent both these detrimental complications, but its use is limited by severe systemic side effects which can be overcome through localized drug delivery from medical devices such as sutures.

In the current study, we aimed to develop a novel biosuture that consist of natural polymers and is able to provide sustained, localized dexamethasone release. The biosuture was characterized in terms of mechanical properties, surface morphology, swelling, degradation and drug releasing behaviour in addition to FTIR, XRD, TGA and DSC analysis. The coated biosutures showed a maximum strength of 2.59N, which exceeds the minimum requirements of the USP. The biosutures displayed gradual degradation over a period of 28 days, while the drug release profile indicated an initial burst release, followed by a lag phase and finally linear drug release over 7 days. Altogether, the results suggest that the newly developed biosuture can provide a viable alternative to the synthetic polymer sutures that are currently on the market, while carving a way towards preventing ischemic reperfusion injury and no-reflow during MVS.

Poster: A novel monofilament, absorbable, drug-eluting biopolymeric suture.

A NOVEL MONOFILAMENT, ABSORBABLE, DRUG-ELUTING BIOPOLYMERIC SUTURE

Kara M. de la Harpe¹, Thashree Marimuthu¹, Pierre P.D. Kondiah¹, Yayha E. Choonara¹
¹Wits Advanced Drug Delivery Platform Research Unit, Department of Pharmacy and Pharmacology, School of Therapeutic Science, Faculty of Health Sciences, University of the Witwatersrand, Johannesburg, 7 York Road, Parktown, 2193, South Africa.

INTRODUCTION

- Sutures are one of the most widely used medical devices with a huge global market of over \$37 billion [1].
- Yet, all the suture materials that are currently available hold high risks of complications, such as infection, chronic inflammation, and tissue granulation, that can lead to surgical failure with devastating consequences for the patient. Hence, there is a great need for a new, advanced suture material [2].
- In recent years, natural polymers (e.g., chitin, cellulose and alginate) have received increasing attention as raw materials for suture material development, largely due to their desirable qualities, such as excellent biocompatibility, similarity to the native extracellular matrix and effective biodegradation, which can improve the safety and therapeutic efficacy of suture materials [3].
- Absorbable sutures also hold immense potential as drug delivery devices as they can provide local, sustained drug delivery, directly to the site of injury without the need for an additional foreign object to be introduced to the wound bed or for a second removal procedure, which can be painful and traumatic to the patient [4].

AIM AND OBJECTIVES

The goal of this study is to create a new suture material that consists of natural polymer with well-known biocompatibility and biodegradability; has a monofilament design; can degrade in an acceptable time frame and is capable of localized drug delivery.

METHODS

- Fabrication of the biopolymeric suture:** Extrusion of the biopolymeric suture formulation (Table 1) into a crosslinker bath of BaCl₂ (2% w/v) followed by drying and coating with a lipid-drug layer (Table 1) as shown in Fig. 1.
- Chemical characterization:** Crosslinking and coating was confirmed with Fourier Transform Infrared Spectra (PerkinElmer Spectrum 2000 FTIR Spectrometer).
- Mechanical characterization:** Stress-strain curves were constructed from data obtained with the Texture Analyser (TA.XT Plus, Stable Micro Systems, England), according to USP guidelines. Data was also used to obtain relevant parameters such as force at break, tensile strength, elongation at break and Young's modulus. All measurements were performed 10x and expressed as average ± standard deviation.
- Morphological characterization:** The coated and uncoated biopolymeric sutures were imaged with a Phenom™ SEM (FEI Company, USA) after coating with carbon and palladium/gold.
- In vitro characterization:** Degradation and drug release were determined by incubating the biopolymeric sutures in phosphate buffered saline (pH=7.4) at 37°C and 25 rpm. Degradation was evaluated as a function of weight loss over time and drug release measured spectrophotometrically at 241 nm using the nanophotometer (Implen, GmbH, Germany).

Human embryonic kidney cells (HEK 293) were employed to study the cytotoxicity of the biopolymeric sutures. Cells were seeded in 96-well plates and treated with biopolymeric suture extracts (500µg/ml). After incubation for 48 hours, XTT-assays were carried out according to standard protocols. Absorbance was measured at 450 nm with a multiplate reader (VICI™ X, Perkin Elmer, SA) and the data used to quantify cell viability. Statistical analysis was performed using student's t-tests and data marked by (*) for p<0.05 and (**) for p<0.01.

RESULTS

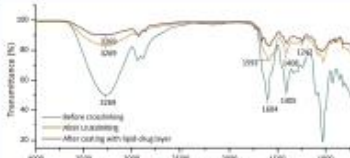


Fig. 2. FTIR spectra of the biopolymeric suture, before and after crosslinking, as well as after coating with the lipid-drug layer.

Biopolymeric suture	Load failure (N)	Tensile strength (N/mm ²)	Elongation at break (%)	Young's modulus (MPa)
Straight configuration				
A. Uncoated	4.06 ± 0.4	300.3 ± 0.4	18.55 ± 0.9	2.04 ± 0.4
B. Coated	4.34 ± 0.7	368.7 ± 0.7	16.57 ± 0.3	2.00 ± 0.3
Knot configuration				
A. Uncoated	2.46 ± 0.2	218.0 ± 0.3	9.47 ± 0.4	1.51 ± 0.4
B. Coated	2.59 ± 0.4	229.7 ± 0.4	10.26 ± 0.7	1.58 ± 0.3

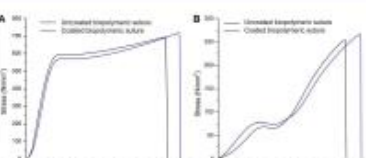


Fig. 3. Stress-strain curves of the uncoated and coated biopolymeric sutures in the (A) straight configuration and (B) knotted configuration.




Fig. 4. SEM Images of (A,D) uncoated and (B,C) coated biopolymeric sutures in the straight configuration, (D) knot of the uncoated suture.




Fig. 5. Photographs of the biopolymeric sutures, reflecting their size.

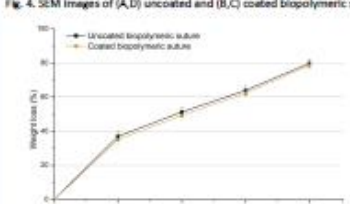


Fig. 6. Degradation profiles of the biopolymeric sutures.

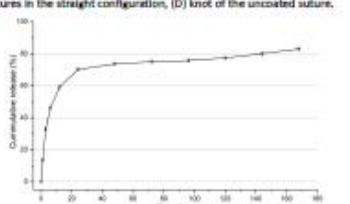


Fig. 7. Cumulative drug release profile of dexamethasone from the coated biopolymeric suture.


CONCLUSION

The developed biopolymeric sutures show promising results that suggest it will be able to act as an alternative to current synthetic sutures with the added benefit of local, sustained drug delivery.

FUTURE PROSPECTS

Haemolysis and platelet activation assays are currently underway to further assess the biocompatibility of the biopolymeric sutures. Future prospects include in vivo evaluation of the biopolymeric sutures using a Sprague dawley rat model.

ACKNOWLEDGEMENTS



REFERENCES

1. J.B. Aghajani, C.C. Aghajani, Surgical sutures: the largest textile implant material, Woodhead Publishing Limited, 2004, https://doi.org/10.1533/9781845694247_441.
2. N.D. Devita Jr. Complications Associated with Sutures, *Consultant, Spine Surgery*, (2012) 79-79.
3. R. Pandey, C. Kishor, G. Singh, Compositing Biopolymers for Biomedical Applications, *Trends Biotechnol.*, 24 (2006) 462-468. <https://doi.org/10.1016/j.tbiotec.2006.03.002>
4. Ayala, A., Aguilera, G., Chander, J., Mahara, R. and Nagpal, M., 2018. Drug-eluting sutures: A recent update. *Journal of Applied Pharmaceutical Science*, 9(9), pp.133-123.

Appendix C: Accolades

1) Postgraduate Merit Award



2) Young Scientist of the Year Award, APSSA 2019.

*The Academy of Pharmaceutical Sciences of the
Pharmaceutical Society of South Africa*



congratulates

Kara de la Harpe

*as the winner of the Young Scientist competition
(Laboratory Sciences)
at the APSSA conference 2019*

Chairman

10 October 2019

Date

3) Best student poster presentation. School of Therapeutic Sciences Biannual Research Day 2021.



SCHOOL OF THERAPEUTIC SCIENCES BIENNIAL RESEARCH DAY 2021

BEST STUDENT POSTER PRESENTATION

AWARDED TO

KARA DE LA HARPE

14 September 2021


Professor Hellen Myezwa
Head of school


Professor Benita Olivier
Research day chairperson

Sponsors



Appendix D: Ethical clearance



R49 Professor YE Choonara

HUMAN RESEARCH ETHICS COMMITTEE (MEDICAL) CLEARANCE CERTIFICATE NO. M180978

NAME: Professor YE Choonara
(Principal Investigator)

DEPARTMENT: School of Therapeutic Sciences
Department of Pharmacy and Pharmacology
Medical School
University

PROJECT TITLE: *Development of a biohybrid, platelet-based drug-delivery vehicle for the potential treatment of ischaemic stroke*


DATE CONSIDERED: 28/09/2018

DECISION: Approved unconditionally

CONDITIONS: Change of Principal Investigator noted on 02/09/2021

NOTE: If contact information regarding student study participants is required, please contact the Registrar's office - <Nicoleen.Potgieter@wits.ac.za>

SUPERVISOR: Not applicable

APPROVED BY: 
Dr CB Penny, Chairperson, HREC (Medical)

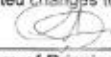
DATE OF APPROVAL: 16/11/2018

This Clearance Certificate is valid for 5 years from the date of approval. An extension may be applied for.

DECLARATION OF INVESTIGATORS

To be completed in duplicate and **ONE COPY** returned to the Research Office secretariat on the 3rd floor, Phillip Tobias Building, Parktown, University of the Witwatersrand, Johannesburg.

I/we fully understand the conditions under which I am/we are authorized to carry out the above-mentioned research and I/we undertake to ensure compliance with these conditions. Should any departure be contemplated from the research protocol as approved, I/we undertake to submit details to the Committee. **I agree to submit a yearly progress report.** When a funder requires annual re-certification, the application date will be one year after the date when the study was initially reviewed. In this case, the study was initially reviewed in «Missing mail merge field» and therefore reports and re-certification will be due in the month of «Missing mail merge field» each year. Unreported changes to the study may invalidate the clearance given by the HREC (Medical).



Signature of Principal Investigator

18 October 2021

Date